Feasibility of Bipolar DC Grids on Ships

An Insight into Quantitative Benefits

A. Abhyankar

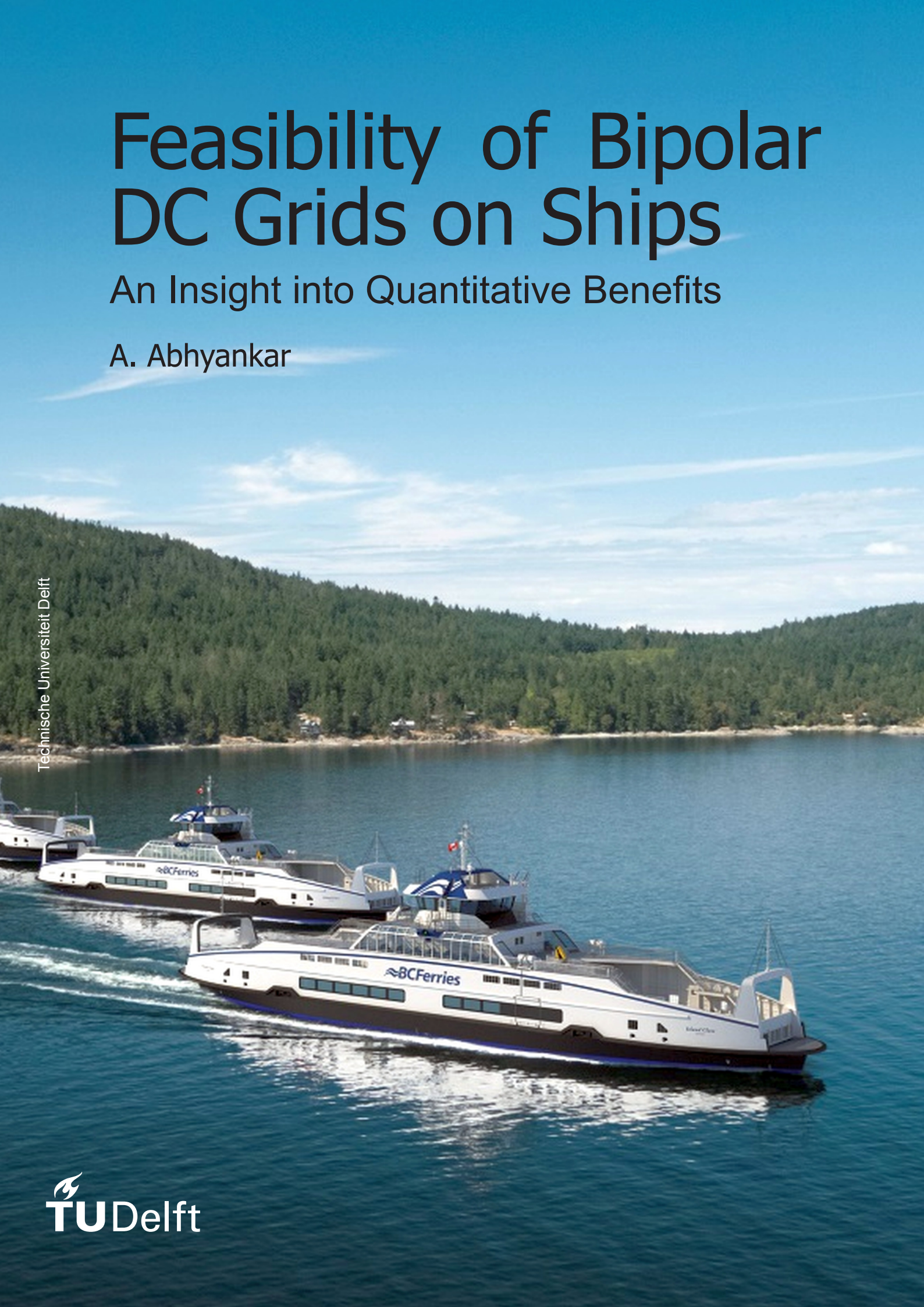

Technische Universiteit Delft

TU Delft

Feasibility of Bipolar DC Grids on Ships

An Insight into Quantitative Benefits

by

A. Abhyankar

to obtain the degree of Master of Science
at the Delft University of Technology,
to be defended publicly on Thursday, August 31, 2023 at 2:30 PM.

Student number:	5532264	
Project duration:	December 8, 2022 – August 31, 2023	
Thesis committee:	Prof. dr. ir. P. Bauer,	TU Delft, committee chair
	Dr. ir. Z. Qin,	TU Delft, thesis supervisor
	Dr. ir. H. Ziar,	TU Delft, external member
	Ir. S. Yadav,	TU Delft, daily supervisor

Cover Image : - Schottel GmbH

TU Delft

Summary

Global average temperatures are setting new records in comparison to the previous decade, primarily due to the accumulation of greenhouse gases such as CO_2. The growth potential in emerging economies worsens the current global situation. These CO_2 emissions are needed to be curtained and efforts are underway from the world governments and international organisations. The emissions target set by the International Maritime Organisation seems far-fetched given the forecast for the growth of the shipping sector. Although electrification is proven to reduce emissions, the energy efficiency metrics (EEDI, EEXI) are incapable to provide the quantitative benefits that can be realised by switching to a bipolar DC (BiDC) grid as compared with the AC grid.

This thesis aims to evaluate the feasibility of BiDC grids over the complete operating profile of the ship by comparing ten arrangements, five for AC and five for DC, with the Key Performance Indicators (KPIs). The arrangements are two diesel generators (AC1 & DC1), two diesel generators and battery (AC2 & DC2), two diesel generators, battery, and shore power (AC3 & DC3), one diesel generator and battery (AC4 & DC4), one diesel generator, battery, and shore power (AC5 & DC5). The comparison is made for key performance indicators like CO_2 emissions, fuel consumption, electrical power requirement, propulsion power cable losses, capital costs, operating costs, propulsion system weight, and load-carrying capacity of the ship. In this study, a ferry is chosen for the comparison between the two grid architectures as it is the least promising ship class due to its operating characteristics.

To establish the required background knowledge for the reader of this thesis, the literature for the current emission regulations, the different propulsion systems, and the differences in AC and DC grids are presented. The ship's propulsion and auxiliary power demand are not freely available and are in the possession of the ship operator. Therefore, first, a preliminary methodology was developed for estimating the ship's mechanical power requirements. Second, the ship's electrical power requirements are estimated from the understanding of the literature. The cable power losses are also calculated for the AC and BiDC grid topology. Third, the diesel generator model was developed from the data points of a marine diesel generator for the AC and BiDC grid operation, i.e. the fixed speed and variable speed operation. This model provides the specific fuel oil consumption as a function of loading on the diesel generator. Finally, an optimization problem was formulated for all the ten arrangements for minimising the CO_2 emissions over the complete operational profile of the ship.

The power losses, as well as the electrical power requirements, were found to be lower for the BiDC grid as compared to the AC grid. The number of cables required was also less, resulting in lower cable weight in the BiDC grid topology. Overall, the results showed that the minimum emissions achieved over the ship's operation were lower for the BiDC grids than for the AC grid. For the selected configuration, a similar result was seen in terms of emissions. It was observed that the availability of shore power did not affect the trend seen in fuel consumption, where the fuel consumed over the ship's operations was higher for the AC arrangements as compared to their DC counterparts. The capital costs for the DC arrangements were seen to be higher than for the AC arrangements, with an exception in the DC4 arrangement that can be attributed to the elimination of the rectifier connected to the diesel generator, the diesel generator itself, the rectifier unit in the VFD, and the three winding transformer. The operating costs were observed to be lower for the DC arrangements as compared to the AC arrangements, except for the DC5 arrangement, which was observed to be marginally higher than its AC counterpart. The system weight was found to be lower for the AC arrangements as compared to the DC arrangement without shore power availability. However, the reverse was seen for arrangements with shore power connection due to the increased weight of the shore transformer. This was also reflected in the load carrying capacity of the ship. Furthermore, these results depend on the operating profile of the ship, the shore infrastructure, the diesel generator and battery configuration and their technical parameters. However, these findings demonstrate the possible potential of BiDC grids in emission reduction from the shipping sector.

Acknowledgment

The journey over the past seven months working on my thesis has taught me many lessons that not only encouraged my personal growth but also made me discover the frontier of the known unknown. A humble experience, I must say. I will be forever indebted towards this prestigious institution and my research group, DCE&S. I will be eternally grateful to call it my alma mater.

I would like to express my most in-depth gratitude towards my thesis supervisors Prof. Zian Qin and Prof. Pavol Bauer. Their guidance, both technical and personal, have been invaluable throughout my thesis. Furthermore, I would take this opportunity to thank my daily supervisor, Ir. Sachin Yadav. His technical insights and feedback have been beneficial for this thesis. I will be permanently grateful to have them as my supervisors. Similarly, I would appreciate my colleagues not only from the DCE&S research group but also from my master's and different faculties.

Likewise, I would also express my appreciation towards my family members and dear friends. My mom, dad and big sister for video calls, moral support and love, and my friends from back home and in Delft. My parents are my role models. That being said, I will be forever in debt for the way they have shown me and also for accepting the path I have chosen. They have set the bar high through their achievements and discipline. Last but not least, my warm cup of coffee. Thank you.

I look forward to forging a new relationship with the Delft University of Technology.

With profound gratitude and a sense of accomplishment,
A. Abhyankar,
Delft, August 2023

Contents

Nomenclature

Abbreviations

3L-NPC	Three Level Neutral-Point Clamped
AC	Alternating Current
AC1	Arrangement AC1
AC2	Arrangement AC2
AC3	Arrangement AC3
AC4	Arrangement AC4
AC5	Arrangement AC5
AFE	Active Front End
AIS	Automatic Information System
BiDC	Bipolar DC
CII	Carbon Intensity Indicator
CPP	Controllable Pitch Propeller
CSI	Current Source Inverter
DAB	Dual Active Bridge
DC	Direct Current
DC1	Arrangement DC1
DC2	Arrangement DC2
DC3	Arrangement DC3
DC4	Arrangement DC4
DC5	Arrangement DC5
DFE	Diode Front End
DP	Dynamic Positioning
DPO	Dynamic Programming Optimization
DWT	Dead-Weight Tonnes
ECA	Emission Control Area
EEDI	Energy Efficiency Design Index
EEOI	Energy Efficiency Operating Index
EEXI	Energy Efficiency Existing Ship Index
ESS	Energy Storage Systems

GA	Genetic Algorithm
GDP	Gross Domestic Product
GHG	Greenhouse Gas
ICCT	International Council on Clean Transportation
ICE	Internal Combustion Engine
IEC	International Electrotechnical Commission
IEEE	Institute of Electrical and Electronics Engineers
IEP	Integrated Electric Propulsion
IMO	International Maritime Organisation
IPCC	Intergovernmental Panel on Climate Change
LF	Loading Factor
LFP	Lithium Iron Phosphate
LTO	Lithium Titanate Oxide
LVAC	Low Voltage Alternating Current
LVDC	Low Voltage Direct Current
LWT	Light-Weight Tonnes
m/m	Mass by Mass
MARPOL	International Convention for the Prevention of Pollution from Ships
MCR	Maximum Continuous Rating
MDO	Marine Diesel Oil
MEPC	Marine Environment Protection Commitee
MILP	Mixed Integer Linear Programming
MINLP	Mixed-Integer Non-Linear Programming
NMC	Nickel Manganese Cobalt Oxide
NPC	Neutral-Point Clamped
NSGA-II	Non-Dominated Sorting Genetic Algorithm-II
OD	Optimal Dispatch
ODS	Ozone Depleting Substances
OSV	Offshore Supply Vessel
PM	Particulate Matter
PSO	Particle Swarm Optimization
PSV	Platform Supply Vessel
RO-RO	Roll on - Roll off Ship
RPM	Revolutions per Minute

SFOC	Specific Fuel Oil Consumption
SMES	Superconducting Magnetic Energy Storage
THD	Total Harmonics Distortion
UC	Unit Commitment
UDC	Unipolar DC
VFD	Variable Frequency Drive
VOC	Volatile Organic Compounds
VSI	Voltage Source Inverter
XLPE	Cross-Linked Polyethylene

Variables

α	a factor to convert the price of fuel
β	Temperature coefficient of resistance
$\cos(\theta_{AUX})$	Power factor for auxiliary load
$\cos(\theta_{Motor})$	Power factor of induction motor
Δt	Optimization time step
Δ	The difference in SFOC values at full loading conditions for different diesel generators
η_H	Hull efficiency
η_P	Propeller efficiency
η_R	Relative rotative efficiency
η_S	Shaft efficiency
η_{BiDC}	Efficiency of rectifier connected with the diesel generator
η_{Ch}	Efficiency of battery during charging
η_{Dis}	Efficiency of battery during discharging
η_{gen}	Efficiency of generator
$\eta_{Inv_{AUX}}$	Auxiliary inverter efficiency
$\eta_{Inv_{Motor}}$	Motor inverter efficiency
η_{Motor}	Induction motor efficiency
$\eta_{Sh_{BiDC}}$	Efficiency of rectifier connected with shore power
$\eta_{Sh_{Trans}}$	Efficiency of transformer connected with shore power
$\eta_{Transformer_{AUX}}$	Auxiliary transformer efficiency
η_{TWT}	Three winding transformer efficiency
η_{VFD}	Variable frequency drive efficiency
∇	Maximum displacement of the ship
ρ	Sea water density

Bat_{Cap}	Battery Capacity
Bat_{Cost}	The cost of battery bank
Bat_{Weight}	The weight of battery bank
$BatC$	The cost of Battery bank in $ per kWh
C_B	Block coefficient
C_D	Dead-weight coefficient
C_f	Emission factor for the fuel in use
C_{Ch}	Charging C-rate for the battery
C_{Dis}	Discharging C-rate for the battery
$Capex$	The cost of the propulsion system, excluding the cost of propulsion motors and power cables
CI_{Elec}	The cost index of electronic components
CI_{TF}	The cost index for power transformer
$Cost_{Fuel}$	The purchasing cost of fuel
$Cost_{Shore}$	The purchasing cost of electricity from shore infrastructure
D	Draught of the ship
$DCConv_{Cost}$	The cost of DC-DC converter connected to the battery in BiDC grid
$DCConv_{Rated}$	The power rating for DC/DC converter connected to the battery
$DCConv_{Weight}$	The weight of the DC-DC converter connected to the battery in the BiDC grid
DG_{Cost}	The cost of a diesel generator
DG_{Weight}	The weight of a diesel generator
DGC	The cost of diesel generator in $ per kW
$DGRect_{Cost}$	The cost of rectifier connected to the diesel generator in BiDC grid
$DGRect_{Rated}$	The power rating for diesel generator rectifier
$DGRect_{Weight}$	The weight of the rectifier connected to the diesel generator in the BiDC grid
E_{AC1}	Emissions from arrangement AC1
E_{AC2}	Emissions from arrangement AC2
E_{AC3}	Emissions from arrangement AC3
E_{AC4}	Emissions from arrangement AC4
E_{AC5}	Emissions from arrangement AC5
E_{DC1}	Emissions from arrangement DC1
E_{DC2}	Emissions from arrangement DC2
E_{DC3}	Emissions from arrangement DC3
E_{DC4}	Emissions from arrangement DC4
E_{DC5}	Emissions from arrangement DC5

EF_{CO2}	Emission factor of CO_2
EF_{Sh}	Emission factor of shore power
f	Skin friction coefficient
I_{AC}	Current flowing through the cables during operation on AC grid
$I_{B_{AC}}$	AC design current
$I_{B_{DC}}$	DC design current
$I_{CAP_{AC}}$	AC current carrying capacity of the cable
$I_{CAP_{DC}}$	DC current carrying capacity of the cable
I_{DC}	Current flowing through the cables during operation on BiDC grid
$Inv_{BatCost}$	The cost of inverter connected to the battery in AC grid
$Inv_{BatRated}$	The power rating for the inverter connected to the battery bank
$Inv_{BatWeight}$	The weight of the inverter connected to the battery in the AC grid
$InvAux_{Cost}$	The cost of inverter connected with auxiliary loads
$InvAUX_{Rated}$	The power rating for the auxiliary inverter
$InvAux_{Weight}$	The weight of inverter connected with auxiliary loads
$InvMotor_{Cost}$	The cost of the inverter connected with the propulsion motor
$InvMotor_{Rated}$	The power rating for the propulsion motor inverter
$InvMotor_{Weight}$	The weight of the inverter connected with the propulsion motor
L	Length of the ship at waterline
L_{SB2M}	Length of cable between switchboard and motor
M	Margin for resistance increase
$Max(P_{R_{AC}})$	Maximum power requirement in AC grid
$Max(P_{R_{DC}})$	Maximum power requirement in DC grid
n	a coefficient that depends on ships hull
N_G	Number of diesel generator
N_P	Number of propeller drive
NC_{AC}	Number of cables for AC
NC_{DC}	Number of cables for DC
P	75 percent of installed shaft power
P_D	Delivered power
P_E	Effective power
P_P	Propulsion power
$P_{AC_{losses}}$	AC cable losses during operation
$P_{AUX_{ACSB}}$	AC auxiliary power required at switchboard

$P_{AUX_{DCSB}}$	DC auxiliary power requirement at switchboard
P_{AUX}	Auxiliary power
$P_{Ch_{Min}}$	Minimum power delivered by the battery while charging
$P_{Ch}(t)$	Charging power delivered by battery
$P_{DC_{losses}}$	DC cable losses during operation
$P_{DG1}(t)$	Power delivered by diesel generator 1
$P_{DG2}(t)$	Power delivered by diesel generator 2
$P_{DGRated}$	Rated power of diesel generator
$P_{Dis_{min}}$	minimum power delivered by the battery while discharging
$P_{Dis}(t)$	Discharging power delivered by battery
P_{Motor}	Rated power of motor
$P_{P_{ACSBWL}}$	AC propulsion power required at switchboard without cable losses
$P_{P_{DCSBWL}}$	DC propulsion power required at switchboard without cable losses
$P_{P_{MAX}}$	Maximum propulsive power
$P_{R_{AC}}$	Total electrical power for AC grid at the switchboard
$P_{R_{DC}}$	Total electrical power for DC grid at the switchboard
$P_{Sh_{Max}}$	Maximum power delivered by the shore infrastructure
$P_{Sh_{Min}}$	Minimum power delivered by the shore infrastructure
$P_{Sh}(t)$	Power delivered from the shore
R	Total resistance in calm water conditions
R_E	Eddy-making resistance
R_F	Frictional resistance
R_R	Residual resistance
R_T	Total resistance
R_W	Wave-making resistance
R_{0AC}	Ambient resistance per meter for AC
R_{0DC}	Ambient resistance per meter for DC
$R_{AC}(T_R)$	Resistance per meter at temperature T_R for AC
R_{APP}	Resistance due to wind and appendages
$R_{DC}(T_R)$	Resistance per meter at temperature T_R for DC
S	Wetted surface area
$SFOC_{AC}(LF_t)$	Specific fuel consumption of a fixed speed diesel generator as a function of Load factor (LF)
$SFOC_{DC}(LF_t)$	Specific fuel consumption of variable speed diesel generator as a function of Load factor (LF)

$ShoreRect_{Cost}$	The cost of rectifier for shore connection
$ShoreRect_{Rated}$	The power rating for the shore power rectifier
$ShoreRect_{Weight}$	The weight of rectifier for shore connection
$SoC(t)$	State of charge of battery
SoC_0	Inital SoC value
SoC_f	Final SoC value
SoC_{max}	Maximum SoC level for the battery
SoC_{min}	Minimum SoC level for the battery
T	Total voyage time
t	Time
T_0	Ambient temperature
T_R	Temperature at which the resistance is computed
T_S	Time spent at the shore
T_V	Travel time between ports
$TFAux_{Cost}$	The cost of transformer for auxiliary loads
$TFAux_{Rated}$	The power rating for the auxiliary transformer
$TFAux_{Weight}$	The weight of the transformer for auxiliary loads
$TFProp_{Cost}$	The cost of propulsion transformer
$TFProp_{Rated}$	The rated power for the propulsion transformer
$TFProp_{Weight}$	The weight of propulsion transformer
$TFShore_{Cost}$	The cost of transformer for shore connection
$TFShore_{Rated}$	The power rating for the shore power transformer
$TFShore_{Weight}$	The weight of transformer for shore connection
V	Velocity in meter per second
V_M	Mass displacement
V_S	Volume displacement
V_{AC}	AC voltage line to line
V_{DC}	DC voltage between positive and negative poles
V_k	Velocity in knots
V_{ref}	Velocity at design load
VFD_{Cost}	The cost of variable frequency drive
VFD_{Rated}	The rated power for the variable frequency drive
VFD_{Weight}	The weight of variable frequency drive
W	Width of the ship
$Weight_{sys}$	The propulsion system weight, excluding the weight of the propulsion motor

List of Figures

List of Tables

1

Introduction

This chapter aims to provide the reader with an introduction to the report and to build a foundation for the key aspects that are dealt with through the course of each chapter. The author provides background and motivation in section 1.1 followed by a problem definition and formulating the research question in section 1.2. Furthermore, the thesis methodology, which provides an insight into how the research question is tackled, is explained in section 1.3. The report's structure is highlighted in section 1.4. Subsequently, the limitations for the research question and methodology are presented in section 1.5. Finally, section 1.6 concludes the chapter with a summary.

1.1. Background and Motivation

The relentless growth in the CO_2 emissions regardless of the efforts of global powers, pressed upon by the alarming projections from the people of academia, pose an inevitable threat to survival if this trend is not reversed. This growth in CO_2 emissions has a direct impact on the greenhouse effect of our planet and increases average temperatures, leading to global warming. The Intergovernmental Panel on Climate Change (IPCC) highlights the impact of different levels of rise in temperature on nature and biological life [100]. Although governments from around the world in 2014 agreed to sign the Paris Agreement, in hindsight, it has not proven to decrease CO_2 emissions. As a result, we saw a relative growth of 4.25 per cent in CO_2 emissions from the world in the year 2021, compared to 2014 levels [106]. The Covid-19 pandemic resulted in a drop in energy demand by 5.1 per cent in 2020, thus reducing emissions, although the sustainable economic recovery expected did not happen and pushed the world towards fossil fuels like coal, natural gas and oil [52]. Although the emissions from developed economies are decreasing, the emissions from emerging economies like India and China are on the rise [52]. This is mostly due to the increase in Gross Domestic Product (GDP). This growth is followed by trade, and currently, 90 per cent of global trade is carried by ships [51, 60]. The forecast from the International Council on Clean Transportation (ICCT) states that by the year 2050, the volume of global trade carried from ocean-going ships could account for 80 per cent of commerce by volume and cause about 17 per cent of the anthropogenic CO_2 emissions [49, 42]. The emissions from the shipping sector accounted for 3 per cent in 2021 and around 70 per cent of that was contributed by international maritime trade and commerce [68]. Therefore, the rising CO_2 emissions from the shipping sector present a great threat to our fight against climate change and to achieve a net-zero scenario. As per IMO [58], the emission target for a 50 per cent reduction from the 2008 levels seems far-fetched considering the future growth in this industry mainly due to economic development in emerging economies.

The shipping sector contributes not only to CO_2 emissions but also to NO_x, SO_x, particulate matter (PM), ozone-depleting substances (ODS) and volatile organic compounds (VOCs) emissions. The International Maritime Organization (IMO) has introduced regulations to reduce these emissions. The International Convention for the Prevention of Pollution from Ships (MARPOL) was adopted in 1973 with five annexes [59]. Consequently, in 1999, annexure VI was added that dealt with air pollution

from ships. This annexure included regulations for SO_x, NO_x, ODS and PM emissions [67]. Although direct regulations on CO_2 emissions are not yet mandated, various energy efficiency metrics like the Energy Efficiency Design Index (EEDI), Energy Efficiency Operational Index (EEOI), Energy Efficiency Existing Ship Index (EEXI) and Carbon Intensity Indicator (CII) have been introduced to assist in reducing greenhouse gas (GHG) emissions. EEDI, EEOI, CII and EEXI are all sister metrics with subtle measurement differences. All these metrics provide data regarding the efficiency at which the cargo is transported, in other words, it provides information on the amount of CO_2 emitted on transporting a metric tonne of cargo for one nautical mile. The major drawback of EEDI is, the metric to estimate CO_2 emissions is not dynamic and thus fails to capture the complete extent of CO_2 emission that occurs at other load points of the engine [66, 81]. Electrifying the ship's propulsion system has proven to increase the system efficiency and also reduce the emissions [13, 109]. This has led to an increase in opting for diesel-electric propulsion systems for newly built ships [85]. The two methods for power distribution that have been contending since the dawn of their discovery are AC and DC power systems. The major difference is in the operation of the generator, where a fixed-speed generator and a variable-speed generator are used in AC and DC systems, respectively. International Maritime Organization [66] provides guidelines to measure a ship's EEDI, where the ship's reference velocity is considered along with a static load point of the diesel engines and the Specific fuel oil consumption (SFOC) at that load point. However, this load point happens to be in the region where the diesel engine operates at its optimum Specific fuel oil consumption. In an AC system, due to the constraint on the speed i.e. frequency of the generator, the Specific fuel oil consumption and loading follow an inverse relation. Consequently, in AC systems, EEDI fails to capture the critical load points where the SFOC deviates from the optimum and results in higher fuel consumption. Whereas, in a DC system where a variable speed generator is used, it can operate at the near-optimum SFOC over the operational range. Thus, the EEDI methodology fails to capture the benefits of switching to a DC power system. Therefore, this thesis is mainly targeted towards the emission reduction that can be realised by switching to a DC grid over the extent of the ship's operational profile while comparing different aspects of the shipboard microgrid.

1.2. Research Question

The previous section presented the background and motivation for doing this work. This section will introduce the problem definition, which is derived from section 1.1 followed by the main research question that is dealt with in this work. The emissions from the shipping sector need to reduce to meet the targets set by IMO. Therefore, electrification for newly built ships has begun. As stated earlier, the EEDI metric fails to capture the energy efficiency at variable load points. Therefore, the EEDI estimation for an AC system as well as a DC system at the load point specified in the guidelines of International Maritime Organization [66] would provide a similar value and therefore, the quantitative benefits of switching to a DC grid maybe not be visible.

Problem Definition

> **The CO_2 emissions are on the rise and the emissions target set by the International Maritime Organisation seems far-fetched. Although electrification is proving to reduce emissions, the energy efficiency metrics (EEDI, EEXI) are incapable to provide the quantitative benefits that can be realised by switching to a bipolar DC (BiDC) grid.**

For this, a shipboard AC microgrid with two diesel generators is considered the status quo. This thesis also takes into account the effect of including a battery bank for the propulsion system, as well as the use of shore power to quantify and compare the key performance indicators (KPI) observed for AC and BiDC grids. These ten arrangements are listed below:-

- AC1 – AC grid with two diesel generators (status quo).
- AC2 – AC grid with two diesel generators and battery bank.
- AC3 – AC grid with two diesel generators, battery bank and shore power.

- AC4 – AC grid with one diesel generator and battery bank.
- AC5 – AC grid with one diesel generator, battery bank and shore power.
- DC1 – DC grid with two diesel generators.
- DC2 – DC grid with two diesel generators and battery bank.
- DC3 – DC grid with two diesel generators, battery bank and shore power.
- DC4 – DC grid with one diesel generator and battery bank.
- DC5 – DC grid with one diesel generator, battery bank and shore power.

The KPIs considered are **cable power losses, electrical power requirements, emissions, fuel consumption, capital cost, operating cost, system weight, and dead-weight tonnage (DWT)** of the AC and DC grid architectures. The research question that will be answered through this thesis is defined below, along with its sub-questions:-

What are the quantitative benefits of switching to a bipolar DC grid compared to an AC grid?

1. How does the electrical power requirement change for AC and BiDC grids?
2. What is the effect of switching to a BiDC grid on power cable losses and sizing?
3. What are the changes in CO_2 emissions observed as we switch from the status quo to other arrangements?
4. What is the effect on fuel consumption for each arrangement as compared with the status quo?
5. What is the effect of each arrangement on the capital cost of the system?
6. What is the effect on the operating cost of the ship for different arrangements compared with the status quo?
7. How does the system weight vary for each arrangement compared with the status quo?
8. How does each arrangement affect the load carrying capacity (DWT) of the ship?

1.3. Thesis Methodology

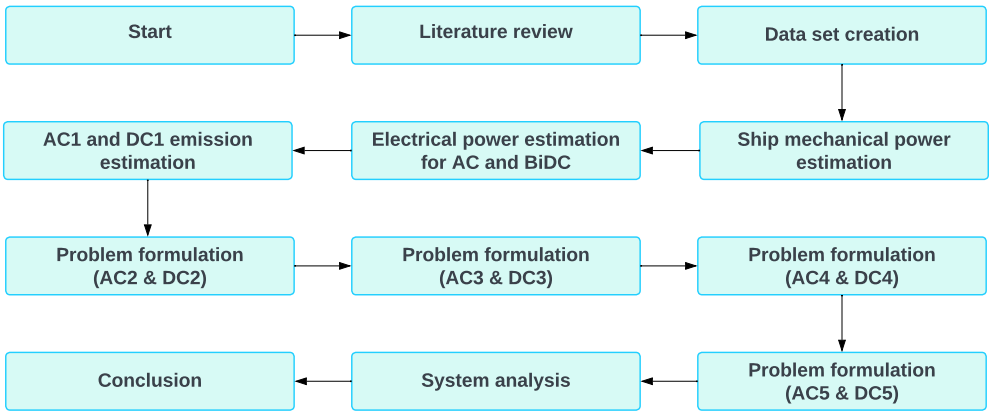

Figure 1.1: Thesis methodology

This section presents the thesis methodology to assist in answering the research question described in section 1.2. The methodology is shown in Figure 1.1. The literature review was performed to

understand and learn about the shipboard propulsion systems. The working of different components for AC and DC grid architecture, as well as the inherent differences between these topologies. The current emission regulations were studied to assist in creating a catalogue for diesel generators, and batteries. The different optimization types were reviewed. The ship's propulsion profile was not available, therefore, a methodology was developed to assist in estimating the ship's mechanical power propulsion. The backward calculations for calculating the electrical power requirements were performed for AC and BiDC grids from the learnings of the literature review. Finally, ten arrangements were defined for this study. The AC1 and DC1 arrangements are used to estimate the emission from the ship's voyage. From the review of optimization types and previous work done on this topic, optimization problem formulation was done for minimizing the emissions from the ship's operations for arrangements AC2, AC3, AC4, AC5, DC2, DC3, DC4 and DC5. Finally, the system analysis is performed to evaluate the KPIs.

1.4. Thesis Outline

The report provides the background and motivation for the thesis in this chapter, along with the research question that is answered in this report. The current emissions regulations will be introduced and the differences in AC and DC shipboard microgrids along with the components that make up these topologies, establishing the necessary background information, will be explained in chapter 2. The next chapter will dive deep into the ship's mechanical and electrical power estimation methodology by introducing a schematic electrical diagram for the propulsion system of the ship in chapter 3. The chapter 4 will present the outcome of different studies that have been done, introducing the research gap and the optimization problem will be formulated for all ten arrangements. This chapter also models a diesel generator for Specific Fuel Oil Consumption (SFOC) as a function of Load Factor (LF) for fixed speed and variable speed operation. After minimising the emissions for all configurations, the system analysis is performed for the selected configuration in chapter 5. This chapter will introduce the methodology to estimate the Key Performance Indicators (KPIs) like fuel consumption, operating cost, capital costs, propulsion system weight and load carrying capacity of the ship. The results of the methodologies explained in chapter 3, chapter 4 and chapter 5 will be presented and explained in chapter 6. Finally, the finding from the thesis for the research question formulated will be answered in chapter 7. This chapter will also put forward recommendations for the future.

1.5. Limitations

The work carried out using the methodology expressed in section 1.3 has some limitations. The aspects that have not been taken into account or not permitted by the methodology that is used to address the research question are listed below:-

1. The power imbalance is not possible to simulate or introduce in the optimization problem formulation. Thus, the ship's power transients are not taken into account and the shipboard microgrid is assumed to be balanced with no transient behaviour throughout the ship's voyage.
2. The efficiency values for the various components (transformers, AC to DC converters, Inverters, etc.) in the shipboard microgrid are taken constant, thus the changes in efficiency are decoupled with the power requirements, which is not what happens in reality. This limitation exists as a consequence of the optimization problem formulation requirements in MATLAB®.
3. The bipolar DC grid is prone to voltage imbalances due to unbalanced load requirements. This effect is not taken into account, as it is limited by the methodology of this study.
4. The ship's real power requirements are not available. Therefore, the preliminary power estimation methodology is developed from the literature that provides insight into the power requirements, although the use of real data would assist in getting more accurate estimates.
5. The ship's power profile has a significant impact on the emissions of the ship because of the loading requirements on the diesel generator. We have performed this work on a Ferry, and therefore it limits our understanding of the benefits of using bipolar DC architecture on other ships like Platform Supply Vessels (PSVs), Yachts, Tugboats, etc.

6. For the capital cost and system weight estimation, the absence of bipolar DC grid standards and regulations makes the availability of industrial components like circuit breakers and power electronic converters for the specified ratings difficult to obtain and therefore, not included in this thesis.

1.6. Summary

This chapter has introduced the background and motivation in section 1.1. This provides the reasoning for the research question formulated in section 1.2. Furthermore, The approach/methodology that is used to answer the research question was described in section 1.3. The report's structure was highlighted in section 1.4. Finally, the limitations of the research and the methodology are also penned in section 1.5.

2

Background

This chapter is aimed at providing the reader with the background information that is used in this thesis. First, the current emission regulations are introduced in section 2.1. The propulsion system is one of the most important systems in the operation of ships. This is responsible for the mammoth feat of transporting goods and passengers across the gigantic Atlantic as well as the Pacific Ocean. Therefore, the types of propulsion systems and their characteristics are discussed in section 2.2. Furthermore, a comparative study on the type of grid topology (AC and DC) used in diesel-electric and hybrid propulsion systems is presented in detail in section 2.3. The different components making up an AC or a DC microgrid like diesel generators, energy storage systems, power conditioning devices, etc. are described in section 2.4. Subsequently, some case studies are also introduced that showcase the potential of emission reduction by using these propulsion architectures in section 2.5. Finally, the chapter is concluded with a chapter summary in section 2.6.

2.1. Current Emission Regulations

The exhaust gases emitted from the ships and the required regulations are described in International Maritime Organization [67]. These regulations are proposed for exhaust gases like SO_x, NO_x, PM, ODS and VOC emissions. The regulations for ODS and VOCs are not discussed here, as they are not directly related to the exhaust gas emissions from the ship. Therefore, they fall outside the envelope of this thesis. ODS emissions are a result of usage and leakage of refrigerants, and VOC emissions are mainly applicable to oil tankers during port operations.

2.1.1. NO_x emissions

The NO_x emissions are defined under regulation 13 of the MARPOL, annexure VI [67]. They apply to each marine engine with a power output of more than 130 kW, and also to any marine diesel engine that has gone through major modification on or after the 1st of January 2000. The emission requirements are classified based on the time of the ship's construction as well as the engine's rated rpm, as shown in Table 2.1. As it can be seen in Table 2.1 the regulations enforced are stricter for newer ships and ships that will be built in the future. Furthermore, the regulations also tighten as we move to engines running on higher rpm from lower rpm.

Table 2.1: NO_x emission limits [67]

Tier	Ship Construction date on or after	Total weighted cycle emission limit (g/kWh) n = engine's rated speed (rpm)		
		n < 130	n = 130 – 1999	n ≥2000
I	1 January 2000	17.0	$45*n^{-0.2}$	9.8
II	1 January 2011	14.4	$44*n^{-0.23}$	7.7
III	1 January 2016	3.4	$9*n^{-0.2}$	2.0

Emission control area (ECA) is a special area defined under the regulations implemented in Annexure VI of the MARPOL [67]. Currently, NO_x ECA are defined in the North American region, the US Caribbean Sea, the North Sea and the Baltic Sea. The ECA's are presented in Figure 2.1. The coordinates defining the sea area can be found in Appendix VII of MARPOL Annexure VI [67]. As per the amendment, tier III emission standards are imposed on the ships in ECA's. The American ECA's are applicable for ships constructed on or after 1st January 2016, whereas the European ECA's are relevant to ships constructed on or after 1st January 2021. However, the emission standard that must be fulfilled outside the ECA is the Tier II limits.

Figure 2.1: MARPOL annexure VI emission control areas [31]

2.1.2. SO_x and particulate matter emissions

The SO_x and particulate matter emissions are defined under regulation 14 of the MARPOL, annexure VI [67]. Table 2.2 describes the history of SO_x and PM emission limits imposed by the IMO. Currently, a global limit of 0.50 per cent mass by mass (m/m) of fuel is enforced outside the ECA. This regulation came into force for ships operating outside the ECA on and after 1st January 2020. The ECA's described in Figure 2.1 are valid for the SO_x and PM emissions as well. Furthermore, inside an ECA, the sulphur content limit of 0.1 per cent m/m is applied to the fuel that is utilized in the ship operations. This regulation was mandated for ships operating on and after 1st January 2015. As a result, the ship operators are enforced to use low sulphur fuels within the ECA. Currently, a global sulphur cap has been imposed as shown in Table 2.2 to eliminate the use of higher sulphur content fuels.

Table 2.2: SO_x and PM emission limits [67]

Outside an ECA established to limit SO_x and particulate matter emissions	Inside an ECA established to limit SO_x and particulate matter emissions
4.50% m/m prior to 1 January 2012	1.50% m/m prior to 1 July 2010
3.50% m/m on and after 1 January 2012	1.00% m/m on and after 1 July 2010
0.50% m/m on and after 1 January 2020	0.10% m/m on and after 1 January 2015

2.1.3. CO_2 emissions

In July 2011, Marine Environment Protection Committee (MEPC) 62, introduced a new chapter in the MARPOL annexure VI targetted towards the regulations on the carbon intensity of international shipping [50, 67]. Even though the regulations do not pertain to domestic voyages, the amendment recommended that the national regulatory agency ensure that new ships that are constructed and operated are by the requirements of chapter 4 of MARPOL annexure VI [67]. This regulation aimed to motivate shipbuilders and to promote and install energy-efficient components on ships. The fundamental equation that encapsulated the idea of EEDI is given below [50, 103]: -

$$EEDI = \frac{P * SFC * C_f[g]}{DWT * V_{ref}[t.nm]} \tag{2.1}$$

Where,
$EEDI$ = Energy Efficiency and Design Index [g-CO_2 / t.nm]
P = 75 per cent of the installed shaft power [kW]
$SFOC$ = Specific fuel oil consumption at 75 percent loading [g-CO_2/kWh]
C_f = Emission factor for the fuel in use [t-CO_2/t-Fuel]
DWT = Dead-Weight Tonnage [Tonnes]
V_{ref} = Velocity at design load [knots]

The guidelines introduced EEDI in four phases, with each phase accounting for higher energy efficiency from phase 0 (reference line). The reference line (phase 0) depends on the class of ship and DWT described in table 2 of chapter 4 in MARPOL annexure VI [67]. Furthermore, the reduction in each phase depend on the type of ship for which the EEDI was being calculated, as well as the transport capacity of that ship. The lower the EEDI value, the higher the energy efficiency, as the amount of CO_2 emitted for transporting one metric tonne of cargo for one nautical mile decreases. Currently, Phase II is in operation where the EEDI reduction is required to be 15/20 per cent depending on the ship class and tonnage as shown in Figure 2.2. Along similar lines, the EEXI was adopted that deals with the energy efficiency of existing ships. For both the kind of ships (New and Existing) the attained EEDI and EEXI are mandated to be below the required EEDI and EEXI, respectively. Currently, the required EEDI and EEXI are asked to be 85/80 per cent (depending on the type of ship) of the phase 0 EEDI, and EEXI values. Equation 2.1 highlights the drawback of this methodology. The EEDI estimation is carried out at a static condition and thus fails to capture the dynamic behaviour of the ship i.e. effect of different loading conditions, the effect of ship velocity other than the reference velocity and finally, the effect of variation in the cargo carrying capacity of the ship.

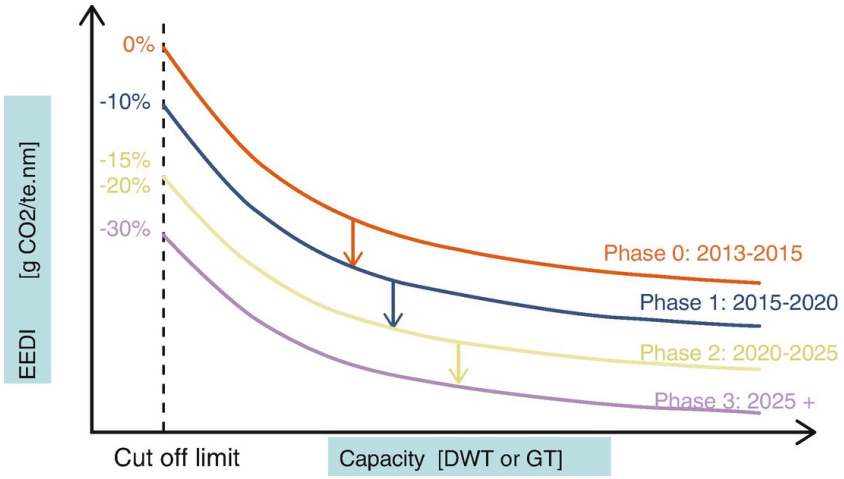

Figure 2.2: Concept of required EEDI, reduction factor, cut-off limits, and EEDI phases [103]

2.2. Modern Propulsion Systems on Ships

The early attempts for the commercial use of electricity on ships came about through the lighting applications on the *SS Columbia* in the 1880s [114]. The propulsion system was a mechanical propulsion system powered by steam turbines that used a DC electrical system for the lighting [114]. Later, the inventions of a diesel engine, transformer, and an AC induction motor paved the way for the first diesel-electric propulsion system that was used on the *SS Vandal* in 1903 [114]. Various other technologies were explored during the world war like nuclear-powered propulsion for submarines, and turbo-electric propulsion for naval ships, later in 1987 due to disruptive advancements in solid-state technology, the all-electric ship *Queen Elizabeth II* was inaugurated [113]. The steam turbine was inefficient, and therefore, after the invention of the diesel engine, it replaced the old turbo-electric propulsion system giving birth to diesel-electric propulsion [113]. Presently, merchant ships still use mechanical propulsion, whereas cruise ships and military ships have moved on to electric propulsion [117]. This transition was motivated because of the potential for fuel savings due to efficiency

improvements, room savings in the engine room, as well as increased flexibility in power distribution [117].

The propulsion system on ships can be broadly classified into mechanical, electrical and hybrid propulsion [39]. The hybrid propulsion system can further be classified into series hybrid, parallel hybrid and series-parallel hybrid propulsion architectures [34, 61, 41, 138]. The types of propulsion systems are highlighted in Figure 2.3.

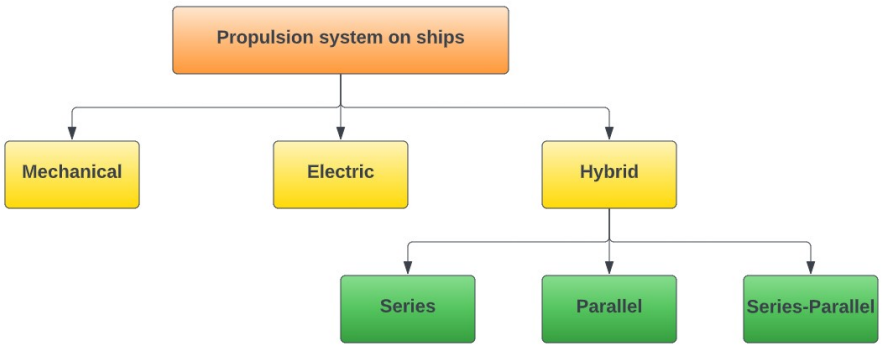

Figure 2.3: Classification of the propulsion system in ships

Firstly, the mechanical propulsion is shown in Figure 2.4a. It consists of a prime mover (commonly a diesel engine, a gas turbine can also be used in some cases) that is connected to the propeller through a shaft and gearbox. The prime mover operates at very high rpm and a direct coupling with the propeller results in high losses, therefore, a reduction gearbox is used to improve the efficiency of the system [87]. An experimental study conducted by Geertsma et al. [35] indicates that up to 30 per cent in fuel savings can be achieved by using a controllable pitch propeller (CPP) as compared with the baseline control strategy with fixed combinator curves. Furthermore, one large generation unit is required to propel the ship. As a result, even for lower load demands, the thermal unit is operated at an inefficient point, leading to higher fuel consumption and thus lower energy efficiency [87]. On the contrary, the splitting of a large generational unit into multiple smaller units provided energy efficiency improvements as well as lower fuel consumption compared to the mechanical propulsion [39]. This efficiency increase was achieved because of the ability to switch them off during lower load demands. The Figure 2.4b highlights the envelope of increased efficiency. Thus, the inefficient nature of the mechanical propulsion system was replaced by electric propulsion.

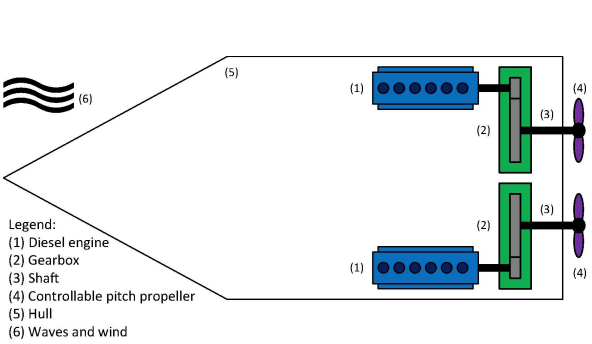

(a) Mechanical propulsion [35]

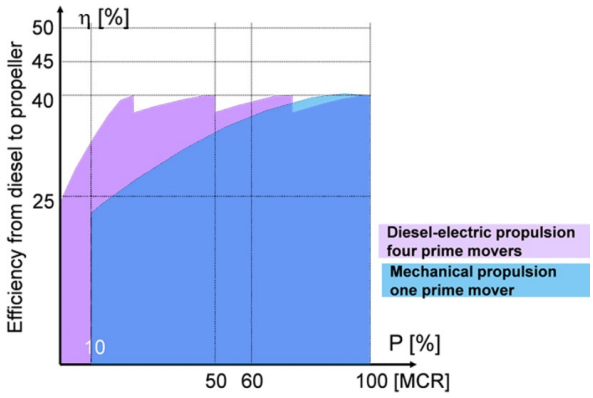

(b) The increased efficiency on using diesel-electric propulsion [39]

Figure 2.4: The mechanical propulsion system and the efficiency improvement achieved on switching to electric propulsion

Secondly, the electric propulsion consists of multiple diesel generators and the whole system is integrated on the electrical side [87]. The advancement in the AC drives has motivated the ship designers to accommodate multiple diesel generators for propulsive and auxiliary power needs [87].

As seen in Figure 2.4b, the benefits are visible in the electric propulsion, being more efficient. In this architecture, the diesel generator produces the necessary electrical power and the redundant mechanical linkages are reduced to flexible cable routing, which results in better space utilization. It also provides the electrical motor, the freedom to be oriented in a position that is optimum for energy efficiency improvements [117]. The electrical line diagram for electric propulsion is shown in Figure 2.5. This is an AC power architecture, and Kumar and Zare [76] highlights this to be a common scheme used for ferries.

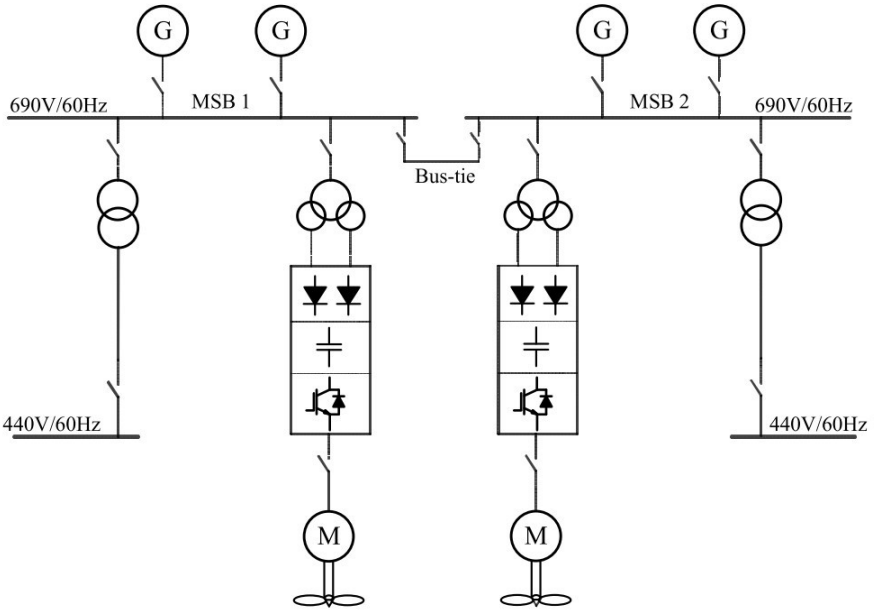

Figure 2.5: Electrical line diagram for electrical propulsion system [76]

Finally, the hybrid propulsion system is shown in Figure 2.6. In a hybrid propulsion system, multiple energy sources are used for power distribution. These power sources can be internal combustion engines, fuel cells, batteries, supercapacitors or renewable energy sources like solar and wind. The energy distribution in a hybrid propulsion system mainly takes place by electrical means. The majority of current ship hybrid propulsion systems operate on AC architecture, however, the DC integration schemes look more promising because of their simplicity and higher energy conversion efficiency [41, 42]. Hybrid propulsion can be further classified into three types, depending upon the integration of ICE in the power system, and are shown in Figure 2.6.

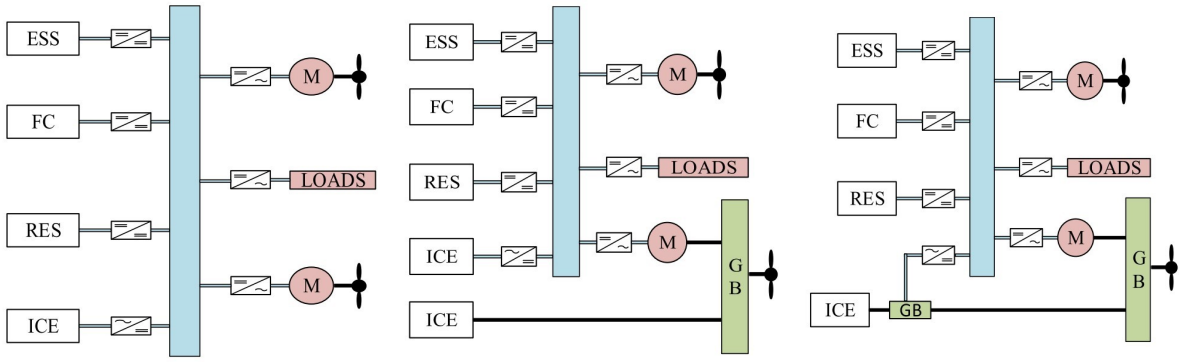

Figure 2.6: The hybrid propulsion system with series, parallel and series-parallel configurations [61, 41, 138]

Figure 2.6a presents the series hybrid propulsion system. In this system, the diesel generator is directly connected to the main bus. The other power sources are also connected to the main distribution bus

Table 2.3: Comparison between series, parallel and series-parallel propulsion and ships that commonly use these power systems. Adapted from Inal, Charpentier, and Deniz [61].

Architecture	Advantages	Disadvantages
Series	Engine downsizing and modular system	Multiple energy conversion
	Zero noise and emission availability	Loss of energy during conversions and relatively lesser efficiency
	Mature technology, precise control	Only electrical propulsion available
	Less fuel consumption and emission	
Parallel	Zero-emission operation option	Complex propulsion
	Both mechanical and electrical propulsion availability	Need of robust control for higher efficiency
	Reduced electrical chain and motor size	Additional mechanical linkages
	Sizing optimization available	
Series-Parallel	Zero-emission operation option	Complex system architecture
	Increased freedom in operation modes	Higher cost
	Both mechanical and electrical propulsion availability	Same challenges as of series configuration
	Higher efficiency at lower loads and higher loads	

along with the main propulsion as well as auxiliary loads. The addition of batteries can assist in turning off the engines when the fuel consumption is high in part-load consumption [34]. Figure 2.6b describes the series hybrid propulsion system. In this configuration, the combination of mechanical and electrical propulsion is achieved by incorporating a gearbox and establishing a parallel connection between the electric motor and the propeller. This enables the operation of the propeller in dual or single mode [138]. On the mechanical side, A diesel engine is directly coupled to the gearbox and on the electrical side, various power sources can be used to provide the electrical power needed for propulsion. The excess power can also be transmitted back to the electrical side as a result of using a motor generator setup. Finally, Figure 2.6c highlights the series-parallel hybrid propulsion system, as the name suggests it is a combination of series and parallel hybrid propulsion architectures. This configuration enables it to operate in different operational modes like fully mechanical, fully-electric, series, parallel or both [61]. The advantages and disadvantages of these propulsion systems are highlighted in Table 2.3.

2.3. Comparative Study of AC and DC Microgrid

In the previous section, different types of propulsion systems were introduced. In this section, we look at some benefits and limitations of electric and hybrid AC propulsion architecture compared with its DC counterpart. The difference between AC and DC microgrids is explained by comparing power quality, stability, cable losses, power density, grid protection as well as volume and weight of the system. The inherent characteristics of voltage imbalances for the BiDC grid are highlighted, along with strategies to minimize/neutralise these imbalances. Finally, the different types of system architectures are presented and compared.

The shipboard microgrid inherently forms a weak grid. The vessel's electric propulsion can be designed to operate on AC or DC power system architectures. The DC system can be further divided into Unipolar (UDC) and Bipolar DC (BiDC) systems [136]. Figure 2.5 describes an AC microgrid that operates at 690 V_{AC} and 60 Hz. The diesel generator operates at a fixed speed (rpm) and supply power at a

Table 2.4: The standardised voltage levels for power generation and distribution on ships [136, 56, 55]

Power	IEEE Std. 45.1	IEEE Std 1709-2018
Generation	AC: 120V, 208V, 230V, 240V, 380V, 450V, 480V, 600V, 690V, 2400V, 3300V, 4160V, 6600V, 11kV, 13.8kV DC: 120V, 240V	DC: 1.5kV, 3kV, 6kV, 12kV, 18kV, 24kV, 30kV
Distribution	AC: 115V, 200V, 220V, 230V, 350V, 440V, 460V, 575V, 660V, 2.3kV, 3.15kV, 4kV, 6.3kV, 10.6kV, 13.2kV DC: 12V, 24V, 28V, 115V, 230V, 270V, 380V	none

certain voltage to the bus bars. Some standards define voltage levels for generation and distribution on ships. The IEEE Std 45.1 and 1709-2018 are some of these standards. The Table 2.4 highlights the standard voltage levels for generation and distribution for AC and DC power systems [56, 55]. As per IEEE [56], the LVAC and LVDC are used if the total installed capacity on the vessel is less than 4 MW. The auxiliary load is supplied with the help of a transformer, whereas the electric motor is driven by a variable frequency drive (VFD) that is supplied by a three-winding transformer. This is mostly done to reduce the harmonics generated by the use of a 12-pulse system [7].

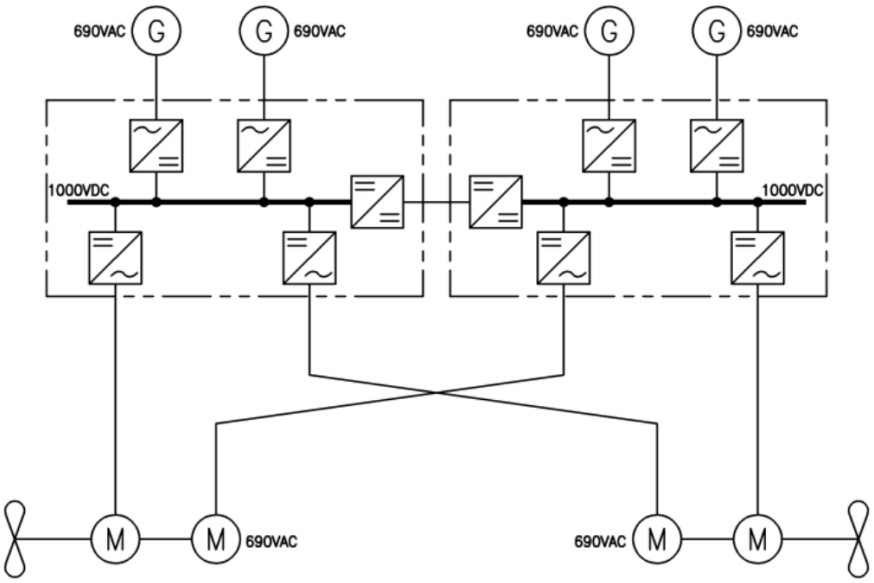

Figure 2.7: UDC grid for a double ended ferry [7]. The DC grid eliminates the transformer, reducing weight.

Figure 2.7 presents the DC power grid operating at 1000 V_{DC}. The inherent AC components like diesel generator and electric motor are connected to the DC bus using rectifiers and inverters respectively. This is contrary to what is seen in Figure 2.5 where these components are connected using transformers to the bus. The auxiliary load is also supplied via inverters compared to a transformer in AC microgrids. A case study performed on a double-body research vessel concluded that on switching to a DC IEP, a 41 per cent and 56 per cent reduction in footprint and weight was observed [21]. This weight reduction can be contributed to the absence of rectifying transformers. Figure 2.8 presents the DC power grid operating between +350V_{DC} and -350V_{DC}. In BiDC, an additional point of connection is present that increases the power density as compared to UDC [136]. In addition to this, it also provides higher flexibility to connect multiple power generators like diesel generators, batteries, and propulsion and auxiliary loads at different voltage levels.

Yadav, Qin, and Bauer [136] has presented three ways a BiDC grid can be generated on ships and assist in maintaining the voltage level for which the BiDC grid is built. These generation methods are shown in Figure 2.9. First, using a synchronous generator coupled with three winding transformers and two twelve pulse rectifiers. Second, to generate a BiDC grid using a dual stator generator and two twelve pulse rectifiers and finally using two synchronous generators to form a BiDC grid using

two twelve pulse rectifiers. The voltage imbalances are constitutional to BiDC grids because of the unbalanced load demand, this can lead to a shift in the voltage level of the neutral line conductor [136]. To counter the voltage imbalances, balancing converters are used.

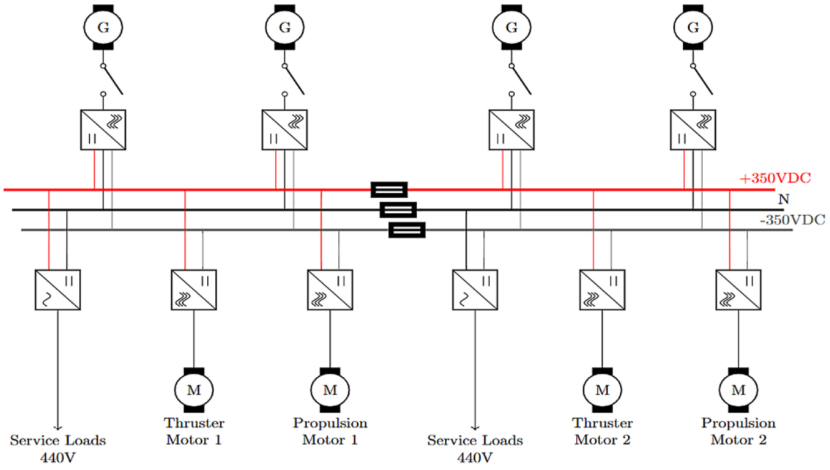

Figure 2.8: BiDC grid for a platform supply vessel. The UDC consists of two poles (positive and negative) shown in Figure 2.7 whereas Bipolar DC consists of two poles and a neutral (positive, neutral, and negative) [136].

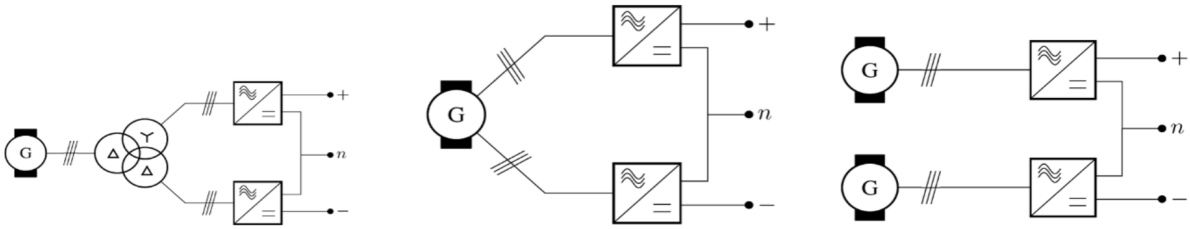

Figure 2.9: Methods for producing Bipolar DC grid [136]. The image on the right uses a three winding transformer and twelve pulse rectifiers. Next, the middle image uses a dual stator generator and two twelve pulse rectifiers and finally, the right image uses two synchronous generators to form a BiDC grid using two twelve pulse rectifiers

The AC grid needs to control and regulate voltage, frequency, reactive power and phase angle parameters to have a functioning stable grid whereas in a DC grid, the only variable that is monitored is voltage [70]. Also, the generators that are required to be operated must be synchronous. Consequently, this requirement leads to more time for the generator to come online and support the grid [70]. On the contrary, a major advantage that a DC grid provides is the grid and generator synchronization is not necessary, providing faster response time in case of a generator's mechanical or electrical failure. Also, the use of power drives (VFD) for electrical motors for propulsion causes harmonics in the system because of the rectifier part of the VFD, to minimise these harmonic distortions three winding transformers are usually installed before the VFD to provide a 30-degree phase shifted input to the rectifier, this helps in reducing the Total Harmonics Distortions (THD) [70]. Consequently, this rectifier part of the VFD can be eliminated completed, and instead, an inverter can be used to drive the motor [70]. Therefore, the DC grid reduces the power losses as a power conversion step in reduced as well as improves the harmonics in the system.

In AC microgrids, the current has a natural zero crossing because of the defining nature of the transmission. The voltage is maintained at a certain voltage level as shown in Table 2.4 and operated at 50 or 60 Hz and includes ferromagnetic components like the transformer whereas in the DC microgrid, the transformer is replaced by semiconductor-based power electronic devices like inverters, rectifiers [21]. These voltage-source converters have DC link capacitors that store an immense amount of energy [7]. Whenever a fault occurs in a DC bus, this stored energy in the DC link capacitors is released. Consequently, the magnitude of fault current during electrical faults is higher compared to AC. In addition to this, the current is difficult to interrupt, as the zero crossing available in AC microgrids is

not present in DC grids [7, 21]. This increases the chances of arc formation when the circuit breaker contacts are opened to clear the fault, and thus can become prone to fire hazards. The rate of energy release from these capacitors present in the power conditioning devices along with battery and diesel generator is simulated in Ayers [7], the author further highlights the contribution of different energy sources in the total fault current and energy released. Although the energy released decreases and plateaus for DC bus capacitors, the energy released from the battery and the diesel generator keeps on increasing. Thus, DC circuit breakers must be designed to minimize and protect the circuit from fault current as well the overvoltages that occur during faults [7]. Subsequently, to safeguard the grid, sometimes, the power conditioning devices themselves are switched off as they cannot sustain high magnitudes of current for long periods [136]. Due to this, the issue like selectivity, detection, and the ability to isolate the fault and keep the grid operational are developed. Compared to UDC, the BiDC grid provides more reliability to faults and becomes more promising to be deployed on shipboard microgrids [134].

Another issue that needs attention in power systems is grounding. The inefficient grounding method used can lead to current conduction and can result in corrosion of the ship [136]. In BiDC grids with multiple power generators and multiple unbalanced load requirements supplied at different voltage levels can lead to power unbalancing issues and can result in the current flow through the neutral of the BiDC grid or to circulate within the grid [136]. Thus, the correct grounding scheme is necessary to avoid this current flow and increase the ship's safe operation. These protection issues form a challenge for the implementation of DC grids.

An issue that pertains to the use of BiDC on ships is the issue of power balancing. This unbalance is due to the unequal load demand from the individual voltage levels of the BiDC grid. This imbalance can cause a shift in the neutral voltage towards either positive or negative and can result in the tripping of critical components connected with the BiDC grid [136]. Yadav, Qin, and Bauer [136] also describes three methods on how this imbalance can be tackled. First, the two three-level converters connected to form the BiDC grid can be controlled, and thus the required power imbalance can be overcome. Another approach is to intelligently control the two three-level converters connected to the dual-stator generator on one end and on the other to form the BiDC grid to balance the power demand, regulating the voltage of the BiDC grid. Finally, connecting balancing converters to the BiDC grid. The topologies used in balancing converters are Boost, Sepic, Zeta, Cuk, B6 and three-level topologies. Out of these, the three-level converter topologies are mature for BiDC implementation [136].

The alternating nature of the AC grid leads to cable induction losses. These losses occur as the direction of the current changes, depending on the frequency of operation [7]. In addition to this, another phenomenon that affects the AC microgrid cables is the skin friction effect. The effect affects the current density of the cable cross-section, where the current carrying capacity of the cable near its centre reaches zero and increases exponentially as we move towards the outer portion of the cable [7, 96]. This increases the cable sizing for power transmission along with its insulation in the AC grid compared to its DC counterpart. The benefits are substantial of switching to a DC grid as compared to an AC grid. To summarize, the advantages and disadvantages of a DC grid over an AC microgrid are briefed in Table 2.5.

The system architecture deployed on the ship can be Radial, Zonal or Ring type [134]. The qualitative comparison of these grid architectures for the DC grid is presented in Xu et al. [134]. The radial type of system architecture consists of two DC buses connected through a bus tie. The power generation, electric load from motors and auxiliary equipment are delivered symmetrically [134]. This type of system is cost-effective and not complicated. Second, the zonal type also consists of two DC buses, although they are connected at the bow and stern of the ship using two breakers [134]. The system is divided into zones and the energy consumers are connected to both the DC buses. In case of fault, the faulted DC bus is disconnected, and the electricity for the load is supplied from the opposite bus. This redundancy increases the reliability of this grid architecture and is therefore used in naval vessels. Finally, the ring topology is similar to a zonal type in normal operation where the DC bus ties are closed forming a ring. However, in case of a fault, the nearest circuit breaker to the fault is disconnected, and the grid is stabilized. Contrary to the zonal system, the energy consumers do not have a second bus for

Table 2.5: The advantages and disadvantages of DC microgrid over AC microgrid [21, 7, 136, 70, 55, 56, 134, 135]

DC	Advantages	Disadvantages
1	The easy integration of energy storage technologies and fuel cells as compared to AC grid.	DC Fault current is difficult to control
2	The collective weight and volume of the components forming an DC is less as compared to the AC counterpart	The selectivity and detection issues during faults and isolation of the fault itself is difficult
3	The cable induction losses and the power transmitting capability in DC grid is better compared to AC grid.	Lack of standards for UDC and BiDC grid, affecting the development of commercial components
4	The degrees of freedom are less in a DC grid compared to an AC grid where voltage is measured and maintained in DC compared to voltage, frequency, reactive power and rotor angle in AC	The power stability issues as a result of using a higher number of power electronic components
5	The lack of grid synchronization in terms of rotor angle helps in powering up the generator to support the grid faster than in AC grid.	The power imbalances in BiDC grid and pertaining losses
6	The availability of multiple voltage levels help in integrating the loads as per their working voltage.	
7	The variable speed operation of diesel generator assist in reducing the fuel consumption and carbon footprint.	
8	The power quality is higher as a result of reduction in harmonic distortions	

power delivery, unlike the zonal grid topology [134]. Yadav, Van Der Blii, and Bauer [137] performed dynamic modelling and stability analysis using a state-space model of a radial and a zonal architecture for a ferry and concluded that the zonal architecture provided higher stability and more power damping capabilities for power transients compared to the radial architecture. Most of the present ships are retrofitted, and radial architecture is dominated by traditional propulsion system described in section 2.2 remains cost-effective and with the added complexity in zonal architecture for power flow control and protection, the implementation of zonal architecture remains far from reality in commercial ships [134, 137].

2.4. Shipboard Microgrid Components

In the previous section, we highlighted the difference between AC and DC microgrids comparing power quality, stability, cable losses, power density, grid protection as well as volume and weight of the system as a whole. This section is aimed at providing an overview of the components that create an integrated electric propulsion (IEP) system. Although the propulsion system can be vast and quite extensive when studied on a minute scale, this thesis focuses on the components that act as near as possible to the grid. Consequently, propulsion components like the rudder, propellers, etc. are not considered in this thesis. The IEP can be primarily grouped into three divisions namely, power production, power distribution and power consumption. The power production consists of diesel generators, batteries, fuel cells, supercapacitors, gas turbines, etc. This thesis is aimed at finding the benefits of a bipolar DC grid as compared to the AC grid. Therefore, diesel generators and batteries are only considered. Although, fuel cells have shown great potential and some studies have been conducted to quantify their benefits in emissions reduction and as a power generator in ships with pilot/commercial projects like the Hyseas III, Hyship, Nemo H2, etc. [12, 133, 128, 80, 99, 101, 132]. Next, the power distribution consists of power conditioning devices along with cables, busbars for power transmission as well as

protection devices like fuses and circuit breakers. The transformer forms a distinctive feature in an AC grid, whereas solid-state technology forms the backbone of a DC grid [21]. Finally, the power consumption accounts for the power requirements for the electric motor for propulsion, manoeuvring, and the auxiliary energy consumption by the ship's communication, emergency, navigation, and control systems as well as the loads like refrigeration, air-conditioning and heating [80].

2.4.1. Power production

Power production for the onboard electric grid, either AC or DC, can be done with a variety of technologies. The generator is connected to a prime mover and forms the main source of energy production. The function of prime mover can be realised with a diesel engine, dual fuel engine (Methanol, Liquefied Natural Gas (LNG), Liquefied Petroleum Gas (LPG), etc.), fuel cells and others. Battery technology stores energy in chemical form and delivers this energy in an electrical form whenever demanded by the grid. This section explains the diesel engine-driven generators and batteries used in the production of electric power on ship microgrids.

Diesel Generator

Diesel engine is a mature technology and promising when it comes to operating in harsh marine environments. Therefore, the majority of ship builders opt for marine diesel engines as a prime mover MAN Energy Solutions [82], Caterpillar [18], Wartsila [131], Mitsubishi Heavy Industries [88], Cummins Inc. [24], and Rolls-Royce [107] and are catalogued in Appendix A. Diesel engines can be divided into three types namely, low-speed, medium speed and high-speed diesel engines. According to IACS [48], the marine diesel engine operating below 300 rpm are low-speed engines, whereas engines operating between 300-1400 rpm are medium-speed engines. Finally, high-speed diesel generators operate above 1400 rpm which are also commonly used in diesel-electric propulsion. The prime mover is a diesel engine connected to an alternator to produce electrical power. The commonly used alternator on the shipboard microgrid is a rotor wound synchronous generator [124]. This type of generator can also be used in variable speed operation by making modifications to the voltage and frequency controllers [124]. As per the IEEE [56], commercial vessels are mandated to bring their generators online within 30 seconds. The load steps are required to be within 33 per cent of the MCR and the engines take 5 secs to restore to a steady state as shown in Figure 2.10. For an emergency start, the diesel generator can reach its MCR within 10 seconds. This shows the fast response of the diesel generators that support the weak shipboard AC microgrid, as the frequency is also a constraint in operation that is needed to be fixed at 50 or 60 Hz.

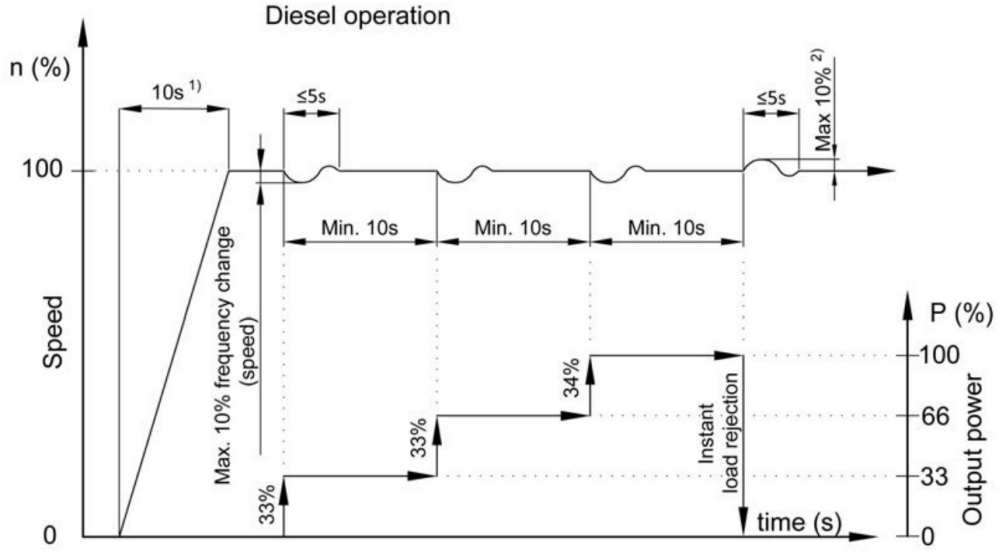

Figure 2.10: The cold start of a diesel generator as well as the load transients and the recovery time to reach steady state as described in Wartsila [130].

In AC microgrids, as the frequency (50 or 60 Hz) is a design constraint fundamental to the system, the generators are constrained to run at a fixed speed. At this fixed speed of operation, the diesel engines and specific fuel oil consumption (SFOC) have an inverse relation. This relationship is shown in Figure 2.11. The loading on the diesel generator affects the SFOC with decreasing load resulting in an increase in specific fuel oil consumption. The Figure 2.11 also highlights the specific fuel oil consumption of a variable-speed diesel generator used in DC grid operations. The specific fuel oil consumption increases marginally as compared to a fixed-speed diesel generator. This is realised due to the freedom of operating the diesel generator at variable speed, eliminating the constraint of frequency imparted due to AC grid architecture. This change is also highlighted in Figure 2.11 where at 560 kW loading the fuel consumption was reduced by 23 percent. Consequently, the CO_2 emissions arising due to shipping operation can be reduced by switching to variable speed diesel generator. Various studies conducted by Kim and Jeon [71], Hansen, Wendt, and Olav Lindtjørn [40], Hansen, Lindtjørn, and Vanska [38], and Chang et al. [21] have shown the emission reduction potential for variable speed diesel generators. Mobarra, Rezkallah, and Ilinca [89] studied the performance of variable speed diesel generators to operate the diesel engine at optimal load point and has shown up to 40 per cent reduction in lowering the CO_2 emissions. Finally, depending upon AC or DC grid, the diesel generator is configured directly with the switchboard in AC and uses a rectifier after the generator to produce DC voltage [76, 71, 136].

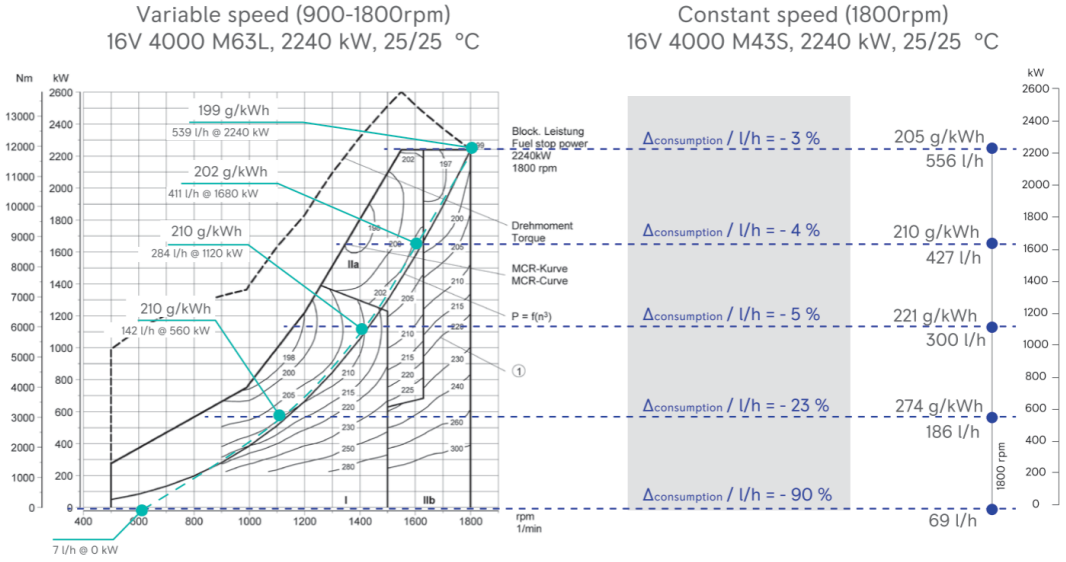

Figure 2.11: The SFOC relationship with loading on the diesel engine for fixed speed and variable speed diesel generator [36].

Energy Storage System

The energy storage system (ESS) primarily functions to store energy in any form when available in excess and to deliver power whenever the energy is in deficit in the system. Subsequently, many ESS are developed and range from mechanical, chemical, and electrical methods of storing energy (electricity) [91]. Furthermore, based on system working and environmental conditions, a typical energy storage solution consisting of one or more technologies is chosen. Dedes, Hudson, and Turnock [27] assessed the potential of energy storage to reduce emissions by conducting a study on 31 vessels of five different types and concluded that depending on storage system, vessel condition and vessel type, the reduction could be up to 0.32 million tonnes in NO_x, 0.07 million tonnes in SO_x and 4.1 million tonnes in CO_2. Another simulation study was published by, Peralta et al. [97] where the Platform Supply vessel's voyage was divided into segments and the emission reduction for four different types of configurations was estimated. The four configurations were main diesel generator, main diesel generator and battery, main diesel and auxiliary generator, and finally main diesel, auxiliary and battery together. Two types of battery technologies were studied (LTO and LFP) and the emission reduction for LFP was higher compared to LTO. However, they both assisted in the efficient operation of diesel

generators by charging the battery in part-load conditions and discharging during high energy needs, ensuring optimum loading on the diesel generators [97].

For marine environments, the most suitable ESS are Batteries, Supercapacitors, Flywheels, Superconducting Magnetic Energy Storage (SMES) and Fuel cells [91]. Figure 2.12 presents the power and energy densities for these energy storage systems. Flywheels, SMES and supercapacitors have higher power density as compared to different battery types as well as fuel cells. However, technologies like battery storage and fuel cells have higher energy density. The technologies with high power density tend to have lower response times compared to high energy density technologies [92]. This is due to the high power requirements within a very short time, typically less than microseconds. The response times for other ESS are in microseconds. These higher energy densities and higher power density technologies should be used in combinations, as shown by De Smet et al. [26]. The study performed by De Smet et al. [26] presented a comparative assessment between a single battery (Either high power or high energy) and a two parallel battery system, one being high energy dense and the other with high power capabilities and showed that although the system efficiency changes were not significant, the weight reductions were estimated to be 30 per cent. The system cost was reduced by 28 per cent and 14 per cent for monotype LTO and NMC batteries, respectively. In transportation, the requirements from ESS are mostly inclined towards high energy density technologies with long discharge times, although higher power density components are required during acceleration or when the possibility of sudden power changes is present [32]. The presence of pulsed loads on shipboards demands the ESS to have high power density to operate efficiently and avoid power disturbances [32]. Lithium-ion and Nickel based batteries are the most suited battery for transportation, mainly due to their high energy density [32]. As per the report of Helgesen, Henningsgård, and Aarseth Langli [43], the most used battery chemistry in marine applications is Li-NMC due to its flexible design for energy and power density. The commercially available batteries are ABB [2], Corvus Energy [22], Kongsberg [72], Echandia [30], and Kongsberg [73] and are catalogued in Appendix A.

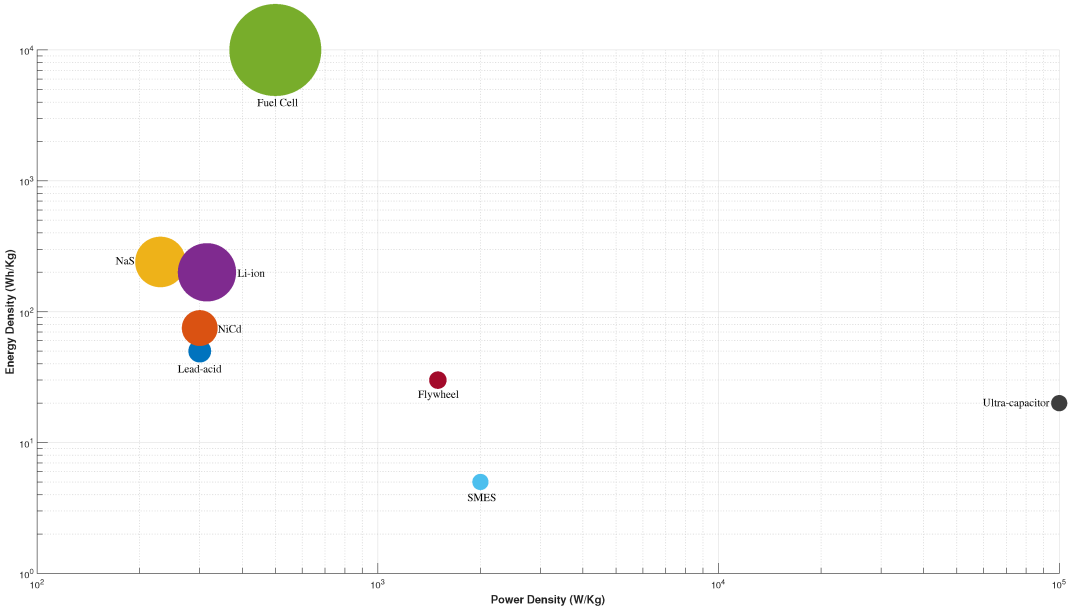

Figure 2.12: Ragone plot for different ESS suitable for shipboard microgrids [91].

The typical ESS on shipboard microgrids performs the function described in Figure 2.13. These functions are described in detail in the work of Hansen and Wendt [39] and Mutarraf et al. [91]. First, the ESS can act as a backup for generators by establishing an active connection with the grid. The ESS units are active and running, ready to step in on loss of generating capacity. This function can assist in reducing the number of generators to be kept online, increasing the fuel efficiency of the system. Second, the ESS can be connected in a smaller capacity performing the functions as before but near an electrical load, ensuring high power availability during load transients. Third, a large capacity of ESS

can act as a power generator, with higher response times to average out the power requirements from the diesel generators, improving the fuel efficiency of engines. Fourth, the ESS can provide support during sudden load changes and assist the diesel generators to follow this load change smoothly. this can be of major advantage for slower-running engines or with hybrid power propulsion with shaft generators. Fifth, the ESS can be used to charge, discharge and support the working of the diesel generators such that they operate at the least possible emission load point. This function helps in producing power at its peak efficiency. Finally, the engines can be turned off completed and the load requirements for propulsion as well as auxiliary systems can be supplied with the ESS resulting in comparatively quiet operation, reducing noise and vibrations. This function is most advantageous near harbours or in ECA's described in section 2.1 where strict emission regulations are needed to be achieved. The grid integration for ESS is done using a DC/DC converter for the DC grid and in the case of the AC grid, this connection is performed using an inverter. The main design and selection criterion from the available topologies is the provision for bi-directionality of power flow so that the ESS can charge and discharge.

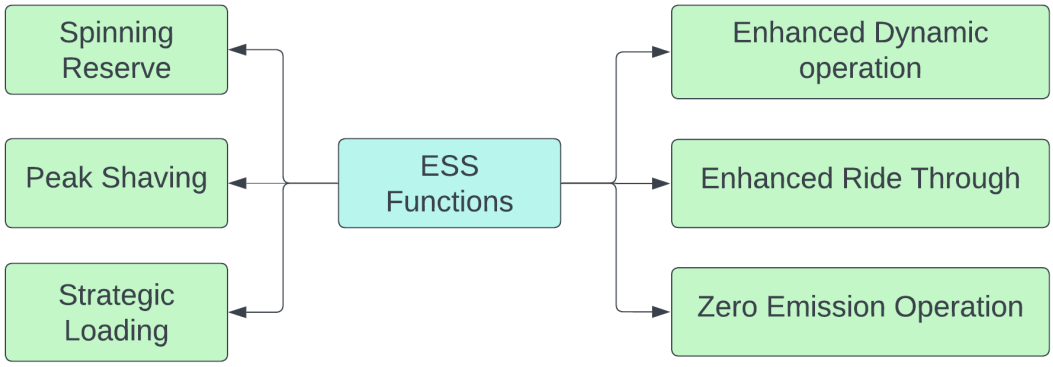

Figure 2.13: The functions performed by ESS on a shipboard microgrid

2.4.2. Power distribution

The electricity distribution on the shipboard microgrid happens mainly from different electrical components like the transformer, electronic power conditioning components, protection devices and most importantly electrical power cables. They serve to maintain the required stability and protection criteria to avoid any catastrophic failures of the weak grid network by maintaining the desired voltage levels.

Transformer

The main purpose of a transformer is to provide protection as well as desirable voltage levels at the output of the transformer [76]. A transformer is used exclusively in AC systems, as it takes an AC voltage as input and provides AC voltage at the output. This output voltage can be either higher or lower than the input voltage. The three winding transformers are used to provide a phase-shifted output to the rectifiers that assists in reducing the THD in the system. Transformers have also been shown to reduce high-frequency noise because of their good damping qualities, therefore reducing the propagation of noise through the system [76].

Switchboard

The switchboard consists of protection devices and power management devices like AC and DC circuit breakers, fast fuses and power electronic converters[76]. For the scope of this thesis, the power electronic components are only considered. The main function of the switchboard is to distribute the power received from the generators reliably and efficiently to multiple power consumers. In AC systems, as the power production on ships from the diesel generators is three-phase, the switchboard

consists of three thick copper plates called bus bars running horizontally throughout the length of the main switchboard [76]. In BiDC systems, the number of bus bars would remain the same (Positive, Neutral, Negative poles), although a rectifier is installed between the generator and the bus bars to provide rectified voltage and current. As the diesel generators are directly connected to the main bus bars, protection from overcurrent is provided by circuit breakers. In case of fault, the circuit breaker can trip and isolate the faulty generator from the main bus bars, providing protection. The high power loads like electric motors for propulsion are directly connected to the main bus bar [76]. Low power loads are connected to a transformer and then to a smaller distribution board as shown in Figure 2.5. These connections are often made using AC or DC circuit breakers to provide protection and isolation from faults. The discussions of AC and DC circuit breakers are out of the scope of this thesis, although commercially available DC circuit breakers are found to operate below 250, 500, 750, 1000, and 1500 Volts depending on the manufacturer [29, 1, 108]. This limits the scope of this thesis to low-voltage DC grids.

The power electronics that condition the electricity in the grid are AC-DC converters (Rectifiers), DC-AC converters (Inverters), DC-DC converters and VFDs. First, the rectifiers can be divided into uncontrolled rectifiers, half-controlled and fully controlled rectifiers operated by diodes, thyristors and IGBTs or MOSFETs respectively [136, 76, 134]. They take the responsibility of stabilising the DC voltage at the output. The rectifiers can also be divided into two-level and multi-level rectifiers. Two-level rectifiers are commercially available in the marine industry. The multi-level rectifier is preferred for high voltage and high power requirements, as the series or parallel connections reduce the voltage or current stresses on the switches [134]. It provides a modular approach to a medium voltage system that can provide higher fault tolerance, bypassing the faulty submodule [134]. The number of components is higher in multi-level rectifiers compared to two-level rectifiers and this leads to higher losses especially in switching and conduction, reducing the efficiency [134]. For a diesel generator where power only flows in one direction, bi-directionality is not required. The active rectifiers can be used to stabilise the DC output voltage as well as promote variable speed operation of diesel generators compared to using a diode rectifier constrained by the output power developed by the generator [134, 21, 38].

Second, the Inverter topologies are reviewed in Xu et al. [134]. Depending on the motor, the inverter topology is selected. The active rectifiers are used to control a DC motor, the induction motors require voltage source inverters (VSIs) whereas the synchronous motors use voltage source inverters and current source inverters (VSIs and CSIs). The inverters are also divided into two-level and multi-level topologies. The widely used inverter topology for high-power applications is the three-level neutral point clamped (NPC) topology, as this topology provides lower stresses on the switches, higher quality of voltage and current output [134]. 3L-NPC is prone to unequal loss distribution, to overcome this active NPC is used by using two switches and a freewheeling diode instead of a clamping diode. The use of switches provides active clamping and assists in reducing unequal loss distribution. The NPC provide benefits but at the expense of additional weight, space, and hardware cost. Therefore, for small ships, two-level inverters are considered.

Third, the DC-DC converters are used to interface DC components like batteries with the DC grid. For high-power applications, isolated converters are preferred [134]. The most common type is the Dual Active Bridge (DAB) because of its benefits like soft-switching, galvanic isolation, high power density and bidirectional power flow [134]. The last quality is important for the integration of batteries. DAB consists of two full-bridge converters with DC capacitors and a high-/medium-frequency transformer. The presence of a DC capacitor makes this converter difficult to control the fault current [134]. Another topology used in maritime is the NPC-based DC/DC converters that are suitable for short voyages.

Finally, VFDs are a combination of rectifiers and inverters. They are used for AC power with a fixed voltage and fixed frequency input and provide variable frequency and variable voltage as output [76]. Therefore, they are used in starting and controlling the Induction motor. They also help in improving the power factor of the electric motor, reducing the reactive power losses [96].

The major disadvantage of the BiDC grid is the voltage imbalances that occur due to unbalanced load requirements from different connections of the BiDC grid (positive-negative, positive-neutral,

negative-neutral). The failure of the grid due to instability from voltage imbalances is taken care of by so-called voltage balancing topologies of power converters. Pires et al. [98] has reviewed an exhaustive set of power converter topologies for voltage balancing for the BiDC grid. These power converters are divided according to the integration schemes of different components like the generators, batteries, and load in the BiDC grid as well as standalone voltage balancing converter topologies. This classification is shown in Figure 2.14 and it highlights the topologies that are suitable for a particular component and its integration in the BiDC grid. The centralized architecture refers to the power converters forming the BiDC grids connected to the AC system, whereas the decentralized architecture is one where the voltage balancers are connected to the weak portions of the BiDC grid. Another distinction that is studied in Pires et al. [98] is isolated type and non-isolated type converters. The isolated types include a solid-state transformer to provide protection by separating the input and output voltage terminals.

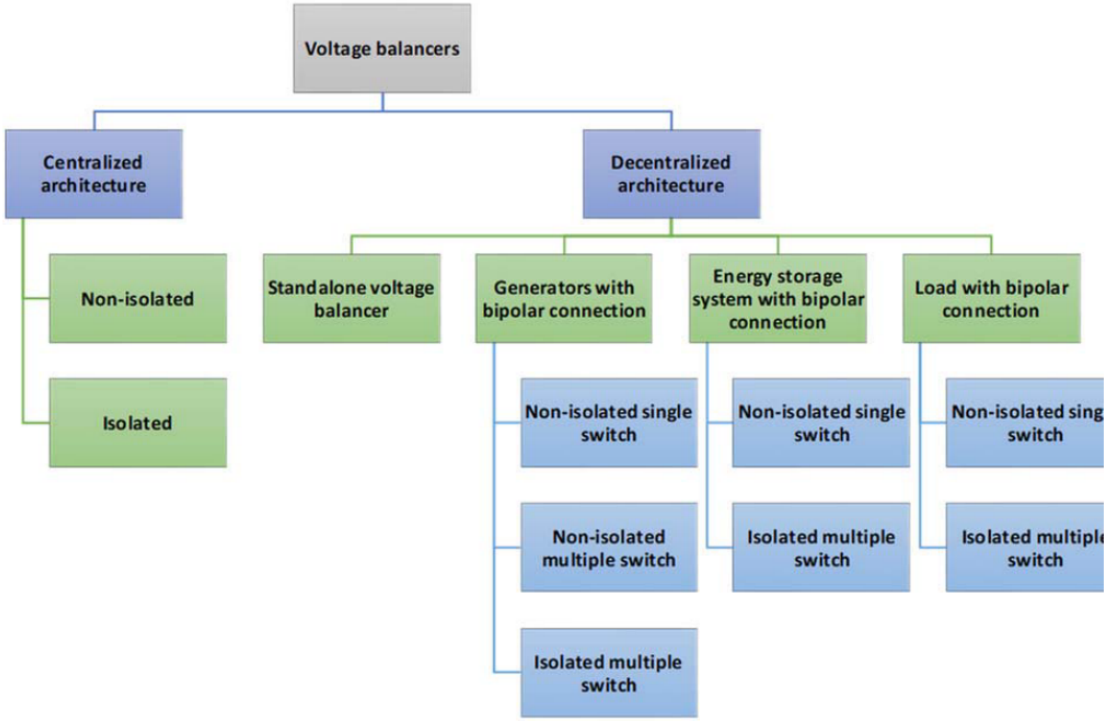

Figure 2.14: Classification of BiDC voltage balancer topologies according to the different components and their integration with the BiDC grid [98].

Power Cables

The standard for power cable used in shipboard microgrids are defined by IEEE [57]. The marine environment is harsh and therefore requires additional measurements for power distribution. As per Prysmian Group [102], the power cables are made of stranded annealed copper to make them flexible and corrosion-resistant, they need to be fire-resistant in case of fire on ships, the maximum conductor temperature should not be allowed to go above 90^{o} Celsius and the insulation is required to sustain that temperature and in case of fire, the insulation should burn without emitting toxic halogens. Therefore, the commonly used power cable insulation material is cross-linked polyethylene (XLPE) [46]. Finally, these cables are tested as per IEC standards. According to IEEE [57], the cable should be provided with armour, where physical damage to the cable is possible leading to mechanical failure. It also states that short circuit considerations are also to be taken care of and the cable should be able to sustain the fault current. The skin friction effect and the grouping effect of cable on the current carrying capacity are also important factors to be considered in cable design and installations [57]. The cables designed for AC that do not contain silicon can also be used for DC voltages up to 2000 V [57]. The companies that provide power and instrumentation cables for shipboard microgrids are Prysmian Group [102], Top Cable [120], R & M Electrical group Ltd. [104], and Honest Cable [46].

2.4.3. Power consumption

The power consumption is mainly divided into two parts, namely, propulsive/thruster loads and service/auxiliary loads [76]. Induction motors are commonly used in electric propulsion, mainly because of their cost-effective and rugged construction [96]. The motor is finally connected to the propeller using a mechanical shaft linkage. In an AC microgrid, the speed (rpm) of the motors is controlled by the VFDs described before, and the integration is made directly with the main bus bars using a phase-shifted three-winding transformer to reduce the voltage ripples (fluctuations) developed due to rectification in the VFD. A catalogue of Induction motors is shown in ABB [3] that are used in marine applications. In DC microgrids, the rectification part of the VFD and the three winding transformers can be eliminated and inverters with Active Front End (AFE) are used to provide the necessary variable frequency and voltage to the induction motor as shown in Figure 2.7 and Figure 2.5. Therefore, the lesser use of components increases the efficiency of the operation in DC grids over AC grids.

The auxiliary loads consist of heating and refrigeration demand, navigation and control systems, and emergency systems, these are considered low-power applications. In an AC microgrid, a transformer is used to integrate these loads on the main bus bar, whereas, in a DC microgrid, an inverter is used.

2.5. Case Studies

This section highlights case studies that have been done on DC grids and variable speed operation of diesel generators in real life. The first case study is on a 10-ton fishing boat, conducted by Son, Lee, and Sul [115]. The DC IEP consists of a diesel generator and a battery bank. The DC system is Unipolar and operates at 650 Voltage. The weight reduction for DC IEP was 2 tonnes. The study was performed in the summer and winter seasons. The study estimated saving 67 Kg (-18.4 per cent) of fuel in summer over a single trip, whereas 234 Kg (-22.7 per cent) was in winter. The cumulated fuel consumption is shown in Figure 2.15.

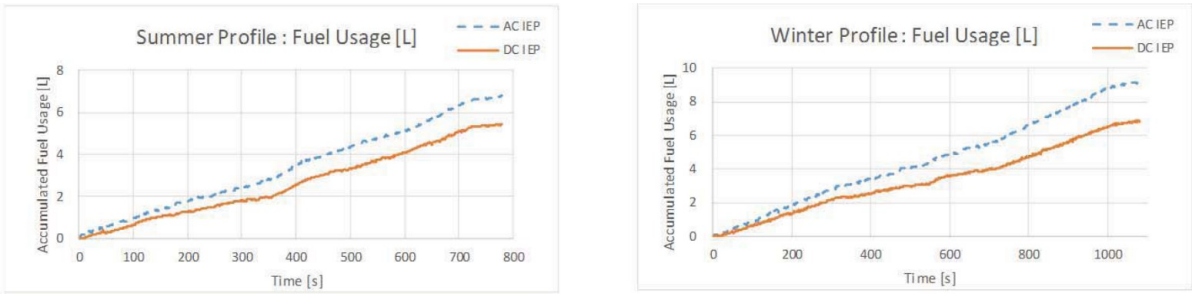

Figure 2.15: The cumulated fuel consumption for the fishing boat in summer (left) and in winter (right) [115].

The second case study is on a double body research vessel performed by Chang et al. [21]. The ship DC bus IEP system consists of two independent DC buses that are interlinked with bus ties. The DC bus architecture is unipolar DC operating at 1000 Voltage, powered by a main diesel generator and an auxiliary generator on each side of the bus tie. The DC IEP has shown a 56 per cent reduction in weight as compared with the AC counterpart, mainly due to the absence of transformers. The study was conducted for a 53-day voyage where the ship was 20 per cent in cruising mode and the rest of the time in dynamic positioning (DP), docking, and manoeuvring modes as shown in Figure 2.16a. The study concluded that compared to AC microgrid, the fuel consumption in cruising mode was similar in DC IEP with 5 per cent, 6 per cent and 9 per cent reduction in manoeuvring, dynamic positioning and docking modes as shown in Figure 2.16b. The fuel saving in cruise mode is negligible, as in both AC and DC architectures the diesel generators work at optimum levels. Overall, the average fuel saving observed throughout a 53-day voyage was 6 per cent.

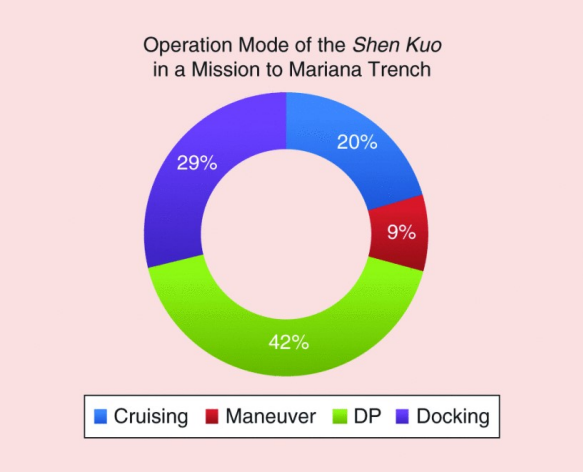

(a) The percentage division of different operating modes like cruise, DP, docking and manoeuvring [21].

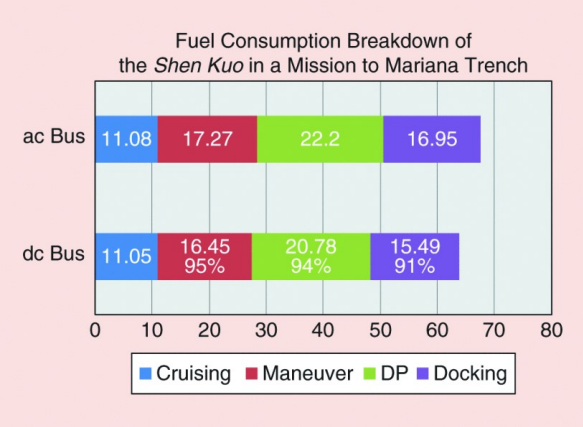

(b) The fuel saving observed in each operating mode [21].

Figure 2.16: The operational modes of the vessel in the study, as well as the fuel reductions observed in each operating mode, conducted for a 53-day voyage [21].

2.6. Summary

This chapter assisted in establishing the adequate background required for this thesis. The current emission regulations were introduced in section 2.1. These regulations provide a base to narrow down the diesel generators that are used in this study. The section 2.2 describes the characteristics of different propulsion types like mechanical, electrical and hybrid systems. Subsequently, the advantages and disadvantages of propulsion architectures are highlighted. This narrowed down the propulsion system to be chosen for this study. Consequently, the section 2.3 puts forward a comparison of system-level differences to form respective grid topologies. Finally, the operational technical differences of these components for AC and DC shipboard microgrids are highlighted in section 2.4. Finally, section 2.5 showcases the experimental studies that have been performed and the findings from them.

3

Ship Power Estimation

The chapter 2 assisted in establishing the required knowledge for maritime ship propulsion systems, as well as the qualitative differences between AC and DC shipboard microgrids. The emission regulations were introduced that helped in narrowing down the dataset creation of diesel generators as well as the lack of commercial availability of DC circuit breakers provided a limitation for this thesis to be confined to LVDC. The section 3.1 describes the methodology to estimate the ship's mechanical power requirements for propulsion, and auxiliary electrical power is assumed as a per cent of this mechanical power. The electrical layout for ten arrangements is presented in section 3.2. Furthermore, the power balance in AC and DC microgrids occurs at the bus bars in the switchboard and hence the electrical power is calculated using the electrical line diagrams described in section 3.2 based upon background knowledge attained in section 2.2. This electrical power estimation methodology is highlighted in section 3.3. This section also presents the methodology to estimate the cable losses for the AC and the BiDC grid, along with the cable sizing procedure leading to estimating the total electrical power requirements on the distribution and consumption side. Finally, the chapter is concluded with a chapter summary in section 3.4.

3.1. Ship's Mechanical and Auxiliary Power Estimation

The ship's propulsion and auxiliary power demand are recorded in the ship's data management system. This data is not freely available and is in the possession of the ship operator. The propulsion power demand varies with time and depends on the ship's operational, voyage parameters and environmental conditions. Thus, not only the operational parameters but also the environmental conditions are taken into account at the time of designing the ship's propulsion system. Usually, the environmental factors (fouling, wind resistance, etc.) are taken into account with a certain margin [9, 90, 17]. The methodology given in this section is preliminary and aims to provide a practical estimate of the ship's propulsion power demand. The ship's propulsion power requirements are an important variable for formulating the optimization problem and thus realizing our objective (min. emissions). The vessel's speed and design parameters are taken as input, and backward calculations for the mechanical power requirements are estimated. Mechanical power means the power that needs to be delivered to the propeller. The ship's power requirements are mainly divided into two main groups: - propulsion loads and auxiliary/hotel loads [9, 90, 76]. The average auxiliary power is defined as a percentage of the propulsion power with a certain standard deviation from the mean value.

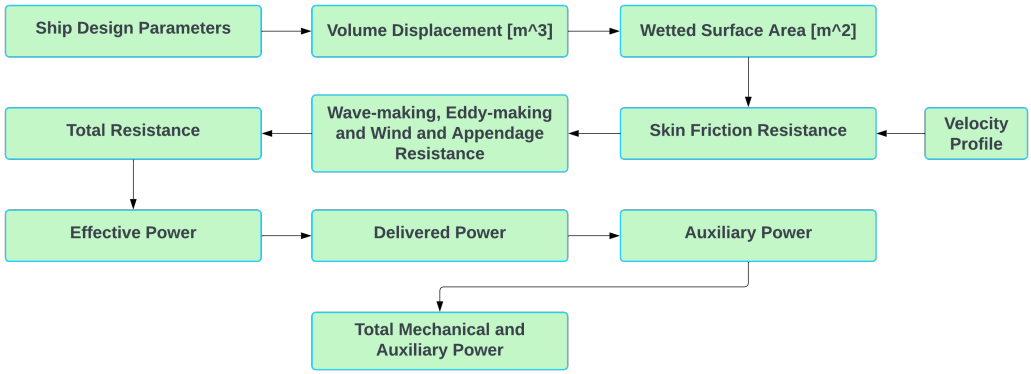

Figure 3.1: The flowchart describing the methodology used in estimating the ship's mechanical and auxiliary power.

The methodology is described in Figure 3.1. The ship's propulsion system has to perform work to overcome the total resistance (R_T) to maintain a certain speed at sea. According to Barrass [9], the total resistance can be divided into four main categories. They are Frictional resistance (R_F), Wave-making resistance (R_W), Eddy-making resistance (R_E), Resistance due to wind and appendages (R_{APP}). Therefore, the total resistance (R_T) is the sum of all four resistances $(R_T = R_F + R_W + R_E + R_{APP})$. The 2^{nd} and 3^{th} resistances are considered together as residual resistance (R_R). The resistance from wind and appendages is not considered in calm water conditions and is added later as a percentage of the total resistance in calm waters (R). Thus, the total resistance equation for calm water conditions is given as [9, 90]: -

$$R[N] = R_F[N] + R_R[N] \tag{3.1}$$

Where,
R = Total resistance in calm water conditions [N]
R_F = Frictional resistance [N]
R_R = Residual resistance [N]

William Froude had come up with an empirical formula in the late 1860s to estimate the frictional resistance of the ship. This formula is as follows [9, 90, 17]: -

$$R_F[N] = f * S * V_k^n \tag{3.2}$$

Where,
f = Skin friction coefficient which depends on the length of the ship, hull roughness and density
S = Wetted surface area $[m^2]$
V_k = Velocity of ship $[knots]$
n = A coefficient which depends on the ship's hull

The value for coefficient n is taken as 1.825 [90, 9, 17]. Furthermore, the value for skin friction coefficient f is taken from Table 3.1. These values are given in Molland, Turnock, and Hudson [90]. Table 3.1 shows only the range of values of our interest. One can observe the inverse relation between skin friction coefficient (f) and the length of the vessel (L) in Figure 3.2 which shows the complete range of calculations made by Froude. Thus, from the Equation 3.2 and with the assumption for the R_F/R value, we can estimate the total resistance of the ship in calm water conditions.

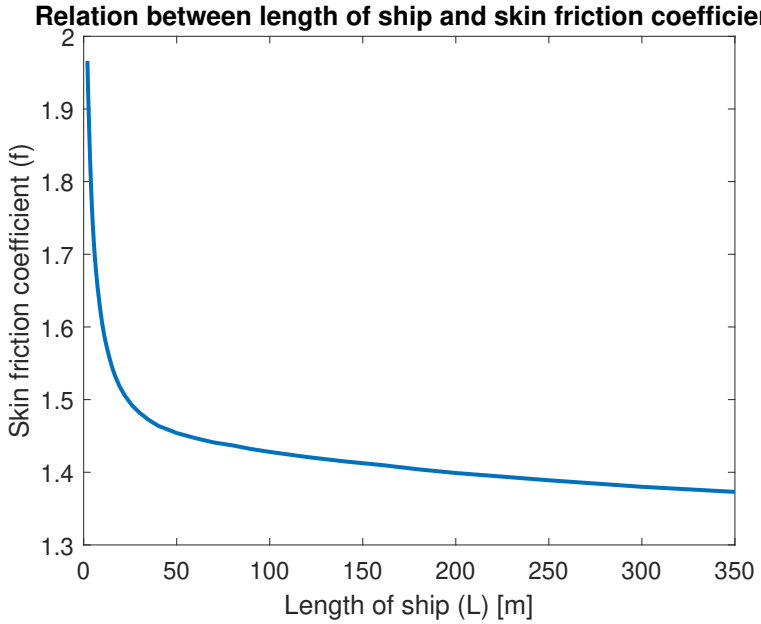

Figure 3.2: Relationship between the length of the ship (L) and the skin friction coefficient (f) calculated by Froude [90]. The value for the skin friction coefficient reduces exponentially for smaller lengths and tends to become linear for longer ship lengths.

Table 3.1: Froude's skin friction f values. adapted from Molland, Turnock, and Hudson [90]

Length (m)	f	Length (m)	f
20	1.515	45	1.459
22	1.506	50	1.454
24	1.499	60	1.447
26	1.492	70	1.441
28	1.487	80	1.437
30	1.482	90	1.432
35	1.472	100	1.428
40	1.464	120	1.421

The wetted surface area is calculated using the hydro-static programs [75]. But, for an approximate estimation of the wetted surface, different formulas have been proposed in the past by D.W.Taylor in Barrass [9], Holtrop and Mennen in Holtrop and Mennen [45], Denny and Mumford in Kristensen and Lützen [75], Froude in Molland, Turnock, and Hudson [90] and others. The formula proposed by Denny and Mumford has shown that the calculated area deviated by 7 per cent when compared with the wetted surface area of the original ship [75]. Thus, for our power estimation, a variant of the Denny Mumford formula for double-ended ferries is used as described in Kristensen and Lützen [75]. The formula is as follows: -

$$S[m^2] = 1.11 * (\frac{V_S[m^3]}{D[m]} + 1.7 * L[m] * D[m]) \tag{3.3}$$

Where,
V_S = Volume displacement $[m^3]$
L = Length $[m]$
D = Draught $[m]$

Equation 3.3 takes into account the volume displacement of the ship to calculate the wetted surface area. Furthermore, to evaluate the volume displacement (V_S), the mass displacement (V_M) is divided by the density of the seawater. However, if the mass displacement of the ship is not known, it can

be estimated using the Block coefficient (C_B) and Dead-weight coefficient (C_D) [9, 90]. The formula to calculate the volume displacement is given below: -

$$V_S = \frac{V_M[tonnes] * 1000[kg/tonnes]}{\rho[kg/m^3]} \tag{3.4}$$

Where,
V_M = Mass displacement [$tonnes$]
ρ = Density of seawater [kg/m^3]

The R_F/R ratio depends on the velocity-length ratio defined in Barrass [9] and is used to estimate the percentage of frictional resistance to resistance in calm water conditions. Furthermore, the total resistance (R_T) can be evaluated using the relationship between the wind and appendage resistance and resistance in calm water conditions. Therefore, using the methodology proposed above, the total resistance (R_T) of the ship can be computed.

$$R_T[N] = R_F[N] + R_W[N] + R_E[N] + R_{APP}[N] \tag{3.5}$$

Where,
R_T = Total Resistance of ship [N]
R_W = Wave-making resistance [N]
R_E = Eddy-making resistance [N]

Thus, the effective power (P_E) requirement for maintaining a velocity (V) of the ship can be estimated using the formula given below [17, 9, 90, 75]: -

$$P_E[W] = R_T[N] * V[m/s] \tag{3.6}$$

Where,
V = Velocity of ship [m/s]
P_E = Effective power [W]

The effective power (P_E) is the power delivered to the water through the propeller and does not consider the losses that are needed to be taken to estimate the required power produced by the power generation system of the ship. Therefore, for the evaluation of the delivered power (P_D) which is the power delivered to the propeller, the hull efficiency (η_H) and the propeller efficiency (η_P), relative rotative efficiency (η_R) and shaft efficiency (η_S) values are taken into account. The equation for the delivered power (P_D) then becomes [75, 17]: -

$$P_D[W] = \frac{P_E[W]}{\eta_R * \eta_S * \eta_P * \eta_H} \tag{3.7}$$

Where,
P_D = Delivered power [N]
η_R = Relative rotative efficiency [-]
η_H = Hull efficiency [-]
η_S = Shaft efficiency [-]
η_P = Propeller efficiency [-]

The ship's resistance value changes throughout its lifetime, which affects the losses that take place in the power delivery to the propellers. This happens due to an increase in roughness of the hull as a consequence of fouling, rusting of the hull and/or biological growth of weed or barnacle [90]. The increase in roughness value can be 10-30 per cent per year, as stated by Molland, Turnock, and Hudson [90]. Thus, an appropriate margin is taken into account when evaluating the propulsion power P_P of the ship. Molland, Turnock, and Hudson [90] states a margin (M) of 15 per cent over the delivered power to account for this change. For ships operating near the coast, this margin can be neglected. Therefore, the equation for propulsion power is stated below ([90, 75]): -

$$P_P[W] = P_D[W] * \left[1 + \frac{M}{100}\right] \tag{3.8}$$

Where,
P_P = Propulsion power [W]
M = Margin for resistance increase [%]

The mean auxiliary power demand (P_{AUX}) is assumed to be a percentage of the maximum propulsive power $(P_{P_{MAX}})$ requirement, with a standard deviation to account for the change in load requirements. The Equation 3.1 to Equation 3.8 are used to estimate the ship's total power requirement. The proposed methodology in this section is used to estimate the power requirement of the ship selected for this study, i.e. *Island Discovery*. The results obtained are explained in section 6.1. The following section will describe the ship's electrical layout for arrangements AC1 to AC5 and DC1 to DC5 used for the optimization problem for the ship used in this study.

3.2. Electrical Layouts for the Ship

In the previous section, a methodology for mechanical power production based on the ship's design and operational data was estimated. The methodology is described in Figure 3.1. This section will present the schematic electrical line diagrams for AC and DC grids based on the common electrical layouts. The propulsion architecture used in this study is a series hybrid propulsion system, as the ships that operate on LVAC and LVDC have this type of propulsion system in common. These layouts are used to estimate the power requirement at the switchboard for both grids in comparison. This power requirement is estimated taking into account the efficiency of the components used to form this islanded microgrid, as well as reactive power losses in the case of an AC grid. In total, ten arrangements have been studied, AC1-AC5 are based on the AC grid whereas DC1-DC5 are based on the DC grid architectures.

The Table 3.2 describes the ten arrangements used in this work. The all-inclusive electrical layout diagram is presented in Figure 3.3a for AC architecture designed for 3 phase 690V 50Hz, whereas Figure 3.3b highlights the BiDC architecture operating at 1400V (+700V N -700V). The '✓' symbol means the component is used, and the '✗' symbol means the component is not considered in that specific arrangement from the ten arrangements for AC and DC grid.

Table 3.2: The definition of all ten arrangements used in this study for an AC as well as a DC grid. The first five arrangements (AC1-AC5) are for AC described by Figure 3.3a whereas the next five (DC1-DC5) arrangements are highlighted with Figure 3.3b.

Arrangement	Grid	DG1	DG2	Battery Bank	Shore Power
AC1	AC	✓	✓	✗	✗
AC2	AC	✓	✓	✓	✗
AC3	AC	✓	✓	✓	✓
AC4	AC	✓	✗	✓	✗
AC5	AC	✓	✗	✓	✓
DC1	DC	✓	✓	✗	✗
DC2	DC	✓	✓	✓	✗
DC3	DC	✓	✓	✓	✓
DC4	DC	✓	✗	✓	✗
DC5	DC	✓	✗	✓	✓

The Figure 3.3a consists of a diesel generator providing the required voltage level for the main bus bar situated in the switchboard. A battery bank is inherently a DC power source and is integrated into the AC grid using a Bi-directional inverter topology. The propulsive load is connected directly using a three winding transformer and the variable voltage and variable frequency are provided to the motor by a variable frequency drive (VFD) giving control over the rpm of the motor as well as improving the power factor. The shore power is integrated with the help of a transformer to provide necessary galvanic isolation as well as protection in case of faults.

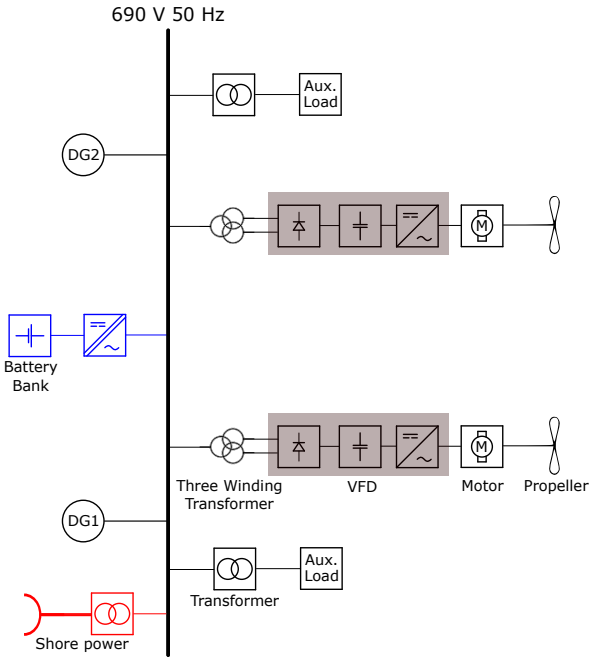

(a) The AC grid architectures for AC1-AC5 arrangements. The arrangements are two DG, two DG and battery, Two DG, battery and shore power, One DG with battery, and one DG with battery and shore power.

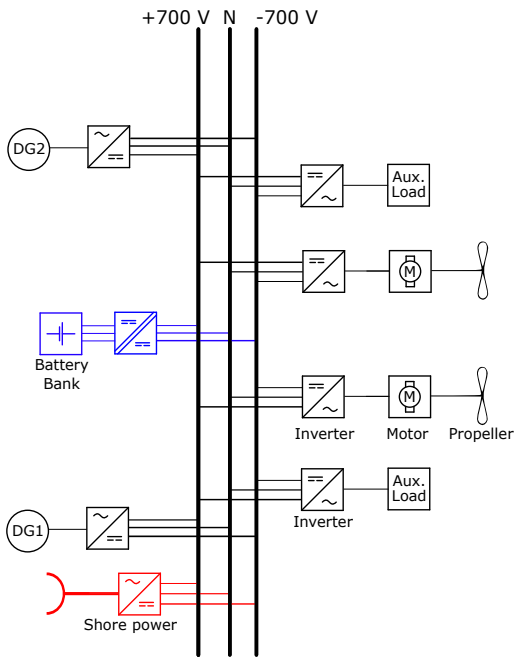

(b) The DC grid architectures for DC1-DC5 arrangements. The arrangements are two DG, two DG and battery, Two DG, battery and shore power, One DG with battery, and one DG with battery and shore power.

Figure 3.3: The electrical line schematics for AC and BiDC grid, with the electrical components that form the respective grids.

The Figure 3.3b is made up of diesel generators connected through three-phase rectifiers to form a BiDC grid. The battery bank is connected to the main bus bar via a bidirectional DC/DC converter. The transformers are replaced by inverters and power the auxiliary load, whereas the rectifier part of the VFD is omitted and uses only inverters with AFE to drive the propulsion motor. The three-winding transformer is also eliminated, as harmonics, as a result of the rectification process in the VFD, do not occur. The shore power is incorporated using three phase rectifier.

The electrical layout for the AC and DC microgrid presented in Figure 3.3 are used to estimate the electrical power for the AC and DC microgrid, respectively. The electrical power requirement will remain the same for all the AC arrangements as well as all DC arrangements. The backward calculations are done to estimate the power requirements according to the components used to form the respective microgrids. The following section will provide the methodology to estimate AC and DC electrical power.

3.3. Electrical Power Estimation for AC and DC Microgrid

This section is aimed at estimating the electrical power requirements at the switchboard for the AC and BiDC grid. The components that make up the grid in respective architectures, with their efficiency values, are taken into account for the calculations. The information from the section 3.2 is used in this section. Finally, the cable losses are also estimated in subsection 3.3.1. Therefore, realising the electrical power requirements for the AC and BiDC grid architectures.

AC Grid

The electrical power requirements for the AC grid are calculated taking into account the efficiency values for the components connected in the flow of electricity and calculating in the reverse direction to the flow of electricity. The auxiliary load is connected to the switchboard with a transformer. In section 3.1, the auxiliary power was estimated after the transformer. The Equation 3.9 describes the formula to calculate the auxiliary electrical power requirements of the ship throughout the voyage.

$$P_{AUX_{ACSB}}[W] = \frac{P_{AUX}[W]}{\eta_{Transformer_{AUX}} * \cos(\theta_{AUX})} \tag{3.9}$$

Where,
$P_{AUX_{ACSB}}$ = AC auxiliary power required at switchboard [W]
$\eta_{Transformer_{AUX}}$ = Auxiliary transformer efficiency
$\cos(\theta_{AUX})$ = Power factor for auxiliary load

The power for main propulsion is estimated using Equation 3.8. However, this equation provides the total mechanical power for propulsion, and therefore it is necessary to calculate the electrical power per propeller drive. To calculate the electrical power of the main propulsion, the Equation 3.10 is used and takes into account efficiency values for the three winding transformers, VFD, Induction motor and the reactive power losses.

$$P_{P_{ACSBWL}}[W] = \frac{\left(\frac{P_P}{N_P}\right)[W]}{\eta_{Motor} * \eta_{VFD} * \eta_{TWT} * \cos(\theta_{Motor})} \tag{3.10}$$

Where,
$P_{P_{ACSBWL}}$ = AC propulsion power required at switchboard without cable losses per propeller drive [W]
η_{Motor} = Induction motor efficiency
η_{VFD} = Variable frequency drive efficiency
η_{TWT} = Three winding transformer efficiency
$\cos(\theta_{Motor})$ = Power factor of induction motor
N_P = Number of propeller drive

BiDC Grid

In the BiDC microgrid, similar to the AC grid, the electrical power estimation is calculated according to the component efficiencies that make up the BiDC grid up to the switchboard. The auxiliary power is calculated using the Equation 3.11 as an inverter is used to provide the AC power to the auxiliary load. The reactive power losses are also considered. In addition to this, the electrical propulsion power at the switchboard for the BiDC grid is also computed using Equation 3.12 as per the efficiencies of components making the BiDC connection to the switchboard. Subsequently, the efficiencies of the inverter connected to the motor, efficiency of the motor itself and reactive power losses are considered.

$$P_{AUX_{DCSB}}[W] = \frac{P_{AUX}[W]}{\eta_{Inv_{AUX}} * \cos(\theta_{AUX})} \tag{3.11}$$

Where,
$P_{AUX_{DCSB}}$ = DC auxiliary power required at switchboard [W]
$\eta_{Inv_{AUX}}$ = DC auxiliary inverter efficiency

$$P_{P_{DCSBWL}}[W] = \frac{\left(\frac{P_P}{N_P}\right)[W]}{\eta_{Motor} * \eta_{Inv_{Motor}} * \cos(\theta_{Motor})} \tag{3.12}$$

Where,
$P_{P_{DCSBWL}}$ = DC propulsion power required at switchboard without cable losses per propeller drive [W]
$\eta_{Inv_{Motor}}$ = Inverter efficiency connected to motor

This section provided the electrical power for AC and DC grid for its auxiliary power as well as propulsion power. However, the cable power losses and sizing is taken into account and is addressed in subsection 3.3.1.

3.3.1. Cable sizing and losses

The cable sizing is done as per the IEC [53]. The commercially available cable is used along with the derating factors provided in the datasheet. For AC and BiDC grids, the rated load demand along with the losses is used to calculate the design current for the system working at the operating voltage. The total number of cables, with their cross-section, was determined by taking into account the design current with a safety factor. The current flowing through the cables is estimated along with the resistance for a 25^{o} C temperature rise. Consequently, the power losses are calculated. Finally, the electrical power at the switchboard is estimated taking into account the component efficiencies, and cable losses for the main propulsion drives and component efficiencies for auxiliary loads. The detailed procedure for AC and BiDC grids is explained below.

AC Grid

The design current is calculated using the rated power of the motor, the line-to-line voltage, motor efficiency, VFD efficiency and the reactive power losses. The efficiency of the three-winding transformer is not taken into consideration, as the cabling after the transformer is considered in this study. The cabling for the auxiliary load is also not taken into account, as the transformer in AC and inverter in DC are assumed to be installed in the switchboard leading to the marginal cable run. The Equation 3.13 is used to estimate the design load current for an AC grid operating at V_{AC} V.

$$I_{B_{AC}}[A] = \frac{P_{Motor}[W]}{\sqrt{3} * V_{AC}[V] * \eta_{Motor} * \eta_{VFD} * \cos(\theta_{Motor})} \tag{3.13}$$

Where,
$I_{B_{AC}}$ = AC design current [A]
P_{Motor} = Rated power of the motor [W]
V_{AC} = AC voltage line to line [V]

The installation of the cable and environment affect the current carrying capacity of the cable. These factors are quantified in IEC [53] standard. Commercial marine cable manufacturers for electrical power applications provide the current carrying capacity of their cable type for derating factors for a particular cross-section of the cable. The cables with higher cross-sections have higher current carrying capacity and vice versa. In an AC grid, the cables consist of three conductors per phase, this is done to minimise the self-induction losses between them. The Figure 3.4 showcases the cross-section of the cable used in this study. Also, the design current ($I_{B_{AC}}$) is the maximum current required for continuous operation. However, the cables are required to withstand the short-circuit current that flows through the cables in case of fault. According to Bussmann [16], the magnitude of short-circuit current flowing through the induction motor in case of fault is around 4 to 6 times the design current. However, circuit breakers react in ms to a fault. Therefore, the design current value is taken with a safety factor to determine the number of cables. In this study, the safety factor is taken at 20 per cent. The number of cables required can be determined as per the Equation 3.14. The marine cable catalogue provides data for the current carrying capacity of cable with their respective cross-sections. Therefore, the cable size and number can be determined.

Figure 3.4: The cross-section of a marine cable used in this study. It consists of three wires per phase made up of annealed copper strands protected by XLPE insulation. The outermost insulation is also made of XLPE insulation as well [46].

$$NC_{AC} = \frac{1.2 * I_{B_{AC}}[A]}{I_{CAP_{AC}}[A]} \tag{3.14}$$

Where,
NC_{AC} = AC number of cables
$I_{CAP_{AC}}$ = AC current carrying capacity of the cable [A]

The number of cables (NC_{AC}) is rounded up to the closest integer. The voltage drop for starting and short-circuit conditions is calculated according to the values specified in the marine cable catalogue. The per cent drop in voltage must be below 3 per cent and 10 per cent of continuous and short circuit conditions [54].

The current flowing through the cables can be calculated based on the power requirements of the motor. These requirements are estimated in section 3.1 and section 3.3. The Equation 3.15 estimates the current flowing through the cables during operational conditions. I_{AC} is required to be less than over equal to the $1.2 * I_{B_{AC}}$ value, as the latter current value is for the conservative design conditions.

$$I_{AC}[A] = \frac{\left(\frac{P_P}{N_P}\right)[W]}{\sqrt{3} * V_{AC}[V] * \eta_{Motor} * \eta_{VFD} * \cos(\theta_{Motor})} \tag{3.15}$$

Where,
I_{AC} = Current flowing through the cables during operation on AC grid [A]

The XLPE insulation temperature limit is 90° C. Therefore, the cable losses are calculated for 25° C temperature rise. The resistance per meter of the cable at + 25° C is calculated according to the equation described in Equation 3.16. This equation takes the value of resistance per meter at ambient temperature and estimates the resistance at any other temperature. The ambient resistance values are taken from the catalogue and differ for different cable sizing taken into account from Equation 3.14. The length of the cable is also used in calculating the resistance and is assumed to be equal for AC and DC grids.

$$R_{AC}(T_R)[\Omega] = L_{SB2M}[m] * (R_{0AC}[\Omega/m] * (1 + \beta[1/K] * (T_R[K] - T_0[K]))) \tag{3.16}$$

Where,
$R_{AC}(T_R)$ = Resistance per meter at temperature T_R for AC $[\Omega/m]$
R_{0AC} = Ambient resistance per meter for AC $[\Omega/m]$
β = Temperature coefficient of resistance $[1/K]$
T_R = Temperature at which the resistance is computed [K]
T_0 = Ambient temperature [K]
L_{SB2M} = Length of cable between switchboard and motor

Finally, the cable losses can be estimated during the operation of the ship. The losses can be calculated as shown in Equation 3.17.

$$P_{AC_{losses}}[W] = I_{AC}^2[A^2] * R_{AC}[\Omega] \tag{3.17}$$

Where,
$P_{AC_{losses}}$ = AC cable losses during operation [W]

The total electrical power requirement for the AC microgrid taking into consideration all the components between the switchboard and the auxiliary loads and induction motor with their efficiency values as well as the cable losses that incur during the power flow is given in Equation 3.18.

$$P_{R_{AC}}[W] = N_P * P_{AC_{losses}}[W] + N_P * P_{P_{ACSBWL}}[W] + P_{AUX_{ACSB}}[W] \tag{3.18}$$

Where,
$P_{R_{AC}}$ = Total electrical power for AC grid at the switchboard [W]
$P_{P_{ACSBWL}}$ = AC propulsion power required at switchboard without cable losses [W]
$P_{AUX_{ACSB}}$ = AC auxiliary power required at switchboard [W]

BiDC Grid

The procedure for cable sizing and losses remains the same for the BiDC grid. First, the design current is estimated according to the Equation 3.19. The operating voltage of the BiDC grid is the voltage rating between the positive and the negative pole of the grid and is taken as V_{DC}. The formula is as follows: -

$$I_{B_{DC}}[A] = \frac{P_{Motor}[W]}{V_{DC}[V] * \eta_{Motor} * \eta_{Inv_{Motor}} * \cos(\theta_{Motor})} \tag{3.19}$$

Where,
$I_{B_{DC}}$ = DC design current [A]
V_{DC} = DC voltage between positive and negative poles [V]

Consequently, the number of cables can be determined using a similar design methodology used for the AC grid. The construction of the cable remains the same where per-phase conductors in the cable act as positive, negative and neutral poles of the BiDC grid. The required cross-section of the cable with its current rating is computed as shown in Equation 3.20. The current rating of the cable in the catalogue already constitutes the effect derating factor.

$$NC_{DC} = \frac{1.2 * I_{B_{DC}}[A]}{I_{CAP_{DC}}[A]} \tag{3.20}$$

Where,
NC_{DC} = DC number of cables
$I_{B_{DC}}$ = DC design current [A]
$I_{CAP_{DC}}$ = DC current carrying capacity of the cable [A]

The current flowing through the cable during operation is calculated using the power estimated in section 3.1 and section 3.3. The mechanical power requirements remain the same for both the AC and BiDC grid, and the current flowing through the cables is calculated as shown in Equation 3.21.

$$I_{DC}[A] = \frac{\left(\frac{P_P}{N_P}\right)[W]}{V_{DC}[V] * \eta_{Motor} * \eta_{INV_{Motor}} * \cos(\theta_{Motor})} \tag{3.21}$$

Where,
I_{DC} = Current flowing through the cables during operation [A]

The resistance per meter for the cable cross-section can be found in the catalogue of Prysmian Group [102]. The XLPE insulation can withstand temperatures up to 90^{o} C. However, the resistance is calculated for the 25 ^{o} C temperature rise. This resistance value is further used in estimating the cable losses observed in the BiDC grid. The Equation 3.22 highlights the formula to estimate the resistance value.

$$R_{DC}(T_R)[\Omega] = L_{SB2M}[m] * (R_{0DC}[\Omega/m] * (1 + \beta[\Omega/mK] * (T_R[K] - T_0[K]))) \tag{3.22}$$

Where,
$R_{DC}(T_R)$ = Resistance per meter at temperature T_R for DC $[\Omega/m]$
R_{0DC} = Ambient resistance per meter for DC $[\Omega/m]$
T_R = Temperature at which the resistance is computed [K]

Finally, the cable losses can be estimated during the operation of the ship. The losses can be calculated as shown in Equation 3.23.

$$P_{DC_{losses}}[W] = I_{DC}^2[A^2] * R_{DC}[\Omega] \tag{3.23}$$

Where,
$P_{DC_{losses}}$ = DC cable losses during operation [W]

The total electrical power requirement for the DC microgrid taking into consideration all the components between the switchboard and the auxiliary loads and induction motor with their efficiency values as well as the cable losses that incur during the power flow is given in Equation 3.24.

$$P_{R_{DC}}[W] = N_P * P_{DC_{losses}}[W] + N_P * P_{P_{DCSBWL}}[W] + P_{AUX_{DCSB}}[W] \tag{3.24}$$

Where,
$P_{R_{DC}}$ = Total electrical power for DC grid at the switchboard [W]
$P_{P_{DCSBWL}}$ = DC propulsion power required at switchboard without cable losses [W]
$P_{AUX_{DCSB}}$ = DC auxiliary power required at switchboard [W]

The Equation 3.18 and Equation 3.24 provide the total electrical power at the switchboard for AC and BiDC grids. This provides the power demand for the power balancing constraint that is formulated during the optimization problem formulation for respective grid architectures in section 4.4. The weights for the cables can also be estimated from the cable catalogue of Prysmian Group [102] and used in system weight estimation.

3.4. Summary

This chapter was aimed at developing the ship's power profile. Subsequently, the section 3.1 describes the methodology to develop the mechanical power required for the ship. The knowledge from chapter 2 was used to develop an electrical layout for the ship for both AC and BiDC architectures. The electrical layout for all ten arrangements was presented in section 3.2. Furthermore, from this understanding, the electrical power estimation was done considering the efficiency values of the electrical components that make up the respective grid in section 3.3. The cable losses and sizing are also presented in this section by using industry-available marine power cables.

4

Optimisation Problem Formulation

In this chapter, the optimization problem is formulated for all ten arrangements. The section 4.1 highlights the different types of optimizations. Further, the literature related to the optimization for a shipboard microgrid is reviewed, and the research gap is highlighted in section 4.2. Consequently, the practical considerations based on the knowledge acquired from chapter 2, section 4.1 and section 4.2 are highlighted in section 4.3. The Specific Fuel Oil Consumption (SFOC) of a diesel generator is modelled as a function of loading (load factor) and the model for fixed speed and variable speed operation is developed, leading to formulating the optimization problem for all ten arrangements in section 4.4.

4.1. Optimisation Problem Types

The optimization process refers to finding the optimal solution (maximum/minimum) for your objective, taking into account the restrictions that are placed on it. Every optimization problem is made up of three main components, the objective function (f(x)) that defines a mathematical relation for a parameter that has to be minimised, the decision variables (x) that take into account the feasible region defined by the constraints to take values that affect the objective function and the constraints (g(x)) that define a feasible region for the decision variables to take values from and evaluate the minimum/maximum objective value. The mathematical representation of a typical optimization problem is shown in Equation 4.1 highlighting the three components that are used to formulate an optimization problem.

$$\begin{array}{lcll} Obj.\,function & :- & min./max. & f(x_i) \\ Decision\ variables & :- & x_i & i \in [1,2,3,4,5] \\ s.t\ Constraint & :- & g_j(x_i) \leq 0 & i \in [1,2] \\ s.t\ Bounds & :- & x_i \geq 0 & i \in [1,2,3,4,5] \end{array} \tag{4.1}$$

The Figure 4.1 highlights the different types of optimization problems. The broader overview of these optimization types is given in Hillier and Lieberman [44]. The linear programming (LP) optimization problem consists of linear objective functions as well as linear constraints to establish a feasible region. In non-linear optimization problem formulations, the objective function and/or the constraints formulated are non-linear. In both the previous two types (LP and NLP), the decision variables are allowed to take real values. However, in mixed integer linear programming (MILP) and mixed integer non-linear programming (MINLP), some decision variables are restricted to take integer values. For an optimization problem, the decision variables can have either continuous, integer or Binary (Integer but limited to 0 and 1). The respective constraints on the objective function and/or constraints from the linear programming and non-linear programming problems apply to mixed integer linear programming and mixed integer non-linear programming, respectively. There are numerous techniques to solve these optimization problem formulations types like Branch and Bound (BAB), Genetic Algorithm (GA), and Particle Swarm Optimization (PSO). In this study, the Matlab's® in-built function, 'fmincon' is used.

The ‘fmincon’ is used to solve dynamically constrained non-linear optimization problems. The ‘interior point method’ is an optimization technique used in our optimization problem to find the optimum solution for the objective function.

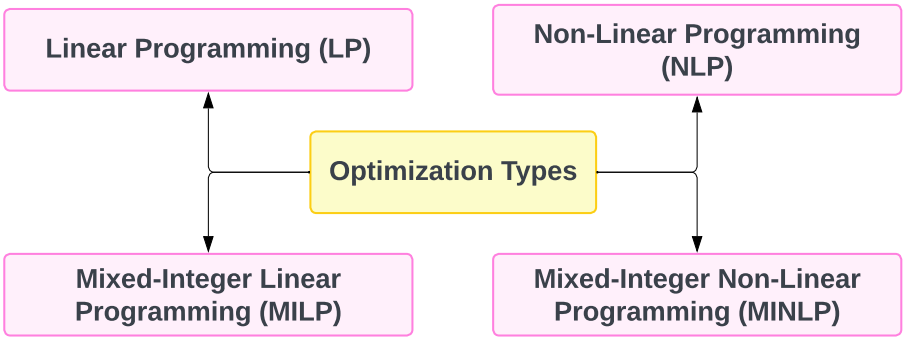

Figure 4.1: The types of optimization problems

4.2. Optimization in Academic Literature

The section 4.1 highlighted the different optimization types present. These optimization types depend upon the optimization problem formulations for the objective function and constraints. This section is going to present the work done in the past on energy management for the shipboard grids. Various power production sources, batteries as well as different propulsion types have been worked on in the literature. However, the hybrid propulsion type and its literature are presented as it is the most commonly used type of propulsion for ferries, platform supply vessels, etc. as highlighted in section 2.2. Consequently, studies with only diesel generators and batteries are included in the literature. These studies are presented below. Similar work has also been done in Lan et al. [77], Wu and Bucknall [132], Pivetta, Dall’Armi, and Taccani [99], Wang et al. [129], Pourrahmani et al. [101], Vieira et al. [126], Luna et al. [79], Rafiei, Boudjadar, and Khooban [105], Banaei et al. [8], and Han, Charpentier, and Tang [37] but is not considered in this thesis as they differ in the sources of power production. These papers also include renewable technologies and fuel cells in optimization for the propulsion system. The work on optimal sizing of energy storage systems (ESS) for shipboard applications is also presented in Barrera-Cardenas, Mo, and Guidi [10], Tjandra et al. [119], Boveri et al. [14], and Divyajot, Kumar, and Fozdar [28] and falls beyond the scope of this thesis.

Mashayekh et al. [86] performed an optimal generation dispatch problem for a ferry operating between Nanaimo and Vancouver. The study conducted optimization taking into account different battery sizes. The problem was formulated on Matlab® and solved using the inbuilt function *fmincon*. The unit commitment problem was solved first (generator on/off states) before solving the optimal dispatch problem. The generators were forcefully turned off when they reached the shore. The constraints on generator limits were only applicable if the generator was on. Other constraints like the ramping limit on the generator, battery energy storage limit, and dynamic constraint for energy storage were implemented in this work. This paper failed to evaluate and incorporate the cable losses, and efficiencies of the components that make up the grid as well as the battery efficiency, the battery power limits were not included in this work. Finally, the shore power constraints were also not included in this study. However, a fuel consumption model for the diesel generator was modelled as a quadratic function, which is similar to the reality of generators operating at fixed rpm in AC grids. Also, a transient penalty function was added to avoid load fluctuations on the generator, forcing the battery to fulfil these load transients. The objective of this study was to minimize the total generation costs as well as find the optimal battery capacity such that it is not oversized. The preliminary economic analysis was done to determine the optimum energy storage size over the lifetime of the ship. The paper also concluded that the optimum size for energy storage highly depends on the operational profile of the ship.

Kanellos [69] has proposed a three-stage optimization problem for minimizing the operational costs of a cruise ferry. The first two stages are solved using Dynamic Programming Optimization (DPO) while the third stage was solved using Particle Swarm Optimization (PSO). The problem is formulated to optimize the ship's operating costs, taking into account the velocity constraints of the ships. The paper also incorporates the velocity with the propulsion power needed to maintain that velocity along with constraints on generator operating limits, generator ramping limits, and battery storage limits as well as the power delivered by the battery during charging and discharging. The paper also includes the constraints on blackout prevention and minimum time for the generator off-state. As the six generators that provide power to the ship are free to turn on and off to converge to a globally optimum solution. The optimization problem solves the unit commitment and optimal dispatch problem simultaneously. A constraint on the emission of CO_2 is included as EEOI, an energy efficiency metric that is explained in section 2.1. This constraint limits the grams of CO_2 emitted to transport a tonne of cargo for a nautical mile. The work optimizes the ship's speed to counter the emissions from the ships. Wang and Meng [127] highlights that sailing speed reduction also known as slow steaming can reduce fuel consumption leading to emission reduction. The results highlight the reduction in operational costs of using battery storage and propulsion adjustments.

Shang, Srinivasan, and Reindl [110] has formulated a multi-objective optimization problem with two objectives namely, the operational cost and the energy-efficient cargo transport as formulated in EEOI. The EEOI is used to quantify the CO_2 emissions observed throughout the particular journey, to quantify it. The optimization includes diesel generators that operate within the specified limits of the DG or can be completely turned off. The paper also includes constraints for minimum generator off time. The ESS has operational constraints along with the maximum and minimum power that the ESS can deliver in the power balance of the ship at every load step of the optimization. The distance constraint and sailing speed constraints are included to optimize the voyage for minimizing the costs and emissions. The charging and discharging efficiencies are formulated as well. Although the paper performs optimization on a conceptualised vessel speed profile, the electrical parameters like the converter losses and the cable losses are not taken into consideration in this study. The two case simulations consisting of four and six DGs respectively with different energy capacities of ESS are performed using the optimization formulation. The results showcase a reduction in fuel costs as well as emissions on joint generation voyage scheduling that is integrated with ESS as compared to fixed voyage scheduling with DGs alone. The degree of reduction in emissions is dependent on the energy capacity of the ESS.

Skjong et al. [112] formulated a mixed integer linear programming (MILP) optimization problem to minimize the emissions for electric ships. The paper also proposes a logic-based algorithm for energy management systems. The comparison of these two approaches is done on three configurations for a ferry, a platform supply vessel and a seismic research vessel. The configurations are four fixed-speed DGs, three fixed-speed DGs and one variable-speed DG and finally, four fixed-speed DGs and energy storage systems. This paper has used the real data obtained from the ships used in this study, as well as the fuel consumption data points for the diesel generator. As the generator can switch on and off, the problem simultaneously solves unit commitment and optimal dispatch problems. The constraints taken into account are the power balance of the microgrid, the generator power limits, the battery power limits and the energy capacity limits for it. The research gap that is not addressed in this work is the cable losses that occur during power distribution. Also, the converter efficiency is not taken into account. The shore power is not considered as well. The work is performed on the AC grid only, and a comparison for the DC grid is missing. These constraints are for the MILP approach used for energy management systems. The results for ferry indicate a marginal difference in optimised solution for all configurations for both EMS approaches. Both approaches indicate a 10.2 per cent reduction in emissions for four DG and an ESS configuration. The results for the PSV indicate a similar trend, with the same configuration resulting in a 12.6 per cent reduction in emissions for both energy management approaches. Finally, the seismic survey vessel also showed a reduction in emissions for the configuration with four DGs and ESS. The emissions were reduced by 10.3 per cent for both the MILP and logic-based approaches for energy management systems. The variable speed operation of the diesel generator assisted in reducing the emissions, but the extent of reduction was highest for a configuration with an energy storage system.

Boveri et al. [15] has solved a sizing problem for a cruise ship operating on AC grid architecture. The

work highlights two approaches to sizing a propulsion system on large vessels. They are deterministic and probabilistic approaches. The deterministic approach is based on load factor analysis, load data from similar ships or carrying out detailed field measurements. This approach is direct but can result in oversizing as a result of conservative design methodology used during the design and sizing of generator sizes. The stochastic approach takes into account a probability distribution function for every load that will be present on the ship, and a cumulative probability distribution is calculated. This research takes account of these two approaches and optimizes installation and management costs for the generator sizing. The four different simulations considered are homogenous sizing of generators with a deterministic approach, heterogenous sizing of generators with a deterministic approach, homogeneous sizing of generators with a stochastic approach and finally, heterogeneous sizing of generators with a stochastic approach. The constraints that are considered are the power balance, generator power limits and reserve capacity constraints. The constraints for cable losses, generator efficiency, converter efficiency, and the comparison between AC and DC grids are not implemented in this work. Finally, the results show a reduction in sizing for the generators in stochastic sizing with homogenous generators the most with 36.5 per cent in costs whereas 25.6 per cent in installed power. Therefore, this work highlights the stochastic approach of sizing to be cost-effective however, field measurements are needed to validate the results.

Valera-Garcia and Atutxa-Lekue [123] has formulated a multi-objective optimization problem to generate a Pareto set for the objective function. The objectives considered were the minimization of ESS size, ESS energy consumption as well as the minimization of fuel consumption. The DG model for fuel consumption estimation was a polynomial function. The optimization is performed for a small portion of the total mission profile of the offshore supply vessel. A non-real simplified load profile is developed for this study. The two power distributions are operated at 690 V_{AC} 60Hz and 1100 V_{DC}. For AC the gen sets are operating at fixed speed whereas variable speed operation is considered in DC distribution. The following optimization was performed in Matlab® using NSGA-II and the fuel consumption results showed a 14 per cent reduction in DC distribution as compared with the AC topology when no ESS is used for both cases. In addition to this, the same load profile was used to evaluate the AC topology with ESS. The spinning reserve constraint used in this study restricted the switching off of gen sets. However, In the case of ESS, the gen-sets were turned off to satisfy the spinning reserve constraint as well as reduce the fuel consumption. The fuel consumption reduction offered with ESS on board on AC distribution was found to be as competitive as the DC distribution. The constraints considered in this research were the generator ramp rate, power balance, converter efficiency, comparison for AC and DC grid topology and most importantly the spinning reserve constraint. However, the cable losses, battery efficiency the dynamic constraint on the battery are not considered.

Zaccone, Campora, and Martelli [139] has researched minimizing the emissions for a pleasure craft. The AC and DC grids are compared with different capacities for design and off-design conditions. The constraints used for the optimization problem formulation are power balance, the limits on the generator, comparison between AC and DC grids with fixed speed and variable speed operation. The generator rpm and loading on the DG are used to estimate the SFOC from the lookup table for the fuel consumption. The switch on and off of generators is also included in this research, and the effect of this on AC and DC grid operation is also studied. The cable losses and converter efficiencies are not considered. The results show that the variable speed operation allows the DG to operate at optimal fuel consumption point as compared to fixed speed operation. From the different sizes of engines available, the biggest sizes are selected as an optimum as they are more efficient at the design conditions. For the off-design conditions, two approaches are studied, one with equal load sharing and the other with unequal load sharing. For equal load sharing, the variable speed operation offered better fuel consumption compared to fixed speed. For unequal load sharing, it was observed that the first DG offered more stable behaviour, with the next DGs speeding up and contributing to the increasing load demand. The fuel consumption study highlights that the DC system has proven to be more fuel-saving at lower speed/load operations.

Table 4.1: Summary of optimization for energy management for hybrid/electric ships

Work	Grid and Ship type	Objective	Algorithms		DG Fuel Model	Constraints	Research Gap
			Component Sizing	Energy management			
[86]	AC grid on Ferry	Single Min. Generation cost.	MATLAB® *fmincon*		Quadratic	Generator power limits, Generator ramp rate, Battery storage limits, Dynamic constraint on battery, Power balance, Solving for optimal dispatch alone.	Cable losses, Battery efficiency, Converter efficiencies, Battery power limits, No comparison between AC and DC, Shore power, Solving UC problem.
[69]	AC grid on Cruise-Ferry	Single Min. Operational cost.	✗	PSO + DP	Quadratic	Generator power limits, Generator ramp rate, Generator loading constraint, Battery storage and power limits, Dynamic constraint on battery, Power balance, EEOI constraint, Black out prevention constraint, Velocity constraint, Distance travelled, Solving for OD and UC.	Cable losses, Battery efficiency, Converter efficiencies, No comparison between AC and DC, Shore power.
[110]	AC grid on Cruise ship	Multi. Emissions and Operational cost.	✗	NSGA-II	Not Included, taken in monetary unit	Distance constraint, Sailing speed constraint, Power balance, Generator power limits, Generator ramp rate, Reserve capacity, Battery efficiency, Battery power and energy limits, Initial and final SoC limits, Dynamic constraint on battery, Solving for OD and UC.	Cable losses, converter efficiency, No comparison between AC and DC, Shore power.
[112]	AC grid on Ferry, Platform supply vessel, Seismic survey vessel	Single Min. Emissions	✗	MILP	Real data point from genset supplier	Power balance, Generator power limits, Battery energy and power limits, Solving for OD and UC.	Cable losses, Converter efficiency, Battery efficiency, No Comparison between AC and DC, Shore power.
[15]	AC grid on Cruise ship	Single Min. Installation and management cost.	GA	✗	Polynomial	Generator power limits, Reserve capacity, Power balance	Cable losses, Converter efficiency, No comparison between AC and DC, Shore power.
[123]	AC and DC grid on PSV	Multi. Min. fuel consumption ESS energy consumption and ESS size	NSGA-II		Polynomial	Generator ramp rate. Power balance, Reserve capacity, Battery power and SoC limits Converter efficiency, Comparison between AC and DC	Cable losses, Battery efficiency, Shore power, Dynamic constraints on battery, Generator power limits
[139]	AC and DC grid on Pleasure craft	Single Min. Emissions	✗	MATLAB® *GA*	Engine load diagram (Lookup table)	Generator rpm, Generator power limits Power balance, Comparison between AC and DC, converter efficiency, Solving for OD and UC.	Shore power, Cable losses.
[95]	DC grid on Ferry	Single Min. Fuel consumption	✗	MINLP	Real data point from genset supplier	Power balance, Generator power limits, HSG power limits, Shore power limits, Battery power and energy constraints, Initial and Final SoC, SoC limits.	Cable losses, Converter efficiency, Battery efficiency, No comparison between AC and DC
This thesis	AC and BiDC grid on Ferry	Single Min. CO_2 Emissions	✗	MATLAB® *fmincon*	Quadratic & Linear	Generator power limits, Battery storage and power constraints, Dynamic constraint on Battery, Power balance, Cable losses, Battery efficiency, Initial and Final, SoC limits, converter efficiency, Shore power, Equal power generation, Comparison between AC and DC grid.	Solving UC problem

Oo et al. [95] performed a sizing and energy management study on a ferry with shaft generators. The vessel is considered to be operating on DC-bus architecture. The hybrid shaft generators can provide power from the battery as well as during low power demand to operate and serve to charge the battery for future use. The propellers are connected to the diesel engine and an alternator through a gearbox. The optimization is formulated as an MINLP with an energy management algorithm with initialization to fulfil the battery recharging requirements. The constraints considered in this research were the minimum and maximum power limits on the diesel engine and the alternators, the power balance constraint, shore power limits, battery power and energy constraints, the SoC limits and the initial and final SoC requirements. The main finding from this study highlighted the importance of shore infrastructure in reducing fuel consumption and therefore the emissions from diesel engines. The larger battery capacity also significantly contributed to minimizing fuel consumption. Finally, the constraints that were not incorporated in this study are the cable losses, converter efficiency, the battery efficiency.

Research Gap

The studies in the literature have incorporated the batteries in the optimization problem. These researchers have initialised the battery in the problem formulation with high energy storage. Therefore, the use of battery energy has proven to be a significant factor to reduce emissions. The battery has to be recharged, and the power for this charging is not incorporated in most studies, nor the emissions that occur in doing so. The cable losses that occur in power transmission and the component efficiency on the power production, distribution, and consumption side are not fully considered. The comparative study on the AC and DC grid topologies for the worst-case scenarios is necessary to estimate the feasibility of the BiDC grids on ships. This worst-case scenario is a ship that travels at its optimal speed for most of the duration, i.e. a Ferry. The qualitative advantages of variable speed operation over fixed speed operation of a diesel generator are known, and they provide significant emission and fuel consumption reductions as a result of it. One such mode of operation is the dynamic positioning mode in PSVs. The mixed integer formulation is also not a worst-case scenario because the switched-off engine is not going to produce any emissions and the use of energy from the battery will conclude a reduction in emissions, although the recharging of the battery is necessary to consider. Therefore, the ship in this thesis was considered to be a ferry, with initial and final SoC values incorporating the emissions from the recharging of the battery. This recharging can occur with the help of gen sets when the ferry is in port where the propulsion requirements are none, or with the supply of electrical power from shore infrastructure. This was done to estimate the feasibility of the BiDC grid and the total emission reductions that can be realised over the ship's operational profile.

4.3. Practical Considerations of Problem Formulation

After introducing the background required in chapter 2 and presenting the research that has been done so far in section 4.2. This section will establish the practical considerations taken into account for carrying out this work. The following considerations were taken into account:-

1. The diesel generator included in the dataset should compel to tier III NO_x emission standards. The regulations are represented in subsection 2.1.1.

2. The diesel generator included in the dataset should run on low sulphur fuels as per the regulation mentioned in subsection 2.1.2 i.e. the diesel generators should oblige to the tier III regulations. The list of the dataset is shown in Appendix A.

3. The batteries are catalogued from various manufacturers and are shown in Appendix A. The batteries are catalogued only if they are used in marine applications.

4. The diesel generators are kept on during the whole operation for AC1, AC2, AC4 and DC1, DC2, and DC4. This is done because of the grid-forming nature of these diesel generators in AC as well as BiDC grids.

5. The diesel generators are turned off for arrangements AC3, AC5, DC3, and DC5 when the ship reaches the shore and the shore infrastructure provides the required energy demand.

6. The shore power i.e. the necessary infrastructure included in the optimization for arrangements AC3, AC5, DC3, and DC5 is assumed to be available at the ports at which the ship operates. Cavotec [19, 20] provides the required technical and operational details for shore power to include in the problem formulation.

7. The average efficiency values for electronic and electrical components are assumed.

8. The DC power electronics components are not commercially available for MVDC systems [42, 92]. Therefore, it limits our work to ships that can operate on LVDC power systems.

9. According to IEEE STD 45.1, LVAC and LVDC can only be used when the total generation capacity is not greater than 4MW [56]. This limits our work to ferries, yachts, platform supply vessels (PSVs), etc.

10. The propulsion architecture used in this study is a series hybrid propulsion system. This is because the ships that operate on LVAC and LVDC have this type of propulsion system to be found in common [76].

11. The State of Charge (SoC) estimation is done using coulomb counting and does not take into account the electrochemical behaviour of the battery. The battery degradation model is not incorporated in the problem formulation.

12. The diesel generators have quick response and reach maximum continuous rating within a minute as described in subsection 2.4.1. Figure 2.10 also shows the load transients and the time taken to reach steady-state. Therefore, the ramping constraints on the diesel generators are not taken into consideration in forming our optimization problem.

13. The fixed-speed diesel generator also operates within the same operating range as a variable-speed diesel generator shown in Figure 2.11.

14. The charging and discharging of the battery occur at constant power. Therefore, the change in voltage in batteries while charging and discharging is compensated by appropriate current flow.

4.4. Problem Formulation

The previous sections highlighted the different optimization types in section 4.1, the research done on different energy management systems on shipboard microgrids is explained in section 4.2, the electrical layout was finalized in section 3.2 and the electrical power requirements at the switchboard were evaluated from the mechanical power estimated from section 3.1 in section 3.3. Consequently, cable losses for AC, as well as DC, are evaluated. The practical considerations made in section 4.3 are used to formulate the optimization problem in this section. The decision variable for each arrangement, with the objective function to be minimised and the constraints that apply to that specific arrangement, are formulated in this section. The overview of the optimization methodology is presented in Figure 4.2.

The optimization formulation uses the electrical power estimated for AC and BiDC grid from section 3.3, depending upon the arrangement for which the optimization is carried out. The data set for diesel generators and batteries is described in Appendix A. The algorithm, developed, starts with the first diesel generator and battery bank available in the catalogue. Furthermore, for that specific configuration, the optimal dispatch problem is solved to find a feasible solution. If an optimum solution is found, the results are stored. If the configuration is insufficient to provide a feasible solution, the next battery bank from the catalogue created is selected until the battery data set is exhausted. Consequently, the next diesel generator is chosen, and the process continues by selecting the first battery bank from the catalogue. Finally, as the feasible solution for all diesel generators and battery bank configurations is completed, the results are plotted for each arrangement. These results consist of power profiles for each configuration for which a feasible solution exists and an SoC plot along with the range of emissions for all feasible configurations for that particular arrangement.

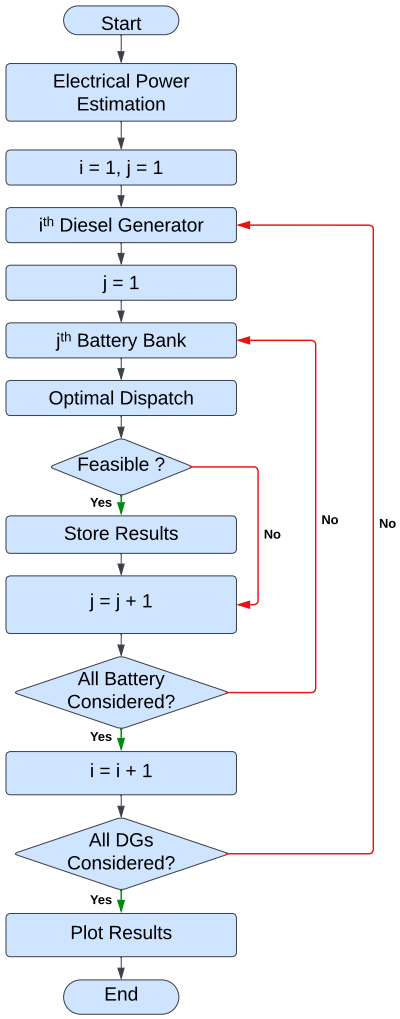

Figure 4.2: Optimization methodology

Decision variables

Equation 4.2 describes the decision variables for each arrangement. The arrangements are described in Table 3.2. The ferry operates with a total voyage time assumed to be of T hours. This total time can be divided into T_V, time to reach port B from port A and T_S time spent in the port. The latter time is the time required to unload and load cars, and people, onto the ship. The former is the travel time between ports. For the arrangements with shore power, the diesel generator is turned off and the shore power is said to satisfy the electrical demand of the ship. By quantifying the on and off state of the generator, the unit commitment problem is solved before the optimal dispatch problem.

$$
Arrangement \begin{cases} AC1, DC1 & : & P_{DG1}(t),\ P_{DG2}(t) & \forall t \in T \\ AC2, DC2 & : & P_{DG1}(t),\ P_{DG2}(t),\ P_{Dis}(t),\ P_{Ch}(t),\ SoC(t) & \forall t \in T \\ AC3, DC3 & : & \begin{cases} P_{DG1}(t),\ P_{DG2}(t) & \forall t \in T_V \\ P_{Sh}(t) & \forall t \in T_S \\ P_{Dis}(t),\ P_{Ch}(t),\ SoC(t) & \forall t \in T \end{cases} \\ AC4, DC4 & : & P_{DG1}(t),\ P_{Dis}(t),\ P_{Ch}(t),\ SoC(t) & \forall t \in T \\ AC5, DC5 & : & \begin{cases} P_{DG1}(t) & \forall t \in T_V \\ P_{Sh}(t) & \forall t \in T_S \\ P_{Dis}(t),\ P_{Ch}(t),\ SoC(t) & \forall t \in T \end{cases} \end{cases} \tag{4.2}
$$

Where,
t = Time [min]
T = Total voyage time [min]
T_S = Time spent at the shore [min]
T_V = Travel time between ports [min]
$P_{DG1}(t)$= Power delivered by diesel generator 1 [W]
$P_{DG2}(t)$= Power delivered by diesel generator 2 [W]
$P_{Dis}(t)$= Discharging power delivered by battery [W]
$P_{Ch}(t)$= Charging power delivered by battery [W]
$P_{Sh}(t)$= Power delivered from the shore [W]
$SoC(t)$ = State of charge of battery [-]

The arrangements considered in this study are presented in Table 3.2. The AC1 and DC1 arrangements are not included in the optimization problem, as other decision variables are absent. The diesel generator from the catalogue is selected only if the condition in Equation 4.3 is satisfied. Once the diesel generator is selected from the catalogue, only two constraints are active, and using these the emissions for arrangement AC1 and DC1 can be estimated. These constraints are defined in Equation 4.9 and Equation 4.10.

$$\begin{aligned} AC1 \quad &: \quad P_{DGRated} * \eta_{gen} \quad \geq \frac{Max(P_{R_{AC}})}{N_G} \\ DC1 \quad &: \quad P_{DGRated} * \eta_{gen} * \eta_{BiDC} \quad \geq \frac{Max(P_{R_{AC}})}{N_G} \end{aligned} \tag{4.3}$$

Where,
$P_{DGRated}$ = Rated power of diesel generator [W]
η_{gen} = Efficiency of generator [-]
η_{BiDC} = Efficiency of rectifier connected with the diesel generator
$Max(P_{R_{AC}})$ = Maximum power requirement in AC grid [W]
$Max(P_{R_{DC}})$ = Maximum power requirement in DC grid [W]
N_G = Number of diesel generators [-]

The emissions from the operation of the ship from point A to point B are to be minimised. The arrangements AC1 and DC1 are straightforward and do not require any optimization, since they do not have other decision variables that can affect the emissions from the operation of the ship over the duration of travel. The diesel generators follow the load changes with time and supply the necessary power to the switchboard. These emissions are directly related to the fuel consumption of the diesel generator that is dependent on the Load Factor (LF_t) of the diesel generator. The Load Factor (LF_t) can be defined as the ratio of the delivered power at a particular time divided by the rated power of the diesel generator. Consequently, the emissions from the operation of the ship for AC1 and DC1 can be estimated as shown in Equation 4.4.

$$\begin{aligned} E_{AC1} \quad = \quad & \left\{ \begin{array}{l} \sum_{t=1}^{T} \left(P_{DG1}(t)[kW] * \Delta t[h] * EF_{CO2} \left[\frac{g_{CO2}}{g_{Fuel}}\right] * SFOC_{AC}(LF_t) \left[\frac{g_{Fuel}}{kWh}\right] \right) \\ + \sum_{t=1}^{T} \left(P_{DG2}(t)[kW] * \Delta t[h] * EF_{CO2} \left[\frac{g_{CO2}}{g_{Fuel}}\right] * SFOC_{AC}(LF_t) \left[\frac{g_{Fuel}}{kWh}\right] \right) \end{array} \right. \\ E_{DC1} \quad = \quad & \left\{ \begin{array}{l} \sum_{t=1}^{T} \left(P_{DG1}(t)[kW] * \Delta t[h] * EF_{CO2} \left[\frac{g_{CO2}}{g_{Fuel}}\right] * SFOC_{DC}(LF_t) \left[\frac{g_{Fuel}}{kWh}\right] \right) \\ + \sum_{t=1}^{T} \left(P_{DG2}(t)[kW] * \Delta t[h] * EF_{CO2} \left[\frac{g_{CO2}}{g_{Fuel}}\right] * SFOC_{DC}(LF_t) \left[\frac{g_{Fuel}}{kWh}\right] \right) \end{array} \right. \end{aligned} \tag{4.4}$$

Where,
E_{AC1} = Emissions from arrangement AC1
E_{DC1} = Emissions from arrangement DC1
Δt = Optimization time step [h]
$SFOC_{AC}(LF_t)$ = Specific fuel oil consumption of a fixed speed diesel generator as a function of Load factor (LF) [g_{Fuel}/kWh]
$SFOC_{DC}(LF_t)$ = Specific fuel oil consumption of variable speed diesel generator as a function of Load

factor (LF) [g_{Fuel}/kWh]
EF_{CO2} = Emission factor of CO_2 [g_{CO2}/g_{Fuel}]
$P_{DG1}(t)$ = Power delivered by diesel generator 1 at time t [kW]
$P_{DG2}(t)$ = Power delivered by diesel generator 2 at time t [kW]

Diesel generator model

The CO_2 emissions are dependent on fuel consumption. Therefore, a diesel generator model is developed to evaluate the specific fuel oil consumption. As seen in Figure 2.11, the SFOC is a function of loading on the diesel generator also known as the loading factor and the rpm of the generator. The empirical equations for estimation of SFOC for a fixed-speed diesel generator are given by Kristenen [74] and IMO [58]. However, the relations are for AC grid connected diesel generator i.e. operating on fixed speed. These studies have not included variable speed operation of generators. Therefore, the SFOC data points shown in Figure 2.11 for fixed speed and variable speed generators are used to develop a model for our optimization problem that supports fixed speed and variable speed generation.

Table 4.2: The SFOC data points for variable speed and fixed speed diesel generator, as shown in Figure 2.11 [36]

LF	AC SFOC [g/kWh]	DC SFOC [g/kWh]
100	205	199
75	210	202
50	221	210
25	274	210

These data points are presented in Table 4.2 and a curve fitting is done to develop a diesel generator model for fixed as well as variable speed operation. The diesel generators in the catalogue have different SFOC values at full load conditions compared to the data points used to develop the model. Therefore, the values of SFOC at full load conditions of other diesel generators and the difference between these values are incorporated in the model to showcase the similar nature of fuel consumption for individual diesel generators. The differences at full loading as presented in Table 4.2 in SFOC in fixed speed and variable speed operation are also incorporated in the DG model. The fixed-speed diesel generator model and variable-speed diesel generator model are presented in Figure 4.3a. The SFOC curve for different generators is highlighted in Figure 4.3b with SFOC at 100 per cent LF as a reference.

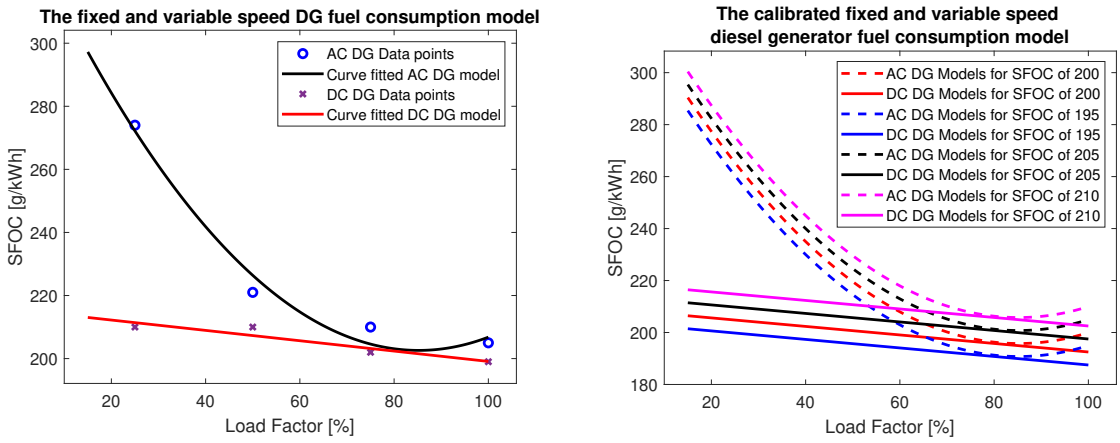

(a) The Specific fuel oil consumption model as a function of load factor for fixed and variable speed diesel generator

(b) The Specific fuel oil consumption model for satisfying all the diesel generators from the catalogue

Figure 4.3: The fixed speed and variable speed diesel generator model for the real data points on the right from Table 4.2 and for calibrated SFOC value for different diesel generators on the left

The SFOC equations as a function of LF are presented in Equation 4.5 and Equation 4.6 for fixed speed and variable speed diesel generators, respectively. The fixed speed DG model is curve fitted as

a polynomial equation, whereas the variable speed DG model is modelled as a linear equation. The R^2 values are also highlighted for the curve fitting for these developed models, and it can be noted that the SFOC is a function of the loading factor of the diesel generator. The term Δ in the function is added to calibrate the regression model to produce the same nature of SFOC curve for fixed and variable speed diesel generators, different from the one used in developing this fuel consumption model.

$$SFOC_{AC}(LF_t)[g/kWh] \quad = \quad 0.0192 * LF_t^2 - 3.272 * LF_t + 342 + \Delta \quad \rightarrow R^2 = 0.9785 \tag{4.5}$$

Where,
LF_t = Load factor of the diesel generator at time t
Δ = The difference in SFOC values at full loading conditions for different diesel generator

$$SFOC_{DC}(LF_t)[g/kWh] \quad = \quad -0.164 * LF_t + 215.5 + \Delta \quad \rightarrow R^2 = 0.8871 \tag{4.6}$$

Objective function

The objective for all the arrangements is to minimize the CO_2 emissions. The Equation 4.7 highlights the objective function for minimization of emissions using optimal dispatch of available power sources for AC grid architecture, whereas Equation 4.8 highlights the objective function for minimizing the emissions for available power sources for DC architecture.

$$Min. \begin{cases} E_{AC2} : \begin{cases} \sum_{t=1}^{T} \left(P_{DG1}(t)[kW] * \Delta t[h] * EF_{CO2} \left[\frac{g_{CO2}}{g_{Fuel}}\right] * SFOC_{AC}(LF_t) \left[\frac{g_{Fuel}}{kWh}\right] \right) \\ + \sum_{t=1}^{T} \left(P_{DG2}(t)[kW] * \Delta t[h] * EF_{CO2} \left[\frac{g_{CO2}}{g_{Fuel}}\right] * SFOC_{AC}(LF_t) \left[\frac{g_{Fuel}}{kWh}\right] \right) \end{cases} \\ E_{AC3} : \begin{cases} \sum_{t=1}^{T_V} \left(P_{DG1}(t)[kW] * \Delta t[h] * EF_{CO2} \left[\frac{g_{CO2}}{g_{Fuel}}\right] * SFOC_{AC}(LF_t) \left[\frac{g_{Fuel}}{kWh}\right] \right) \\ + \sum_{t=1}^{T_V} \left(P_{DG2}(t)[kW] * \Delta t[h] * EF_{CO2} \left[\frac{g_{CO2}}{g_{Fuel}}\right] * SFOC_{AC}(LF_t) \left[\frac{g_{Fuel}}{kWh}\right] \right) \\ + \sum_{t=T_V+1}^{T} \left(P_{Sh}(t)[kW] * \Delta t[h] * EF_{Sh} \left[\frac{g_{CO2}}{kWh}\right] \right) \end{cases} \\ E_{AC4} : \sum_{t=1}^{T} \left(P_{DG1}(t)[kW] * \Delta t[h] * EF_{CO2} \left[\frac{g_{CO2}}{g_{Fuel}}\right] * SFOC_{AC}(LF_t) \left[\frac{g_{Fuel}}{kWh}\right] \right) \\ E_{AC5} : \begin{cases} \sum_{t=1}^{T_V} \left(P_{DG1}(t)[kW] * \Delta t[h] * EF_{CO2} \left[\frac{g_{CO2}}{g_{Fuel}}\right] * SFOC_{AC}(LF_t) \left[\frac{g_{Fuel}}{kWh}\right] \right) \\ + \sum_{t=T_V+1}^{T} \left(P_{Sh}(t)[kW] * \Delta t[h] * EF_{Sh} \left[\frac{g_{CO2}}{kWh}\right] \right) \end{cases} \end{cases} \tag{4.7}$$

$$Min. \begin{cases} E_{DC2} : \begin{cases} \sum_{t=1}^{T} \left(P_{DG1}(t)[kW] * \Delta t[h] * EF_{CO2} \left[\frac{g_{CO2}}{g_{Fuel}}\right] * SFOC_{DC}(LF_t) \left[\frac{g_{Fuel}}{kWh}\right] \right) \\ + \sum_{t=1}^{T} \left(P_{DG2}(t)[kW] * \Delta t[h] * EF_{CO2} \left[\frac{g_{CO2}}{g_{Fuel}}\right] * SFOC_{DC}(LF_t) \left[\frac{g_{Fuel}}{kWh}\right] \right) \end{cases} \\ E_{DC3} : \begin{cases} \sum_{t=1}^{T_V} \left(P_{DG1}(t)[kW] * \Delta t[h] * EF_{CO2} \left[\frac{g_{CO2}}{g_{Fuel}}\right] * SFOC_{DC}(LF_t) \left[\frac{g_{Fuel}}{kWh}\right] \right) \\ + \sum_{t=1}^{T_V} \left(P_{DG2}(t)[kW] * \Delta t[h] * EF_{CO2} \left[\frac{g_{CO2}}{g_{Fuel}}\right] * SFOC_{DC}(LF_t) \left[\frac{g_{Fuel}}{kWh}\right] \right) \\ + \sum_{t=T_V+1}^{T} \left(P_{Sh}(t)[kW] * \Delta t[h] * EF_{Sh} \left[\frac{g_{CO2}}{kWh}\right] \right) \end{cases} \\ E_{DC4} : \sum_{t=1}^{T} \left(P_{DG1}(t)[kW] * \Delta t[h] * EF_{CO2} \left[\frac{g_{CO2}}{g_{Fuel}}\right] * SFOC_{DC}(LF_t) \left[\frac{g_{Fuel}}{kWh}\right] \right) \\ E_{DC5} : \begin{cases} \sum_{t=1}^{T_V} \left(P_{DG1}(t)[kW] * \Delta t[h] * EF_{CO2} \left[\frac{g_{CO2}}{g_{Fuel}}\right] * SFOC_{DC}(LF_t) \left[\frac{g_{Fuel}}{kWh}\right] \right) \\ + \sum_{t=T_V+1}^{T} \left(P_{Sh}(t)[kW] * \Delta t[h] * EF_{Sh} \left[\frac{g_{CO2}}{kWh}\right] \right) \end{cases} \end{cases} \tag{4.8}$$

Where,
E_{ACi} = Emissions from AC arrangement i [g_{CO2}]
E_{DCi} = Emissions from DC arrangement i [g_{CO2}]
P_{Sh} = Power delivered by shore power [kW]
EF_{Sh} = Emission factor of shore power [g_{CO2}/kWh]

Constraints

The shipboard microgrid with two diesel generators delivers equal power at every optimization time step. The reason to include this as a constraint is motivated by the weak grid on ships. With multiple diesel generators on board, the load transients are equally shared to prevent the grid to become unstable and collapse. The failure of the grid can result in dangerous situations at sea, and therefore this constraint is added by looking at the qualitative benefit it offers to the operation of the shipboard microgrid. For all the arrangements with two diesel generators, the constraint is formulated as shown in Equation 4.9.

$$\begin{array}{rcll} AC1, AC2, DC1, DC2 & : & P_{DG1}(t)[kW] = P_{DG2}(t)[kW] & \forall\ t \in T \\ AC3, DC3 & : & P_{DG1}(t)[kW] = P_{DG2}(t)[kW] & \forall\ t \in T_V \end{array} \tag{4.9}$$

The power supplied by the power sources at all time steps are required to satisfy the power demand of the ship. The constraint can be formulated as shown in Equation 4.10. The component efficiencies are taken into account for the consumer side of the switch and are derived in section 3.3. The component efficiencies on the generator side of the switchboard are taken into account when formulating the power balance constraint. The generator side consists of an alternator connected to the diesel engine, a transformer for connection with the shore power infrastructure, an additional rectifier for the BiDC grid to convert AC to DC and a shore power connection through a rectifier unit. In addition to this, the battery is connected through a bidirectional DC/DC converter in the BiDC grid, whereas a bidirectional DC AC converter is used. The efficiency of these components and the battery itself are also taken into account.

$$\begin{array}{lcl}
AC1: & P_{DG1}(t) * \eta_{gen} + P_{DG2}(t) * \eta_{gen} = P_{R_{AC}}(t) & \forall t \in T \\
AC2: & P_{DG1}(t) * \eta_{gen} + P_{DG2}(t) * \eta_{gen} + P_{Dis}(t) * \eta_{Dis} - \frac{P_{Ch}(t)}{\eta_{Ch}} = P_{R_{AC}}(t) & \forall t \in T \\
AC3: & \begin{cases} P_{DG1}(t) * \eta_{gen} + P_{DG2}(t) * \eta_{gen} + P_{Dis}(t) * \eta_{Dis} - \frac{P_{Ch}(t)}{\eta_{Ch}} = P_{R_{AC}}(t) & \forall t \in T_V \\ P_{Sh}(t) * \eta_{Sh_{Trans}} + P_{Dis}(t) * \eta_{Dis} - \frac{P_{Ch}(t)}{\eta_{Ch}} = P_{R_{AC}}(t) & \forall t \in T_S \end{cases} \\
AC4: & P_{DG1}(t) * \eta_{gen} + P_{Dis}(t) * \eta_{Dis} - \frac{P_{Ch}(t)}{\eta_{Ch}} = P_{R_{AC}}(t) & \forall t \in T \\
AC5: & \begin{cases} P_{DG1}(t) * \eta_{gen} + P_{Dis}(t) * \eta_{Dis} - \frac{P_{Ch}(t)}{\eta_{Ch}} = P_{R_{AC}}(t) & \forall t \in T_V \\ P_{Sh}(t) * \eta_{Sh_{Trans}} + P_{Dis}(t) * \eta_{Dis} - \frac{P_{Ch}(t)}{\eta_{Ch}} = P_{R_{AC}}(t) & \forall t \in T_S \end{cases} \\
DC1: & P_{DG1}(t) * \eta_{gen} * \eta_{BiDC} + P_{DG2}(t) * \eta_{gen} * \eta_{BiDC} = P_{R_{AC}}(t) & \forall t \in T \\
DC2: & P_{DG1}(t) * \eta_{gen} * \eta_{BiDC} + P_{DG2}(t) * \eta_{gen} * \eta_{BiDC} + P_{Dis}(t) * \eta_{Dis} - \frac{P_{Ch}(t)}{\eta_{Ch}} = P_{R_{AC}}(t) & \forall t \in T \\
DC3: & \begin{cases} P_{DG1}(t) * \eta_{gen} * \eta_{BiDC} + P_{DG2}(t) * \eta_{gen} * \eta_{BiDC} + P_{Dis}(t) * \eta_{Dis} - \frac{P_{Ch}(t)}{\eta_{Ch}} = P_{R_{AC}}(t) & \forall t \in T_V \\ P_{Sh}(t) * \eta_{Sh_{BiDC}} + P_{Dis}(t) * \eta_{Dis} - \frac{P_{Ch}(t)}{\eta_{Ch}} += P_{R_{AC}}(t) & \forall t \in T_S \end{cases} \\
DC4: & P_{DG1}(t) * \eta_{gen} * \eta_{BiDC} + P_{Dis}(t) * \eta_{Dis} - \frac{P_{Ch}(t)}{\eta_{Ch}} = P_{R_{AC}}(t) & \forall t \in T \\
DC5: & \begin{cases} P_{DG1}(t) * \eta_{gen} * \eta_{BiDC} + P_{Dis}(t) * \eta_{Dis} - \frac{P_{Ch}(t)}{\eta_{Ch}} = P_{R_{AC}}(t) & \forall t \in T_V \\ P_{Sh}(t) * \eta_{Sh_{BiDC}} + P_{Dis}(t) * \eta_{Dis} - \frac{P_{Ch}(t)}{\eta_{Ch}} = P_{R_{AC}}(t) & \forall t \in T_S \end{cases}
\end{array} \tag{4.10}$$

Where,
$\eta_{Sh_{Trans}}$ = Efficiency of transformer connected with shore power
$\eta_{Sh_{BiDC}}$ = Efficiency of rectifier connected with shore power
η_{Dis} = Efficiency of battery during discharging
η_{Ch} = Efficiency of battery during charging

The State of Charge (SoC) of the battery is an important parameter that influences the optimal dispatch of power, minimizing the emissions. The SoC describes the amount of energy available in the battery,

like a measure of water present in a well. The SoC is affected by the charging and discharging of the battery. When the battery is charged, the SoC increases and vice versa. One of the methods to estimate SoC is Coulomb counting, and it is presented in Franco [33]. The equation is discretized for our optimization problem with a time step of Δt. The SoC of the battery and the constraint for it is formulated in Equation 4.11.

$$\begin{matrix} AC2, AC3, AC4, AC5, \\ DC2, DC3, DC4, DC5 \end{matrix} \quad : \quad SoC(t) = SoC(t-1) + \frac{P_{Ch}[kW] * \Delta t[h]}{Bat_{Cap}[kWh]} - \frac{P_{Dis}[kW] * \Delta t[h]}{Bat_{Cap}[kWh]} \quad \forall \ t \in T \tag{4.11}$$

Where,
Bat_{Cap} = Battery capacity [kWh]

This forms the dynamic constraint in our optimization problem that depends on the value of the previous optimization time step. The charging and discharging cannot happen at the same time, i.e. the battery can either deliver power to the electrical loads through the switchboard or receive power through the switchboard leading to discharging and charging of the battery, respectively. To incorporate this, a non-linear constraint is formulated and presented in Equation 4.12.

$$AC2, AC3, AC4, AC5, DC2, DC3, DC4, DC5 \quad : \quad P_{Dis}(t)[kW] * P_{Ch}(t)[kW] = 0 \quad \forall \ t \in T \tag{4.12}$$

The battery is assumed to be fully charged at the start and at the end of the voyage. This is done to evaluate the feasibility of the grid to achieve repeatability of the optimal dispatch profile for the ship's operational profile. The initial and final SoC constraints are formulated as shown in Equation 4.13 and Equation 4.14, respectively.

$$AC2, AC3, AC4, AC5, DC2, DC3, DC4, DC5 \quad : \quad SoC_0 = 0.85 \tag{4.13}$$

Where,
SoC_0 = Initial value of SoC

$$AC2, AC3, AC4, AC5, DC2, DC3, DC4, DC5 \quad : \quad SoC_f = 0.85 \tag{4.14}$$

Where,
SoC_f = Final value of SoC

The diesel generator model developed from the data points shown in Figure 2.11 and Habermass and Thurner [36] also highlight the operating limits of a diesel generator. For variable speed operation, the diesel generator can run over a rpm range of 900 rpm (900-1800 rpm) and can deliver power from 300 kW to 2240 kW. Therefore, the minimum LF on the diesel generator can be constrained to 15 per cent. The same is considered for a fixed-speed diesel generator. The operating limits for diesel generator 1 and diesel generator 2 are formulated as shown in Equation 4.15 and Equation 4.16, respectively.

$$\begin{matrix} AC2, AC4, DC2, DC4 \quad : \quad 0.15 * P_{DGRated}[kW] \leq P_{DG1}(t)[kW] \leq P_{DGRated}[kW] \quad \forall \ t \in T \\ AC3, AC5, DC3, DC5 \quad : \quad 0.15 * P_{DGRated}[kW] \leq P_{DG1}(t)[kW] \leq P_{DGRated}[kW] \quad \forall \ t \in T_V \end{matrix} \tag{4.15}$$

$$\begin{matrix} AC2, DC2 \quad : \quad 0.15 * P_{DGRated}[kW] \leq P_{DG2}(t)[kW] \leq P_{DGRated}[kW] \quad \forall \ t \in T \\ AC3, DC3 \quad : \quad 0.15 * P_{DGRated}[kW] \leq P_{DG2}(t)[kW] \leq P_{DGRated}[kW] \quad \forall \ t \in T_V \end{matrix} \tag{4.16}$$

The State of Charge of the battery is also limited by the battery capacity. Typically, the reason for the use of NMC batteries in marine is the deep cycle they provide [43]. This is also reflected by the catalogue created in Appendix A that presents the commercial batteries used in this study along with their technical parameters. The battery is not recommended to use all the energy capacity they store

to prevent battery damage and promote a longer lifetime of the battery. Therefore, the SoC limits are constrained in the Equation 4.17.

$$AC2, AC3, AC4, AC5, DC2, DC3, DC4, DC5 \quad : \quad SoC_{min} \leq SoC(t) \leq SoC_{max} \quad \forall \ t \in T \tag{4.17}$$

Where,
SoC_{min} = Minimum SoC level for the battery
SoC_{max} = Maximum SoC level for the battery

Appendix A presents the battery catalogue for marine applications with the capacity, charging and discharging power limits and the weights of the battery banks from different manufacturers. The C-rate is a measure of how fast the battery can be charged or discharged, assuming the charging and discharging process is carried out at constant power. 1 C-rate takes 1 hour to discharge, whereas a battery with 2 C-rate takes 30 mins to discharge. The same logic can be applied to charging the batteries. Therefore, the C-rates given in the catalogue form the basis for the operational limits on the charging and the discharging power of the battery. These limits are formulated for discharging and charging in Equation 4.18 and Equation 4.19, respectively.

$$AC2, AC3, AC4, AC5, DC2, DC3, DC4, DC5 \quad : \quad P_{Dis_{Min}}[kW] \leq P_{Dis}(t)[kW] \leq \frac{Bat_{Cap}}{\left(\frac{1}{C_{Dis}}\right)}[kW] \quad \forall \ t \in T \tag{4.18}$$

Where,
$P_{Dis_{Min}}$ = Minimum power delivered by the battery while discharging [kW]
C_{Dis} = Discharging C-rate for the battery [kW]

$$AC2, AC3, AC4, AC5, DC2, DC3, DC4, DC5 \quad : \quad P_{Ch_{Min}}[kW] \leq P_{Ch}(t)[kW] \leq \frac{Bat_{Cap}}{\left(\frac{1}{C_{Ch}}\right)}[kW] \quad \forall \ t \in T \tag{4.19}$$

Where,
$P_{Ch_{Min}}$ = Minimum power delivered by the battery while charging
C_{Ch} = Charging C-rate for the battery

Finally, the shore power minimum and maximum power constraints are defined in Equation 4.20. The technical parameters for shore power are defined in Cavotec [19, 20].

$$AC3, DC3, AC5, DC5 \quad : \quad P_{Sh_{Min}}[kW] \leq P_{Sh}(t)[kW] \leq P_{Sh_{Max}}[kW] \quad \forall \ t \in T_S \tag{4.20}$$

Where,
$P_{Sh_{Min}}$ = Minimum power delivered by the shore infrastructure
$P_{Sh_{Max}}$ = Maximum power delivered by the shore infrastructure

The Emission estimation for AC1 and DC1 as well as the optimization formulation for AC2, AC3, AC4, AC5, DC2, DC3, DC4 and DC5 as per the arrangements shown in Table 3.2 and the constraints corresponding to the respective arrangements are formulated from Equation 4.2 to Equation 4.20. The constraints differ from arrangement to arrangement, along with the parameters selected for the diesel generator and battery.

Finally, the Table 4.3 highlights the optimization setup used in Matlab® for the inbuilt ‘fmincon’ function. The main reason to alter the default values was to provide stricter stopping criteria for the optimizer.

Table 4.3: Optimization parameter setup used

Sr. No.	Parameter	Default Value	My Value
1	Max. Iterations	1000	500
2	Max. Function Evaluations	3000	10^6
3	Constraint Tolerance	10^{-6}	10^{-10}
4	Optimality Tolerance	10^{-6}	10^{-10}

4.5. Summary

The optimization problem was formulated in this chapter. An overview of the structure of an optimization problem along with the types was introduced in section 4.1. The literature review was done and the findings from it, highlighting the research gap, were presented in section 4.2. Following this, practical considerations were established based upon the knowledge gained from chapter 2, chapter 3 and were listed in section 4.3. Finally, the optimization problem was formulated in section 4.4 along with the diesel generator model for fixed speed and variable speed operation.

5

System analysis

The chapter 4 formulated the optimization problem for all arrangements with respective decision variables, objective functions and constraints. This chapter is aimed at estimating the other key performance indicators like capital cost, operating cost, fuel consumption, system weight, and load carrying capacity (DWT) for each arrangement for which a feasible solution is present for the selected configuration of the diesel generator and/or battery. The fuel consumption is calculated in section 5.1. The operating cost includes the fuel cost as well as the cost of electricity from the shore infrastructure depending upon the selected arrangement as shown in section 5.2. The capital costs of the propulsion system exclude the propulsion motors and the estimation methodology is presented in section 5.3. The weight of the propulsion system is assessed as the procedure described in section 5.4. The ship is considered to be travelling at maximum displacement irrespective of the arrangement and the configurations within, leading to evaluating the load carrying capacity of the ship from the system weight calculations in section 5.5. Finally, the chapter is concluded with a summary in section 5.6

5.1. Fuel Consumption

The fuel consumption can be estimated for each feasible solution in every arrangement by calculating the cumulative fuel consumption over the ship's operational profile. The feasible solution provides the optimal dispatch profile for diesel generators and/ or batteries. For every optimization time step, the specific fuel oil consumption can be calculated according to the diesel generator model developed for AC and DC grid in section 4.4. The SFOC is calculated as per the loading factor on the diesel generator obtained from the optimal dispatch profile and the summation leads to estimating the total fuel consumption as shown in Equation 5.1.

$$FC[g_{Fuel}] = \begin{cases} AC1, AC2 : \begin{cases} \sum_{t=1}^{T} P_{DG1}(t) * SFOC_{AC}(LF_t) * \Delta t \\ + \sum_{t=1}^{T} P_{DG2}(t) * SFOC_{AC}(LF_t) * \Delta t \end{cases} & \forall t \in T \\ AC3 : \begin{cases} \sum_{t=1}^{T_V} P_{DG1}(t) * SFOC_{AC}(LF_t) * \Delta t \\ + \sum_{t=1}^{T_V} P_{DG2}(t) * SFOC_{AC}(LF_t) * \Delta t \end{cases} & \forall t \in T_V \\ AC4 : \sum_{t=1}^{T} P_{DG1}(t) * SFOC_{AC}(LF_t) * \Delta t & \forall t \in T \\ AC5 : \sum_{t=1}^{T_V} P_{DG1}(t) * SFOC_{DC}(LF_t) * \Delta t & \forall t \in T_V \\ DC1, DC2 : \begin{cases} \sum_{t=1}^{T} P_{DG1}(t) * SFOC_{DC}(LF_t) * \Delta t \\ + \sum_{t=1}^{T} P_{DG2}(t) * SFOC_{DC}(LF_t) * \Delta t \end{cases} & \forall t \in T \\ DC3 : \begin{cases} \sum_{t=1}^{T_V} P_{DG1}(t) * SFOC_{DC}(LF_t) * \Delta t \\ + \sum_{t=1}^{T_V} P_{DG2}(t) * SFOC_{DC}(LF_t) * \Delta t \end{cases} & \forall t \in T_V \\ DC4 : \sum_{t=1}^{T} P_{DG1}(t) * SFOC_{DC}(LF_t) * \Delta t & \forall t \in T \\ DC5 : \sum_{t=1}^{T_V} P_{DG1}(t) * SFOC_{DC}(LF_t) * \Delta t & \forall t \in T_V \end{cases} \quad (5.1)$$

5.2. Operating Cost

The operating cost considered in this study is the fuel cost and the average electricity cost from the shore infrastructure. The operating cost for each set of diesel generators and batteries for every arrangement in which the feasible solution exists can be computed as per Equation 5.2.

$$
Opex[\$] = \begin{cases}
AC1, AC2 : \begin{cases} \sum_{t=1}^{T} \alpha * P_{DG1}(t) * SFOC_{AC}(LF_t) * Cost_{Fuel} * \Delta t \\ + \sum_{t=1}^{T} \alpha * P_{DG2}(t) * SFOC_{AC}(LF_t) * Cost_{Fuel} * \Delta t \end{cases} & \forall t \in T \\
AC3 : \begin{cases} \sum_{t=1}^{T_V} \alpha * P_{DG1}(t) * SFOC_{AC}(LF_t) * Cost_{Fuel} * \Delta t \\ + \sum_{t=1}^{T_V} \alpha * P_{DG2}(t) * SFOC_{AC}(LF_t) * Cost_{Fuel} * \Delta t \\ + \sum_{t=T_V+1}^{T} P_{Sh}(t) * Cost_{Shore} * \Delta t \end{cases} & \forall t \in T \\
AC4 : \sum_{t=1}^{T} \alpha * P_{DG1}(t) * SFOC_{AC}(LF_t) * Cost_{Fuel} * \Delta t & \forall t \in T \\
AC5 : \begin{cases} \sum_{t=1}^{T_V} \alpha * P_{DG1}(t) * SFOC_{DC}(LF_t) * Cost_{Fuel} \Delta t \\ + \sum_{t=T_V+1}^{T} P_{Sh}(t) * Cost_{Shore} * \Delta t \end{cases} & \forall t \in T \\
DC1, DC2 : \begin{cases} \sum_{t=1}^{T} \alpha * P_{DG1}(t) * SFOC_{DC}(LF_t) * Cost_{Fuel} * \Delta t \\ + \sum_{t=1}^{T} \alpha * P_{DG2}(t) * SFOC_{DC}(LF_t) * Cost_{Fuel} * \Delta t \end{cases} & \forall t \in T \\
DC3 : \begin{cases} \sum_{t=1}^{T_V} \alpha * P_{DG1}(t) * SFOC_{DC}(LF_t) * Cost_{Fuel} * \Delta t \\ + \sum_{t=1}^{T_V} \alpha * P_{DG2}(t) * SFOC_{DC}(LF_t) * Cost_{Fuel} * \Delta t \\ + \sum_{t=T_V+1}^{T} P_{Sh}(t) * Cost_{Shore} * \Delta t \end{cases} & \forall t \in T \\
DC4 : \sum_{t=1}^{T} \alpha * P_{DG1}(t) * SFOC_{DC}(LF_t) * Cost_{Fuel} * \Delta t & \forall t \in T \\
DC5 : \begin{cases} \sum_{t=1}^{T_V} \alpha * P_{DG1}(t) * SFOC_{DC}(LF_t) * Cost_{Fuel} * \Delta t \\ + \sum_{t=T_V+1}^{T} P_{Sh}(t) * Cost_{Shore} * \Delta t \end{cases} & \forall t \in T
\end{cases} \tag{5.2}
$$

Where,
α = a factor to convert the price of fuel [tonne/g]
$Cost_{Fuel}$ = the purchasing cost of fuel [$/tonne]
$Cost_{Shore}$ = the purchasing cost of electricity from shore infrastructure [$/kWh]

5.3. Capital Cost

The section 3.2 highlights the differences in AC and BiDC grid for the ship. The motor-rated capacity is not changing for both the grid architectures. The component efficiencies that make up the grid are considered for sizing these components. In the AC grid, the components that are connected between the motor and the switchboard as shown in Figure 3.3a are VFDs and three winding transformers. The VFD power rating has to supply the rated power of the motor, as well as the motor losses that occur during operation. Consequently, the power rating of the VFD can be estimated as shown in Equation 5.3. The transformer is required to be rated at a power rating that not only supplies the rated motor power but also satisfies the VFD losses and motor losses. Therefore, the power rating for the transformer can be calculated as shown in Equation 5.3.

$$
\begin{aligned}
VFD_{Rated}[kW] &= \frac{P_{Motor}[kW]}{\eta_{Motor} * \cos(\theta_{Motor})} \\
TFProp_{Rated}[kVA] &= \frac{P_{Motor}[kW]}{\eta_{VFD} * \eta_{Motor} * \cos(\theta_{Motor})}
\end{aligned} \tag{5.3}
$$

Where,
VFD_{Rated} = Rated power for the variable frequency drive
$TFProp_{Rated}$ = Rated power for the propulsion transformer

For the auxiliary and shore power transformers, the maximum value of auxiliary power and shore power are taken for the sizing and the power factor value for auxiliary power is considered. The estimation is shown in Equation 5.4.

$$\begin{aligned} TFAux_{Rated}[kVA] &= \frac{maximum(P_{AUX})[kW]}{\cos\theta_{AUX}} \\ TFShore_{Rated}[kVA] &= maximum(P_{Sh_{Max}})[kW] \end{aligned} \tag{5.4}$$

Where,
$TFAux_{Rated}$ = The power rating for the auxiliary transformer
$TFShore_{Rated}$ = The power rating for the shore power transformer

Finally, the bidirectional inverter rating connected with the battery bank can be sized as per the maximum power during discharge allowed by the battery. The power rating is estimated as highlighted in Equation 5.5.

$$Inv_{BatRated}[kW] = \frac{Bat_{Cap}}{\left(\frac{1}{C_{Dis}}\right)}[kW] \tag{5.5}$$

Where,
$Inv_{BatRated}$ = The power rating for the inverter connected to the battery bank

In the BiDC grid, the VFD with its rectification part can be eliminated, along with the three winding transformers leading to an inverter connection to the propulsion motor as shown in Figure 3.3b. The power rating for the motor inverter can be calculated using the motor efficiency and motor power factor, as highlighted in Equation 5.6.

$$InvMotor_{Rated}[kW] = \frac{P_{Motor}[kW]}{\eta_{Motor}*\cos(\theta_{Motor})} \tag{5.6}$$

Where,
$InvMotor_{Rated}$ = The power rating for the propulsion motor inverter

The power rating for the auxiliary inverter and the shore power rectifier is dependent on the maximum power requirements. The shore power is constrained by the shore power infrastructure, whereas the auxiliary power is limited by the auxiliary load demand. The inverter power rating for auxiliary and rectifier power rating for shore connection is estimated as per Equation 5.7.

$$\begin{aligned} InvAUX_{Rated}[kW] &= \frac{maximum(P_{AUX})[kW]}{\cos\theta_{AUX}} \\ ShoreRect_{Rated}[kW] &= maximum(P_{Sh_{Max}})[kW] \end{aligned} \tag{5.7}$$

Where,
$InvAUX_{Rated}$ = The power rating for the auxiliary inverter
$ShoreRect_{Rated}$ = The power rating for the shore power inverter

The diesel generator in the BiDC grid is connected to the main distribution network using a rectifier. The maximum power delivered by the diesel generator is limited by the diesel generator's power rating and efficiency. The battery bank is integrated into the network using a bidirectional DC/DC converter, the maximum power rating for this converter is limited by the maximum power delivered by the battery during discharge. The power rating for both the power electronic conversion devices can be evaluated as shown in Equation 5.8.

$$\begin{aligned} DGRect_{Rated} &= P_{DGRated}[kW] * \eta_{gen} \\ DCConv_{Rated} &= \frac{Bat_{Cap}}{\left(\frac{1}{C_{Dis}}\right)}[kW] \end{aligned} \tag{5.8}$$

Where,
$DGRect_{Rated}$ = The power rating for diesel generator rectifier
$DCConv_{Rated}$ = The power rating for DC/DC converter connected to the battery

The ratings for all the components in the AC and BiDC grid are rounded up to the nearest number divisible by 50 or 100 except for the battery and diesel generator. The sizing for these components is already done as per the industry availability as shown in Appendix A. The rounding up of rated power is done to have an integer value, as it is not common to find commercial industrial components in decimal power ratings. The inverter and DC/DC converter are connected to the battery in AC and BiDC grid, respectively. The power rating of these components is dependent on the battery characteristics, especially, the maximum power during discharge. In the BiDC grid, the power rating of the rectifier unit connected to the diesel generator is dependent on the sizing of the diesel generator. The power rating for all other electrical components respective to the AC and BiDC grid does not change, as the power requirements of AC and BiDC grid topologies remain the same irrespective of the arrangement.

Vásquez and Andrés [124] formulated the cost curves for electrical components like induction motors, VFD and transformers. This study was performed in 2014 and therefore highlights the 2014 US Dollar prices. To convert these values to 2023 US Dollar prices, the respective component/industry cost index is used. The data on three winding transformers is not easily available as compared to conventional transformers [124]. Also, the main reason for the use of these types of transformers is to provide a phase shift of 30^{o} to reduce harmonics that are generated as a result of the rectification process in the variable frequency drive. To overcome this, two parallel conventional transformers can also be used, with the secondary side of the first transformer connected in the Delta configuration and the secondary side of the second transformer connected in the Wye configuration. This approximation is used to estimate the capital cost of the propulsion transformers. For the shore transformers, the sizing is dependent on the shore infrastructure for power delivery. The variable frequency drive is constitutionally made of two parts:- the rectifier part and the inverter part, with a DC link capacitor to separate them. Therefore, The cost of the rectifier, inverter, and DC/DC converter is assumed to be equal to half of the VFD cost as they use a similar number of semiconductor devices in the construction of these devices. The modified cost curves for VFD, rectifiers, inverters, DC/DC converters and transformers from the work of Vásquez and Andrés [124] are given in Equation 5.9.

$$\begin{aligned}
DG_{Cost}[\$] &= PDG_{Rated} * DGC \\
Bat_{Cost}[\$] &= Bat_{Cap} * BatC \\
TFProp_{Cost}[\$] &= CI_{TF} * (2 * (9.4821 * \left(\frac{TFProp_{Rated}}{2}\right) + 12029)) \\
TFShore_{Cost}[\$] &= CI_{TF} * (9.4821 * TFShore_{Rated} + 12029) \\
TFAux_{Cost}[\$] &= CI_{TF} * (9.4821 * TFAux_{Rated} + 12029) \\
VFD_{Cost}[\$] &= CI_{Elec} * (208.9 * VFD_{Rated} - 2185.5) \\
Inv_{BatCost}[\$] &= CI_{Elec} * (104.45 * Inv_{BatRated} - 1092.75) \\
DGRect_{Cost}[\$] &= CI_{Elec} * (104.45 * DGRect_{Rated} - 1092.75) \\
DCConv_{Cost}[\$] &= CI_{Elec} * (104.45 * DCConv_{Rated} - 1092.75) \\
ShoreRect_{Cost}[\$] &= CI_{Elec} * (104.45 * ShoreRect_{Rated} - 1092.75) \\
InvAux_{Cost}[\$] &= CI_{Elec} * (104.45 * InvAux_{Rated} - 1092.75) \\
InvMotor_{Cost}[\$] &= CI_{Elec} * (104.45 * InvMotor_{Rated} - 1092.75)
\end{aligned} \tag{5.9}$$

Where,
DGC = The cost of diesel generator in $ per kW
$BatC$ = The cost of Battery bank in $ per kWh
DG_{Cost} = The cost of a diesel generator
Bat_{Cost} = The cost of battery bank
$TFProp_{Cost}$ = The cost of propulsion transformer
$TFShore_{Cost}$ = The cost of transformer for shore connection
$TFAux_{Cost}$ = The cost of transformer for auxiliary loads
VFD_{Cost} = The cost of variable frequency drive
$Inv_{BatCost}$ = The cost of inverter connected to the battery in AC grid
$DGRect_{Cost}$ = The cost of rectifier connected to the diesel generator in BiDC grid

$DCConv_{Cost}$ = The cost of DC-DC converter connected to the battery in BiDC grid
$ShoreRect_{Cost}$ = The cost of rectifier for shore connection
$InvAux_{Cost}$ = The cost of inverter connected with auxiliary loads
$InvMotor_{Cost}$ = The cost of the inverter connected with the propulsion motor
CI_{TF} = The cost index for power transformer
CI_{Elec} = The cost index of electronic components

The total capital cost for each arrangement can be estimated by adding the cost of all components that make up the respective grid topology. The cost of power cables is neglected in this study, as they have a negligible impact on the total capital cost in AC and BiDC grids. The cost of the motor is also not considered in this study, as the sizing is not changing and remains constant for all arrangements. The generalised formula for the capital cost of AC and BiDC grid is shown in Equation 5.10. The generalised formula is used to calculate the total capital cost according to the components that make up that particular arrangement. If certain components are not present in a particular arrangement, then the costs for them are considered zero in this generalised formula.

$$Capex[\$]: \quad \begin{matrix} AC & = & \left\{ \begin{matrix} N_G * DG_{Cost} + N_P * (VFD_{Cost} + TFProp_{Cost}) \\ +N_{Aux} * TFAux_{Cost} + Bat_{Cost} + Inv_{BatCost} + TFShore_{Cost} \end{matrix} \right. \\ BiDC & = & \left\{ \begin{matrix} N_G * (DG_{Cost} + DGCRect_{Cost}) + N_P * (InvMotor_{Cost}) \\ +N_{Aux} * InvAux_{Cost} + Bat_{Cost} + DCConv_{Cost} + ShoreRect_{Cost} \end{matrix} \right. \end{matrix} \tag{5.10}$$

Where,
$Capex$ = The cost of the propulsion system, excluding the cost of propulsion motors and power cables

5.4. System Weight

The total weight of the system consists of weights of all the components that make up the grid, as shown in Figure 3.3 for AC and BiDC grid for each arrangement. The weight of the diesel generator and the battery bank is listed in Appendix A. Vásquez and Andrés [124] has also worked on curve fitting the transformer weights as a function of power rating from the industrial transformer data. The weight of the transformer can be estimated as shown in Equation 5.11. The weight of the propulsion transformer is calculated by multiplying the weight of the conventional transformer by two, with a power rating of half of the propulsion transformer. The weights of the VFD, Induction motor, and power electronic converters can be estimated from datasheets.

$$TF_{weight}[KG] \quad = \quad 2.0005 * TF_{Rated} + 155.76 \tag{5.11}$$

Where,
TF_{Weight} = Transformer weight as a function of power rating
TF_{Rated} = Power rating of the transformer

The generalised formula for system weight estimation is presented in Equation 5.12. If certain components are not present in a particular arrangement, then the weights for them are considered zero in this generalised formula. The system weight is considered in the light-weight tonnes of the ship, along with other weights.

$$Weight_{Sys}: \quad \begin{matrix} AC & = & \left\{ \begin{matrix} N_G * DG_{Weight} + N_P * (VFD_{weight} + TFProp_{Weight}) \\ +N_{Aux} * TFAux_{Weight} + Bat_{Weight} + Inv_{BatWeight} + TFShore_{Weight} \end{matrix} \right. \\ BiDC & = & \left\{ \begin{matrix} N_G * (DG_{Weight} + DGCRect_{Weight}) + N_P * (InvMotor_{Weight}) \\ +N_{Aux} * InvAux_{Weight} + Bat_{Weight} + DCConv_{Weight} + ShoreRect_{Weight} \end{matrix} \right. \end{matrix} \tag{5.12}$$

Where,
$Weight_{sys}$ = The propulsion system weight, excluding the weight of the propulsion motor

DG_{Weight} = The weight of a diesel generator
Bat_{Weight} = The weight of battery bank
$TFProp_{Weight}$ = The weight of propulsion transformer
$TFShore_{Weight}$ = The weight of transformer for shore connection
$TFAux_{Weight}$ = The weight of transformer for auxiliary loads
VFD_{Weight} = The weight of variable frequency drive
$Inv_{BatWeight}$ = The weight of the inverter connected to the battery in the AC grid
$DGRect_{Weight}$ = The weight of the rectifier connected to the diesel generator in the BiDC grid
$DCConv_{Weight}$ =The weight of the DC-DC converter connected to the battery in the BiDC grid
$ShoreRect_{Weight}$ = The weight of rectifier for shore connection
$InvAux_{Weight}$ = The weight of inverter connected with auxiliary loads
$InvMotor_{Weight}$ = The weight of the inverter connected with the propulsion motor

5.5. Load Carrying Capacity

The total weight that the ship can hold is expressed as the maximum mass displacement. It accounts for the weight of the ship as well as the load carrying capacity of the ship. The weight of the ship consists of the weight of the ship's hull, the propulsion system weight, the ballast, the machinery on the ship and so on. This is also termed the Lightweight Tonnes (LWT) of the ship. In simpler terms, it accounts for all the weight on the ship except the consumables like fuel, drinking water, cargo, passenger weights, etc. The deadweight tonnes (DWT) of the ship refer to the total capacity of the ship that it can transport within the design margin of the shipbuilder. The Equation 5.13 presents the division of the load displacement of the ship as LWT and DWT.

$$\nabla[tonnes] = LWT + DWT \tag{5.13}$$

Where,
∇ = Maximum displacement of the ship
LWT = Lightweight tonnes
DWT = Deadweight tonnes

The changes in the load carrying capacity (DWT) can be estimated as the maximum displacement of the ship is going to remain constant regardless of the changes in the system weight and the ship is going to be operational at its maximum displacement to generate the highest profits. Therefore, the changes in the system weight are reflected in the load carrying capacity of the ship. These changes for each arrangement are compared with the status quo (AC1).

5.6. Summary

This chapter presented the procedure for estimating the remaining key performance indicators (KPIs). The chapter 4 provided the minimum emissions that can be realised for the different configurations of diesel generators and batteries. The shore power was also introduced in some arrangements to understand the effect on the emissions for the AC and BiDC grid. Following the emission data for these feasible solutions, the KPIs were estimated for the selected configuration of the ship in the study. The fuel consumption, operating costs, capital costs, system weight, and load carrying capacity (DWT) were estimated in section 5.1, section 5.2, section 5.3, section 5.4, and section 5.5, respectively.

6

Results

This chapter aims at presenting the results of the methodology described in chapter 3, chapter 4 and chapter 5. The section 6.1 presents the result for the *Island Discovery* ship with the velocity profile and the mechanical power profile. The upper and lower bounds for the mechanical power estimation are also highlighted to showcase the variability for the computation that can occur as a consequence of resistance calculation and environmental factors. The section 6.2 highlights the electrical power requirements of the ship for AC and BiDC grid, along with the cable power losses that occur in delivering power to the propellers. The emission estimation for AC1 and DC1 are presented in section 6.3 along with the capital cost of the system and the operating cost that accounts for fuel consumption alone. The section 6.4 showcases the results for all the feasible configurations for two diesel generators and a battery bank for AC and BiDC grid. A comparison between the results for AC and BiDC grid for two diesel generators, battery bank and shore power is presented in section 6.5. The elimination of one diesel generator led to a propulsion system consisting of one diesel generator and a battery bank. The effect of this on the emissions is highlighted in section 6.6. The results for the previous configuration but with having the availability of shore power and the differences it creates in emission estimation are studied in section 6.7. In addition to these results, a broader comparison is done between all arrangements with all arrangements for the selected configuration for emissions, fuel consumption, capital cost, operating cost, system weight and load carrying capacity in section 6.8. A graphical representation for all the KPIs is presented in section 6.9 to highlight comparative changes in KPIs compared with the status quo. A comparison of the results for arrangement AC4 from the data available from the battery bank provider i.e. Corvus Energy to *Island Discovery* ship is presented in section 6.10. Finally, the chapter is concluded with a summary in section 6.11.

6.1. Mechanical Power Profile for *Island Discovery*

Using the methodology described in Figure 3.1, the typical operational profile can be generated. Although the operational profile can deviate depending on the weather conditions, the profile generated can be used to provide estimates for the optimization problem. The trip duration varies from one trip to another, that is due to environmental and weather conditions like wind and ocean wave speed and direction. Therefore, approximate trip duration is considered for the analysis. For this thesis, a ferry is taken into consideration and the data used is obtained from the Automatic Identification System (AIS) of the ships, which is available on websites like, MarineTraffic [83] and VesselFinder [125] and the following assumptions are made to estimate the mechanical and auxiliary power requirements.

Assumptions: -

1. An average seawater density (ρ) is taken as 1025 kg/m^3 and is assumed to be constant, neglecting seasonal effects [65].
2. The draught (D) of the ship is assumed to be at full load conditions and constant throughout the year.

3. The frictional resistance to resistance in calm waters (R_F/R) ratio is highlighted in Barrass [9] and depends on the speed-length ratio of the ship. In the case of *Island discovery*, this ratio ranges between 35 and 45 per cent, as shown in Figure 6.2b. In our estimation, this ratio is considered to be 37 per cent.

4. The resistance due to wind and appendages (R_{APP}) varies for different ships, the operational region for the ship and ranges from 8-25 per cent and 10-30 per cent as given in Molland, Turnock, and Hudson [90] and Barrass [9] of the total resistance in calm water respectively $(R_F + R_R)$, respectively. This ratio is assumed to be 20 per cent and constant in our power estimation methodology.

5. The hull efficiency (η_H) ranges from 98-99 percent ([9]) and taken as 99 percent in this study.

6. The propeller efficiency (η_P) ranges from 60-75 percent [9, 90, 75]. The (η_P) value in this study is assumed to be at 75 per cent and remains constant throughout the trip.

7. The relative rotative efficiency (η_R) ranges from 0.95-1.05 per cent and is usually considered as unity in propulsion power estimates [75, 90, 17].

8. The shaft efficiency (η_S) is neglected as the propulsion system is electric propulsion where the propeller is directly connected to the motor.

9. Auxiliary loads are assumed to be constant and as a percentage of the propulsion load. A typical value of 20 per cent is chosen. This is assumed to be the mean power requirement for the whole voyage and accordingly, a standard deviation of 5 per cent is considered around this mean value assuming a normal distribution.

The *Island Discovery's* design data sheet is attached in Appendix B. The operational and velocity data is taken from MarineTraffic [83], VesselFinder [125], and BC Ferries [11]. *Island Discovery* operates between the port of Powell River and Blubber Bay in Canada. The technical and operational details of the ship can be found in Table 6.1. Figure 6.1a presents the ship studied in this thesis and Figure 6.1b shows the ferry operation between the ports. The Table 6.2 provides the real-time velocity data points obtained from MarineTraffic [83] with the addition of data points at its cruise speed for the 45-minute journey. These 45 minutes became the total shore-to-shore time. The data is recorded with non-uniform time intervals, and it is converted to a per min velocity profile that is used to develop a mechanical power profile for the ship at a uniform time step. This per min interpolation is done in Matlab® using the inbuilt interpolation function "pchip" to get a finer resolution that can be passed as an optimization time step during the problem formulation. The interpolated velocity in Figure 6.2a and Figure 6.3b shows the power requirements of *Island Discovery* throughout the trip. An approximate time of 15 mins was considered from the BC Ferries [11] website to account for time spent on the shore before departing again for the next voyage.

(a) Island Discovery. The image is obtained from MarineTraffic [83].

(b) The ship's operation between the port of Powell River and Blubber Bay MarineTraffic [83].

Figure 6.1: The image is of the ship studied in this thesis and the route on which it operates. The ship is on the right and the route is on the left MarineTraffic [83].

The Table 6.1 highlights the design and operational details of the ship. The ship travels between the two ports 16 times a day, accounting for 494 trips in a month. Therefore, the annual number of voyages the ship completes is 5928. The maximum displacement of the ship is 1778 tonnes. The displacement is an important factor used in the methodology that gives information regarding the total mass of the water displaced by the weight of the ship. Subsequently, this mass displacement is used to calculate the volume displacement. The estimation of the wetted surface area for the ship using the length, width, and draught i.e. the height of the ship's hull submerged in seawater is done leading to calculating the required resistance values and eventually arriving at the mechanical power requirements of the ship. Table 6.1 also highlights the DWT of the ship i.e. the load carrying capacity of the ship in tonnes along with the IMO registration number for identification, certification, and tracking.

Table 6.1: *Island Discovery*: Technical and Operational details [83, 11].

IMO	9831751		Trip duration	45 mins
Length	81.2 m		DWT	334 tonnes
Breadth	17 m		Draught	3.3 m
Max. Displacement	1778 tonnes		Stop at Shore	15 mins
Trips (Day)	16		Trips (Month)	494

The ship's velocity profile is presented in Table 6.2. The trip duration as per the data points is 30 minutes, although as per the BC Ferries [11] website, the ship's crossing time is 40 mins. Therefore, a conservative voyage time of 45 mins was considered to account for the worst-case scenario. The datasheet for the ferry as shown in Appendix B states the speed at design draught of the ship as 14 knots. However, the ship travels at a cruise speed of around 12 knots. This also provides validation for the optimum load point of the diesel generator as shown in Figure 4.3 which is found to be around 80 per cent loading.

Table 6.2: *Island Discovery*: Real-time velocity data points obtained from AIS data of MarineTraffic [83] with data point additions.

Real-Time	Velocity (kt)		Real Time	Velocity (kt)
2023-03-21 17:34 UTC	0		2023-03-21 17:57 UTC	12.2
2023-03-21 17:36 UTC	3.7		2023-03-21 17:59 UTC	7.4
2023-03-21 17:38 UTC	9.5		2023-03-21 18:01 UTC	3.1
2023-03-21 17:41 UTC	12		2023-03-21 18:03 UTC	0
2023-03-21 17:45 UTC	12.1			

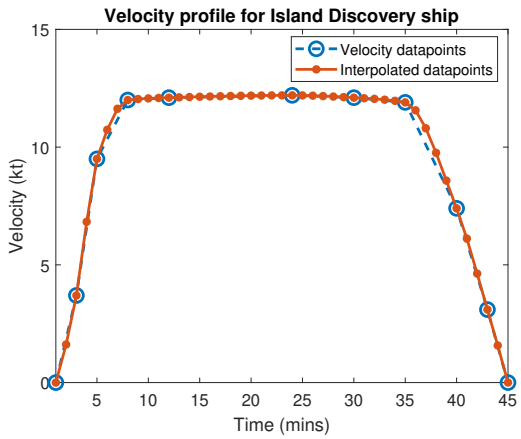

(a) Island Discovery: The interpolated velocity data points using the "pchip" function in Matlab® as well as the real-time velocity data points obtained from the MarineTraffic [83].

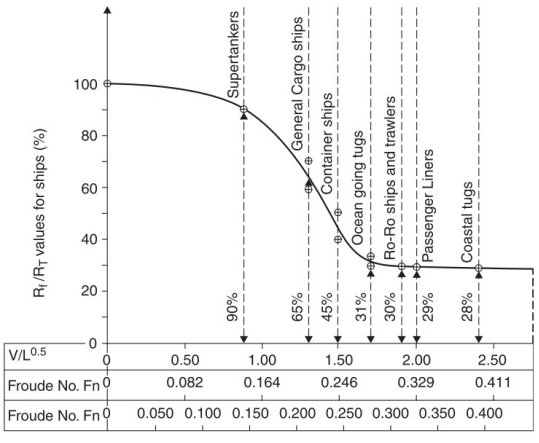

(b) The ratio of friction resistance to resistance in calm water conditions as a function of speed-length ratio for numerous ships operating at different service speeds and lengths Barrass [9].

Figure 6.2: The velocity profile shown in Figure 6.2a on the left and the ratio of frictional resistance to resistance in calm water conditions as a function of speed-length ratio as shown in Figure 6.2b on the right [9].

The velocity data points along with interpolated velocity data points and the frictional resistance to resistance in calm water condition ratio for various ships operating at different design speeds and lengths is shown in Figure 6.2. For *Island Discovery*, the length, and the design velocity of the ship can be used to calculate the speed-length ratio to estimate the percentage of friction resistance that accounts for the resistance in calm water conditions. The value of the speed-length ratio is 1.55 and therefore provides a range of 35 and 45 per cent as highlighted in the assumptions made earlier.

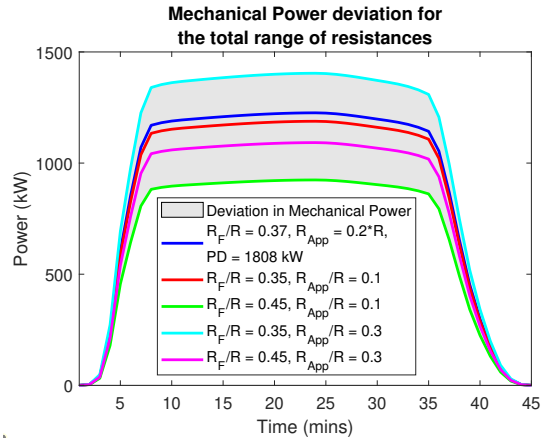

(a) The mechanical power deviation, highlighting the upper and lower bounds for the mechanical load prediction considering different resistance ratios. The figure also presented the values for the resistance ratios assumed to estimate the mechanical power for *Island Discovery*.

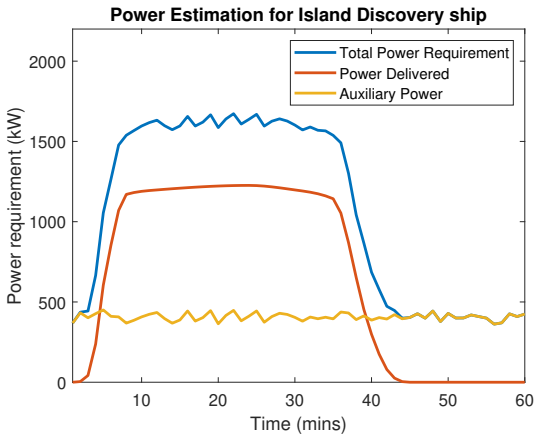

(b) Island Discovery: Estimated operational profile for a single trip using the methodology in section 3.1

Figure 6.3: The area of mechanical power deviation that can occur for assuming different resistance ratio values on the left in Figure 6.3a and the mechanical and auxiliary power requirements for the ship are estimated from the methodology described in section 3.1 on the right.

Figure 6.3 presents the results of the methodology explained in section 3.1. The Figure 6.3a highlights the upper and lower bounds for the deviation of the mechanical power requirements of the ship. The two resistance ratios that affect the power estimation are the frictional resistance to resistance in calm water conditions (R_F/R) ratio and the ratio of total resistance to resistance in calm water conditions (R_{APP}/R). As explained in Barrass [9], the design speed of the vessel has an impact on the residual resistance on the ship. The residual resistance consists of wave-making resistance and eddy-making resistance. The residual resistance as a function of the design speed of the vessel increases exponentially at a faster rate compared to the frictional resistance and contributes more to the resistance in calm water conditions. Therefore, the high-speed vessels have lower R_F/R value compared to slow-moving ships as shown in Figure 6.2b. The wind and appendage resistance depends on the external factors that increase the resistance of the ship. For harsh windy climates, the contribution is higher as compared to the ship sailing through calm seas. It also depends upon the direction of the ship's travel relative to the wind direction, along with the frontal area of the ship that is encountered by the waves and wind. Therefore, a mean value from the range is taken for the *Island Discovery ship*.

Figure 6.3b describes the total power requirements of the ship. The mean auxiliary power is assumed to be 20 per cent of the maximum mechanical power requirements, with a standard deviation of 5 per cent. For a ferry, the constant auxiliary power assumption can be valid as the requirements for the passengers for heating, lighting, and services are necessary. The auxiliary power is assumed to be electrical, whereas the mechanical power is the power delivered to the propeller by the motor. For higher speeds, the mechanical power requirement is more and vice versa, as the ships need to overcome the higher required resistance and maintain the velocity at the desired speed. In the Figure 6.3b, the mechanical power requirement is around 1200 kW at cruise speed (12 kt) as compared to an estimated 1800 kW at design/service speed (14 kt). As explained earlier, at low speed the ship is required to overcome low resistance and also the diesel generator is sized for optimum fuel consumption that occurs at 80-85 per cent of the load factor. The power requirement increases as the ship accelerates and falls steadily as it reaches the end of the journey. The ship reaches its cruise speed in 8–10 mins, and the same amount of time is required to decelerate and dock at the harbour.

6.2. Electrical Power, Cable Sizing and Losses for AC and BiDC grid

This section showcases the results obtained from the electrical power estimation of the ship explained in section 3.3 and the differences between the electrical power requirements for AC and BiDC grids. The section 3.2 is used to understand the different components that make up the respective grid and also use the power conversion efficiencies of these components to calculate the electrical power required. In addition to this, it also provides the results for the cable sizing and losses that occur in power distribution in respective grids.

The cable losses for the propulsion drive in AC and BiDC grid are presented in Figure 6.4a. The losses in the AC grid are higher than in the BiDC grid. The main reason for this is the operating voltage (690 V_{AC} and 1400 V_{DC}) that results in higher current flow from the cables in the AC grid compared with the BiDC grid. The losses are larger at higher power requirements and vice versa, mainly because of the increased current requirements at high power. At maximum power requirement, the losses in the BiDC grid are 41 per cent lower than its counterpart. Another reason that contributes to higher losses in AC is the difference in the resistance values due to different cross-sections of the cable used for AC and the BiDC grid at ambient temperatures, as shown in Table 6.3. These losses can also be attributed to the cable's skin effect phenomenon in AC grids, as the effective cross-section of the cable is affected due to it and has an effect on the resistance of the cable. Therefore, the BiDC grid is more efficient in power distribution as compared to its counterpart.

Table 6.3: Cable parameters for sizing and power loss estimation taken from Prysmian Group [102].

Parameters	AC Grid	BiDC grid
Resistance at 45 ^{o} C (R_{0AC} & R_{0DC})[Ω/Km]	0.168	0.136
Resistance at 70 ^{o} C ($R_{AC}(T_R)$ & $R_{DC}(T_R)$) [Ω/Km]	0.1845	0.1494
Current capacity of cable at 45^{o} C ($I_{Cap_{AC}}$ & $I_{Cap_{DC}}$) [A]	237	272
Voltage Drop [mV/Am]	0.333	0.311
Cable Weight [Kg/Km]	6330	5960
Voltage [V]	690	1400
Length (Switchboard to Motor) (L_{SB2M}) [m]	40	40
Temperature coefficient of Resistance of Copper (β) [1/K]	0.00393	0.00393
Results		
Number of propeller drive (N_P)	2	2
Design Current ($I_{B_{AC}}$ & $I_{B_{DC}}$) [A]	878.3386	749.7969
Design Current Reduction [%]	-	14.63
Number of Cables (NC_{AC} & NC_{DC})	5	4
Weight of Cables [Tonnes]	2.5320	1.9072
Weight Reduction [%]	-	24.67
Voltage Drop (Continuous) [%]	0.3391	0.1666
Voltage Drop (Short Circuit) [%]	1.6956	0.8328

The Figure 6.4b highlights the difference in electrical power requirement for AC and BiDC grids. The difference in power requirement is larger for high power duration as compared to the low power during time spent in the port. The electrical components that make up the AC grid are three winding transformers, variable frequency drives connected to the motor, the auxiliary transformer connected to the auxiliary loads and if the arrangement permits the shore transformer that integrates and forms a connection with the shipboard microgrid. On the BiDC side, these components are replaced by power electronic conversion devices like inverters connected to auxiliary as well as propulsion loads and rectifiers for shore infrastructure to convert the incoming AC power to DC power for integration with the shipboard microgrid. The typical efficiency values for all these components range between 95-98 per cent [6, 63, 47, 62, 64, 5, 118, 4, 94, 93, 26]. The average efficiency values for this study are taken as 0.95 for all electrical components. The generator-side component efficiencies are not included in the power requirements and represent the power requirements at the AC and BiDC switchboards. The

average efficiency value for the inverter (AC) and DC/DC converter (BiDC) coupled with the battery is taken as 0.92 based on the efficiency values seen in the literature [91, 97, 32]. The main reason for the comparatively lower power requirements for the BiDC grid is the absence of additional components required for propulsion power delivery. This could also be explained through the ship's schematic electrical layout, explained in section 3.2 and presented in Figure 3.3 which highlights the requirement of two electrical components for power distribution in AC compared to one device in BiDC grid. The cable losses also contribute to lower power requirements although, the contributions are marginal.

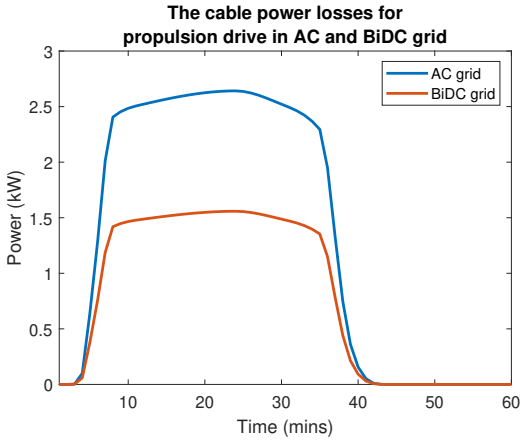

(a) The cable losses estimated for AC and BiDC grid. The cable power losses are higher for AC as compared with BiDC grid

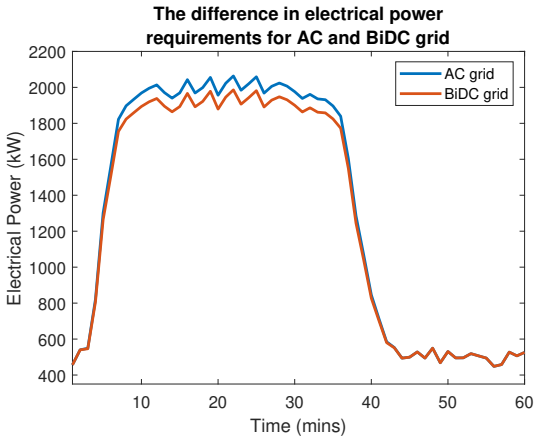

(b) The electrical power estimation for AC and BiDC grid. The electrical power requirements are higher of AC as compared to the BiDC grid

Figure 6.4: The electrical power estimation as per the component efficiencies that incorporate the grid as well as the cable electrical losses for AC and BiDC grid

The cable sizing for DC reduces the total weight of the cable required for the propulsion motor along with the number of cables as shown in Table 6.3. For an AC grid, a cable consisting of four wires (one conductor per phase and a neutral wire) whereas a cable with three wires (positive, negative, and neutral wire) is used that significantly reduces the total weight of the cables. In addition to this, the main reasons for the reduction in the number of cables compared to the AC grid are the higher operating voltage, a higher current carrying capacity of the cable, and lower electrical cable losses. For the AC grid, the number of cables required is five and the weight accounts for 2.532 tonnes, whereas in the BiDC grid, the number of cables is reduced to 4 and a weight reduction of 24.67 per cent is observed.

6.3. Emission Estimation for AC1 and DC1 Arrangements

The emission estimation for the AC1 and DC1 arrangement is straightforward, as it consists of two diesel generators, eliminating the need for optimization problem formulation. The required equations that are to be satisfied for each arrangement are explained in section 4.4. The methodology developed estimates the emissions for each diesel generator sizing catalogued in Appendix A for both the AC and BiDC grid architectures. The solution front for capital costs, operating costs and the system weight for all the possible solutions is shown in Figure 6.5. A total of 14 diesel generator sizing for AC and 12 diesel generator sizing for BiDC grid have an emission estimation. The points in the red asterisks represent the results of diesel generators operating on the AC grid, whereas the blue asterisk highlights the results for the BiDC grid topology.

The effect of increasing the capacity of diesel generators on the emissions is shown in Figure 6.5a. In the AC grid, the emissions are increasing as the capital cost of the system increases. As the power rating on these diesel generators increase, the capital cost of the propulsion system increases. The estimation for the capital cost takes into account all the components that are presented in Figure 3.3 except for the motor and cable costs. The motor cost is neglected, as the same power rating motor is required for propulsion irrespective of the grid in use for *Island Discovery* ship. The cost of power cables is difficult to compute and can be negligible compared to the cost of the propulsion system. The Table 6.4 highlights the necessary parameters used in the optimization problem. The cost index for the

transformer and power electronic components is calculated using the ratio of February 2023, February 2014 and June 2023, June 2014 values, respectively. The values are highlighted in Table 6.4. The oversized diesel generators function at a non-optimum load point, resulting in higher fuel consumption, leading to higher CO_2 emissions. This non-optimum load point operation occurs mainly due to its speed restrictions in the AC grid for its safe operation. In this case, the AC grid is operating at 50 Hz. The diesel model developed for AC in section 4.4 highlights the increase in specific fuel oil consumption for deviation from the optimum load point. In the BiDC grid, the diesel generator is decoupled from the speed at which it operates, leading to near-optimum specific fuel oil consumption over the operational profile of the diesel generator as per the model developed in section 4.4. As a result, the oversized diesel generator also functions at near-optimum specific fuel oil consumption, leading to a flat/marginally decreasing trend for CO_2 emissions. This is a result of the increasing efficiency of diesel generators as a function of larger power capacity and this trend can be observed in Appendix A.

Table 6.4: The value for parameters used in this study

Parameter	Value	Reference		Parameter	Value	Reference
DGC [$/kW]	235	[84]		$Cost_{Fuel}$ [$/ton]	545.32	[111]
$BatC$ [$/kWh]	151	[116]		$Cost_{Shore}$ [$/kWh]	0.1872	[84]
CI_{TF}	1.7160	[121]		$EF_{CO_2}[g_{CO_2}/g_{Fuel}]$	3.206	[58]
CI_{Elec}	0.9625	[122]		$EF_{Shore}[g_{CO_2}/kWh]$	418	[84]

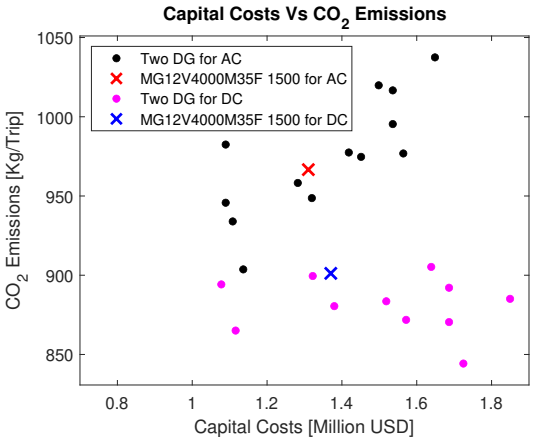

(a) The capital cost versus emissions for different DGs from the catalogue for AC and BiDC grid

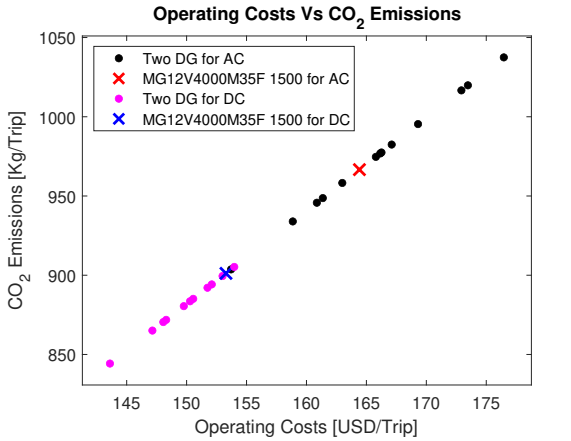

(b) The operating cost versus emissions for different DGs from the catalogue for AC and BiDC grid

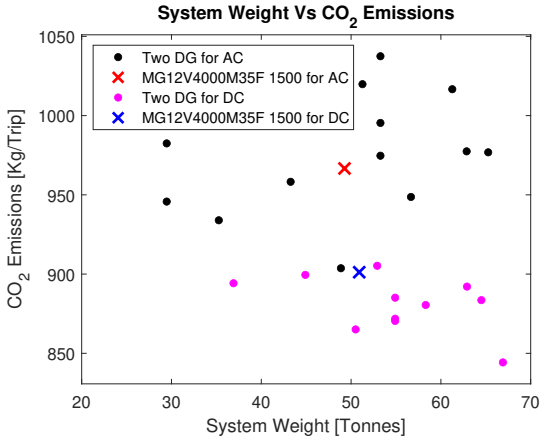

(c) The system weight versus emissions for different DGs from the catalogue for AC and BiDC grid

Figure 6.5: The emission estimation for AC1 and DC1 arrangement, i.e. Two diesel generators. The asterisks are for the component sizing that satisfies the constraint

The operating costs and their relation to the emissions are presented in Figure 6.5b. The emissions follow a direct relation with the operating cost, as the only variable that constitutes it is fuel costs. The fuel consumption is directly related to CO_2 emissions and is quantified using the emission factor. The value of it is presented in Table 6.4. The reduction in fuel consumption reduces the operating costs and emissions. The BiDC grid is proving beneficial in reducing operating costs due to the nature of diesel generator operation. The system weight for different configurations for AC and BiDC grids is shown in Figure 6.5c. The range for the AC and BiDC grid weight is similar, with the BiDC grid being marginally heavier. Although, the emission reductions observed are quite visible for the BiDC grid.

The minimum emission observed for the AC grid is 903.6793 [Kg/Trip] whereas the same value stands at 844.2631 [Kg/Trip] for BiDC grids. For the ship in question, as presented in Appendix B. The diesel generator of 1500 kWe is considered for comparisons, although a minimum emission value can be possible for other configurations. The emissions for the ship's configuration are 966.6350 [Kg/Trip] for the AC grid and 901.1793 [Kg/Trip] for the BiDC grid. The emissions are lower for the range of diesel generators and also for the configuration of *Island Discovery*.

The power profile for both the arrangements for a 1500 kWe diesel generator is shown in Figure 6.6. In both cases, the total electrical power requirement is divided equally between the two diesel generators. The fluctuations in the electrical power are shared by the two diesel generators as per the conditions described in Equation 4.9, as the shipboard microgrids are weak in nature. The diesel generators follow the power profile smoothly in AC as well as BiDC grid. The CO_2 emissions are estimated using the diesel generator model for fixed speed and variable speed, using the loading factor.

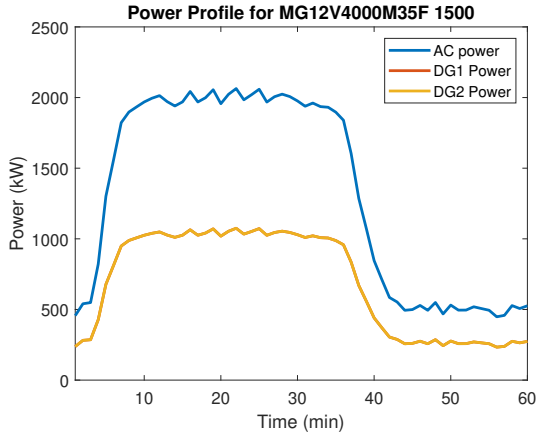

(a) The operational power profile for AC with two diesel generators

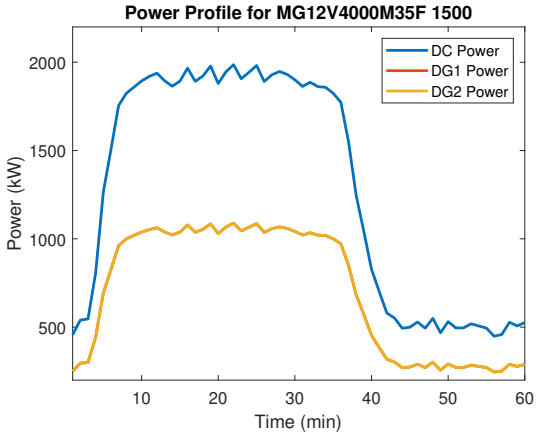

(b) The operational power profile for BiDC with two diesel generators

Figure 6.6: The operational power profiles for AC and BiDC

The BiDC grid results in lower CO_2 emissions as compared to its AC grid counterpart for two diesel generator arrangements.

6.4. Emissions for AC2 and DC2 Arrangement

This arrangement is similar to the previous arrangement except for the addition of the battery. The main idea is to utilise the energy from the battery to help reduce emissions. When the ship is in the port during the loading and unloading phase, the diesel generators should run at an optimum point, reducing specific fuel oil consumption and emissions by charging the battery so that the ship is ready for the next voyage. The constants highlighted in Table 6.4 are also used in this arrangement, along with the average efficiency values for different electrical components, to have similarity between the simulations.

The Figure 6.7a highlights the configurations for which a feasible solution exists, and a comparison between emissions and capital costs is shown. There is an increasing trend in the emissions for

rising capital costs of the system for AC grids. The horizontal lines are for different battery sizes, that only affect the capital costs and do not have an effect on the emissions, meaning the use of the battery is not assisting in reducing emissions for optimal dispatch. The larger diesel generators face the same problem as seen in section 6.3 where the emissions rise due to an increase in specific fuel oil consumption leading to higher emissions. For BiDC grids, the ship's operational emissions follow the same horizontal trend. However, the inherent reduction in CO_2 as seen in section 6.3 is also visible here. The overall trend is flat/marginally decreasing as larger diesel generators are more efficient, having lower specific fuel oil consumption at full loading.

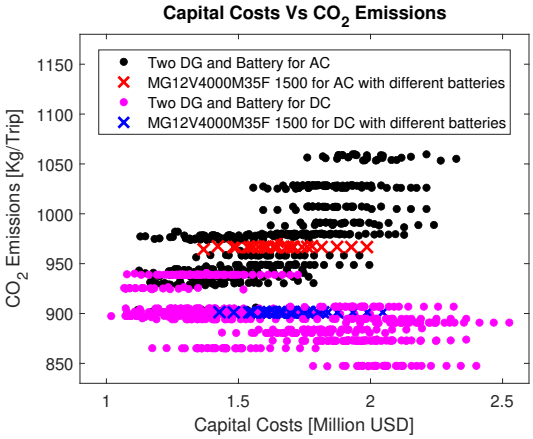

(a) The capital cost versus emissions for different DGs from the catalogue for AC and BiDC grid

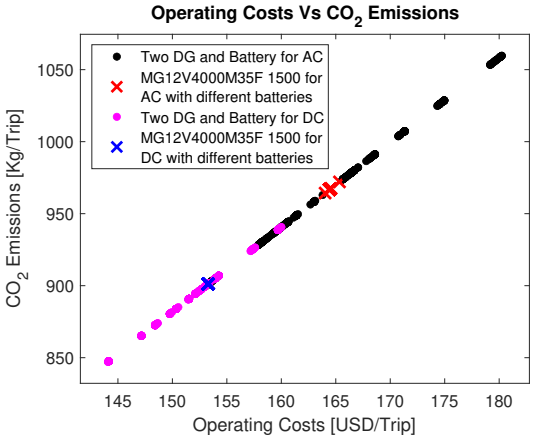

(b) The operating cost versus emissions for different DGs from the catalogue for AC and BiDC grid

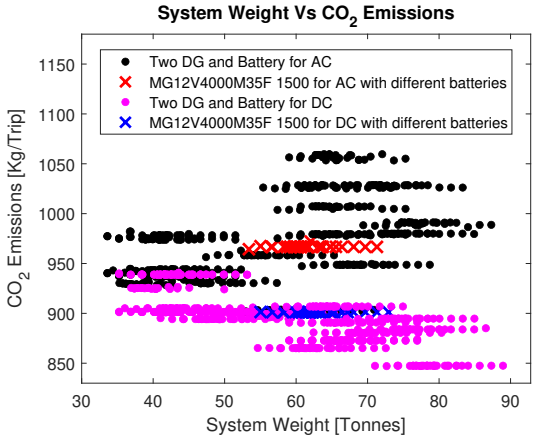

(c) The system weight versus emissions for different DGs from the catalogue for AC and BiDC grid

Figure 6.7: The emission estimation for AC2 and DC2 arrangement, i.e. Two diesel generators and battery bank. The asterisks are for the component sizing that satisfies the constraint

The operational costs and the system weight are compared with the ship's operational emissions in Figure 6.7b and Figure 6.7c, respectively. The linear relation is visible as the operating costs considered are just the fuel expenses. The effect of the addition of a battery on the ship is not assisting in reducing the emissions. This is because the idle shore time of 15 mins for the ship is not justified by the losses that take place during the charging and discharging of the battery. If the energy from the battery is utilised considering the conversion losses for the battery and inverter (AC grid)/ DCDC converter (BiDC) system, then the cumulative emissions from the charging of the battery when the ship is at shore would result in higher emissions than the arrangement with just two diesel generators. The type of propulsion system is a series hybrid propulsion and a disadvantage of these systems is additional losses during energy conversion as highlighted in Table 2.3. The system weight provided in the datasheet is for this configuration, as the ship's original configuration consists of two diesel generators and a battery. Therefore, the 334 tonne of load carrying capacity is for this arrangement.

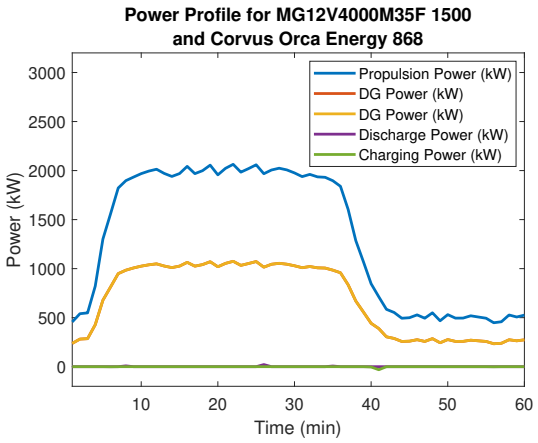

(a) The optimal operational profile for optimal dispatch for AC2 arrangement

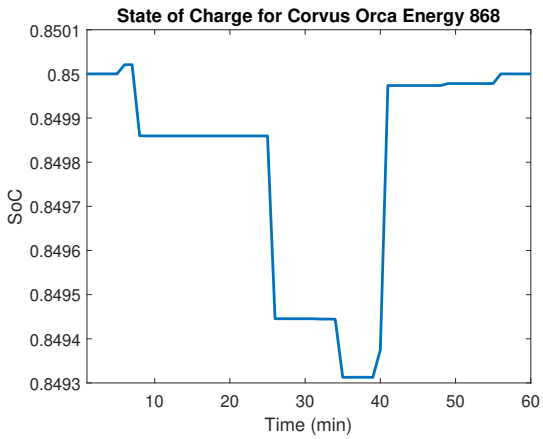

(b) The state of charge of battery for AC2 arrangement

Figure 6.8: The operational profile and SoC of MG12V4000M35F 1500 kWe gen set and Corcus Orca 868 kWh battery bank for AC2 arrangement

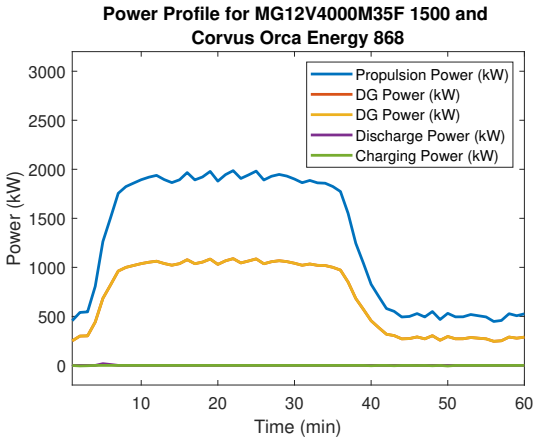

(a) The optimal operational profile for optimal dispatch for DC2 arrangement

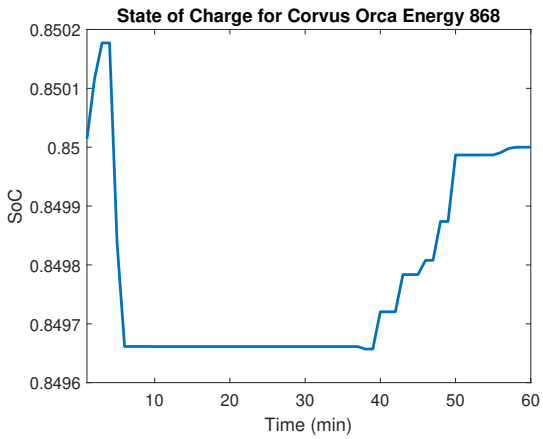

(b) The state of charge of battery for DC2 arrangement

Figure 6.9: The operational profile and SoC of MG12V4000M35F 1500 kWe gen set and Corcus Orca 868 kWh battery bank for DC2 arrangement

The minimum emissions achieved for the AC grid in this arrangement out of the 593 configurations for which a feasible solution exists, is 899.898 Kg/Trip, whereas, in the BiDC grid, out of the 588 configurations the minimum emissions stand at 847.0864 Kg/Trip. The *Island Discovery* ship has a battery bank of 800 kWh capacity installed on the ship, as shown in Appendix B. The battery bank is provided by Corvus Energy [23]. Therefore, for all the arrangements with batteries, the 868 kWh battery from Corvus Energy along with its technical parameters is considered for comparing different arrangements. For the configuration shown in Figure 6.8 for AC grid as well as in Figure 6.9, the trend is similar as in both arrangements the installed capacity of the battery is not utilised because of additional conversion losses that can lead to higher emissions even if the batteries are allowed to charge when power requirements are low during the ships shore time. The emissions for the selected configuration are 966.6350 Kg/Trip for the AC grid and 901.1793 Kg/Trip for the BiDC grid. These emission estimates are marginally higher than the arrangements in section 6.3 as in both cases the SoC of the battery is utilised on a minuscule level and that is reflected in comparatively higher emissions compared to their AC and BiDC counterparts with two diesel generators, respectively. The BiDC grid results in lower CO_2 emissions as compared to its AC grid counterpart for two diesel generators and a battery arrangement.

6.5. Emissions for AC3 and DC3 Arrangement

The third arrangement considered is similar to section 6.4, with an added source for power in the form of a shore connection. The power from shore can be utilised only when the ship is at shore during the 15 minutes of loading and unloading. The idea is to use the energy from the battery and utilise the power from the shore to charge the battery and supply the auxiliary power to the ship's consumers. The diesel generators are switched off as they reach the shore. In this way, the problem is solved for unit commitment and the optimization is performed to obtain an optimal power dispatch profile for minimising the emissions from the operation of the ship. The optimization problem constants are shown in Table 6.4. The Figure 6.10 highlights the change in CO_2 emissions for capital costs, operating costs and propulsion system weight. In the AC grid, the oversizing of the diesel generators leads to an increase in emissions, as seen in Figure 6.5a and Figure 6.7a. In the BiDC grid, the overall emissions from different configurations are found to be lower than their AC counterparts. However, in both arrangements, the emissions for each diesel generator with increasing battery are seen to have a decreasing trend until it flattens out. This is because the increasing battery capacity leads to a higher energy discharge from the battery, which is charged by the shore power as the ship is at the harbour. The flattening of the curves is a result of oversizing the battery, which leads to an increase in capital costs without reducing emissions.

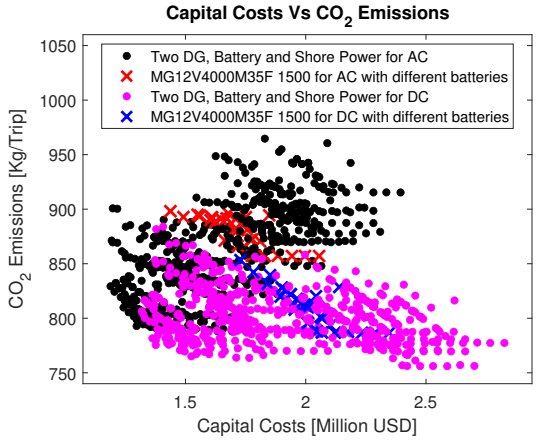

(a) The capital cost versus emissions for different DGs from the catalogue for AC and BiDC grid

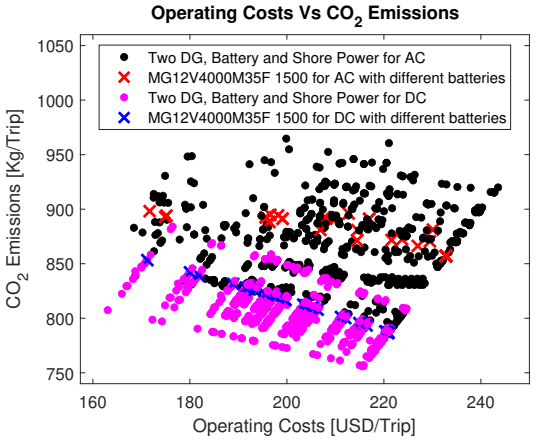

(b) The operating cost versus emissions for different DGs from the catalogue for AC and BiDC grid

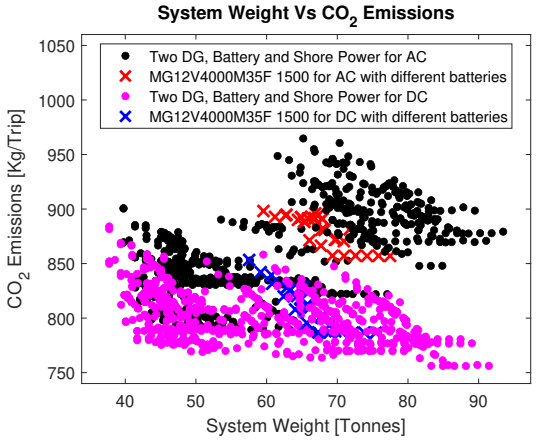

(c) The system weight versus emissions for different DGs from the catalogue for AC and BiDC grid

Figure 6.10: The emission estimation for AC3 and DC3 arrangement, i.e. Two diesel generators, battery bank and shore power. The asterisks are for the component sizing that satisfies the constraint

The Figure 6.10b includes the cost of fuel as well as the average cost of electricity delivered from the shore. For both arrangements, the CO_2 emissions and operating cost have an inverse relation. The

reduction in emissions observed from the increase in capital costs as a result of larger battery capacity is followed by higher operating costs for the use of electricity from the shore. This trend can be seen in the power profiles shown for AC and BiDC grids in Figure 6.11a and Figure 6.12a, respectively. The power from the shore is delivered at maximum capacity to charge the battery, as seen in the SoC of the battery in Figure 6.11b and Figure 6.12b. The available energy from the battery is depleted during the operation of the ship and the depleted capacity is replaced by the energy delivered by the shore power, resulting in emission reduction. The Figure 6.10c highlights the system weight against the ship's emissions. The larger battery capacity is followed by an increase in the propulsion system weight due to an increase in the weight of the battery. Although the range of propulsion weight for both arrangements lies within a comparatively similar range, the minimum emissions achieved for BiDC grids are higher than AC grids when compared amongst all the feasible configurations of diesel generators and battery banks.

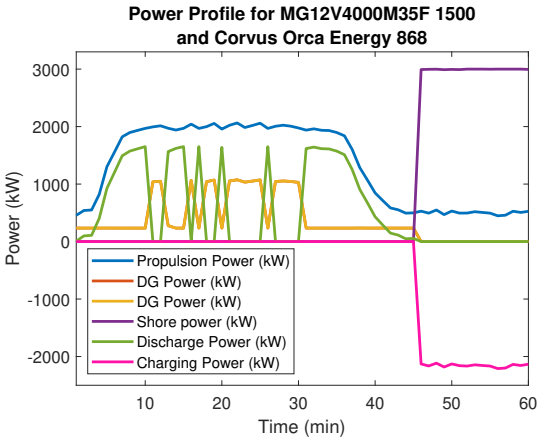

(a) The optimal operational profile for optimal dispatch for AC3 arrangement

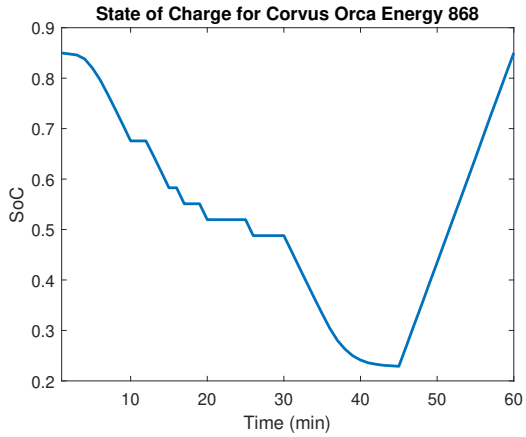

(b) The state of charge of battery for AC3 arrangement

Figure 6.11: The operational profile and SoC of MG12V4000M35F 1500 kWe gen set and Corcus Orca 868 kWh battery bank for AC3 arrangement

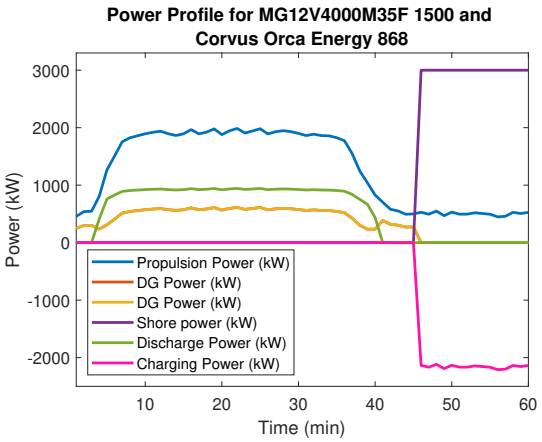

(a) The optimal operational profile for optimal dispatch for DC3 arrangement

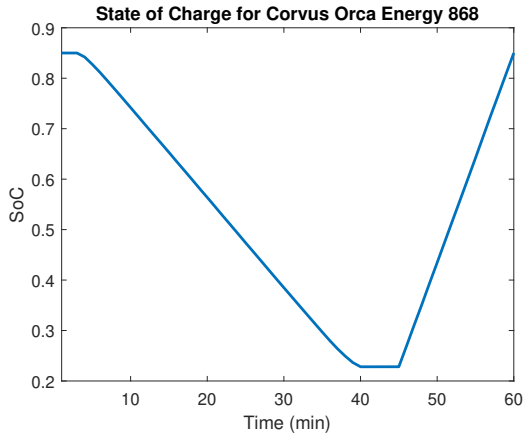

(b) The state of charge of battery for DC3 arrangement

Figure 6.12: The operational profile and SoC of MG12V4000M35F 1500 kWe gen set and Corcus Orca 868 kWh battery bank for DC3 arrangement

The Figure 6.11 and Figure 6.12 highlight the power profile and SoC of the battery bank for the configuration of *Island discovery* ship for AC as well as BiDC grid. The emissions observed for AC and BiDC grids for this configuration are 857.0973 Kg/Trip and 786.9327 Kg/Trip respectively. The CO_2 emissions from the use of shore infrastructure are less when compared with emissions from

section 6.3 and section 6.4. However, the minimum CO_2 emissions observed over the 677 and 682 feasible configurations for AC and BiDC grids stand at 787.9265 Kg/Trip and 756.0871 Kg/Trip for the AC and BiDC grids, respectively.

The minimum emissions calculated for the AC and BiDC grids show that the BiDC grids can emit less CO_2 emissions for the ship's operational profile for two diesel generators, battery, and shore power arrangement. The main reasons for that are the diesel generator operational characteristics for the respective grid highlighted in Figure 2.11, the difference in electrical power requirements as shown in section 6.2 and the availability of shore power as the average emissions from shore electricity are less than the emissions from diesel generators.

6.6. Emissions for AC4 and DC4 Arrangement

The results in this section are presented for an arrangement with one diesel generator and battery for the AC and BiDC grid. The optimization problem constants are highlighted in Table 6.4 and are used for this comparison as well. The main reason to do it is to have uniformity when comparing different arrangements and grids. The CO_2 emissions are compared with the capital costs, operating costs and the weight of the propulsion system in Figure 6.13 for all the feasible configurations. The flat trend in capital costs and emissions was also seen in section 6.4 However, the difference between the two AC grids is visible with the AC2 arrangement on a broader scale showing an increasing trend in emissions with higher capital costs for bigger diesel generators. The elimination of one diesel generator leads to the use of the battery bank to satisfy the remaining power requirements. The feasible solution from the optimization problem formulation yields results only if the battery bank is big enough to satisfy the power and energy demand from the loads. Therefore, the increased capacity for a bigger battery bank results in no further reduction in emissions. The increased capacity only has an impact on the SoC levels of the battery, with higher capacity batteries depleting less and vice versa. Furthermore, the depleted battery is charged with a single diesel generator, leading to optimal load point operation even when the ship is at the harbour. This explains the flat trend seen in Figure 6.13a for both the AC and BiDC grids.

The system weight remains constant and flat for selected diesel generators, and increasing battery capacity because of the increased weight does not assist in reducing the CO_2 emissions as shown in Figure 6.13c. The minimum emissions estimated for AC and BiDC grid for all feasible 302 and 287 configurations are 849.9801 Kg/trip and 813.8636 Kg/Trip, respectively. For the configuration used in *Island Discovery* ship, the emissions from the AC and BiDC grid calculated are 905.5203 Kg/Trip and 900.6764 Kg/Trip, respectively. The Figure 6.14 and Figure 6.15 present the optimal dispatch of diesel generator and battery for the AC and BiDC grid, respectively. The SoC of the battery bank for both arrangements first increases as the ship is accelerating and reaching the cruise speed. After this, the difference in power is supplied by the battery and therefore the SoC decreases till the ship decelerates and reaches the shore. Consequently, the diesel generator supplies the additional power to the battery to charge the battery again and prepare for the next voyage. In doing so, the diesel generator operates at a load point that is more optimal as compared to the arrangement shown in Figure 6.5 leading to a decrease in specific fuel oil consumption and CO_2 emissions.

The Figure 6.13b presents the operating cost of the ship over a single trip for all the feasible configurations. The trend is linearly increasing as the only factor included in estimating the operating costs is fuel prices and the CO_2 emissions are linearly related to the amount of fuel consumption. The AC grid and DC grid operating costs are closely packed, however, the BiDC grid shows larger emission minimization compared to the AC grid. The emission reductions observed from this arrangement (AC4 and DC4) when compared with arrangements shown in section 6.4 are higher for its AC arrangement as compared to its BiDC arrangement. This is mainly possible due to the elimination of one diesel generator, as in AC2 and DC2 arrangements, both power producers operate at sub-optimum load factors leading to higher specific fuel oil consumption resulting in higher operating costs.

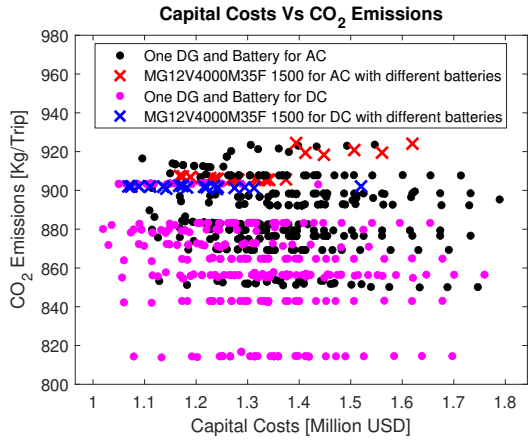

(a) The capital cost versus emissions for different DGs from the catalogue for AC and BiDC grid

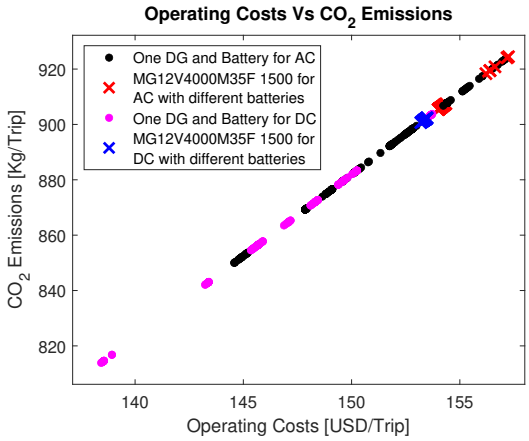

(b) The operating cost versus emissions for different DGs from the catalogue for AC and BiDC grid

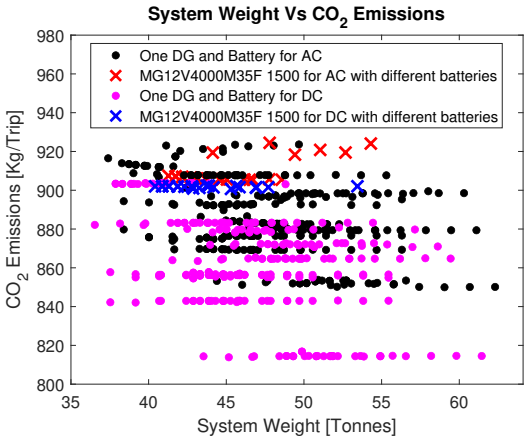

(c) The system weight versus emissions for different DGs from the catalogue for AC and BiDC grid

Figure 6.13: The emission estimation for AC4 and DC4 arrangement, i.e. One diesel generator and battery bank. The asterisks are for the component sizing that satisfies the constraint

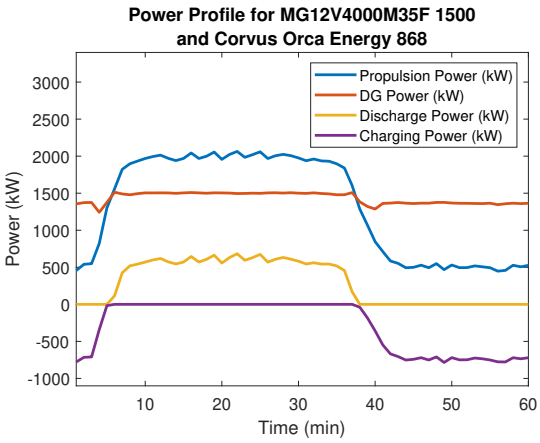

(a) The optimal operational profile for optimal dispatch for AC4 arrangement

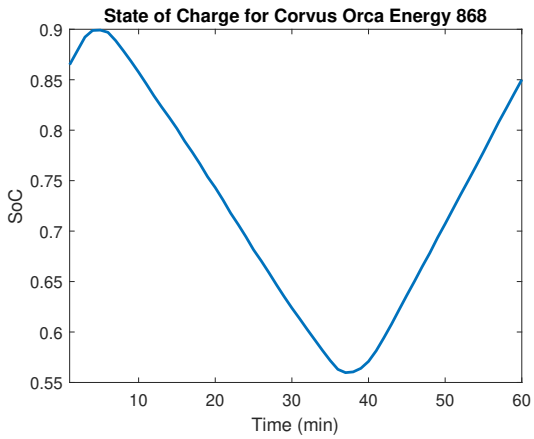

(b) The state of charge of battery for AC4 arrangement

Figure 6.14: The operational profile and SoC of MG12V4000M35F 1500 kWe gen set and Corcus Orca 868 kWh battery bank for AC4 arrangement

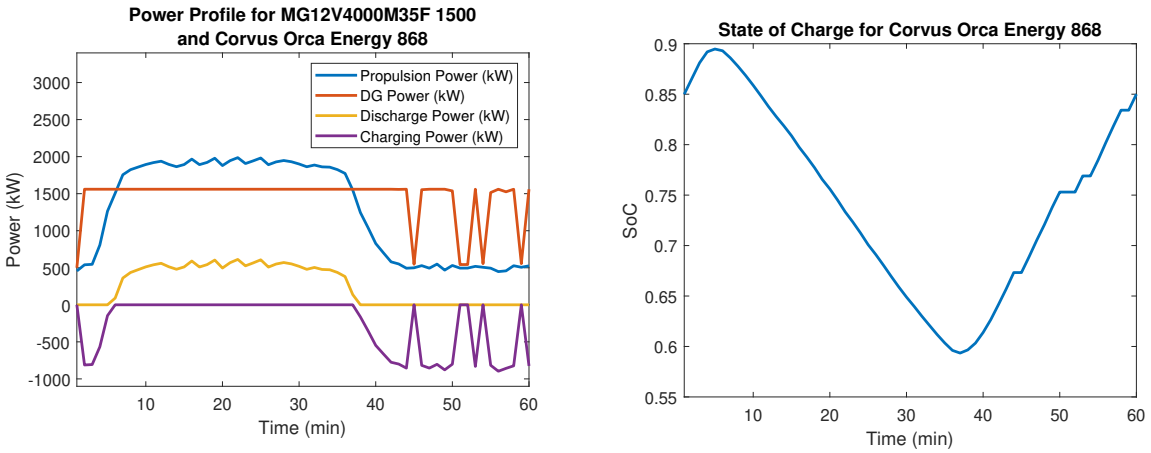

(a) The optimal operational profile for optimal dispatch for DC4 arrangement

(b) The state of charge of battery for DC4 arrangement

Figure 6.15: The operational profile and SoC of MG12V4000M35F 1500 kWe gen set and Corcus Orca 868 kWh battery bank for DC4 arrangement

The elimination of one diesel generator and addition of a battery bank leads to the minimization of emissions for the AC arrangement, as the diesel generator is operated at a better load factor as compared to the arrangement shown in section 6.3. The addition of a battery with two diesel generators is inefficient if shore power is not available, as seen in section 6.4 and Figure 6.10. Here again, the BiDC grid has shown to be more emission-friendly than the configuration running on the AC grid.

6.7. Emissions for AC5 and DC5 Arrangement

This arrangement is similar to the arrangements seen in section 6.6 with the addition of shore power to charge the battery when the ship reaches the shore. Here again, as explained in section 6.5, the unit commitment problem is solved first, and the optimization is performed to minimise the emissions over the ship's operational profile, leading to an optimal dispatch solution. The optimization problem constants are highlighted in Table 6.4 and used for this comparison as well. The emissions from the diesel generators are therefore significantly reduced in all four arrangements (AC3, AC5, DC3 and DC5). However, the emissions over the ship's operational profile occur due to the diesel generator and the electrical received from the shore infrastructure.

The Figure 6.16 presents the results for the emissions for the AC and the BiDC grids in relation to the capital costs, operating costs and the weight of the propulsion system. The capital costs and the CO_2 emissions have an inverse relationship for both arrangements, as shown in Figure 6.16a. The cause for the increase in capital cost is the different diesel generators and battery sizes. However, the decreasing trend seen in the emissions is mainly due to the complete discharge of the battery and with higher battery capacity, leading to a larger fall in emissions. This is also reflected in the operating costs of the system, as shown in Figure 6.16b as the amount of electricity consumed from the shore increases, the emissions decrease. The capital costs at higher values flatten for both cases and the reason can be attributed to the over-sizing of the battery even in the presence of shore power due to the technical and operating power limits that constrain the further depletion of energy content in the batteries. This can be seen in Figure 6.17b and Figure 6.18b as the battery state of charge remains constant as the ship near the harbour for loading and unloading, mainly due to the deceleration of the ship. The system weight increases as we increase the battery capacity, leading to a reduction in the CO_2 emissions as shown in Figure 6.16c. However, the decreasing trend flatten out because of the oversizing of the battery, leading to no change in the emission estimation. In the AC grid, the emissions are higher compared to the BiDC grid.

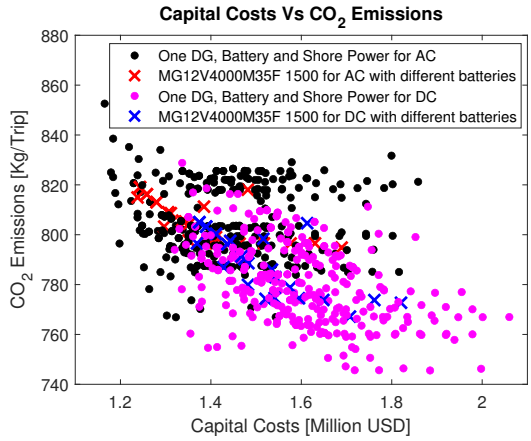

(a) The capital cost versus emissions for different DGs from the catalogue for AC and BiDC grid

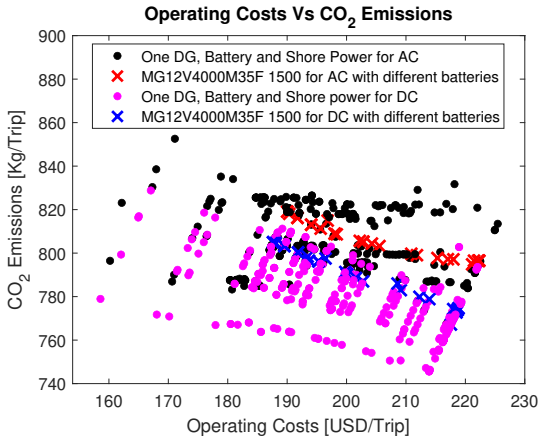

(b) The operating cost versus emissions for different DGs from the catalogue for AC and BiDC grid

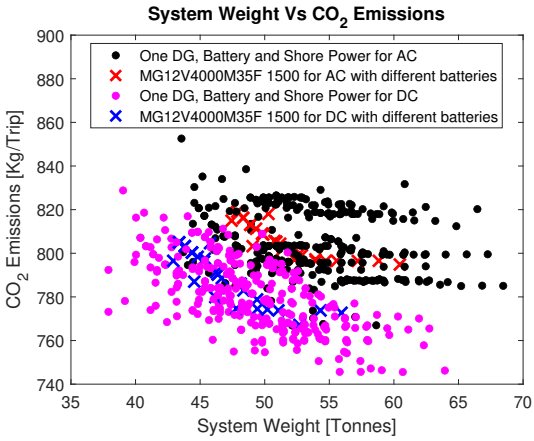

(c) The system weight versus emissions for different DGs from the catalogue for AC and BiDC grid

Figure 6.16: The emission estimation for AC5 and DC5 arrangement, i.e. One diesel generator, battery bank and shore power. The asterisks are for the component sizing that satisfies the constraint

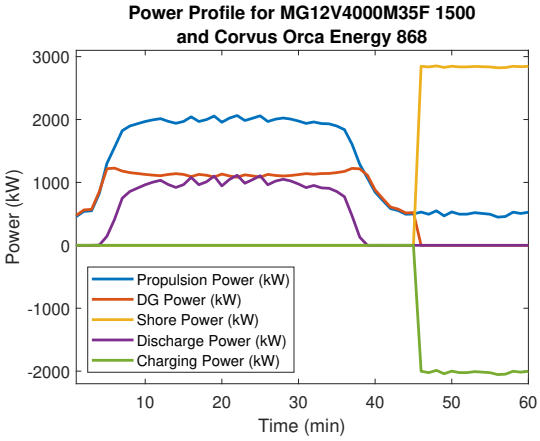

(a) The optimal operational profile for optimal dispatch for AC5 arrangement

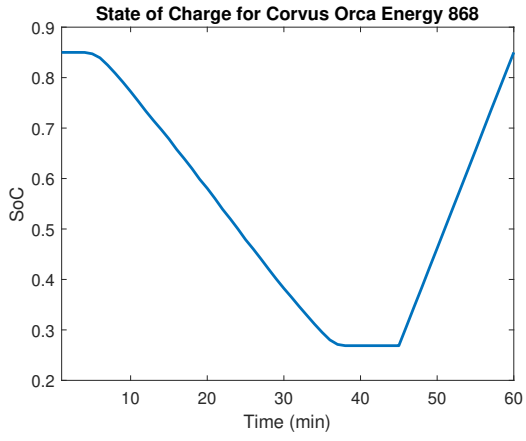

(b) The state of charge of battery for AC5 arrangement

Figure 6.17: The operational profile and SoC of MG12V4000M35F 1500 kWe gen set and Corcus Orca 868 kWh battery bank for AC5 arrangement

The number of feasible configurations for AC and BiDC grids for this arrangement are 330 and 338, respectively. The minimum emission estimations for the AC and BiDC grid are 766.8943 Kg/Trip and

745.5512 Kg/Trip, respectively. The Figure 6.17a and Figure 6.18a highlight the optimal dispatch strategy for minimum emissions for the selected configuration of the diesel generator and battery bank. For the configuration selected for *Island Discovery* ship, the emission estimation is 797.1244 Kg/Trip and 774.6717 Kg/Trip for the AC and BiDC grid, respectively. This is a huge reduction in emissions as compared with the values for the arrangement AC1 and DC1 as shown in section 6.3 which stand at 966.6350 Kg/Trip for the AC grid and 901.1793 Kg/Trip for the BiDC grid.

The Insufficient use of the battery capacity in section 6.6 is fulfilled in this arrangement as the battery can be charged with high power transfer from the shore compared to the limitations from the diesel generator units. Consequently, this leads to minimizing emissions. However, the emissions calculated for the BiDC grid are lower than the estimations for the AC grid.

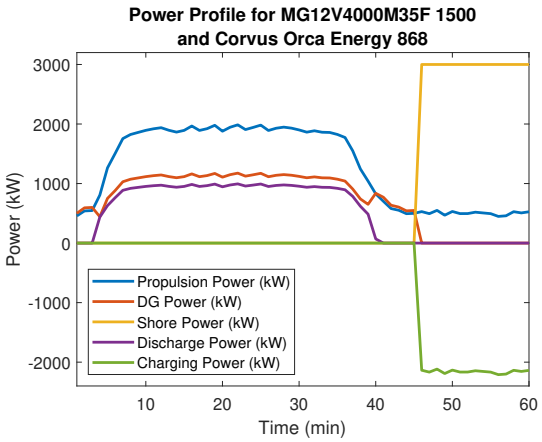

(a) The optimal operational profile for optimal dispatch for DC5 arrangement

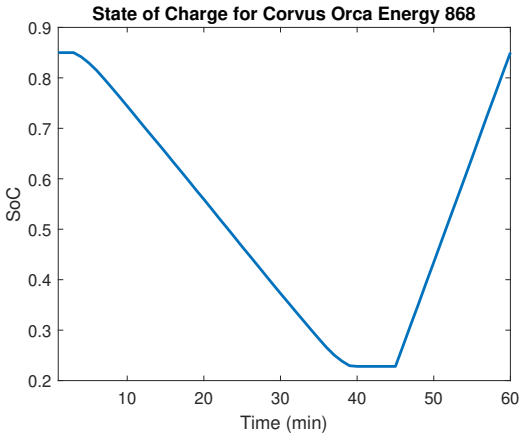

(b) The state of charge of battery for DC5 arrangement

Figure 6.18: The operational profile and SoC of MG12V4000M35F 1500 kWe gen set and Corcus Orca 868 kWh battery bank for DC5 arrangement

6.8. System Analysis

The Table 6.5 for minimum emissions over the operational profile of the ship, Table 6.6 for fuel consumption over the voyage, Table 6.7 for the capital cost of the propulsion system, Table 6.8 for the operating cost of the ship, Table 6.9 for the propulsion system weight and Table 6.10 for the effect on the load carrying capacity, present a comprehensive comparison for the selected *Island Discovery* ship configuration between all the arrangements considered in this study. The key performance indicators are calculated as described in the methodology in chapter 5 whereas the minimum emissions are calculated as per the optimization problem formulation in chapter 4. The weight of these power electronic devices is assumed to be 2.5 tonnes as a conservative value after looking at different datasheets [63, 62, 64, 94, 93]. The rows represent the arrangement with which the arrangement in the column is compared. For example, the arrangement in row (AC5) is compared with the arrangement in column (AC1) and shows a 17.54 per cent reduction in emissions.

Table 6.5: Minimum CO_2 emission estimation comparison for all arrangements for configuration selected for *Island Discovery* ship

arrangement	AC1		AC2		AC3		AC4		AC5		DC1		DC2		DC3		DC4		DC5	
Change	Absolute	Percent	Absolute	Percent	Absolute	Percent	Absolute	Percent	Absolute	Percent	Absolute	Percent	Absolute	Percent	Absolute	Percent	Absolute	Percent	Absolute	Percent
AC1	966.64		-0.18	-0.02	109.54	12.78	61.11	6.75	169.51	21.27	65.46	7.26	65.39	7.26	179.70	22.84	65.96	7.32	191.96	24.78
AC2	0.18	0.02	966.81		109.71	12.80	61.29	6.77	169.69	21.29	65.63	7.28	65.57	7.28	179.88	22.86	66.14	7.34	192.14	24.80
AC3	-109.54	-11.33	-109.71	-11.35	857.10		-48.42	-5.35	59.97	7.52	-44.08	-4.89	-44.15	-4.90	70.16	8.92	-43.58	-4.84	82.43	10.64
AC4	-61.11	-6.32	-61.29	-6.34	48.42	5.65	905.52		108.40	13.60	4.34	0.48	4.27	0.47	118.59	15.07	4.84	0.54	130.85	16.89
AC5	-169.51	-17.54	-169.69	-17.55	-59.97	-7.00	-108.40	-11.97	797.12		-104.05	-11.55	-104.12	-11.55	10.19	1.30	-103.55	-11.50	22.45	2.90
DC1	-65.46	-6.77	-65.63	-6.79	44.08	5.14	-4.34	-0.48	104.05	13.05	901.18		-0.07	-0.01	114.25	14.52	0.50	0.06	126.51	16.33
DC2	-65.39	-6.76	-65.57	-6.78	44.15	5.15	-4.27	-0.47	104.12	13.06	0.07	0.01	901.25		114.31	14.53	0.57	0.06	126.57	16.34
DC3	-179.70	-18.59	-179.88	-18.61	-70.16	-8.19	-118.59	-13.10	-10.19	-1.28	-114.25	-12.68	-114.31	-12.68	786.93		-113.74	-12.63	12.26	1.58
DC4	-65.96	-6.82	-66.14	-6.84	43.58	5.08	-4.84	-0.53	103.55	12.99	-0.50	-0.06	-0.57	-0.06	113.74	14.45	900.68		126.00	16.27
DC5	-191.96	-19.86	-192.14	-19.87	-82.43	-9.62	-130.85	-14.45	-22.45	-2.82	-126.51	-14.04	-126.57	-14.04	-12.26	-1.56	-126.00	-13.99	774.67	

Table 6.6: Fuel consumption estimation comparison for all arrangements for configuration selected for *Island Discovery* ship

Arrangment	AC1		AC2		AC3		AC4		AC5		DC1		DC2		DC3		DC4		DC5	
Change	Absolute	Percent	Absolute	Percent	Absolute	Percent	Absolute	Percent	Absolute	Percent	Absolute	Percent	Absolute	Percent	Absolute	Percent	Absolute	Percent	Absolute	Percent
AC1	301.51		-0.06	-0.02	131.86	77.72	19.06	6.75	145.40	93.14	20.42	7.26	20.40	7.26	153.83	104.17	20.57	7.32	157.66	109.60
AC2	0.06	0.02	301.56		131.91	77.76	19.12	6.77	145.46	93.18	20.47	7.28	20.45	7.28	153.89	104.21	20.63	7.34	157.71	109.64
AC3	-131.86	-43.73	-131.91	-43.74	169.65		-112.79	-39.94	13.55	8.68	-111.44	-39.65	-111.46	-39.65	21.98	14.88	-111.28	-39.61	25.80	17.94
AC4	-19.06	-6.32	-19.12	-6.34	112.79	66.49	282.45		126.34	80.93	1.35	0.48	1.33	0.47	134.77	91.26	1.51	0.54	138.60	96.35
AC5	-145.40	-48.23	-145.46	-48.23	-13.55	-7.98	-126.34	-44.73	156.10		-124.99	-44.46	-125.01	-44.47	8.43	5.71	-124.83	-44.43	12.26	8.52
DC1	-20.42	-6.77	-20.47	-6.79	111.44	65.69	-1.35	-0.48	124.99	80.07	281.09		-0.02	-0.01	133.42	90.35	0.16	0.06	137.24	95.41
DC2	-20.40	-6.76	-20.45	-6.78	111.46	65.70	-1.33	-0.47	125.01	80.08	0.02	0.01	281.11		133.44	90.36	0.18	0.06	137.26	95.42
DC3	-153.83	-51.02	-153.89	-51.03	-21.98	-12.95	-134.77	-47.72	-8.43	-5.40	-133.42	-47.46	-133.44	-47.47	147.67		-133.26	-47.44	3.82	2.66
DC4	-20.57	-6.82	-20.63	-6.84	111.28	65.60	-1.51	-0.53	124.83	79.97	-0.16	-0.06	-0.18	-0.06	133.26	90.24	280.93		137.09	95.30
DC5	-157.66	-52.29	-157.71	-52.30	-25.80	-15.21	-138.60	-49.07	-12.26	-7.85	-137.24	-48.83	-137.26	-48.83	-3.82	-2.59	-137.09	-48.80	143.85	

Table 6.7: Capital cost estimation comparison for all arrangements for configuration selected for *Island Discovery* ship

arrangement	AC1		AC2		AC3		AC4		AC5		DC1		DC2		DC3		DC4		DC5	
Change	Absolute	Percent	Absolute	Percent	Absolute	Percent	Absolute	Percent	Absolute	Percent	Absolute	Percent	Absolute	Percent	Absolute	Percent	Absolute	Percent	Absolute	Percent
AC1	1.31		-0.40	-23.23	-0.47	-26.23	-0.03	-2.22	-0.10	-7.04	-0.06	-4.38	-0.46	-25.83	-0.76	-36.62	0.07	5.64	-0.23	-14.92
AC2	0.40	30.25	1.71		-0.07	-3.91	0.37	27.36	0.30	21.08	0.34	24.55	-0.06	-3.40	-0.36	-17.44	0.47	37.60	0.17	10.82
AC3	0.47	35.56	0.07	4.07	1.78		0.44	32.54	0.37	26.01	0.41	29.62	0.01	0.54	-0.29	-14.08	0.54	43.21	0.24	15.33
AC4	0.03	2.27	-0.37	-21.48	-0.44	-24.55	1.34		-0.07	-4.93	-0.03	-2.20	-0.43	-24.15	-0.73	-35.18	0.10	8.05	-0.20	-12.99
AC5	0.10	7.58	-0.30	-17.41	-0.37	-20.64	0.07	5.19	1.41		0.04	2.87	-0.36	-20.21	-0.66	-31.81	0.17	13.65	-0.13	-8.47
DC1	0.06	4.58	-0.34	-19.71	-0.41	-22.85	0.03	2.25	-0.04	-2.79	1.37		-0.40	-22.44	-0.70	-33.72	0.13	10.48	-0.17	-11.03
DC2	0.46	34.83	0.06	3.52	-0.01	-0.53	0.43	31.83	0.36	25.33	0.40	28.93	1.77		-0.30	-14.54	0.53	42.44	0.23	14.71
DC3	0.76	57.77	0.36	21.13	0.29	16.39	0.73	54.26	0.66	46.66	0.70	50.86	0.30	17.01	2.07		0.83	66.68	0.53	34.23
DC4	-0.07	-5.34	-0.47	-27.33	-0.54	-30.17	-0.10	-7.45	-0.17	-12.01	-0.13	-9.49	-0.53	-29.80	-0.83	-40.00	1.24		-0.30	-19.47
DC5	0.23	17.54	-0.17	-9.76	-0.24	-13.29	0.20	14.92	0.13	9.26	0.17	12.39	-0.23	-12.83	-0.53	-25.50	0.30	24.17	1.54	

Table 6.8: Operating cost estimation comparison for all arrangements for configuration selected for *Island Discovery* ship

arrangement	AC1		AC2		AC3		AC4		AC5		DC1		DC2		DC3		DC4		DC5	
Change	Absolute	Percent	Absolute	Percent	Absolute	Percent	Absolute	Percent	Absolute	Percent	Absolute	Percent	Absolute	Percent	Absolute	Percent	Absolute	Percent	Absolute	Percent
AC1	164.42		-0.03	-0.02	-68.36	-29.37	10.40	6.75	-53.56	-24.57	11.13	7.26	11.12	7.26	-56.51	-25.58	11.22	7.32	-54.42	-24.87
AC2	0.03	0.02	164.45		-68.33	-29.35	10.43	6.77	-53.53	-24.56	11.16	7.28	11.15	7.28	-56.48	-25.56	11.25	7.34	-54.39	-24.85
AC3	68.36	41.58	68.33	41.55	232.78		78.76	51.13	14.80	6.79	79.49	51.86	79.48	51.85	11.85	5.36	79.58	51.94	13.94	6.37
AC4	-10.40	-6.32	-10.43	-6.34	-78.76	-33.83	154.02		-63.96	-29.34	0.74	0.48	0.73	0.47	-66.90	-30.28	0.82	0.54	-64.82	-29.62
AC5	53.56	32.58	53.53	32.55	-14.80	-6.36	63.96	41.53	217.98		64.70	42.21	64.69	42.20	-2.94	-1.33	64.78	42.29	-0.86	-0.39
DC1	-11.13	-6.77	-11.16	-6.79	-79.49	-34.15	-0.74	-0.48	-64.70	-29.68	153.28		-0.01	-0.01	-67.64	-30.62	0.09	0.06	-65.56	-29.96
DC2	-11.12	-6.76	-11.15	-6.78	-79.48	-34.15	-0.73	-0.47	-64.69	-29.67	0.01	0.01	153.30		-67.63	-30.61	0.10	0.06	-65.54	-29.95
DC3	56.51	34.37	56.48	34.34	-11.85	-5.09	66.90	43.44	2.94	1.35	67.64	44.13	67.63	44.12	220.93		67.73	44.21	2.09	0.95
DC4	-11.22	-6.82	-11.25	-6.84	-79.58	-34.19	-0.82	-0.53	-64.78	-29.72	-0.09	-0.06	-0.10	-0.06	-67.73	-30.66	153.20		-65.64	-29.99
DC5	54.42	33.10	54.39	33.08	-13.94	-5.99	64.82	42.08	0.86	0.39	65.56	42.77	65.54	42.76	-2.09	-0.94	65.64	42.85	218.84	

Table 6.9: Propulsion system weight estimation comparison for all arrangements for configuration selected for *Island Discovery* ship

arrangement	AC1		AC2		AC3		AC4		AC5		DC1		DC2		DC3		DC4		DC5	
Change	Absolute	Percent	Absolute	Percent	Absolute	Percent	Absolute	Percent	Absolute	Percent	Absolute	Percent	Absolute	Percent	Absolute	Percent	Absolute	Percent	Absolute	Percent
AC1	49.28		-13.88	-21.98	-20.04	-28.91	3.12	6.76	-3.04	-5.81	-1.62	-3.19	-15.52	-23.95	-18.02	-26.77	3.98	8.79	1.48	3.10
AC2	13.88	28.16	63.16		-6.16	-8.88	17.00	36.82	10.84	20.72	12.26	24.08	-1.64	-2.53	-4.14	-6.15	17.86	39.43	15.36	32.13
AC3	20.04	40.66	6.16	9.75	69.32		23.16	50.16	17.00	32.49	18.41	36.17	4.52	6.97	2.02	3.00	24.02	53.02	21.52	45.01
AC4	-3.12	-6.33	-17.00	-26.91	-23.16	-33.41	46.16		-6.16	-11.77	-4.74	-9.32	-18.64	-28.76	-21.14	-31.41	0.86	1.90	-1.64	-3.43
AC5	3.04	6.16	-10.84	-17.17	-17.00	-24.52	6.16	13.34	52.32		1.41	2.78	-12.48	-19.26	-14.98	-22.26	7.02	15.49	4.52	9.45
DC1	1.62	3.29	-12.26	-19.41	-18.41	-26.56	4.74	10.27	-1.41	-2.70	50.91		-13.90	-21.44	-16.40	-24.36	5.60	12.37	3.10	6.49
DC2	15.52	31.49	1.64	2.59	-4.52	-6.52	18.64	40.38	12.48	23.86	13.90	27.30	64.80		-2.50	-3.71	19.50	43.04	17.00	35.56
DC3	18.02	36.56	4.14	6.55	-2.02	-2.91	21.14	45.79	14.98	28.63	16.40	32.21	2.50	3.86	67.30		22.00	48.56	19.50	40.79
DC4	-3.98	-8.08	-17.86	-28.28	-24.02	-34.65	-0.86	-1.87	-7.02	-13.41	-5.60	-11.01	-19.50	-30.09	-22.00	-32.69	45.30		-2.50	-5.23
DC5	-1.48	-3.00	-15.36	-24.32	-21.52	-31.04	1.64	3.55	-4.52	-8.64	-3.10	-6.10	-17.00	-26.23	-19.50	-28.97	2.50	5.52	47.80	

Table 6.10: Load carrying capacity estimation comparison for all arrangements for configuration selected for *Island Discovery* ship

Arrangment	AC1		AC2		AC3		AC4		AC5		DC1		DC2		DC3		DC4		DC5	
Change	Absolute	Percent	Absolute	Percent	Absolute	Percent	Absolute	Percent	Absolute	Percent	Absolute	Percent	Absolute	Percent	Absolute	Percent	Absolute	Percent	Absolute	Percent
AC1	347.88		13.88	4.16	20.04	6.11	-3.12	-0.89	3.04	0.88	1.62	0.47	15.52	4.67	18.02	5.46	-3.98	-1.13	-1.48	-0.42
AC2	-13.88	-3.99	334.00		6.16	1.88	-17.00	-4.84	-10.84	-3.14	-12.26	-3.54	1.64	0.49	4.14	1.25	-17.86	-5.08	-15.36	-4.40
AC3	-20.04	-5.76	-6.16	-1.84	327.84		-23.16	-6.60	-17.00	-4.93	-18.41	-5.32	-4.52	-1.36	-2.02	-0.61	-24.02	-6.83	-21.52	-6.16
AC4	3.12	0.90	17.00	5.09	23.16	7.06	351.00		6.16	1.79	4.74	1.37	18.64	5.61	21.14	6.41	-0.86	-0.24	1.64	0.47
AC5	-3.04	-0.87	10.84	3.25	17.00	5.19	-6.16	-1.75	344.84		-1.41	-0.41	12.48	3.76	14.98	4.54	-7.02	-1.99	-4.52	-1.29
DC1	-1.62	-0.47	12.26	3.67	18.41	5.62	-4.74	-1.35	1.41	0.41	346.26		13.90	4.18	16.40	4.97	-5.60	-1.59	-3.10	-0.89
DC2	-15.52	-4.46	-1.64	-0.49	4.52	1.38	-18.64	-5.31	-12.48	-3.62	-13.90	-4.01	332.36		2.50	0.76	-19.50	-5.54	-17.00	-4.87
DC3	-18.02	-5.18	-4.14	-1.24	2.02	0.62	-21.14	-6.02	-14.98	-4.34	-16.40	-4.74	-2.50	-0.75	329.86		-22.00	-6.25	-19.50	-5.58
DC4	3.98	1.14	17.86	5.35	24.02	7.33	0.86	0.25	7.02	2.04	5.60	1.62	19.50	5.87	22.00	6.67	351.86		2.50	0.72
DC5	1.48	0.43	15.36	4.60	21.52	6.56	-1.64	-0.47	4.52	1.31	3.10	0.90	17.00	5.11	19.50	5.91	-2.50	-0.71	349.36	

6.9. Comparison for all KPIs for Selected Configuration

The Figure 6.20 presents the per cent changes that occur between each arrangement compared with the status quo (AC1) for the selected configuration of diesel generators and battery banks. The other KPIs like cable weight, and electrical power requirement are not included in these spider plots (Figure 6.19, Figure 6.20). The reason for this is the two KPIs values are the same irrespective of which AC or DC arrangement is selected. The Figure 6.19a presents the changes between AC2 and DC2 with respect to AC1. The Figure 6.19b presents the changes for AC3 and DC3 with respect to the status quo arrangement (AC1). The Figure 6.19c highlights the relative per cent changes for AC4, DC1 and DC4 arrangements. The per cent changes between AC4 and DC1 are comparatively similar, except for the system weight because of the elimination of a diesel generator in AC4. This also proves that the emission reduction achieved by the addition of a battery bank in AC4 can also be achieved by switching to a BiDC grid, as seen in the DC1 arrangement. Finally, the Figure 6.19d presents the changes for AC5 and DC5 with respect to the status quo arrangement (AC1). In all arrangements, the emission reduction and the operating cost that includes fuel costs or fuel costs and the cost of electricity from shore infrastructure achieved by the BiDC grid is higher than its AC counterpart. The fuel consumption is lower in BiDC arrangements as compared with its AC counterparts. However, the fuel consumption reduction from the status quo for arrangements with shore power is significant for both AC and BiDC arrangements. The load carry capacity of the ship is affected marginally and often decreased as either a battery bank is added to the propulsion system or because of the weights of the power electronic devices, leading to an increase in system weight. The capital costs of the arrangements are higher for BiDC arrangements as compared to the AC arrangements, except for the DC4 arrangement, where the capital costs are reduced due to the elimination of components.

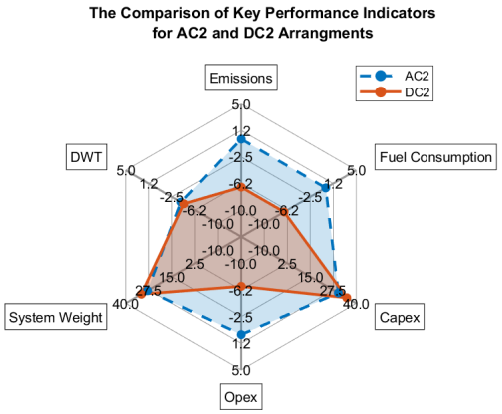

(a) The KPI Comparison for AC2 and DC2 arrangement

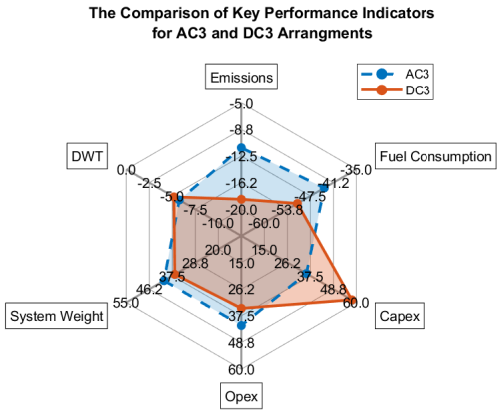

(b) The KPI Comparison for AC3 and DC3 arrangement

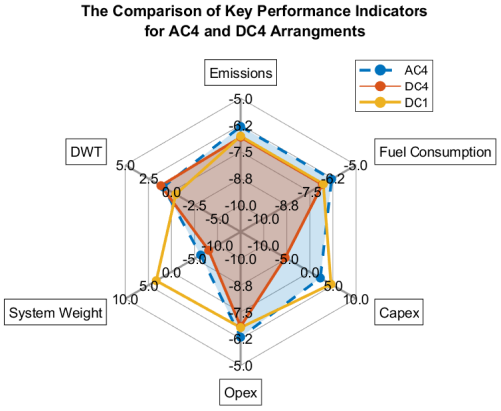

(c) The KPI Comparison for AC4 and DC4 arrangement

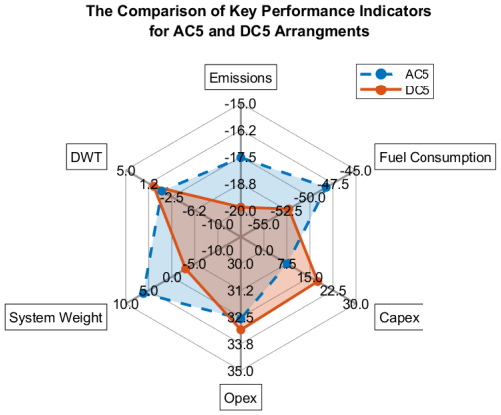

(d) The KPI Comparison for AC5 and DC5 arrangement

Figure 6.19: The spider plots comparing the key performance indicators for AC and DC arrangements with the selected configuration for *Island Discovery Ship*

The Figure 6.20 presents the comparison of all arrangements for KPIs for the selected configuration of diesel generators and batteries with respect to AC1 arrangement. The emissions are reduced for all AC and DC arrangements, with the highest emission reduction occurring in the DC5 arrangement except AC2 where the emissions are marginally increased because of conversion losses in the battery and inverter connected to the AC grid. The fuel consumption is the lowest of the DC5 arrangement followed by DC4, AC5 and AC4. These arrangements are equipped with shore power and also due to switching off the diesel generators in this arrangement after reaching the shore. The capital cost of the system is higher for all arrangements when compared with the status quo, except for the DC4 arrangement. This is due to the elimination of one diesel generator as compared to two diesel generators used in the AC1 arrangement (status quo). For the operating cost, the maximum reduction is observed in the DC4 arrangement. However, the elimination of one diesel generator and using a battery instead reduces the operating cost of the AC grid as a result of charging the batteries during loading/unloading of the ship leading to near optimum operation of the diesel generator, reducing fuel consumption. The maximum displacement of the ship is maintained constant by calculating the propulsion system weight of the ship and estimating the changes that occur in the load carrying capacity (Dead Weight Tonnage) of the ship. This is considered to eliminate the effect of propulsion system weight on the power requirements. Also, a ferry owner would operate his ship at maximum loading to increase economic gains. Considerably, The propulsion system weight increases for all the arrangements except for AC4, DC4 and DC5. However, the weight reduction is lower in DC5 as a result of the additional shore rectifier used to avail the shore electricity connection.

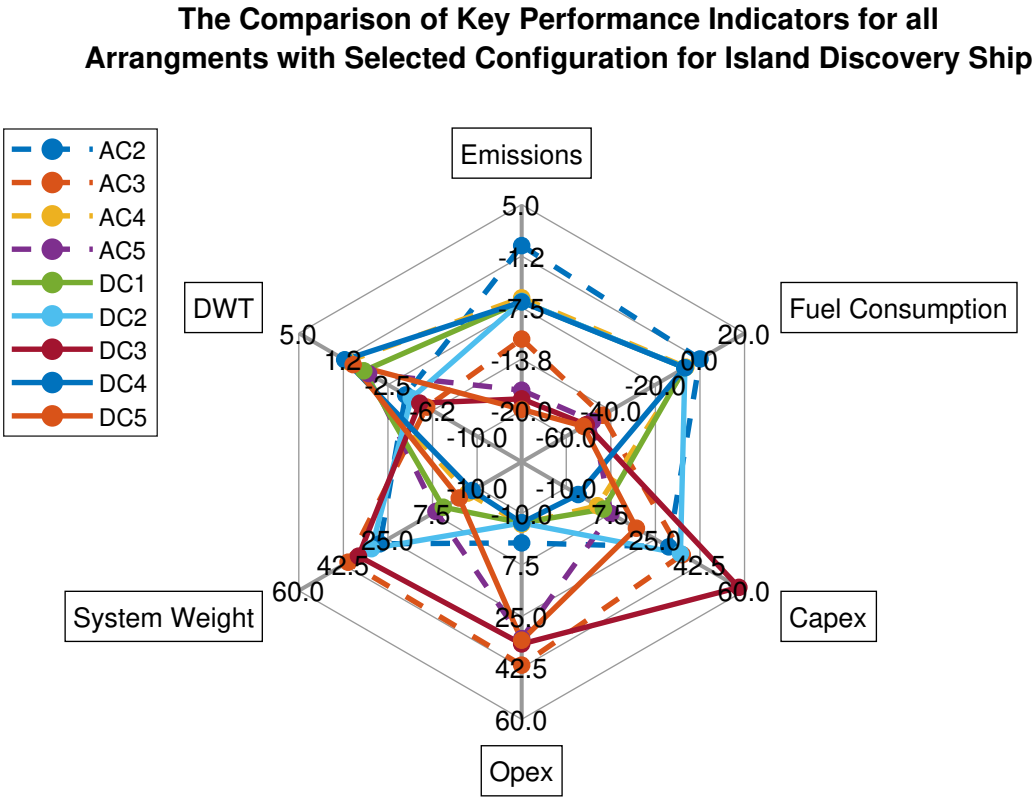

Figure 6.20: The spider plot comparing the Key Performance Indicators with all arrangements

6.10. Validation

The numbers for the AC4 arrangement for emissions reduction as well as the fuel savings observed for a year are given in Figure 6.21. These numbers are compared with the results obtained from the optimisation problem formulated in chapter 4. The *Island Discovery* ship operates 16 trips per day,

leading to 494 trips per month, as shown in Table 6.1. The results from the status quo arrangement of two diesel generators and the AC4 arrangement consisting of a diesel generator and battery are shown in Table 6.11 and compared with the number provided by the battery manufacturer for the *Island Discovery* ship. For the fuel consumption estimation in litres, the density of MDO fuel is considered, as per the guidelines given in International Maritime Organization [66].

Table 6.11: The comparison of the results from the optimization problem and the numbers from Corvus Energy [23]

Arrangement	AC1	AC4	Calculated Reduction	Reduction from [23]	Deviation [%]
Emissions [Ton/Year]	5730.21	5367.92	362.29	397.00	8.74
Fuel Consumption [Ton/Year]	1787.34	1674.34	113.00	-	-
Fuel Consumption [L/Year]	1985933.42	1860374.42	125559.00	148720.00	15.57

Figure 6.21: The reduction in emissions and fuel consumption of *Island Discovery* ship according to the battery provider, Corvus Energy [23]

The deviation in the results of this thesis work and the numbers from Corvus Energy [23] are a result of the following limitations/assumptions made in this thesis:-

1. The diesel generator's specific fuel oil consumption model is developed from a different diesel generator than the one used in *Island Discovery*.
2. The diesel generator installed on the ship is MG12V4000M35F, manufactured by Rolls-Royce [107]. The possibility of different diesel generators cannot be ignored having different SFOC values at full loading.
3. The ship's electrical power estimation is calculated from the velocity profile of the ship. The methodology has numerous assumptions (efficiency values and resistances) that can affect the power estimation.
4. The ship's auxiliary power can be different from what is assumed in this study and can affect the optimal results.
5. The electrical component efficiency values of the ship are assumed to be constant. The efficiency of transformers and VFDs are power dependent and not constant.
6. The trip length and time of voyage are assumed to be constant, and the same power profile is assumed to be repeated for every trip. However, this is not possible due to different weather conditions and the loading of the ship.

However, the results provide confidence in the emission reduction potential for the BiDC grids.

6.11. Summary

This chapter presented the results of the methodologies described in chapter 3, chapter 4 and chapter 5. The mechanical power estimation results were presented in section 6.1. The variability

in the mechanical power because of the resistances was also explained. Following this, the electrical power estimation results for the AC and the BiDC grids were highlighted in section 6.2. It was observed that the power requirements for the AC grid are higher than the BiDC grid. Moreover, the cable sizing also showed that the cable weight can be reduced by switching to the BiDC grid also reducing the cable losses that occur in propulsion drives. The section 6.3, section 6.4, section 6.5, section 6.6, and section 6.7 presented the results for the optimization problem formulation comparing the same arrangement for the AC and the BiDC grid for AC1, DC1, AC2, DC2, AC3, DC3, AC4, DC4, AC5, DC5, respectively. In all the comparisons, the potential for minimum emissions achieved was higher for the BiDC grid than for the AC grid. The lowest emissions achieved were for the DC5 arrangement that consists of one diesel generator, battery, and shore infrastructure. Even for the selected configuration for the *Island Discovery* ship, the arrangements with BiDC grid architecture estimated lower emissions as compared with its AC counterpart. Furthermore, a comprehensive comparison for all the key performance indicators was presented in section 6.8. The rows represent the arrangements that are compared, with the arrangements in each column representing every possible comparison. Moreover, a graphical comparison for all the arrangements with AC1 arrangement was presented in section 6.9. The emission reduction numbers from the battery supplier of *Island Discovery* ship are compared with the results obtained from the optimization problem formulation in section 6.10. The reasons for the deviation between the two numbers were also highlighted in this section.

7

Conclusion and Recommendation

This chapter is intended to conclude the thesis set out with the research question formulated in chapter 1. The concluding remarks are drawn upon from the results presented in chapter 6 and are discussed in section 7.1. Furthermore, the author highlights recommendations in section 7.2 to underline areas for development in future work.

7.1. Conclusion

The CO_2 emissions from the shipping sector are estimated to rise over the coming decades. The International Maritime Organisation (IMO) has introduced measures to counter the CO_2 emissions to achieve the ambitious target. Electrifying the ship's propulsion, cold steaming and using shore electricity have proven to reduce the ship's emissions. This thesis aimed to evaluate the feasibility of Bi-polar DC grid architecture on ships using different Key Performance Indicators (KPIs) like emissions, electrical power requirement, cable losses and weight, system weight, capital cost, operating costs and fuel consumption. Consequently, the main research question was answered.

"What are the quantitative benefits of switching to a bipolar DC grid compared to an AC grid?"

This thesis has developed an optimization problem for a ferry with eligible diesel generators and batteries catalogued to evaluate the feasibility of BiDC grids on ships for different arrangements with different configurations of diesel generators and batteries. The shore infrastructure has also been included to highlight the comparative differences between AC and BiDC grids using the defined KPIs. The sub-questions that assist in answering the main question are explained further.

1: - *"How does the electrical power requirement change for AC and BiDC grids?"*

The methodology for the estimation of the mechanical power and the electrical power requirement was explained in chapter 3. The background knowledge developed from chapter 2 was used to estimate the electrical power requirements, taking into account the components that make up the shipboard microgrid on the distribution and consumption side. Consequently, the schematic shipboard microgrid layout for AC and BiDC grids was developed, which was presented in Figure 3.3. Furthermore, by taking into account the constant efficiency values for the electrical components, the electrical power for AC and BiDC grids was calculated. The comparison was presented and explained in Figure 6.4b and section 6.2, respectively. Over the ship's operational profile, the power requirements for the AC grid are comparatively higher than the BiDC grid. Furthermore, It was seen that at high power, the difference in power requirements was larger between the two grids and vice versa. The low power requirements in BiDC grids were due to the absence of an electrical component i.e. a three winding transformer that increases the overall efficiency of the system. Another reason for BiDC grids to be more efficient was the lower propulsion power cable losses as compared to the AC grid.

2: - *"What is the effect of switching to a BiDC grid on power cable losses and sizing?"*

The cable losses are estimated in subsection 3.3.1. This was done after the electrical power requirement was calculated using the efficiency values for the electrical components that make up the respective grids. The Table 6.3 highlights the results obtained for the cable power losses as well as the cable sizing. The operating voltage plays a crucial role in determining the cable losses, as the current requirements determine the losses that occur in a power cable for constant power. In the AC grid, the operating line-to-line voltage was 690 volts whereas the voltage in the positive and the negative poles of the BiDC grid was 1400 volts, leading to lower current requirements in the BiDC grid as compared to the AC grid. The Figure 6.4a highlights the cable losses that occur over the ship's operational profile. Furthermore, it was observed that in both grid architectures, the high power requirements resulted in larger losses. However, the losses in BiDC grids were lower at all points throughout the ship's voyage when compared with the AC grid power cable losses. For the cable sizing, a weight reduction of 24.67 per cent was observed in BiDC as compared to the AC grid. This decrease was mainly due to reasons like the lower design current requirements for the BiDC grid, the lesser number of conductors used in the cable for the BiDC grid, and the larger current carrying capacity of the cable for the BiDC grid as compared to the AC grid because of the self-induction losses and skin effect phenomenon.

3: - *"What are the changes in CO_2 emissions observed as we switch from the status quo to other arrangements?"*

The emission estimation was performed by formulating an optimization problem to minimise the CO_2 emissions from the ship's operating profile for the AC and the BiDC grid to have the best case comparison between the two grid architectures. The problem formulation was explained in chapter 4, for all ten arrangements. The five AC and BiDC arrangements are defined in Table 3.2. The minimum emissions observed for all the feasible configurations of diesel generators and batteries for all arrangements are presented in section 6.3, section 6.4, section 6.5, section 6.6, and section 6.7. In all the arrangements, the minimum CO_2 emissions achieved were lower for the BiDC grid as compared to the AC grid as shown in Figure 6.5, Figure 6.7, Figure 6.10, Figure 6.13, and Figure 6.16. A comprehensive comparison between each arrangement with each arrangement was presented in Table 6.5. Furthermore, for the selected configuration for the *Island Discovery* ship, it was also observed that the CO_2 for the BiDC grid were lower as compared to the AC grid. The lowest possible emissions were obtained for the DC5 arrangement with one diesel generator, battery bank and shore power availability. The CO_2 emissions estimated were 774.67 Kg/Trip compared to the status quo emissions of 966.64 Kg/Trip, leading to a -19.86 per cent reduction of CO_2 emissions. The emissions for all arrangements with selected configuration were lower than that of the AC1 arrangement except for the AC2 where it was marginally higher, i.e. 0.02 per cent. The decrease can be mainly attributed to the operational characteristic of diesel generators in variable speed (DC) as compared or a fixed speed (AC) operation presented in Figure 2.11 and to the lower electrical power requirements and cable losses. The *Island Discovery* ship was developed as an AC4 arrangement, but here again, it can be seen emitting more CO_2 emissions as compared to the DC4 arrangement by 0.53 per cent, showcasing the benefits of BiDC grids.

4: - *"What is the effect on fuel consumption for each arrangement as compared with the status quo?"*

The CO_2 emissions and fuel consumption of diesel generators have a direct relationship. In other words, the CO_2 emissions from diesel generators are dependent on fuel consumption. The methodology to calculate the fuel consumption was explained in section 5.1. The emission factor of the Marine Diesel Oil (MDO) was used to evaluate the fuel consumption of all the feasible configurations for all ten arrangements. The per cent changes are the same as the emissions for arrangements where the shore power was not incorporated. For arrangements AC3, DC3, AC5 and DC5, the fuel consumption sees a significant drop as the diesel generators are turned off as the ship reaches the shore and the shore infrastructure supplies the required energy demand. A comprehensive comparison between all the arrangements with all arrangements was presented in Table 6.6. The fuel consumption was observed to be lowest for the DC5 arrangement for the selected configuration, accounting for 143.85 Kg/Trip. Furthermore, the fuel consumption for the status quo arrangement was 301.51 Kg/Trip and for the AC4 arrangement was seen to be 282.45 Kg/Trip. One can argue that the differences in fuel consumption between the AC4 and AC1 arrangements (-6.32 per cent) were not significant as

compared to the reduction observed in the DC5 arrangement (-52.29 per cent), but if the fuel savings are to be calculated for a year. The fall in fuel consumption just for AC4 arrangement when compared with AC1 can result in 113 Ton/Year of savings as shown in Table 6.11. Here again, the results can be attributed to the operating characteristics of the diesel generator in variable speed (DC) and fixed speed (AC) operation and the lower electrical power requirements and cable losses. The importance of shore infrastructure to reduce fuel consumption was substantial.

5: - *"What is the effect of each arrangement on the capital cost of the system?"*

The methodology to calculate the capital cost of the propulsion system was explained in section 5.3. The cost of the induction motor was not taken into account in the capital cost estimation, as the motor remains the same for both arrangements. The Table 6.7 highlights the comparison of the capital cost of the system for all arrangements compared with all arrangements. The status quo arrangement was the cheapest among all, except for the DC4 arrangement, where the elimination of a diesel generator and three-winding transformer in the DC4 arrangement made it cheaper by 5.34 per cent. The *Island Discovery* ship is developed around AC4 arrangement, i.e. one diesel generator and battery bank. Here again, the comparison showed that the DC4 arrangement was cheaper by 7.34 per cent. Therefore, the DC4 arrangement was reducing emissions as well as the capital cost of the system. The reason for the decrease in capital cost was mainly due to the elimination of the cost of components like three-winding transformers and variable frequency drives.

6: - *"What is the effect on the operating cost of the ship for different arrangements compared with the status quo?"*

The estimation of the operating costs of the *Island Discovery* ship was explained in section 5.2 for all ten arrangements. The operating costs consist of either the fuel cost or the cost of the fuel along with the average cost of the shore electricity depending upon the arrangement. The operating costs for all ten arrangements are presented in Figure 6.5, Figure 6.7, Figure 6.10, Figure 6.13, and Figure 6.16. The results for the operating costs with the comparison between all arrangements are presented in Table 6.8 for the selected configuration of the ship. In AC arrangements, the operating costs increase for all except for the AC4 arrangement when compared with the AC1 arrangement. This can be explained as a result of a reduction in the fuel consumption of the ship due to the diesel generator's operation at near optimum loading and the absence of shore power, as shown in Figure 6.14a by utilising the battery during travelling and charging while the ship was being loaded/unloaded. For BiDC arrangements, the reduction in emissions reduces fuel consumption, leading to a decrease in the operating costs for arrangements with no shore power. However, the higher emission reduction seen in DC arrangements with shore power was not reflected in the operating costs, as the electricity cost from shore results in higher operating costs. The lowest operating costs are for the DC4 arrangement with a 6.82 per cent reduction when compared with AC1 whereas, a reduction of 0.53 per cent was seen for DC4 when compared with the AC4 arrangement.

7: - *"How does the system weight vary for each arrangement compared with the status quo?"*

The propulsion system weight calculations are explained in section 5.4. The results for the system weight for all the arrangements are shown in Figure 6.5, Figure 6.7, Figure 6.10, Figure 6.13, and Figure 6.16 comparing the respective AC and BiDC arrangements. The comprehensive comparison of the system weight with all the other arrangements was presented in Table 6.9. For AC arrangements, the AC4 arrangement presents a 6.3 per cent reduction in system weight as compared to the AC1 arrangement. This reduction was mainly because of the elimination of a diesel generator, as the battery bank replaced by it weighs lesser compared to it. In DC arrangements, the highest weight reduction was achieved for the DC4 arrangement, accounting for an 8.08 per cent reduction in propulsion weight as compared to the status quo (AC1). This was because of the same reasons as for the AC4 arrangement, along with the reduction in cable weights that further decrease the system weight. For the AC4 arrangement as compared with the other arrangements, the only arrangement that reduces the propulsion weight was the DC4 arrangement with a deduction of 1.64 tonnes for weight accounting for 0.46 per cent. This was possible because of the fall in the cable weights.

8: - *"How does each arrangement affect the load carrying capacity (DWT) of the ship?"*

The ship is supposed to be operating at its maximum displacement, irrespective of the arrangement used. The methodology to calculate the load carrying capacity of the *Island Discovery* ship was presented in section 5.5. The 334-tonne load carrying capacity is for AC2 arrangement, as the ship has two diesel generators and a battery bank. Accordingly, the load carrying capacity was calculated and compared for all arrangements in Table 6.10. The load carrying capacity of the ship increased as compared with the AC2 arrangement for all the arrangements except for the AC3 where the shore transformer was added, DC2 where the power electronic components reduce the DWT by 0.49 per cent and the DC3 arrangement where along with the previous power electronic components, shore rectifier was added resulting in a fall in the load carrying capacity by 1.24 per cent as compared. Here again, the highest increase in load carrying capacity by 5.35 per cent, accounting for 351.86 tonnes instead of 344 tonnes, was seen in the DC4 arrangement. Therefore, it can be said that the BiDC grids have a higher potential to increase the load carrying capacity of the ship at maximum displacement due to the decrease in the cable weight as compared with the AC arrangements.

Finally, after answering the eight sub-questions, the main research question can be answered. When AC arrangements are compared with their DC counterpart. The power losses, as well as the electrical power requirements, were found to be lower for the BiDC grid as compared to the AC grid. The number of cables required was also less, resulting in lower cable weight in the BiDC grid topology. The minimum emissions achieved over the ship's operation were lower for the BiDC grids than for the AC grid. Furthermore, the availability of shore power did not affect the trend seen in fuel consumption, where the fuel consumed over the ship's operations was higher for the AC arrangements as compared to their DC counterparts. The capital costs for the DC arrangements were seen to be higher than for the AC arrangements, with an exception in the DC4 arrangement that can be attributed to the elimination of the rectifier connected to the diesel generator, the diesel generator itself, the rectifier unit in the VFD and the three winding transformer. The operating costs were observed to be lower for the DC arrangements as compared to the AC arrangements, except for the DC5 arrangement, which was observed to be marginally higher than its AC counterpart. The system weight was found to be lower for the AC arrangements as compared to the DC arrangement without shore power availability. However, the reverse was seen for arrangements with shore power connection due to the increased weight of the shore transformer. This was also reflected in the load carrying capacity of the ship. However, the emission reductions in the AC grid after the addition of a battery bank (AC4) can be achieved by only switching to a BiDC shipboard microgrid (DC1), eliminating the use of batteries and reducing capital costs as shown in Figure 6.19c. Furthermore, these results depend on the operating profile of the ship, the shore infrastructure, the diesel generator and battery configuration and their technical parameters. An overall comparison was presented in Figure 6.20 showcasing the key performance indicators for all nine arrangements when compared with the status quo (AC1). The BiDC grids can be the next feasible solution for reducing emissions from the shipping sector.

7.2. Recommendations and Future Work

The author presents recommendations from this study that can be performed in the future to build upon this thesis, as well as provide confidence in the deployment of BiDC architecture on shipboard microgrids.

1. The accuracy of the results can be improved by using real Specific Fuel Oil Consumption (SFOC) data of each diesel generator, the real electrical power profile of the *Island Discovery* ship, and the incorporation of dynamic efficiency values for the electrical components in the optimization problem formulation.
2. The incorporation of the battery degradation model into the optimization problem formulation to evaluate the effect of battery ageing on the CO_2 emissions for optimal power dispatch for AC as well as BiDC grid. The effect on the battery life would be an interesting parameter to study.
3. The optimization problem can be expanded by incorporating the volume and footprint constraints to limit the effect on the gross and net tonnage of the ship, i.e. the volume of available space on the ship for cargo transport.

4. Although this thesis has not taken into consideration the cost of circuit breakers, fuses, relays, etc. in estimating the capital costs, this addition would significantly provide good economic data for shipbuilders to consider deploying BiDC grids. However, the lack of standards in Bipolar DC transmissions and distribution prevents performing an exhaustive comparison at present because of the absence of available industrial components.

5. A cost-benefit analysis comparing the AC and BiDC propulsion architecture over the life-span of the ship including the battery replacement costs, capital costs, operating costs, and the price of carbon emissions to determine the monetary effects over the long term.

6. The addition of alternative power producers like fuel cells, and dual-fuel engines in the optimization problem will assist in a broader comparison of alternative approaches for emission minimization.

7. A multi-objective optimization problem can be formulated to incorporate the operating costs of the ship as an objective function along with the emissions which include the cost of fuel, the cost of shore electricity and the cost of green hydrogen.

8. The effect of switching to BiDC grids on different classes of ships like platform supply vessels, yachts, etc. can be evaluated.

9. The computational time was around 3 to 4 hours on a high-end computer due to the large dataset of diesel generators and batteries. To overcome this, parallel computing was introduced to reduce the computational time. However, the computation time still required is 45–60 minutes for each arrangement, leading to 8–9 hours to obtain results for all arrangements. This time will only increase as we expand the diesel generator and battery dataset. Therefore, a different optimization technique should be looked into to make the optimization methodology faster.

10. A sensitivity analysis for different parameters like the electrical power requirement of the ship considering different scenarios, the economic data like shore electricity cost, fuel cost, the electrical component cost for transformer, power electronic conversion devices, component efficiencies, SFOC data from diesel generators, C-rates for charging and discharging of the batteries, and the shore electricity should be performed to understand its effect on emissions, capital cost, operating cost.

11. A stability and control study for the power system with feasible solutions can be evaluated to further increase the confidence in realizing the BiDC grid architectures on ships.

Bibliography

[1] ABB. *Circuit Breakers Low Voltage*. URL: https://new.abb.com/low-voltage/products/circuit-breakers.

[2] ABB. *Containerized Maritime Energy Storage*. Tech. rep. ABB Marine and Ports, 2023, p. 2. URL: https://new.abb.com/marine/systems-and-solutions/electric-solutions/containerized-maritime-energy-storage-solution.

[3] ABB. *High voltage engineered induction motors*. Tech. rep. ABB, 2021, p. 164. URL: https://library.e.abb.com/public/979075a43be54c43b7ec736d6ef4136d/High%20voltage%20engineered%20induction%20motors%20Technical%20catalog%209AKK103508_RevM_EN_lowres.pdf.

[4] M S Agamy et al. "A high efficiency DC-DC converter topology suitable for distributed large commercial and utility scale PV systems". In: *2012 15th International Power Electronics and Motion Control Conference (EPE/PEMC)*. Novi Sad, Serbia: Institute of Electrical and Electronics Engineers Inc., Sept. 2012. DOI: 10.1109/EPEPEMC.2012.6397420.

[5] Eleftherios I. Amoiralis et al. "Energy efficient transformer selection implementing life cycle costs and environmental externalities". In: *2007 9th International Conference on Electrical Power Quality and Utilisation, EPQU*. Barcelona, Spain: Institute of Electrical and Electronics Engineers Inc., Oct. 2007. ISBN: 8469100572. DOI: 10.1109/EPQU.2007.4424160.

[6] MacIt Aydin, Ersoy Beser, and Hasan Kelebek. "Efficiency Comparison of 2-Level and 3-Level Si IGBT Based Inverters". In: *2023 7th International Conference on Green Energy and Applications, ICGEA 2023*. Singapore, Singapore: Institute of Electrical and Electronics Engineers Inc., Mar. 2023, pp. 126–130. ISBN: 9781665456098. DOI: 10.1109/ICGEA57077.2023.10125768.

[7] Will Ayers. "DC Grids for Ship Propulsion: Benefits and Challenges". In: *SNAME Maritime Convention, SMC 2022*. OnePetro, Sept. 2022, p. 25. DOI: 10.5957/SMC-2022-037. URL: /SNAMESMC/proceedings-abstract/SMC22/3-SMC22/508895.

[8] Mohsen Banaei et al. "Optimal Control Strategies of Fuel cell/Battery Based Zero-Emission Ships: A Survey". In: *IECON Proceedings (Industrial Electronics Conference)*. Vol. 2021-October. IEEE Computer Society, Oct. 2021. ISBN: 9781665435543. DOI: 10.1109/IECON48115.2021.9589512.

[9] C. B. Barrass. *Ship Design and Performance for Masters and Mates*. Elsevier, Jan. 2004, pp. 1–252. ISBN: 9780750660006. DOI: 10.1016/B978-0-7506-6000-6.X5000-4. URL: http://www.sciencedirect.com:5070/book/9780750660006/ship-design-and-performance-for-masters-and-mates.

[10] Rene Barrera-Cardenas, Olve Mo, and Giuseppe Guidi. "Optimal Sizing of Battery Energy Storage Systems for Hybrid Marine Power Systems". In: *2019 IEEE Electric Ship Technologies Symposium, ESTS 2019*. Washington, DC, USA: Institute of Electrical and Electronics Engineers Inc., Aug. 2019, pp. 293–302. ISBN: 9781538675601. DOI: 10.1109/ESTS.2019.8847932.

[11] BC Ferries. *Island Discovery*. 2023. URL: https://www.bcferries.com/on-the-ferry/our-fleet/island-discovery/IDSC.

[12] L. van Biert et al. "A review of fuel cell systems for maritime applications". In: *Journal of Power Sources* 327 (Sept. 2016), pp. 345–364. ISSN: 0378-7753. DOI: 10.1016/J.JPOWSOUR.2016.07.007.

[13] Evert A. Bouman et al. "State-of-the-art technologies, measures, and potential for reducing GHG emissions from shipping – A review". In: *Transportation Research Part D: Transport and Environment* 52 (May 2017), pp. 408–421. ISSN: 1361-9209. DOI: 10.1016/J.TRD.2017.03.022.

[14] Alessandro Boveri et al. “Optimal Sizing of Energy Storage Systems for Shipboard Applications”. In: *IEEE Transactions on Energy Conversion* 34.2 (June 2019), pp. 801–811. ISSN: 08858969. DOI: 10.1109/TEC.2018.2882147.

[15] Alessandro Boveri et al. “Stochastic approach for power generation optimal design and scheduling on ships”. In: *IEEE PES Innovative Smart Grid Technologies Conference Europe (ISGT Europe)*. Vol. 2018-January. Turin, Italy: Institute of Electrical and Electronics Engineers Inc., July 2017, pp. 1–6. ISBN: 9781538619537. DOI: 10.1109/ISGTEUROPE.2017.8260334.

[16] Bussmann. *Short-Circuit Current Calculations*. Tech. rep. Eaton, 2014, p. 10. URL: https://www.eaton.com/content/dam/eaton/products/electrical-circuit-protection/fuses/solution-center/bus-ele-tech-lib-electrical-formulas.pdf.

[17] J. S. Carlton. *Marine propellers and propulsion*. Elsevier, Jan. 2018, pp. 1–585. ISBN: 9780081003664. DOI: 10.1016/C2014-0-01177-X. URL: http://www.sciencedirect.com:5070/book/9780081003664/marine-propellers-and-propulsion.

[18] Caterpillar. *Marine Power Solutions*. Tech. rep. Caterpillar, May 2022, p. 116. URL: https://www.pon-cat.com/application/files/7016/5296/8323/Cat_Marine_Power_Solutions_Guide_May_2022.pdf.

[19] Cavotec. *PowerRampNxG Datasheet*. Tech. rep. Cavotec, Oct. 2021, p. 2. URL: https://www.cavotec.com/en/your-applications/ports-maritime/shore-power/shore-power-systems-for-ports.

[20] Cavotec. *PowerRun LV Datasheet*. Tech. rep. Cavotec, Dec. 2021, p. 2. URL: https://www.cavotec.com/en/your-applications/ports-maritime/shore-power/shore-power-systems-for-ports.

[21] Guomei Chang et al. “DC Bus Systems for Electrical Ships: Recent Advances and Analysis of a Real Case”. In: *IEEE Electrification Magazine* 8.3 (Sept. 2020), pp. 28–39. ISSN: 23255889. DOI: 10.1109/MELE.2020.3005697.

[22] Corvus Energy. *Corvus Orca Energy*. Tech. rep. Corvus Energy, June 2021, p. 2. URL: https://corvusenergy.com/products/energy-storage-solutions/corvus-orca-energy/.

[23] Corvus Energy. *Island Discovery*. 2023. URL: https://corvusenergy.com/projects/island-discovery/.

[24] Cummins Inc. *Cummins Marine Products Guide*. Tech. rep. U.S.A: Cummins, Nov. 2022, p. 140. URL: https://mart.cummins.com/imagelibrary/data/assetfiles/0032264.pdf.

[25] Damen. *Road Ferry 8117 E3 Datasheet*. Tech. rep. Damen Shipyards Group, 2023. URL: https://www.damen.com/vessels/ferries/roro-ferries/road-ferry-8117-e3.

[26] M ; De Smet et al. “Battery Hybrid Energy Storage Systems for Full-Electric Marine Applications”. In: *Processes* 10.11 (Nov. 2022), p. 2418. ISSN: 2227-9717. DOI: 10.3390/PR10112418. URL: https://www.mdpi.com/2227-9717/10/11/2418/htm%20https://www.mdpi.com/2227-9717/10/11/2418.

[27] Eleftherios K. Dedes, Dominic A. Hudson, and Stephen R. Turnock. “Assessing the potential of hybrid energy technology to reduce exhaust emissions from global shipping”. In: *Energy Policy* 40 (Jan. 2012), pp. 204–218. ISSN: 0301-4215. DOI: 10.1016/J.ENPOL.2011.09.046.

[28] Divyajot, Rajesh Kumar, and Manoj Fozdar. “Optimal sizing of hybrid ship power system using variants of particle swarm optimization”. In: *2017 Recent Developments in Control, Automation and Power Engineering, RDCAPE 2017*. Noida, India: Institute of Electrical and Electronics Engineers Inc., May 2018, pp. 527–532. ISBN: 9781509039784. DOI: 10.1109/RDCAPE.2017.8358327.

[29] Eaton. *Circuit breakers*. URL: https://www.eaton.com/mx/en-us/products/electrical-circuit-protection/circuit-breakers.html.

[30] Echandia. *Echandia Energy Datasheet*. Tech. rep. Echandia, Jan. 2022, p. 4. URL: https://echandia.se/products/echandia-energy/.

[31] EGCSA. *Regulations & Guidelines*. 2021. URL: https://www.egcsa.com/regulatory/.

[32] Mustafa Farhadi and Osama Mohammed. "Energy Storage Technologies for High-Power Applications". In: *IEEE Transactions on Industry Applications* 52.3 (May 2016), pp. 1953–1962. ISSN: 00939994. DOI: 10.1109/TIA.2015.2511096.

[33] Alejandro A. Franco. *Rechargeable lithium batteries : from fundamentals to applications*. 1st. Woodhead Publishing, Apr. 2015, p. 412. ISBN: 9781782420903. URL: http://www.sciencedirect.com:5070/book/9781782420903/rechargeable-lithium-batteries.

[34] R. D. Geertsma et al. "Design and control of hybrid power and propulsion systems for smart ships: A review of developments". In: *Applied Energy* 194 (May 2017), pp. 30–54. ISSN: 0306-2619. DOI: 10.1016/J.APENERGY.2017.02.060.

[35] R. D. Geertsma et al. "Pitch control for ships with diesel mechanical and hybrid propulsion: Modelling, validation and performance quantification". In: *Applied Energy* 206 (Nov. 2017), pp. 1609–1631. ISSN: 03062619. DOI: 10.1016/j.apenergy.2017.09.103.

[36] Joerg Habermass and Jochen Thurner. *Variable Speed Generator Sets Offer Advantages for Commercial Ships*. Tech. rep. Rolls Royce MTU, 2023, p. 4. URL: https://www.mtu-solutions.com/content/dam/mtu/technical-article/2020/variable-speed-generator-sets-offer-advantages-for-commercial-ships/21529_Variable%20Speed%20GenSet-Marine_TA_60420_HR.pdf/_jcr_content/renditions/original./21529_Variable%20Speed%20GenSet-Marine_TA_60420_HR.pdf.

[37] Jingang Han, Jean Frederic Charpentier, and Tianhao Tang. "An Energy Management System of a Fuel Cell/Battery Hybrid Boat". In: *Energies* 7.5 (Apr. 2014), pp. 2799–2820. ISSN: 1996-1073. DOI: 10.3390/EN7052799. URL: https://www.mdpi.com/1996-1073/7/5/2799/htm%20https://www.mdpi.com/1996-1073/7/5/2799.

[38] Jan Fredrik Hansen, John O Lindtjørn, and Klaus Vanska. "Onboard DC Grid for enhanced DP operation in ships". In: *2011 Dynamic Positioning Conference*. Maritime Technology Society, Oct. 2011, pp. 1–8.

[39] Jan Fredrik Hansen and Frank Wendt. "History and State of the Art in Commercial Electric Ship Propulsion, Integrated Power Systems, and Future Trends". In: *Proceedings of the IEEE* 103.12 (Dec. 2015), pp. 2229–2242. ISSN: 15582256. DOI: 10.1109/JPROC.2015.2458990.

[40] Jan Fredrik Hansen, Frank Wendt, and John Olav Lindtjørn. "Fuel-efficient power plant featuring variable speed generation system for DP drilling units". In: *2016 Dynamic Positioning Conference*. Maritime Technology Society, Oct. 2016, pp. 1–14.

[41] Arber Haxhiu et al. "Electric Power Integration Schemes of the Hybrid Fuel Cells and Batteries-Fed Marine Vessels - An Overview". In: *IEEE Transactions on Transportation Electrification* 8.2 (June 2022), pp. 1885–1905. ISSN: 23327782. DOI: 10.1109/TTE.2021.3126100.

[42] Arber Haxhiu et al. *Hybrid batteries and fuel cells-based vessel power trains: System integration*. Tech. rep. Helsinki, Finland: ABB Marine and Ports, May 2022, pp. 158–165. URL: https://new.abb.com/news/detail/91041/hybrid-batteries-and-fuel-cells-based-vessel-power-trains-system-integration.

[43] Henrik Helgesen, Sondre Henningsgård, and Andrea Aarseth Langli. *Study on Electrical Energy Storage for Ships*. Tech. rep. European Maritime Safety Agency (EMSA), May 2020, pp. 1–184. URL: https://www.emsa.europa.eu/publications/item/3895-study-on-electrical-energy-storage-for-ships.html.

[44] F S Hillier and G J Lieberman. *Introduction to operations research*. 10th. New York: McGraw-Hill Education, 2015, p. 1010. URL: https://tudelft.on.worldcat.org/oclc/857743855.

[45] J. Holtrop and G. G.J. Mennen. “An approximate power prediction method”. In: *International Shipbuilding Progress* 29.335 (Jan. 1982), pp. 166–170. ISSN: 0020-868X. DOI: 10.3233/ISP-1982-2933501.

[46] Honest Cable. *CJPF/SC Datasheet*. Tech. rep. Honest Cable, 2023, p. 4. URL: https://www.honestcable.com/wp-content/uploads/2018/11/MPRX-CJPF-Honest-Cable.pdf.

[47] Weijie Hua et al. “A datasheet - Based loss model and efficiency analysis for vienna rectifiers using SiC power devices”. In: *2020 IEEE 1st China International Youth Conference on Electrical Engineering, CIYCEE 2020*. Wuhan, China: Institute of Electrical and Electronics Engineers Inc., Nov. 2020. ISBN: 9781728196596. DOI: 10.1109/CIYCEE49808.2020.9332615.

[48] IACS. *UR M71 Type Testing of I.C. Engines - Corr.1*. Tech. rep. International Association of Classification Societies, June 2016, p. 9. URL: https://iacs.org.uk/publications/.

[49] ICCT. *Maritime shipping*. URL: https://theicct.org/sector/maritime-shipping/.

[50] ICCT. *The Energy Efficiency Design index (EEDI) for New Ships*. Tech. rep. The International Council on Clean Transportation, Oct. 2011, p. 9. URL: https://theicct.org/sites/default/files/publications/ICCTpolicyupdate15_EEDI_final.pdf.

[51] ICS. *Shipping and World Trade: World Seaborne Trade*. URL: https://www.ics-shipping.org/shipping-fact/shipping-and-world-trade-world-seaborne-trade/.

[52] IEA. *Global Energy Review: CO2 Emissions in 2021 Global emissions rebound sharply to highest ever level*. Tech. rep. France: International Energy Agency, Mar. 2022, p. 14. URL: https://www.iea.org/reports/global-energy-review-co2-emissions-in-2021-2.

[53] IEC. *IEC 60092-352:2005*. Tech. rep. International Electrotechnical Commission, 2005, p. 49. URL: https://webstore.iec.ch/publication/694.

[54] IEC. *IEC 60364-1:2005*. Tech. rep. International Electrotechnical Commission, 2005, p. 93. URL: https://webstore.iec.ch/publication/1865&preview=1.

[55] IEEE. “IEEE Std 1709™-2018 - IEEE Recommended Practice for 1 kV to 35 kV Medium-Voltage DC Power Systems on Ships”. In: *IEEE Std 1709-2018 (Revision of IEEE Std 1709-2010)* (2018), pp. 1–54.

[56] IEEE. “IEEE Std 45.1™-2017 IEEE Recommended Practice for Electrical Installations on Shipboard–Design”. In: *IEEE Std 45.1-2017* (2017), pp. 1–198. DOI: 10.1109/IEEESTD.2017.8007394. URL: https://ieeexplore.ieee.org/stampPDF/getPDF.jsp?tp=&arnumber=8007394&ref=%20https://ieeexplore.ieee.org/document/8007394.

[57] IEEE. “IEEE Std 45.8™-2016 - IEEE Recommended Practice for Electrical Installations on Shipboard - Cable Systems”. In: *IEEE Std 45.8-2016* (2016), pp. 1–52.

[58] IMO. *Fourth IMO Greenhouse Gas Study*. Tech. rep. London: International Maritime Organization, 2021, p. 534. URL: https://wwwcdn.imo.org/localresources/en/OurWork/Environment/Documents/Fourth%20IMO%20GHG%20Study%202020%20-%20Full%20report%20and%20annexes.pdf.

[59] IMO. *International Convention for the Prevention of Pollution from Ships (MARPOL)*. URL: https://www.imo.org/en/About/Conventions/Pages/International-Convention-for-the-Prevention-of-Pollution-from-Ships-(MARPOL).aspx.

[60] IMO. *Marine Environment*. URL: https://www.imo.org/en/OurWork/Environment/Pages/Default.aspx.

[61] Omer Berkehan Inal, Jean Frédéric Charpentier, and Cengiz Deniz. “Hybrid power and propulsion systems for ships: Current status and future challenges”. In: *Renewable and Sustainable Energy Reviews* 156 (Mar. 2022), p. 111965. ISSN: 1364-0321. DOI: 10.1016/J.RSER.2021.111965.

[62] Ingeteam. *Ingecon H2 C-lyzer Datasheet*. Tech. rep. Ingeteam, 2023, p. 4. URL: https://www.ingeteam.com/fr/en-us/sectors/green-hydrogen/p15_98_708/ingecon-h2-c-lyzer.aspx?_gl=1*5s89xy*_up*MQ..*_ga*MjY0MDYzODIuMTY5MDk3MDc0OA..*_ga_1GVNP88GWM*MTY5MDk3MDc0Ny4xLjAuMTY5MDk3MDc0Ny4wLjAuMA..

[63] Ingeteam. *Ingecon Sun Power B Series Datasheet*. Tech. rep. Ingeteam, 2023, p. 4. URL: https://www.ingeteam.com/en-us/sectors/photovoltaic-energy/p15_24_36/power-b-series.aspx.

[64] Ingeteam. *Ingedrive LV 200 Frequency converters Datasheet*. Tech. rep. Ingeteam, 2023, p. 2. URL: https://www.ingeteam.com/en-us/power-electronics/power-converters/pc28_6_171/ingedrive-lv200.aspx.

[65] Intergovernmental Oceanographic Commission (IOC). *The International thermodynamic equation of seawater – 2010: calculation and use of thermodynamic properties. [includes corrections up to 31st October 2015]*. Tech. rep. Paris, France: UNESCO, 2015, p. 196. DOI: 10.25607/OBP-1338. URL: https://repository.oceanbestpractices.org/handle/11329/286.

[66] International Maritime Organization. *RESOLUTION MEPC.308(73)*. Tech. rep. International Maritime Organization, 2018, p. 36. URL: https://wwwcdn.imo.org/localresources/en/OurWork/Environment/Documents/Air%20pollution/MEPC.308(73).pdf.

[67] International Maritime Organization. *RESOLUTION MEPC.328(76)*. Tech. rep. International Maritime Organization, 2021, p. 88. URL: https://wwwcdn.imo.org/localresources/en/OurWork/Environment/Documents/Air%20pollution/MEPC.328(76).pdf.

[68] IRENA. *A pathway to decarbonise the shipping sector by 2050*. Tech. rep. Abu Dhabi: International Renewable Energy Agency, 2021. URL: https://www.irena.org/publications/2021/Oct/A-Pathway-to-Decarbonise-the-Shipping-Sector-by-2050.

[69] F. D. Kanellos. “Optimal power management with GHG emissions limitation in all-electric ship power systems comprising energy storage systems”. In: *IEEE Transactions on Power Systems* 29.1 (Jan. 2014), pp. 330–339. ISSN: 08858950. DOI: 10.1109/TPWRS.2013.2280064.

[70] Kyunghwa Kim et al. “DC-grid system for ships: a study of benefits and technical considerations”. In: *Journal of International Maritime Safety, Environmental Affairs, and Shipping* 2.1 (Aug. 2018), pp. 1–12. ISSN: 25725084. DOI: 10.1080/25725084.2018.1490239. URL: https://www-tandfonline-com.tudelft.idm.oclc.org/doi/abs/10.1080/25725084.2018.1490239.

[71] Seongwan Kim and Hyeonmin Jeon. “Comparative Analysis on AC and DC Distribution Systems for Electric Propulsion Ship”. In: *Journal of Marine Science and Engineering* 10.5 (May 2022), p. 559. ISSN: 20771312. DOI: 10.3390/JMSE10050559. URL: https://doi.org/10.3390/jmse10050559.

[72] Kongsberg. *20’SAVe Energy ESS deckhouse*. Tech. rep. Kongsberg Maritime, Nov. 2019, p. 2. URL: https://www.kongsberg.com/contentassets/cac0c7ad701b4667ad59176d44704010/31.propsyst-2p_06.11.19.pdf.

[73] Kongsberg. *26’SAVe Energy ESS deckhouse*. Tech. rep. Kongsberg Maritime, Nov. 2019, p. 2. URL: https://www.kongsberg.com/contentassets/cac0c7ad701b4667ad59176d44704010/30.propsyst-2p_06.11.19.pdf.

[74] Hans Otto Kristenen. *Energy demand and exhaust gas emissions of marine engines*. Tech. rep. Technical University of Denmark, Sept. 2015, p. 30.

[75] Hans Otto Kristensen and Marie Lützen. “Prediction of resistance and propulsion power of ships”. In: *Clean Shipping Currents* 1.6 (2012), pp. 1–52.

[76] Dinesh Kumar and Firuz Zare. “A Comprehensive Review of Maritime Microgrids: System Architectures, Energy Efficiency, Power Quality, and Regulations”. In: *IEEE Access* 7 (2019), pp. 67249–67277. ISSN: 21693536. DOI: 10.1109/ACCESS.2019.2917082.

[77] Hai Lan et al. “Optimal sizing of hybrid PV/diesel/battery in ship power system”. In: *Applied Energy* 158 (Nov. 2015), pp. 26–34. ISSN: 0306-2619. DOI: 10.1016/J.APENERGY.2015.08.031.

[78] Leclanche. *Navius MRS-3 Marine Battery System*. Tech. rep. Leclanché Energy Storage Solutions, 2023, p. 8. URL: https://www.leclanche.com/solutions/e-transport-solutions/e-marine/.

[79] Massimiliano Luna et al. “Optimal Management of Battery and Fuel Cell-Based Decentralized Generation in DC Shipboard Microgrids”. In: *Energies* 16.4 (Feb. 2023), p. 1682. ISSN: 1996-1073. DOI: 10.3390/EN16041682. URL: https://www.mdpi.com/1996-1073/16/4/1682/htm%20https://www.mdpi.com/1996-1073/16/4/1682.

[80] Alan Mace. *Fuel Cell Applications for Marine Vessels*. Tech. rep. Ballard, 2019, pp. 1–16.

[81] MAN Energy Solutions. *EEDI*. Tech. rep. Augsburg, Germany: MAN Energy Solutions, 2021, p. 12. URL: https://man-es.com/docs/default-source/document-sync/eedi-eng.pdf?sfvrsn=23fbab95_3.

[82] MAN Energy Solutions. *Marine Engine Programme*. Tech. rep. MAN Energy Solutions, Dec. 2022, p. 242. URL: https://www.man-es.com/marine/products/planning-tools-and-downloads/marine-engine-programme.

[83] MarineTraffic. *Global Ship Tracking Intelligence*. 2023. URL: https://www.marinetraffic.com/en/ais/home/centerx:6.5/centery:52.9/zoom:6.

[84] Maritime Research Institute Netherlands (MARIN). *Sustainable Power @ MARIN*. 2023. URL: https://sustainablepower.application.marin.nl/.

[85] Market Research. *Electric Ship Market by Type (Fully electric, Hybrid), Ship Type (Commercial, Defense), System, Mode of Operation (Manned, Remotely Operated, Autonomous), End Use (Newbuild & Linefit, Retrofit), Power, Tonnage, Range and Region – Global Forecast to 2030*. Tech. rep. MarketsandMarkets, Apr. 2023, p. 350. URL: https://www.marketresearch.com/MarketsandMarkets-v3719/Electric-Ship-Type-Fully-electric-33930912/.

[86] Salman Mashayekh et al. “Optimum sizing of energy storage for an electric ferry ship”. In: *2012 IEEE Power and Energy Society General Meeting*. San Diego, CA, USA: Institute of Electrical and Electronics Engineers Inc., July 2012. ISBN: 9781467327275. DOI: 10.1109/PESGM.2012.6345228.

[87] Timothy J. McCoy. “Electric Ships Past, Present, and Future [Technology Leaders]”. In: *IEEE Electrification Magazine* 3.2 (June 2015), pp. 4–11. ISSN: 23255889. DOI: 10.1109/MELE.2015.2414291.

[88] Mitsubishi Heavy Industries. *Marine product guide*. Tech. rep. Almere, The Netherlands: Mitsubishi Heavy Industries, 2022, p. 114. URL: https://engine-genset.mhi.com/hubfs/00.%20Website/01.%20Marine/02.%20Product/Engine/00.%20Documents/02.%20Brochures/Mitsubishi%20Marine%20Product%20Guide.pdf?hsLang=en.

[89] Mohammadjavad Mobarra, Miloud Rezkallah, and Adrian Ilinca. “Variable Speed Diesel Generators: Performance and Characteristic Comparison”. In: *Energies* 15.2 (Jan. 2022), p. 592. ISSN: 1996-1073. DOI: 10.3390/EN15020592. URL: https://www.mdpi.com/1996-1073/15/2/592/htm%20https://www.mdpi.com/1996-1073/15/2/592.

[90] Anthony F. Molland, Stephen R. Turnock, and Dominic A. Hudson. *Ship Resistance and Propulsion: Practical Estimation of Ship Propulsive Power*. Cambridge University Press, Aug. 2017. ISBN: 9781316494196. DOI: 10.1017/9781316494196. URL: https://doi.org/10.1017/9781316494196.

[91] Muhammad Umair Mutarraf et al. “Energy Storage Systems for Shipboard Microgrids—A Review”. In: *Energies* 11.12 (Dec. 2018), p. 3492. ISSN: 1996-1073. DOI: 10.3390/EN11123492. URL: https://www.mdpi.com/1996-1073/11/12/3492/htm%20https://www.mdpi.com/1996-1073/11/12/3492.

[92] Chalermkiat Nuchturee, Tie Li, and Hongpu Xia. “Energy efficiency of integrated electric propulsion for ships – A review”. In: *Renewable and Sustainable Energy Reviews* 134 (Dec. 2020), p. 110145. ISSN: 1364-0321. DOI: 10.1016/J.RSER.2020.110145.

[93] Omron. *SX AFE Datasheet*. Tech. rep. Omron, 2023, p. 10. URL: https://assets.omron.eu/downloads/datasheet/en/v12/i122e_sx-series_(active_front_end)_variable_frequency_drives_datasheet_en.pdf.

[94] Omron. *SX Datasheet*. Tech. rep. Omron, 2023. URL: https://assets.omron.eu/downloads/datasheet/en/v17/i125e_sx-series_(690_v)_variable_frequency_drives_datasheet_en.pdf.

[95] Thant Zin Oo et al. “Power System Design Optimization for a Ferry Using Hybrid-Shaft Generators”. In: *IEEE Transactions on Power Systems* 37.4 (July 2022), pp. 2869–2880. ISSN: 15580679. DOI: 10.1109/TPWRS.2021.3128239.

[96] Mukund R Patel. *Shipboard Electrical Power Systems*. en. CRC Press, 2011. ISBN: 978-0-429-24633-3. URL: https://www.taylorfrancis.com/books/9781439828175.

[97] César P.O. Peralta et al. “Evaluation of the CO2 Emissions Reduction Potential of Li-ion Batteries in Ship Power Systems”. In: *Energies* 12.3 (Jan. 2019), p. 375. ISSN: 1996-1073. DOI: 10.3390/EN12030375. URL: https://www.mdpi.com/1996-1073/12/3/375/htm%20https://www.mdpi.com/1996-1073/12/3/375.

[98] V. Fernao Pires et al. “DC-DC Converters for Bipolar Microgrid Voltage Balancing: A Comprehensive Review of Architectures and Topologies”. In: *IEEE Journal of Emerging and Selected Topics in Power Electronics* 11.1 (Feb. 2023), pp. 981–998. ISSN: 21686785. DOI: 10.1109/JESTPE.2022.3208689.

[99] D. Pivetta, C. Dall’Armi, and R. Taccani. “Multi-objective optimization of hybrid PEMFC/Li-ion battery propulsion systems for small and medium size ferries”. In: *International Journal of Hydrogen Energy* 46.72 (Oct. 2021), pp. 35949–35960. ISSN: 0360-3199. DOI: 10.1016/J.IJHYDENE.2021.02.124.

[100] H-O Pörtner et al. *IPCC, 2022: Climate Change 2022: Impacts, Adaptation, and Vulnerability. Contribution of Working Group II to the Sixth Assessment Report of the Intergovernmental Panel on Climate Change*. Cambridge, UK and New York, NY, USA: Cambridge University Press, 2022, p. 3056. DOI: 10.1017/9781009325844. URL: http://dx.doi.org/10.1017/9781009325844.

[101] Hossein Pourrahmani et al. “Optimization and dynamic responses of an integrated fuel cell and battery system for an 800 kW ferry: A case study”. In: *Energy Reports* 8 (Nov. 2022), pp. 9757–9776. ISSN: 2352-4847. DOI: 10.1016/J.EGYR.2022.07.144.

[102] Prysmian Group. *Marine Cable Catalogue*. Tech. rep. Prysmian Group, 2023, p. 46. URL: https://baltics.prysmiangroup.com/sites/default/files/atoms/files/Marine-Cables-Catalogue_North-Europe.pdf.

[103] Harilaos N. Psaraftis. *Sustainable shipping: A cross-disciplinary view*. Cham: Springer Nature Switzerland AG, Jan. 2019, pp. 1–477. ISBN: 9783030043308. DOI: 10.1007/978-3-030-04330-8.

[104] R & M Electrical group Ltd. *Marine Cables Catalogue*. Tech. rep. 2023, p. 110. URL: https://www.rm-electrical.com/wp-content/uploads/2019/07/RM-TKF-Marine-Cable-Catalogue.pdf.

[105] Mehdi Rafiei, Jalil Boudjadar, and Mohammad Hassan Khooban. “Energy Management of a Zero-Emission Ferry Boat with a Fuel-Cell-Based Hybrid Energy System: Feasibility Assessment”. In: *IEEE Transactions on Industrial Electronics* 68.2 (Feb. 2021), pp. 1739–1748. ISSN: 15579948. DOI: 10.1109/TIE.2020.2992005.

[106] Hannah Ritchie, Max Roser, and Pablo Rosado. “CO2 and Greenhouse Gas Emissions”. In: *Our World in Data* (2020). URL: https://ourworldindata.org/co2-and-greenhouse-gas-emissions.

[107] Rolls-Royce. *Marine & Offshore Solution Guide*. Tech. rep. Germany: Rolls-Royce MTU solutions, Feb. 2022, p. 59.

[108] Schneider Electric USA. *Circuit Breakers*. URL: https://www.se.com/us/en/product-category/4200-circuit-breakers/?filter=business-4-low-voltage-products-and-systems.

[109] Edward A. Sciberras et al. “Electric auxiliary propulsion for improved fuel efficiency and reduced emissions”. In: *Proceedings of the Institution of Mechanical Engineers Part M: Journal of Engineering for the Maritime Environment* 229.1 (Feb. 2015), pp. 36–44. ISSN: 20413084. DOI: 10.1177/1475090213495824. URL: https://journals-sagepub-com.tudelft.idm.oclc.org/doi/10.1177/1475090213495824.

[110] Ce Shang, Dipti Srinivasan, and Thomas Reindl. “Economic and Environmental Generation and Voyage Scheduling of All-Electric Ships”. In: *IEEE Transactions on Power Systems* 31.5 (Sept. 2016), pp. 4087–4096. ISSN: 08858950. DOI: 10.1109/TPWRS.2015.2498972.

[111] Ship & Bunker. *Rotterdam Bunker Prices*. 2023. URL: https://shipandbunker.com/prices/emea/nwe/nl-rtm-rotterdam.

[112] Espen Skjong et al. “Approaches to Economic Energy Management in Diesel-Electric Marine Vessels”. In: *IEEE Transactions on Transportation Electrification* 3.1 (Mar. 2017), pp. 22–35. ISSN: 23327782. DOI: 10.1109/TTE.2017.2648178.

[113] Espen Skjong et al. “Past, present, and future challenges of the marine vessel’s electrical power system”. In: *IEEE Transactions on Transportation Electrification* 2.4 (Dec. 2016), pp. 522–537. ISSN: 23327782. DOI: 10.1109/TTE.2016.2552720.

[114] Espen Skjong et al. “The Marine Vessel’s Electrical Power System: From its Birth to Present Day”. In: *Proceedings of the IEEE* 103.12 (Dec. 2015), pp. 2410–2424.

[115] Young Kwang Son, Seong Yong Lee, and Seung Ki Sul. “DC Power System for Fishing Boat”. In: *Proceedings of 2018 IEEE International Conference on Power Electronics, Drives and Energy Systems, PEDES 2018*. Institute of Electrical and Electronics Engineers Inc., July 2018, p. 6. ISBN: 9781538693155. DOI: 10.1109/PEDES.2018.8707631.

[116] Statista. *Lithium-ion batteries worldwide*. Tech. rep. Statista, 2021, p. 40. URL: https://www-statista-com.tudelft.idm.oclc.org/study/22772/lithium-ion-batteries-statista-dossier/.

[117] Giorgio Sulligoi, Andrea Vicenzutti, and Roberto Menis. “All-electric ship design: From electrical propulsion to integrated electrical and electronic power systems”. In: *IEEE Transactions on Transportation Electrification* 2.4 (Dec. 2016), pp. 507–521. ISSN: 23327782. DOI: 10.1109/TTE.2016.2598078.

[118] Tame-Power Tronico. *Convy Series V2.4 Datasheet*. Tech. rep. Tame-Power, 2023, p. 5. URL: https://www.tame-power.com/sites/default/files/tame-power/pdf/TAME-POWER-datasheet-convy-V2.4-ed19_800V%20%281%29_0.pdf.

[119] Rudy Tjandra et al. “Optimal Sizing of BESS for Hybrid Electric Ship Using Multi-Objective Particle Swarm Optimization”. In: *ICPE 2019 - ECCE Asia - 10th International Conference on Power Electronics - ECCE Asia*. Busan, Korea (South): Institute of Electrical and Electronics Engineers Inc., May 2019, pp. 1460–1466. ISBN: 9788957083130. DOI: 10.23919/ICPE2019-ECCEASIA42246.2019.8797214.

[120] Top Cable. *Cable catalogue for electric power distribution*. Tech. rep. Top Cable, 2023, p. 204. URL: https://www.topcable.com/downloads/pdf/ENG/TopCable_General_ENG_901001012201.pdf.

[121] U.S Bureau of Labor Statistics. *Producer Price Index by Industry: Electric Power and Specialty Transformer Manufacturing: Power and Distribution Transformers, Except Parts (PCU3353113353111)*. July 2023. URL: https://fred.stlouisfed.org/series/PCU3353113353111.

[122] U.S Bureau of Labor Statistics. *Producer Price Index by Industry: Semiconductor and Other Electronic Component Manufacturing (PCU3344133441)*. July 2023. URL: https://fred.stlouisfed.org/series/PCU3344133441.

[123] Juan Jose Valera-Garcia and Inigo Atutxa-Lekue. “On the optimal design of hybrid-electric power systems for offshore vessels”. In: *IEEE Transactions on Transportation Electrification* 5.1 (Mar. 2019), pp. 324–334. ISSN: 23327782. DOI: 10.1109/TTE.2018.2883870.

[124] M. Vásquez and C. Andrés. “A methodology to select the electric propulsion system for Platform Supply Vessels (PSV).” PhD thesis. São Paulo: Universidade de São Paulo, Apr. 2014. DOI: 10.11606/D.3.2014.TDE-26122014-164655. URL: http://www.teses.usp.br/teses/disponiveis/3/3135/tde-26122014-164655/.

[125] VesselFinder. *Free AIS Ship Tracker*. 2023. URL: https://www.vesselfinder.com/.

[126] Giovani T.T. Vieira et al. “Optimized Configuration of Diesel Engine-Fuel Cell-Battery Hybrid Power Systems in a Platform Supply Vessel to Reduce CO2 Emissions”. In: *Energies* 15.6 (Mar. 2022), p. 2184. ISSN: 1996-1073. DOI: 10.3390/EN15062184. URL: https://www.mdpi.com/1996-1073/15/6/2184/htm%20https://www.mdpi.com/1996-1073/15/6/2184.

[127] Shuaian Wang and Qiang Meng. “Sailing speed optimization for container ships in a liner shipping network”. en. In: *Transportation Research Part E: Logistics and Transportation Review* 48.3 (2012), pp. 701–714. ISSN: 1366-5545. DOI: 10.1016/j.tre.2011.12.003. URL: https://www.sciencedirect.com/science/article/pii/S1366554511001554%20https://www.sciencedirect.com/science/article/pii/S1366554511001554/pdfft?md5=2dfd72b484a698f1b7e802b52c8f6ff1&pid=1-s2.0-S1366554511001554-main.pdf&isDTMRedir=Y%20https://www.sciencedirect.com/science/article/pii/S1366554511001554?via%3Dihub.

[128] Xiaoyu Wang, Jianzhong Zhu, and Minfang Han. “Industrial Development Status and Prospects of the Marine Fuel Cell: A Review”. In: *Journal of Marine Science and Engineering* 11.2 (Jan. 2023), p. 238. ISSN: 2077-1312. DOI: 10.3390/JMSE11020238. URL: https://www.mdpi.com/2077-1312/11/2/238/htm%20https://www.mdpi.com/2077-1312/11/2/238.

[129] Xuezhou Wang et al. “Sizing and Control of a Hybrid Ship Propulsion System Using Multi-Objective Double-Layer Optimization”. In: *IEEE Access* 9 (2021), pp. 72587–72601. ISSN: 21693536. DOI: 10.1109/ACCESS.2021.3080195.

[130] Wartsila. *Product Guide WÄRTSILÄ 14*. Tech. rep. Wartisla Finland Oy, Mar. 2022, p. 106.

[131] Wartsila. *Wartsila Generating Sets*. 2023. URL: https://www.wartsila.com/marine/products/engines-and-generating-sets/generating-sets/wartsila-gensets.

[132] Peng Wu and Richard Bucknall. “Hybrid fuel cell and battery propulsion system modelling and multi-objective optimisation for a coastal ferry”. In: *International Journal of Hydrogen Energy* 45.4 (Jan. 2020), pp. 3193–3208. ISSN: 0360-3199. DOI: 10.1016/J.IJHYDENE.2019.11.152.

[133] Hui Xing et al. “Fuel Cell Power Systems for Maritime Applications: Progress and Perspectives”. In: *Sustainability* 13.3 (Jan. 2021), p. 1213. ISSN: 2071-1050. DOI: 10.3390/SU13031213. URL: https://www.mdpi.com/2071-1050/13/3/1213/htm%20https://www.mdpi.com/2071-1050/13/3/1213.

[134] Luona Xu et al. “A Review of DC Shipboard Microgrids - Part I: Power Architectures, Energy Storage, and Power Converters”. In: *IEEE Transactions on Power Electronics* 37.5 (May 2022), pp. 5155–5172. ISSN: 19410107. DOI: 10.1109/TPEL.2021.3128417.

[135] Luona Xu et al. “A Review of DC Shipboard Microgrids - Part II: Control Architectures, Stability Analysis, and Protection Schemes”. In: *IEEE Transactions on Power Electronics* 37.4 (Apr. 2022), pp. 4105–4120. ISSN: 19410107. DOI: 10.1109/TPEL.2021.3128409.

[136] Sachin Yadav, Zian Qin, and Pavol Bauer. “Bipolar DC grids on ships: possibilities and challenges”. In: *Elektrotechnik und Informationstechnik* 139 (Aug. 2022), pp. 458–467. ISSN: 0932383X. DOI: 10.1007/S00502-022-01036-X/FIGURES/7. URL: https://link-springer-com.tudelft.idm.oclc.org/article/10.1007/s00502-022-01036-x.

[137] Sachin Yadav, Nils H. Van Der Blii, and Pavol Bauer. “Modeling and Stability Analysis of Radial and Zonal Architectures of a Bipolar DC Ferry Ship”. In: *2021 IEEE Electric Ship Technologies Symposium, ESTS 2021*. Institute of Electrical and Electronics Engineers Inc., Aug. 2021. ISBN: 9781728184265. DOI: 10.1109/ESTS49166.2021.9512334.

[138] Yupeng Yuan et al. “A review of multi-energy hybrid power system for ships”. In: *Renewable and Sustainable Energy Reviews* 132 (Oct. 2020), p. 110081. ISSN: 18790690. DOI: 10.1016/j.rser.2020.110081.

[139] Raphael Zaccone, Ugo Campora, and Michele Martelli. “Optimisation of a Diesel-Electric Ship Propulsion and Power Generation System Using a Genetic Algorithm”. In: *Journal of Marine Science and Engineering* 9.6 (May 2021), p. 587. ISSN: 2077-1312. DOI: 10.3390/JMSE9060587. URL: https://www.mdpi.com/2077-1312/9/6/587/htm%20https://www.mdpi.com/2077-1312/9/6/587.

A

DG and Battery Bank Catalog

This Appendix highlights diesel generators and batteries in Table A.1 and Table A.2.

Table A.1: The diesel generators catalogued for optimization [18, 82, 131, 107, 88].

Name	Speed (rpm)	Power (kWe)	Power (kW)	SFOC [g/kWh]	Gen. Efficiency (%)	Mass (Ton)
C9.3 225	1500	225	240	208.8	95.00%	2.4
C9.3 244	1500	244	260	208.8	95.00%	2.4
C9.3 288	1500	288	300	211	95.00%	2.4
C9.3 306	1500	306	320	211	95.00%	2.4
C18 419	1500	419	440	206.6	95.00%	4.2
C18 450	1500	450	470	206.6	95.00%	4.2
C18 486	1500	486	510	204.8	95.00%	4.2
C18 513	1500	513	540	204.8	95.00%	4.2
MAS 650	1500	522	540	205	96.00%	5.9
C18 556	1500	556	590	207.7	95.00%	4.2
C18 581	1500	581	610	207.7	95.00%	4.2
MAS 760	1500	612	640	205	96.00%	6
MAS 850	1500	678	710	202	96.00%	8
Wärtsilä 14 12V14 750	1500	750	780	205	96.00%	5.5
Wärtsilä 20 4L20 760	1000	760	790	199.1	96.00%	14
C32 994 210.3	1500	994	1050	210.3	95.00%	7.1
C32 994 202.1	1500	994	1050	202.1	95.00%	7.1
Wärtsilä 14 16V14 1000	1500	1000	1040	205	96.00%	7.5
C32 1038 210.3	1500	1038	1090	210.3	95.00%	7.1
C32 1038 202.1	1500	1038	1090	202.1	95.00%	7.1
MAS 1350	1500	1081	1130	202	96.00%	10
Wärtsilä 20 6L20 1140	1000	1140	1190	194.9	96.00%	16.8
MAS 1795	1500	1437	1500	200	96.00%	14
MG12V4000M35F 1500	1500	1500	1560	200	96.00%	17
Wärtsilä 20 8L20 1520	1000	1520	1580	195.3	96.00%	20.7
Wärtsilä 20 9L20 1720	1000	1720	1790	194.9	96.00%	23.8
MAN 12V175D-MEV 1786	1800	1786	1860	192	96.00%	19
MAS 2350	1500	1886	1960	199	96.00%	18
MAN 12V175D-MEV 1959	1800	1959	2040	191	96.00%	19
Wärtsilä 26 6L26 1960	1000	1960	2040	195.8	96.00%	23
MAN 6L2738 2015	750	2015	2100	185	96.00%	25
MAN 12V175D-MEV 2189	1800	2189	2280	193.5	96.00%	19

The diesel generator catalogued from various manufacturers, like, Caterpillar [18], MAN Energy Solutions [82], Wartsila [131], Rolls-Royce [107], and Mitsubishi Heavy Industries [88] are presented in Table A.1. The catalogued gen sets are satisfying the Tier III constraints and run on fuels less than 0.1 per cent m/m of sulphur. All the generators below 2.5 MW of capacity were found to operate on MDO except for two models manufactured by MAN Energy Solutions [82]. They are dual-fuel engines and are excluded from this dataset. The marine gen sets manufactured by Cummins Inc. [24] were not catalogued since they were not Tier III equivalent as per the Table 2.1 described in section 2.1. The Table A.1 describes the speed of operation, the electrical power production, mechanical power production, the alternator efficiency the specific fuel oil consumption as well as the mass of the diesel generators. The marine battery manufacturers like Echandia [30], ABB [2], Kongsberg [72, 73], Corvus Energy [22], and Leclanche [78] are also catalogued in Table A.2. The table describes the energy density in kWh the mass of the battery bank as well as the charge and discharge power ratings in C-rates. These parameters for DGs and Batteries were included in forming the optimization problem constraints.

Table A.2: The battery banks catalogued for optimization [30, 2, 72, 73, 22, 78]

Name	Type	Capacity [kWh]	Mass [ton]	Discharge C-rate	Charge C-rate
ABB Container Storage 995	Li-ion	995	13	2.8	2
Kongsberg | 26’ SAVe ESS 532	Li-ion NMC	532	6.9692	2.8	2
Kongsberg | 26’ SAVe ESS 565	Li-ion NMC	565	7.4015	2.8	2
Kongsberg | 26’ SAVe ESS 608	Li-ion NMC	608	7.9648	2.8	2
Kongsberg | 26’ SAVe ESS 678	Li-ion NMC	678	8.8818	2.8	2
Kongsberg | 26’ SAVe ESS 750	Li-ion NMC	750	9.825	2.8	2
Kongsberg | 26’ SAVe ESS 760	Li-ion NMC	760	9.956	2.8	2
Kongsberg | 26’ SAVe ESS 784	Li-ion NMC	784	10.2704	2.8	2
Kongsberg | 26’ SAVe ESS 896	Li-ion NMC	896	11.7376	2.8	2
Kongsberg | 26’ SAVe ESS 912	Li-ion NMC	912	11.9472	2.8	2
Kongsberg | 20’ SAVe ESS 532	Li-ion NMC	532	6.9692	2.8	2
Kongsberg | 20’ SAVe ESS 565	Li-ion NMC	565	7.4015	2.8	2
Kongsberg | 20’ SAVe ESS 608	Li-ion NMC	608	7.9648	2.8	2
Kongsberg | 20’ SAVe ESS 678	Li-ion NMC	678	8.8818	2.8	2
Kongsberg | 20’ SAVe ESS 684	Li-ion NMC	684	8.9604	2.8	2
Kongsberg | 20’ SAVe ESS 760	Li-ion NMC	760	9.956	2.8	2
Leclanché 1079	Li-ion NMC	1079	9.362	2.8	1
Echandia Energy 1068	Li-ion LTO	1068	13.8	2	2
Echandia Power 274	Li-ion LTO	274	4.77	5	5
Corvus Orca Energy 124	Li-ion NMC	124	1.628	3	3
Corvus Orca Energy 248	Li-ion NMC	248	3.256	3	3
Corvus Orca Energy 372	Li-ion NMC	372	4.884	3	3
Corvus Orca Energy 496	Li-ion NMC	496	6.512	3	3
Corvus Orca Energy 620	Li-ion NMC	620	8.14	3	3
Corvus Orca Energy 744	Li-ion NMC	744	9.768	3	3
Corvus Orca Energy 868	Li-ion NMC	868	11.396	3	3
Corvus Orca Energy 992	Li-ion NMC	992	13.024	3	3
Corvus Orca Energy 1116	Li-ion NMC	1116	14.652	3	3
Corvus Orca Energy 1240	Li-ion NMC	1240	16.28	3	3
Corvus Orca Energy 1364	Li-ion NMC	1364	17.908	3	3
Corvus Orca Energy 1488	Li-ion NMC	1488	19.536	3	3
XALT Energy 670	Li-ion	670	8.4	4	1.9

B

Damen *Island Discovery* Datasheet

The Figure B.1 showcases the technical and design details of the ship taken into consideration in this work. The two propulsion motors are rated at 900 kW and the ship's two diesel generators that provide the required electrical power are rated at 1500 kWe. The ship operates at 690V, 3phase 60 Hz @ 1200 rpm.

PICTURE OF SIMILAR VESSEL

GENERAL

Yard number	539320-23
Hull material	Steel
Basic functions	Passenger car ferry
Flag	Canadian
Classification	Bureau Veritas I +HULL +MACH, ro-ro passenger ship, coastal area, AUT-CCS, CLEANSHIP, NDO (1 day), Green Passport, COMF VIB & NOISE, with a rating of 2 for accommodation, InWaterSurvey, Battery System

DIMENSIONS

Length overall	80.80	m
Beam moulded	17.00	m
Depth to main deck moulded	5.70	m
Design draught	3.20	m
Gross tonnage	2277	t

TANK CAPACITIES

Fuel oil	65	m^3
Lube oil	9	m^3
Fresh water	30	m^3
Sewage	30	m^3
Technical fresh water	30	m^3

PERFORMANCES

Speed (at design draught)	14	kn

PROPULSION SYSTEM

Propulsion	2x 900 kW twin-propeller thruster units, electric drive
Propeller	2x 1850 mm ice strength fixed pitch

AUXILIARY EQUIPMENT

Main genset power	2x 1500 kWe, 690V, 3ph / 60 Hz @ 1,200 rpm
Energy storage system	800 kwh Li-Ion battery bank
Emergency genset power	155 kWe, 690V, 3ph / 60 Hz @ 1,800 rpm

ACCOMODATION

Passengers	450
Inside passenger lounge	101 seats
Outside passenger lounge	40 seats
Toilets passenger lounge	2 + 1 accessible toilets
Crew accomodation	1 mess room + pantry, 1 ships office, 1 male changing room and 1 female changing room

Cars on main deck	31
Car line length – main deck	193 m
Trailers on main deck	2
Trailer line length	68 m
Cars on car deck	16
Car lane length – car deck	99 m

NAUTICAL AND COMMUNICATION EQUIPMENT

Wheelhouse equipped with nautical and communications equipment according to national Authorities and owner's requirements.

S- band and X-and radars, ECDIS, Autopilot, Echo sounder, Speed log, GPS navigator, Gyro compass, Magnetic compass, Public address, CCTV, Navtex, AIS, LRIT, VHF, UHF, GDMSS 2, Infotainment system

Figure B.1: The technical and design details of Damen Road Ferry 8117E3, i.e. *Island Discovery* Adapted from [25].

C

Optimization Results for all Arrangements

The optimization algorithm considered all the diesel generators and batteries for each arrangement. There are 32 diesel generators and 32 batteries catalogued as presented in Appendix A leading to a total of 1024 configurations. This chapter presents the results for some of the configurations with feasible solutions i.e. the optimal power dispatch profile for minimum emissions for AC2, AC3, AC4, AC5, DC2, DC3, DC4, and DC5 arrangements.

C.1. AC2 (Two diesel generators and battery)

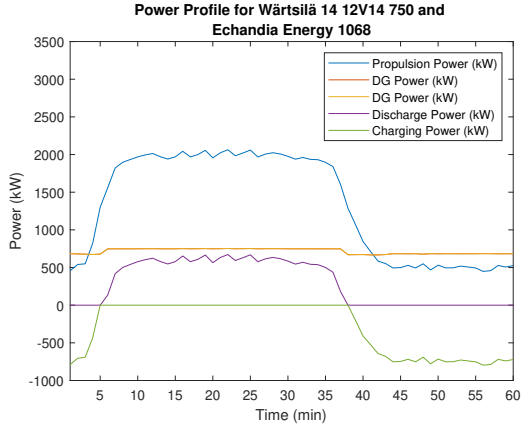

(a) The optimal power profile

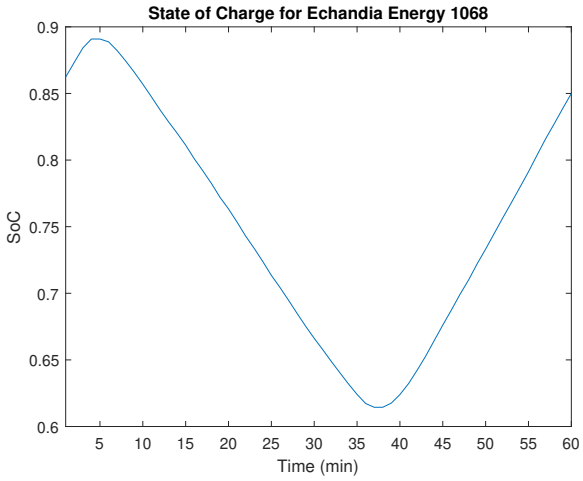

(b) The State of Charge of Battery

Figure C.1: The optimization result for AC2 arrangement

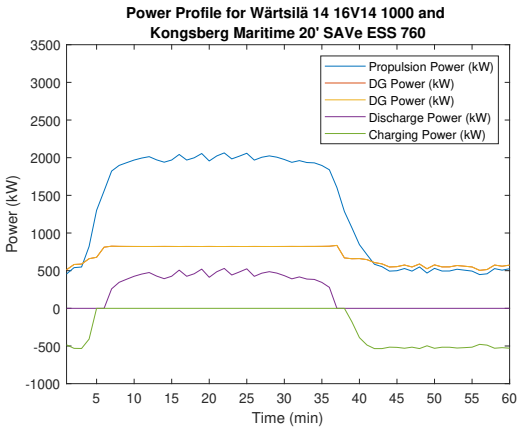

(a) The optimal power profile

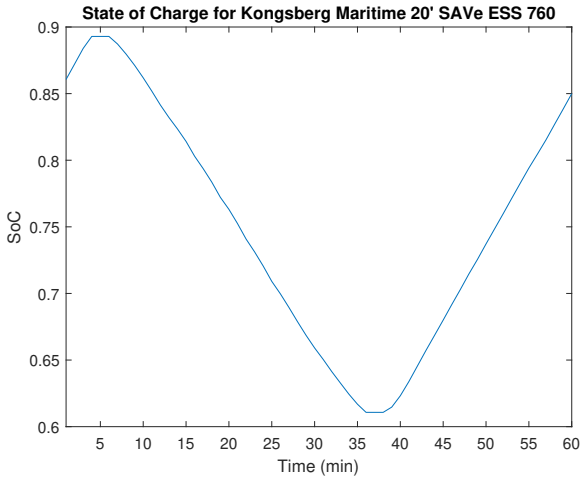

(b) The State of Charge of Battery

Figure C.2: The optimization result for AC2 arrangement

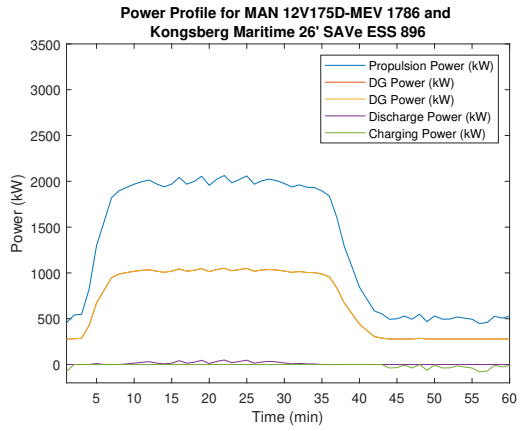

(a) The optimal power profile

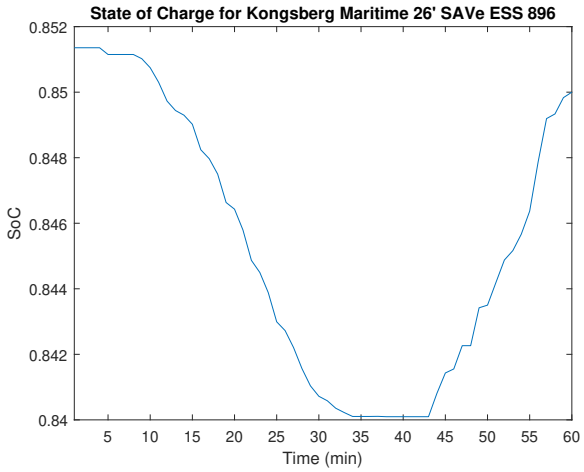

(b) The State of Charge of Battery

Figure C.3: The optimization result for AC2 arrangement

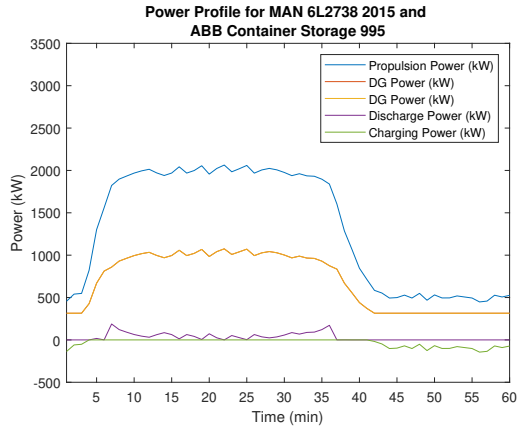

(a) The optimal power profile

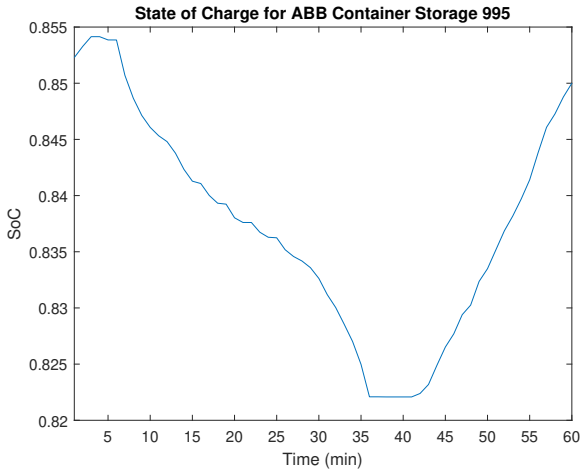

(b) The State of Charge of Battery

Figure C.4: The optimization result for AC2 arrangement

C.2. AC3 (Two diesel generators, battery, and shore power)

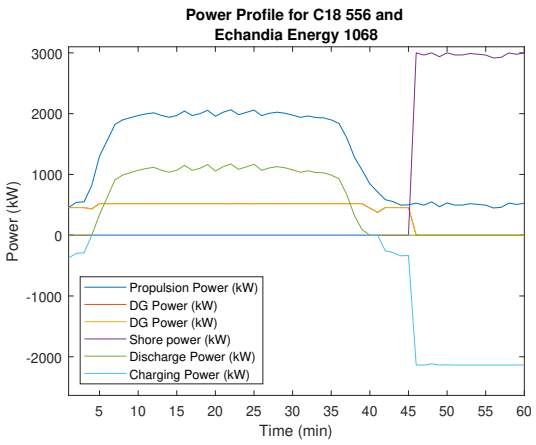

(a) The optimal power profile

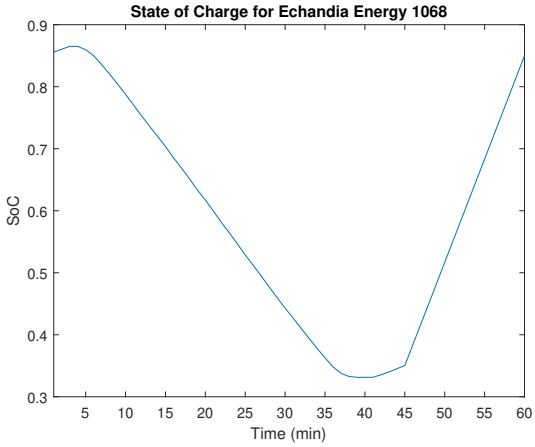

(b) The State of Charge of Battery

Figure C.5: The optimization result for AC3 arrangement

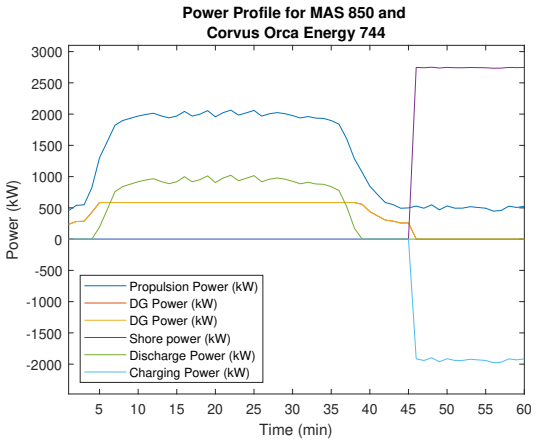

(a) The optimal power profile

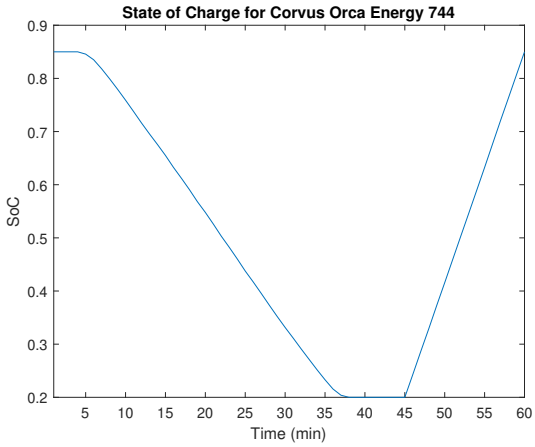

(b) The State of Charge of Battery

Figure C.6: The optimization result for AC3 arrangement

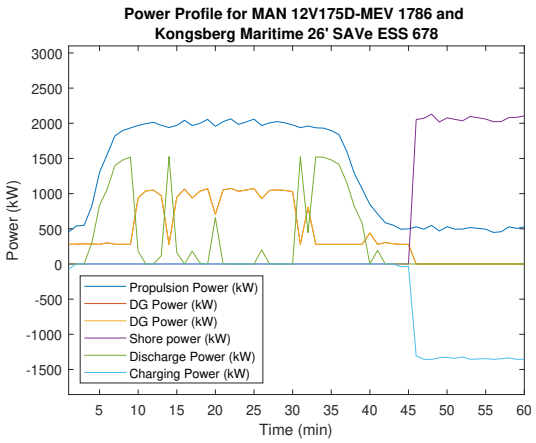

(a) The optimal power profile

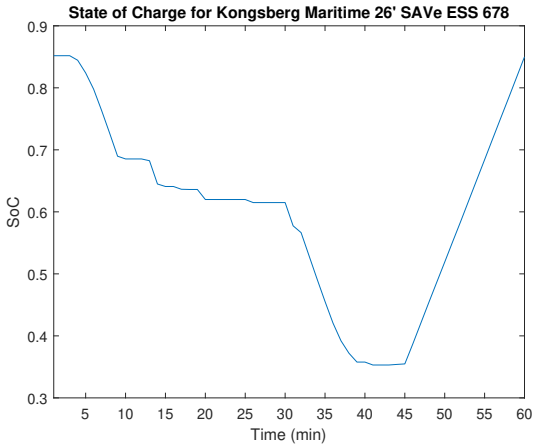

(b) The State of Charge of Battery

Figure C.7: The optimization result for AC3 arrangement

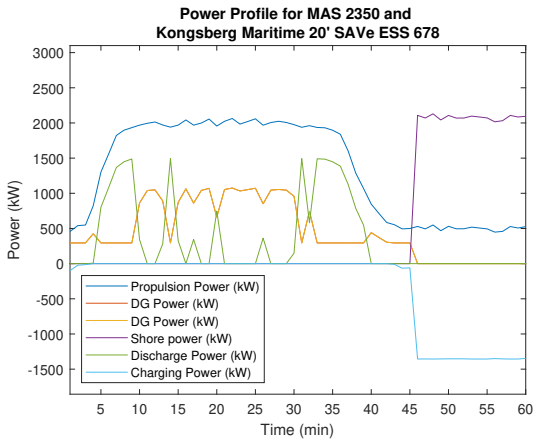

(a) The optimal power profile

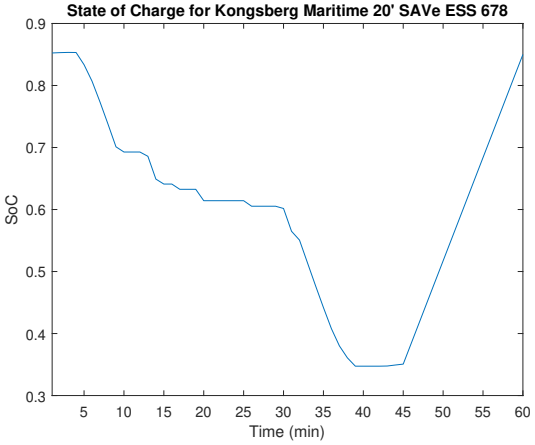

(b) The State of Charge of Battery

Figure C.8: The optimization result for AC3 arrangement

C.3. AC4 (One diesel generator and battery)

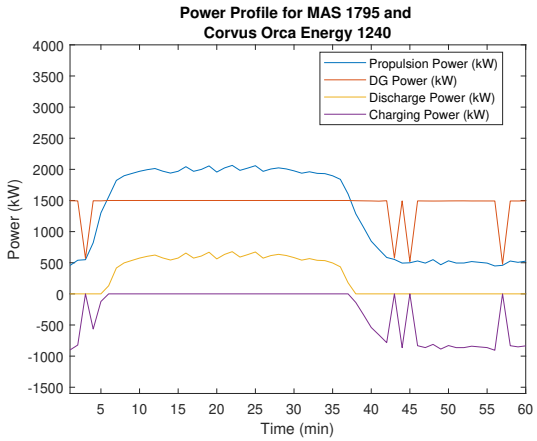

(a) The optimal power profile

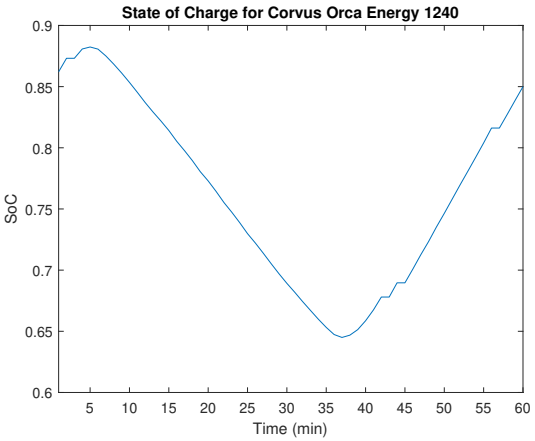

(b) The State of Charge of Battery

Figure C.9: The optimization result for AC4 arrangement

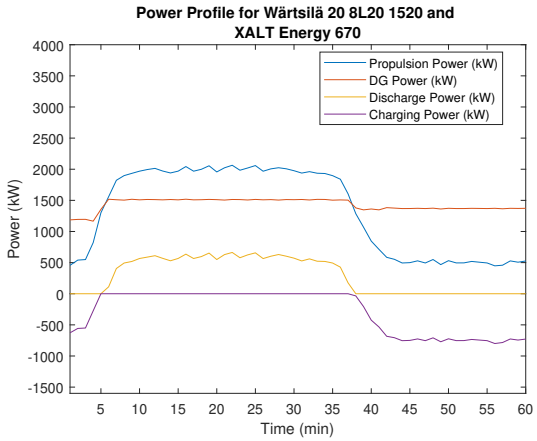

(a) The optimal power profile

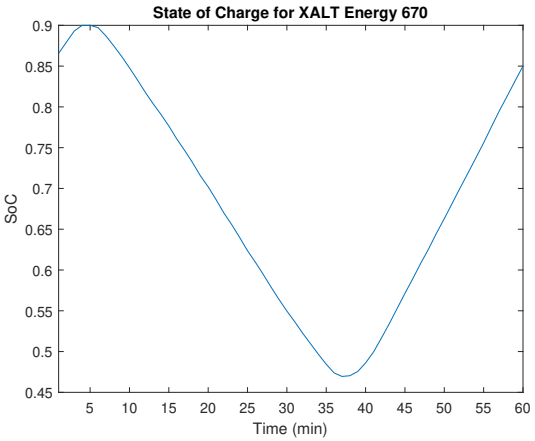

(b) The State of Charge of Battery

Figure C.10: The optimization result for AC4 arrangement

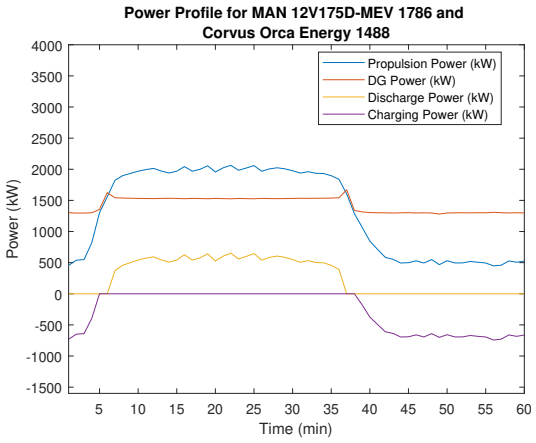

(a) The optimal power profile

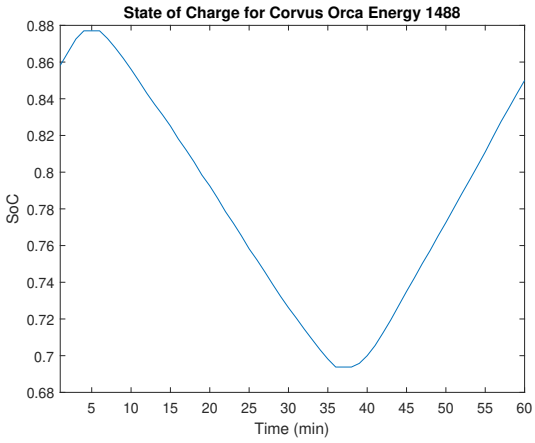

(b) The State of Charge of Battery

Figure C.11: The optimization result for AC4 arrangement

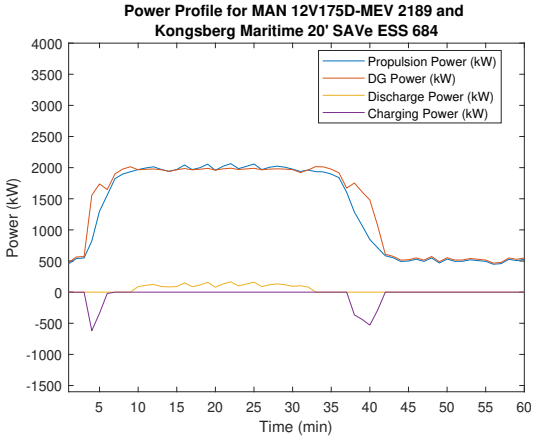

(a) The optimal power profile

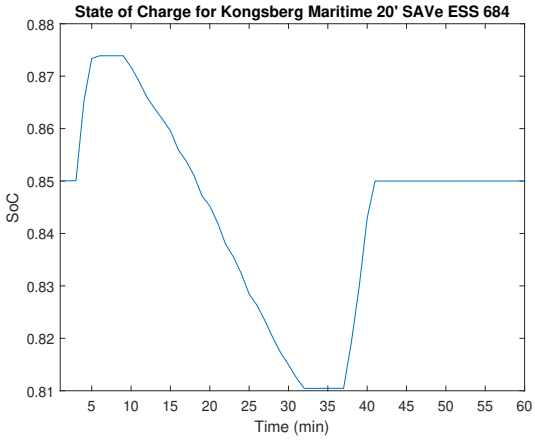

(b) The State of Charge of Battery

Figure C.12: The optimization result for AC4 arrangement

C.4. AC5 (One diesel generator, battery, and shore power)

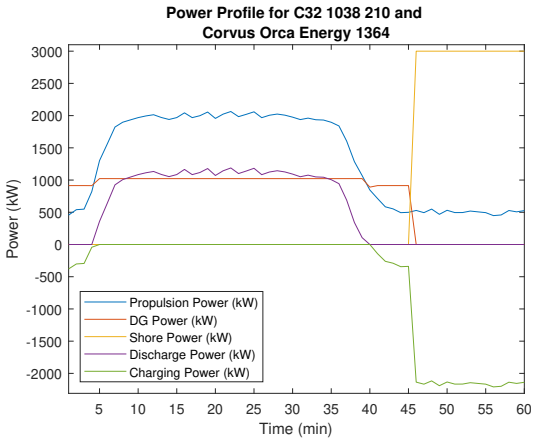

(a) The optimal power profile

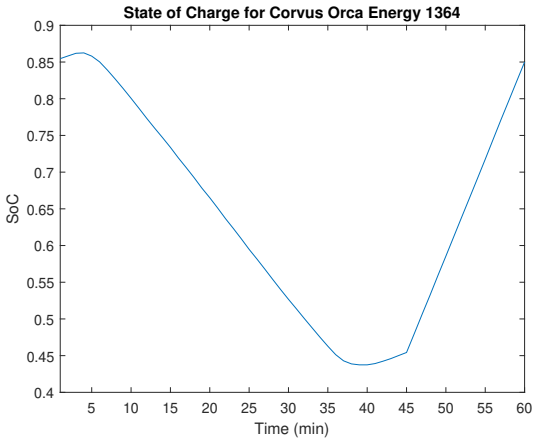

(b) The State of Charge of Battery

Figure C.13: The optimization result for AC5 arrangement

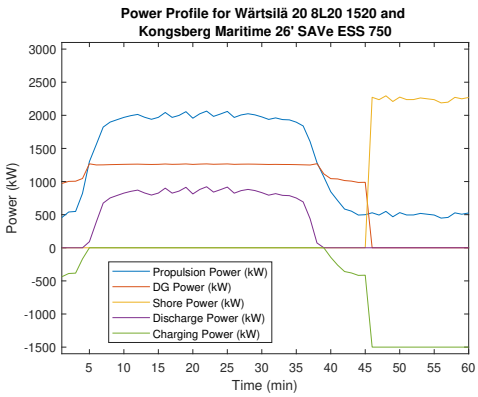

(a) The optimal power profile

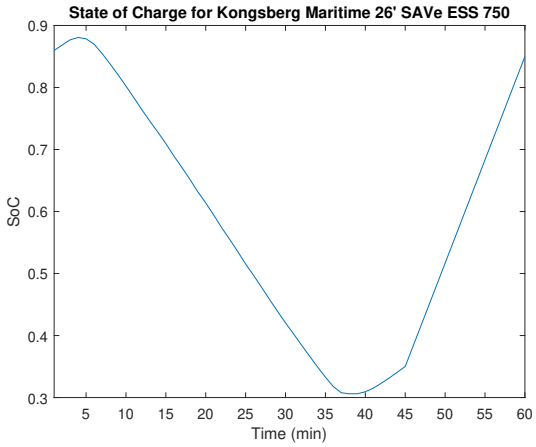

(b) The State of Charge of Battery

Figure C.14: The optimization result for AC5 arrangement

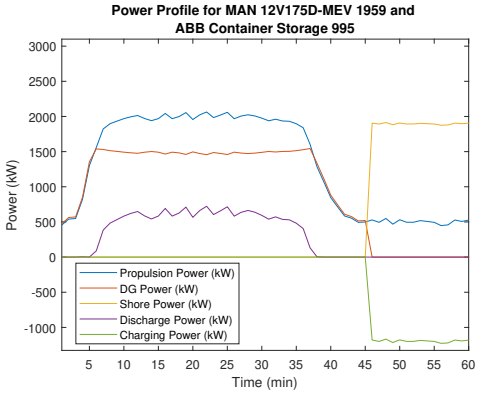

(a) The optimal power profile

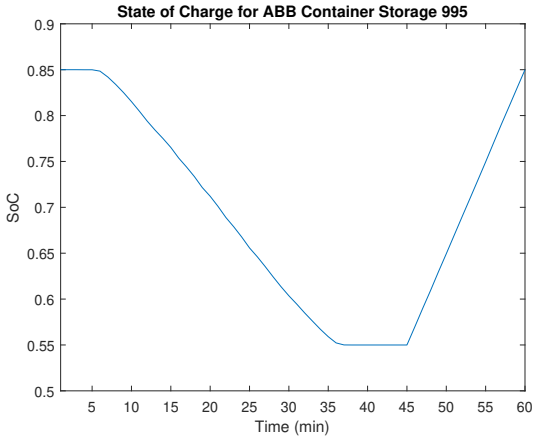

(b) The State of Charge of Battery

Figure C.15: The optimization result for AC5 arrangement

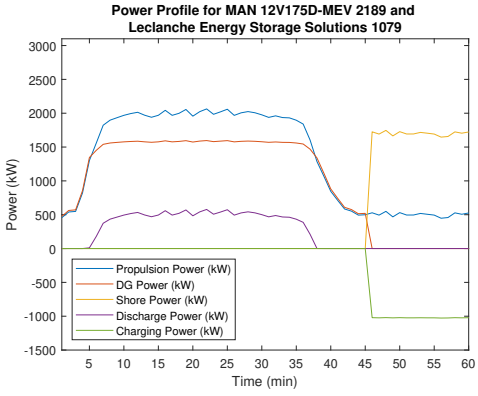

(a) The optimal power profile

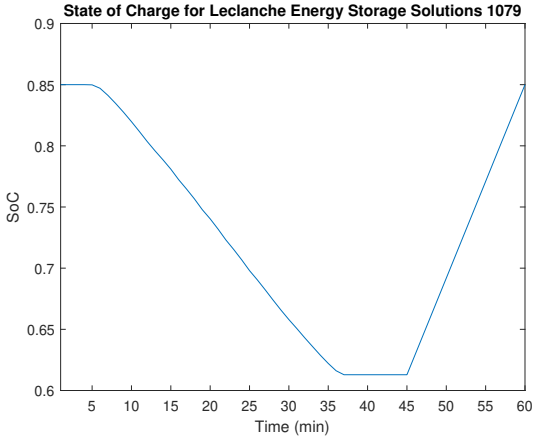

(b) The State of Charge of Battery

Figure C.16: The optimization result for AC5 arrangement

C.5. DC2 (Two diesel generators and battery)

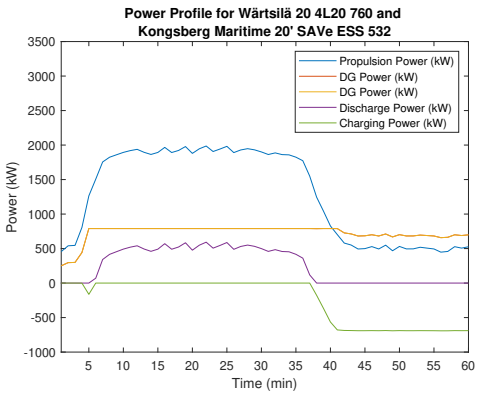

(a) The optimal power profile

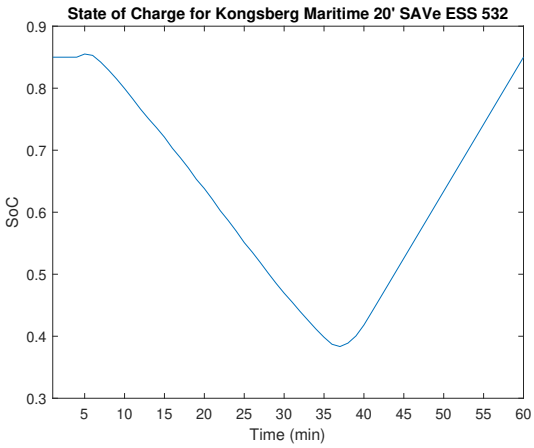

(b) The State of Charge of Battery

Figure C.17: The optimization result for DC2 arrangement

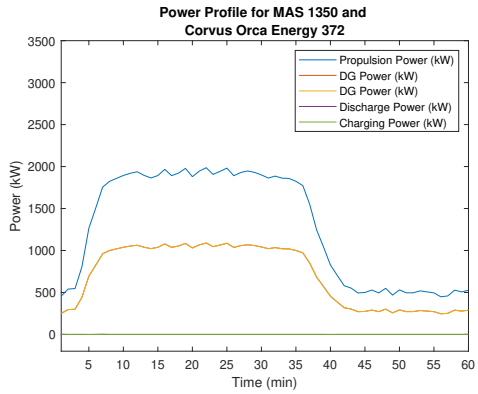

(a) The optimal power profile

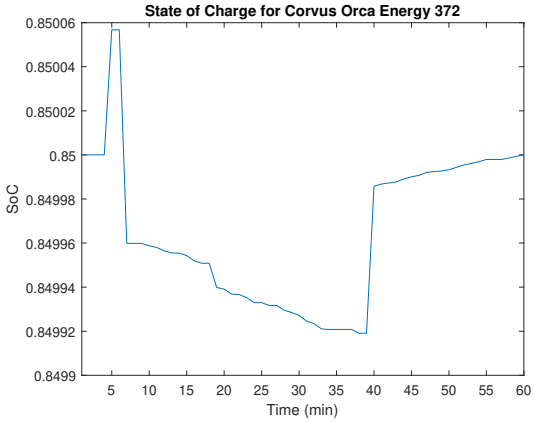

(b) The State of Charge of Battery

Figure C.18: The optimization result for DC2 arrangement

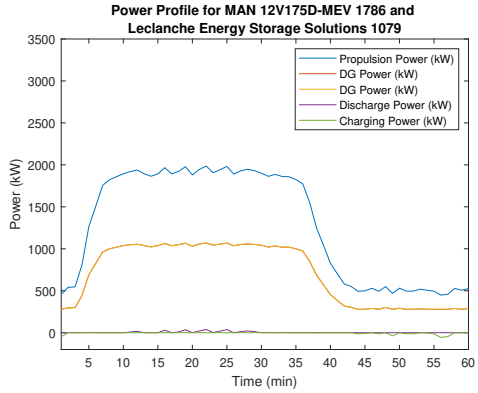

(a) The optimal power profile

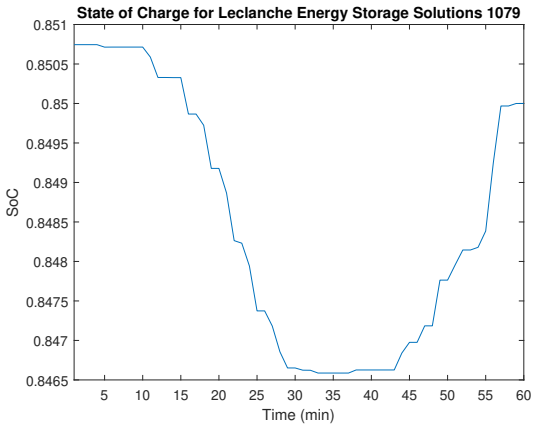

(b) The State of Charge of Battery

Figure C.19: The optimization result for DC2 arrangement

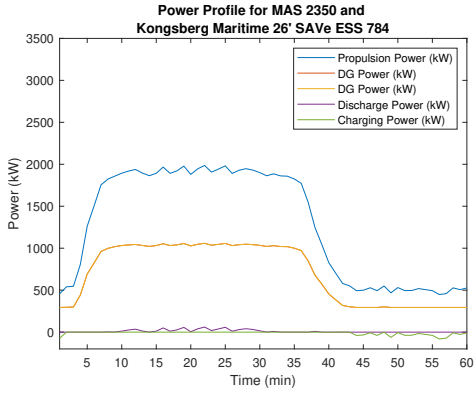

(a) The optimal power profile

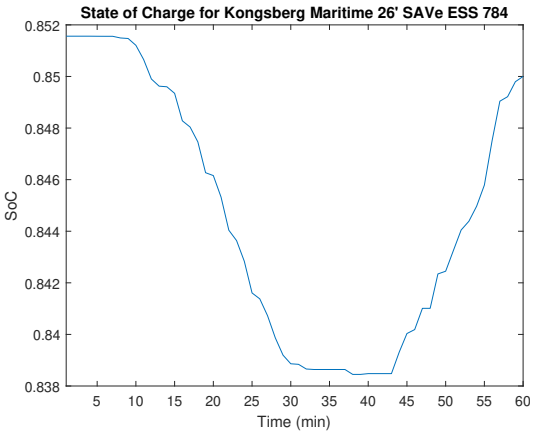

(b) The State of Charge of Battery

Figure C.20: The optimization result for DC2 arrangement

C.6. DC3 (Two diesel generators, battery, and shore power)

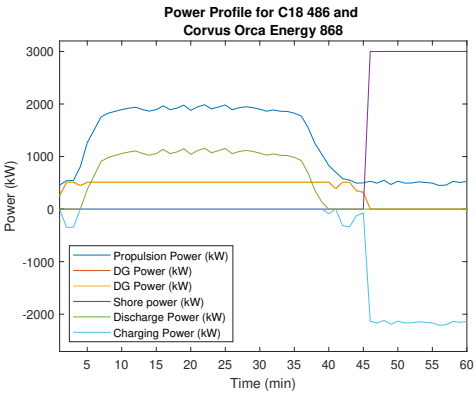

(a) The optimal power profile

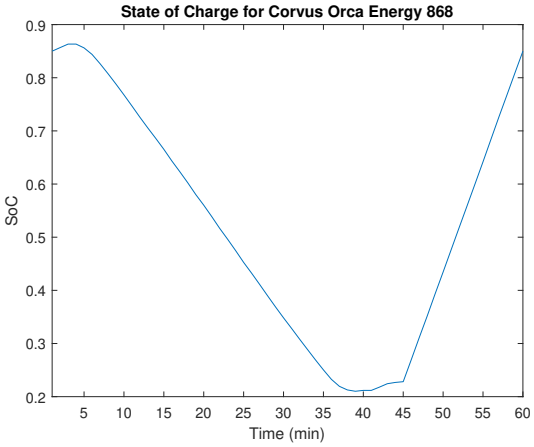

(b) The State of Charge of Battery

Figure C.21: The optimization result for DC3 arrangement

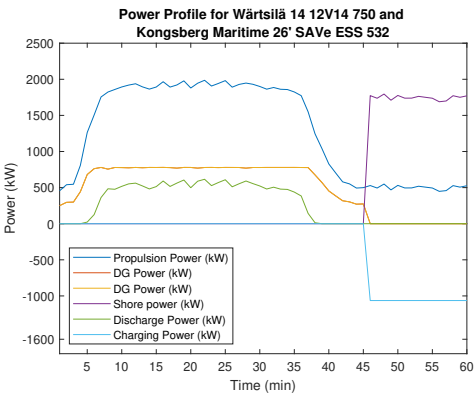

(a) The optimal power profile

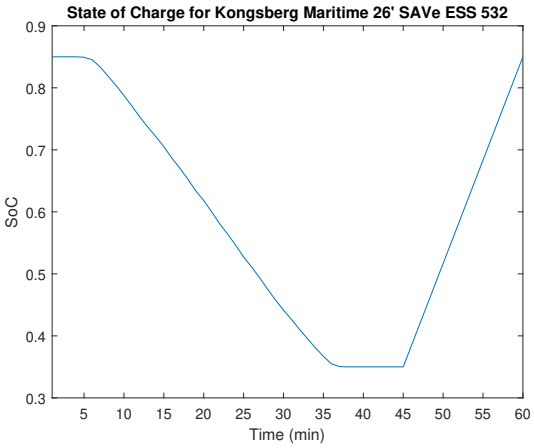

(b) The State of Charge of Battery

Figure C.22: The optimization result for DC3 arrangement

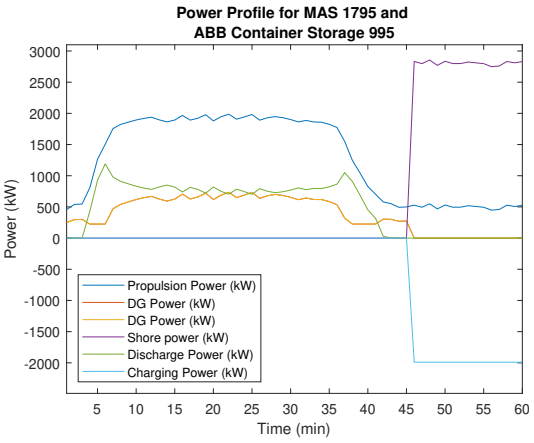

(a) The optimal power profile

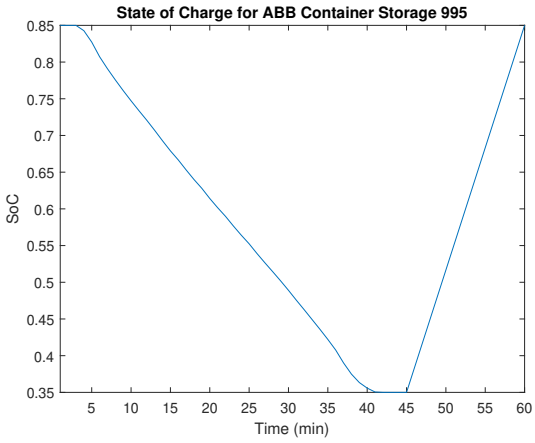

(b) The State of Charge of Battery

Figure C.23: The optimization result for DC3 arrangement

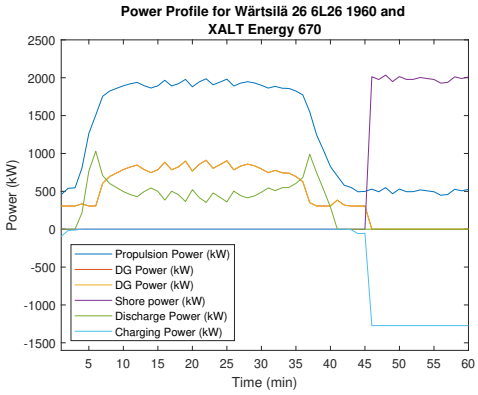

(a) The optimal power profile

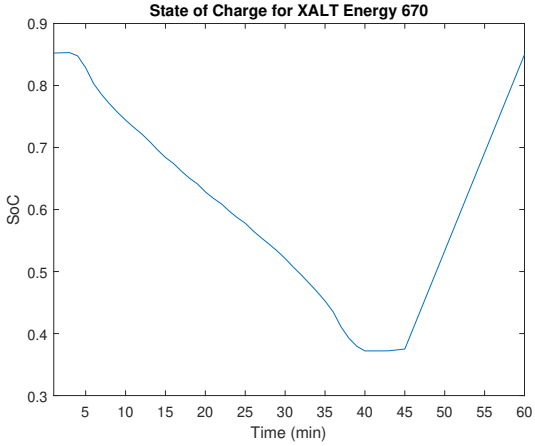

(b) The State of Charge of Battery

Figure C.24: The optimization result for DC3 arrangement

C.7. DC4 (One diesel generator and battery)

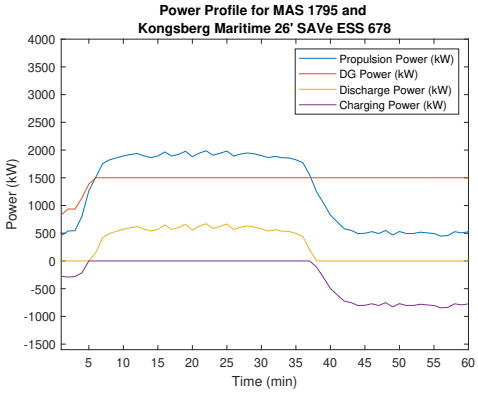

(a) The optimal power profile

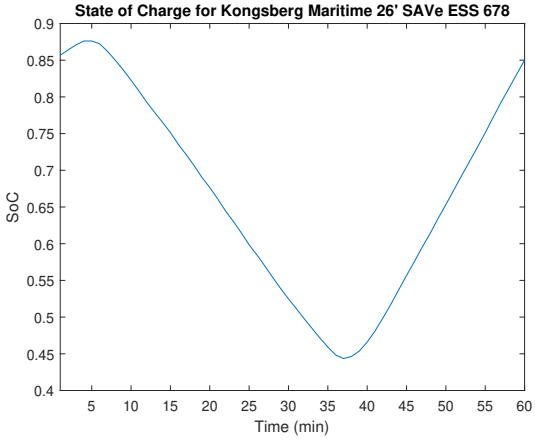

(b) The State of Charge of Battery

Figure C.25: The optimization result for DC4 arrangement

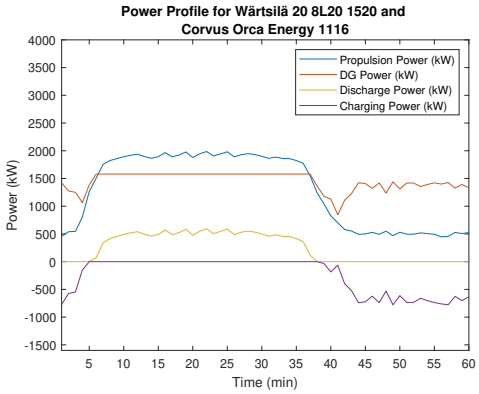

(a) The optimal power profile

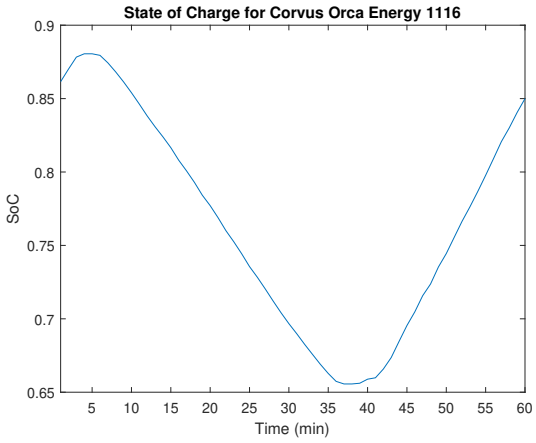

(b) The State of Charge of Battery

Figure C.26: The optimization result for DC4 arrangement

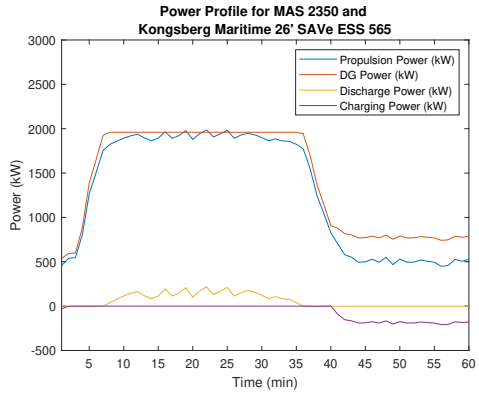

(a) The optimal power profile

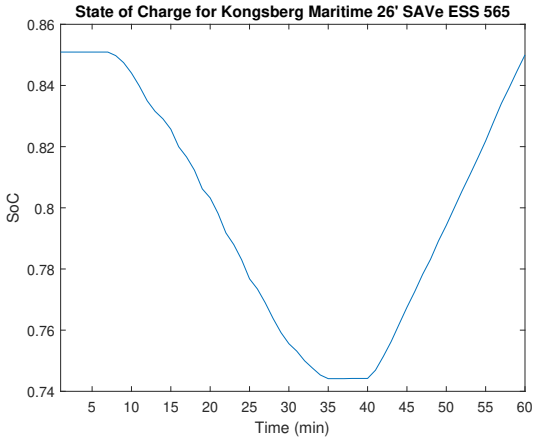

(b) The State of Charge of Battery

Figure C.27: The optimization result for DC4 arrangement

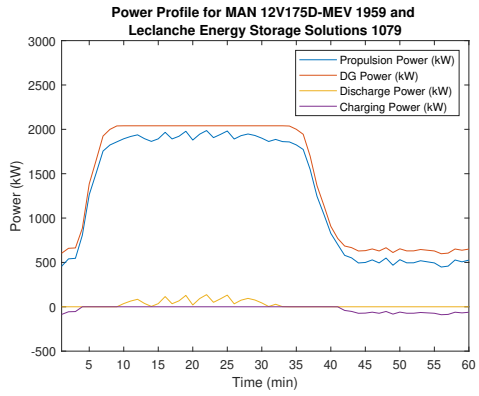

(a) The optimal power profile

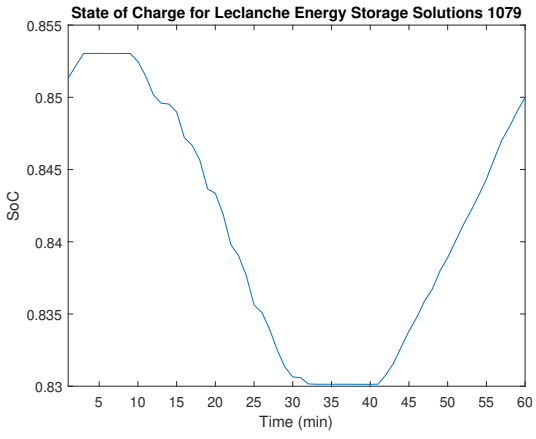

(b) The State of Charge of Battery

Figure C.28: The optimization result for DC4 arrangement

C.8. DC5 (One diesel generator, battery, and shore power)

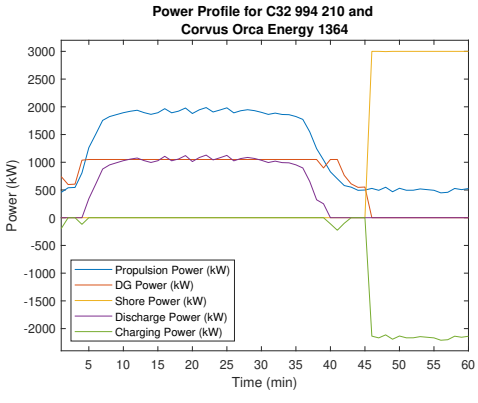

(a) The optimal power profile

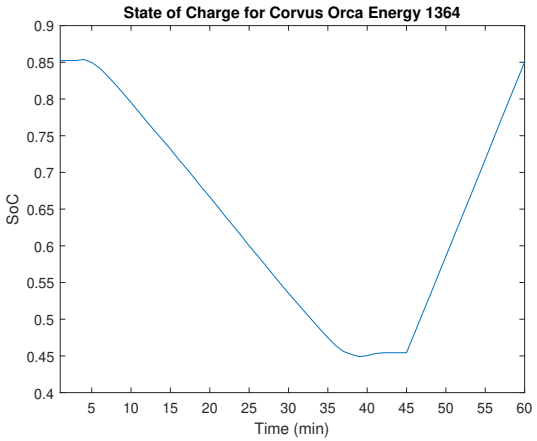

(b) The State of Charge of Battery

Figure C.29: The optimization result for DC5 arrangement

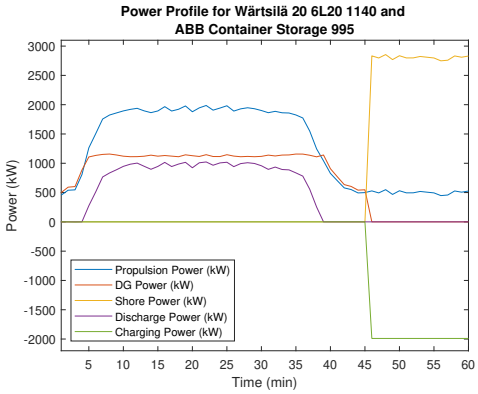

(a) The optimal power profile

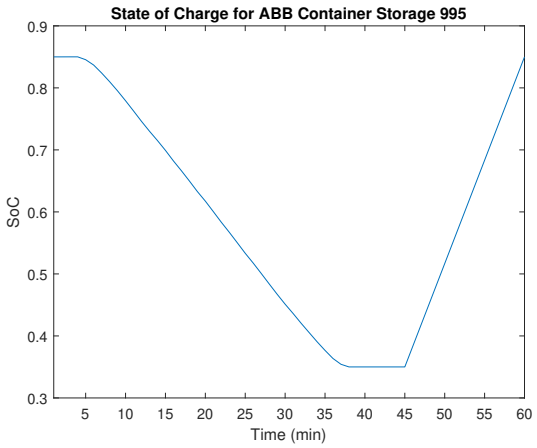

(b) The State of Charge of Battery

Figure C.30: The optimization result for DC5 arrangement

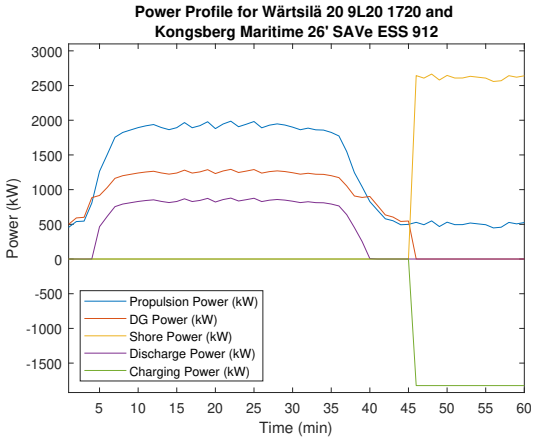

(a) The optimal power profile

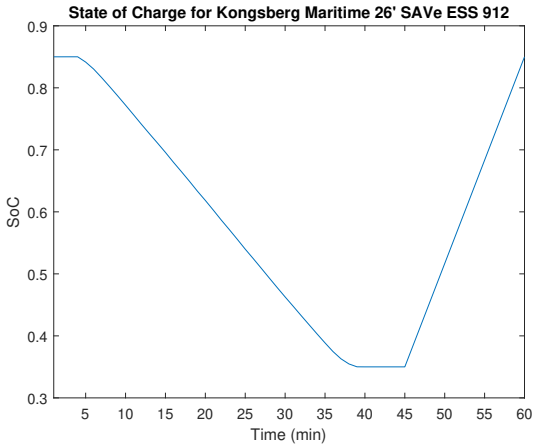

(b) The State of Charge of Battery

Figure C.31: The optimization result for DC5 arrangement

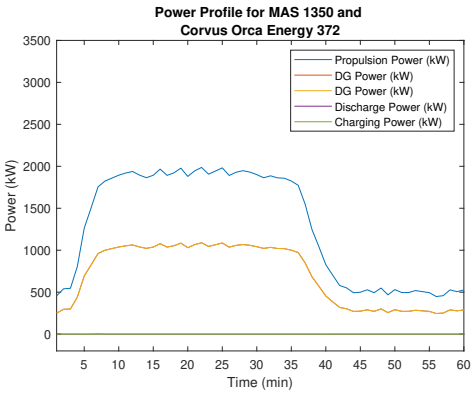

(a) The optimal power profile

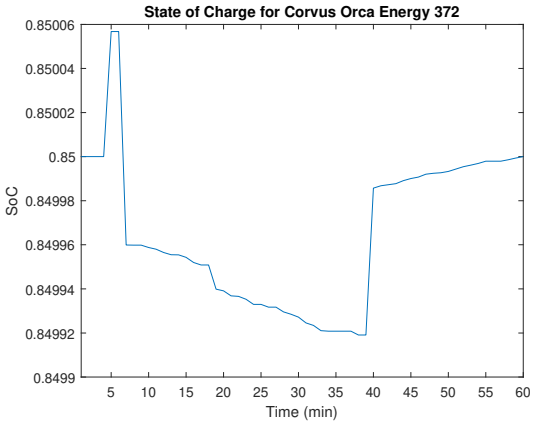

(b) The State of Charge of Battery

Figure C.32: The optimization result for DC5 arrangement

D

Matlab Application for Optimal Dispatch

The application for the optimal dispatch for ship optimising (i.e. minimising) the emissions over the ship's operational profile is developed in the Matlab® GUI.

The application interface is as follows. The top of the application consists of two blank figures. The figure on the left is where the optimal dispatch profile for the selected configuration is plotted if the optimization problem for that particular configuration in a particular arrangement for AC and BiDC grid finds a feasible solution. The plot on the right plots the SoC of the selected battery if the arrangement selected has a battery in it. The application lets the user select the diesel generator and battery from the respective drop-down menu. The selected diesel generator and battery from the selected configuration. The user can also select the type of arrangement from the radio button provided with five options representing the five different arrangements. The user can also select the type of grid he/she wants for the optimization problem to run. Finally, the user can also change the efficiency values for the components that make up the respective AC and BiDC grids, as shown in Figure 3.3. The power factor values are also incorporated along with the voltage levels for the AC and the BiDC grid. This thesis has performed a comparative study between an AC grid operating at 690 V and a BiDC grid operating at +700,-700 (1400 V). However, the application is designed for taking user-defined voltage levels for AC as well as the BiDC grid. Once all the things are selected and completed, the user has to click on the 'Run' button to start the optimization for the selected grid, arrangement, and configuration. If the optimization problem converges to a minimum which is feasible, the results are plotted. To clear the results and reset the application to its default values, the user can click on the 'Reset' button. The default values for the efficiency of the components, the AC and BiDC voltage levels are already programmed in the application.

The results from the optimization problem are shown in the box on the bottom right highlighting the emissions, the capital cost for the system, the operating cost, the weight of the propulsion system, and the result for the optimization problem shown by the exitflag. When the 'Reset' button is pressed, the values from the 'Results' are set to zero for all the fields.

The snapshots from the running of the application are shown in Figure D.1, Figure D.2, Figure D.3, and Figure D.4.

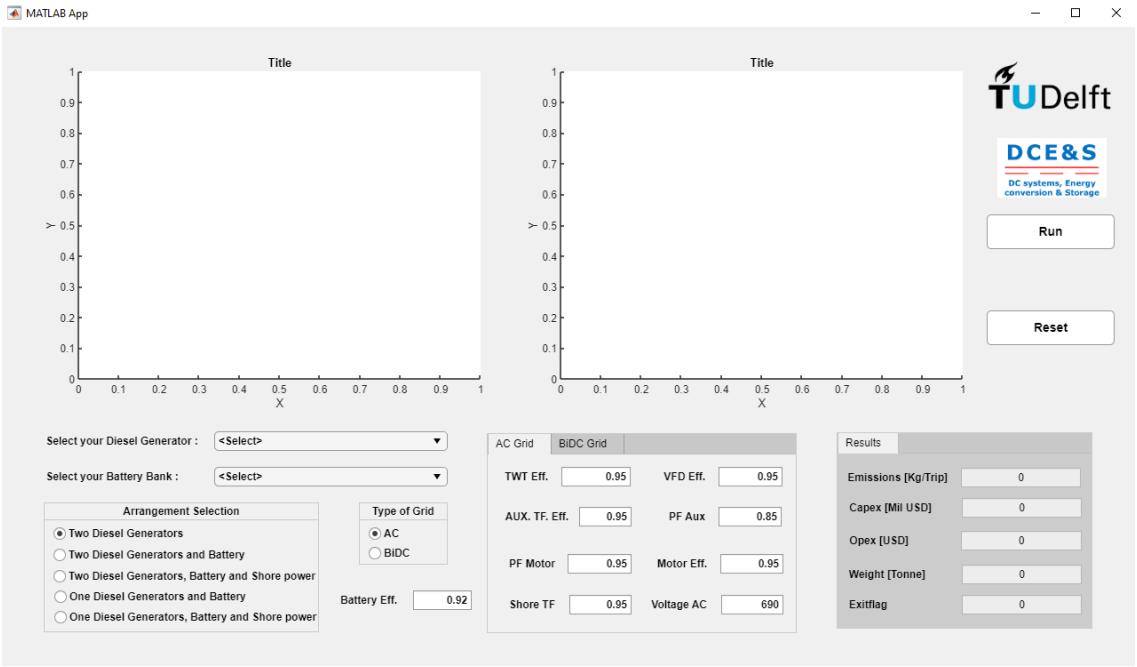

Figure D.1: The main screen of the Application

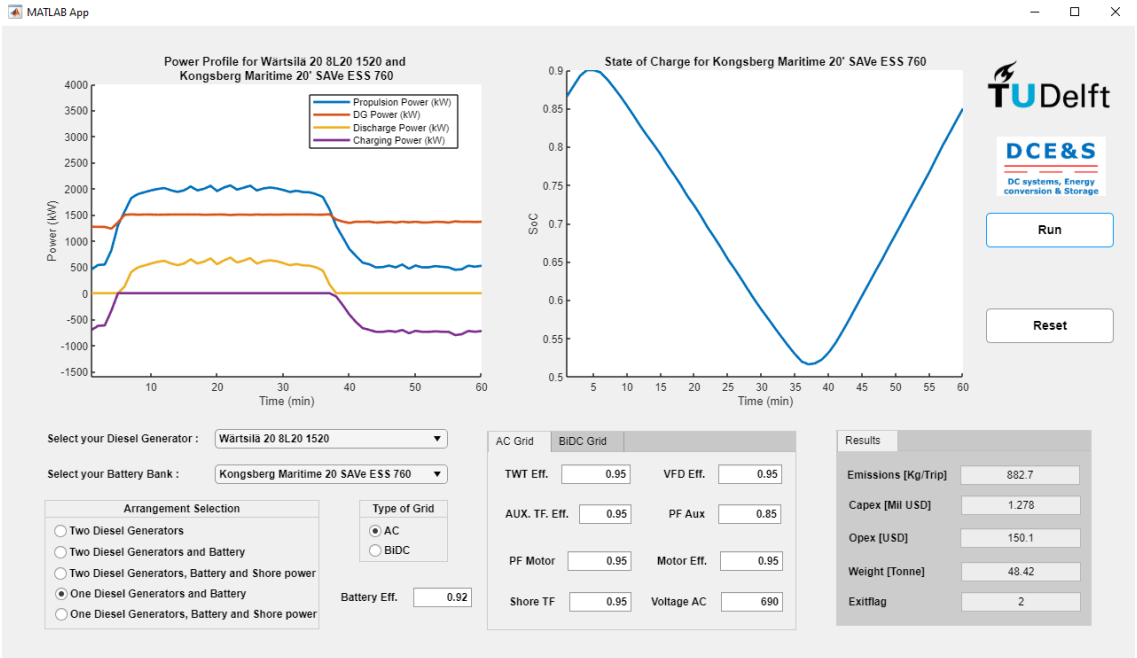

Figure D.2: The results for the AC4 arrangement with the diesel generator and battery, as shown in the figure

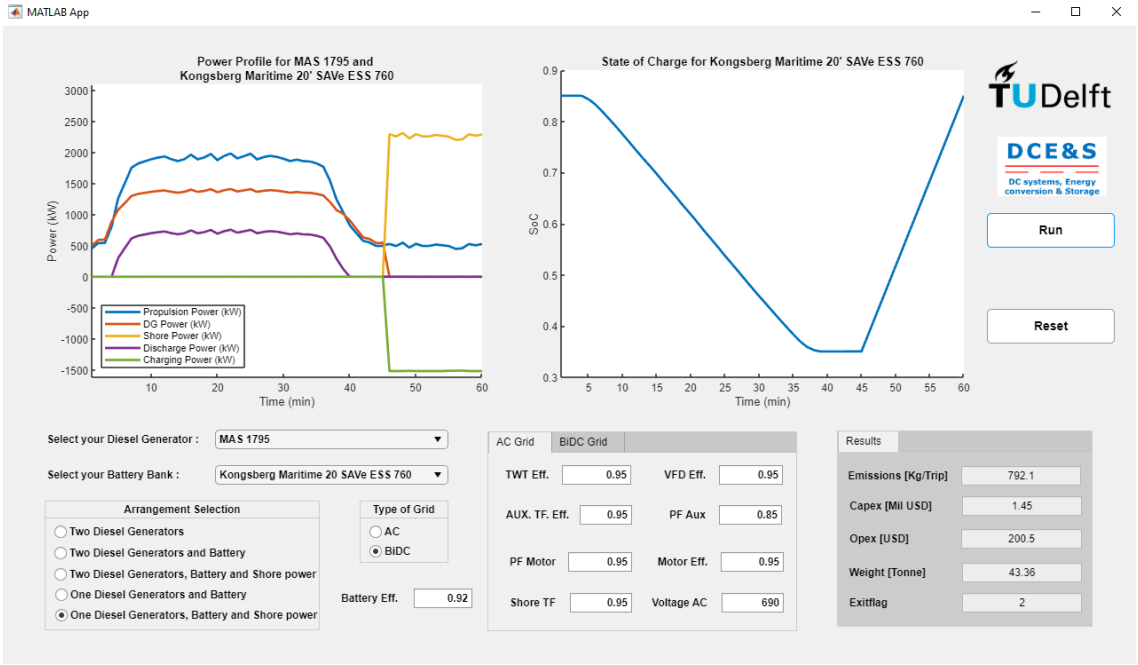

Figure D.3: The results for the DC5 arrangement with the diesel generator and battery, as shown in the figure

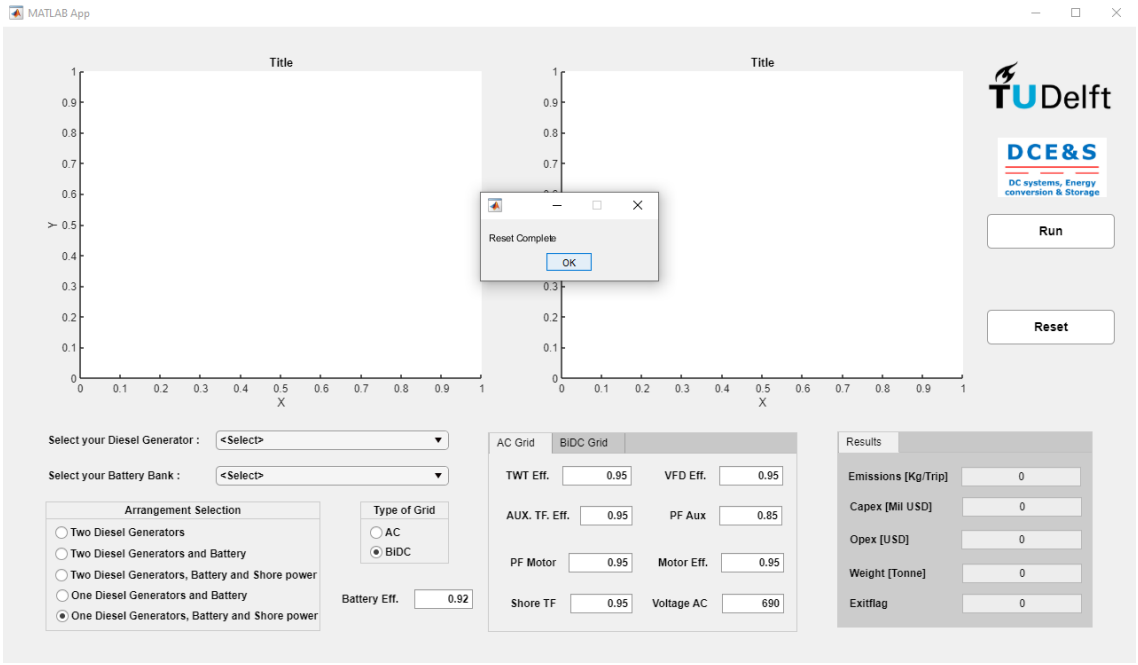

Figure D.4: The results after pressing the reset button on the application